

Biochemical and structural studies on enzymes of menaquinone biosynthesis

Dissertation

zur Erlangung des
Doktorgrades der Naturwissenschaften (Dr. rer. nat.)

der

Naturwissenschaftlichen Fakultät I – Biowissenschaften –

der Martin-Luther-Universität
Halle-Wittenberg,

Vorgelegt

von Camila A. Cotrim

geboren am 03.04.1985 in Campinas (Brasilien)

Gutachter

1. Prof. Dr. Milton T. Stubbs
2. Prof. Dr. Gary Sawers
3. Prof. Dr. Shu-Ming Li

Verteidigt am 13.09.2016

Contents

Contents	i
1. Introduction.....	1
1.1. Isoprenoid quinones.....	1
1.2. Ubiquinone (UQ)	2
1.2.1 Biosynthesis of ubiquinone	2
1.3. Vitamin K.....	4
1.3.1. Menaquinone (MK).....	5
1.3.1.1. Biosynthesis of menaquinone in microorganisms	6
1.3.1.2. Menaquinone biosynthesis as a target for antibacterial drugs	9
1.3.2. Futasolase (MqnB).....	9
1.3.3. Vitamin K in humans.....	10
1.4. Prenyltransferases.....	11
1.4.1. Aromatic prenyltransferases	12
1.4.2. 4-hydroxybenzoate octaprenyltransferase (UbiA)	14
1.4.3. 1,4-dihydroxy-2-naphthoic acid octaprenyltransferase (MenA)	15
1.5. Aims of the work	17
2. Materials and Methods	19
2.1. Materials	19
2.1.1. Chemicals.....	19
2.1.2. Enzymes and Antibodies.....	21
2.1.3. Markers.....	21
2.1.4. Kits	22
2.1.5. Bacteria Strains and Plasmids.....	22
2.1.6. Oligonucleotides.....	23
2.2. Molecular Biology Methods	24
2.2.1. DNA Extraction	24
2.2.2. Polymerase Chain Reaction (PCR)	24
2.2.3. Agarose gel	25
2.2.4. Site-directed mutagenesis.....	26
2.2.5. Digestion.....	26
2.2.6. Ligation	27
2.2.7. Plasmid preparation	27

2.3. Microbiology Methods	27
2.3.1. Preparation of chemically competent <i>E. coli</i> cells	27
2.3.2. Heat shock transformation	27
2.3.3. Gene expression of recombinant proteins in <i>E. coli</i>	28
2.3.4. Preparation of <i>Streptomyces lividans</i> TK24 protoplasts	28
2.3.5. Transformation in <i>Streptomyces lividans</i> TK24 protoplasts	29
2.3.6. Gene expression of recombinant proteins in <i>Streptomyces lividans</i> TK24	29
2.3.7. Cell disruption	29
2.3.8. Generation of <i>menA</i> knockout cells by homologous recombination in bacteriophage P1. 29	
2.3.8.1. Preparation of P1 liquid lysate	29
2.3.8.2. P1 Transduction	30
2.3.9. Complementation assay	30
2.4. Biochemical Methods	31
2.4.1. Polyacrylamide gel electrophoresis (SDS – PAGE)	31
2.4.2. Immunoblotting	32
2.4.3. Alignment	32
2.4.4. Membrane Proteins	32
2.4.4.1. Preparation of membrane fractions	32
2.4.4.2. Solubilization of membrane fraction	33
2.4.5. Purification	33
2.4.5.1. Membrane proteins – TtUbiA and EcMenA	33
2.4.5.1.1. Immobilized metal ion affinity chromatography (IMAC) – Batch mode	33
2.4.5.1.2. TEV digestion	33
2.4.5.1.3. Size Exclusion Chromatography (SEC)	34
2.4.5.2. Fucosyltransferase (TtMqnB)	34
2.4.5.2.1. Heat Treatment	34
2.4.5.2.2. Purification Co-NTA – 5 mL column Äkta system	34
2.4.6. Prenyltransferase Assays	34
2.4.6.1. UbiA prenyltransferase assays	34
2.4.6.2. MenA prenyltransferase assays	35
2.5. Biophysical Methods	35
2.5.1. Protein concentration determination	35
2.5.1.1. RC DC™ Protein Assay	35
2.5.1.2. UV/Vis Spectroscopy	36
2.5.2. Circular Dichroism (CD) spectroscopy	36

2.5.3. Mass spectrometry	37
2.5.3.1. MALDI-TOF Mass spectrometry	37
2.5.3.2. ESI-Mass spectrometry.....	37
2.5.4. Analytical Ultracentrifugation	38
2.6. Crystallography Methods	39
2.6.1. 96-well plate crystallization screening	39
2.6.2. 15-well plate fine screening	39
2.6.3. Ligand Soaking	40
2.6.4. Data collection and data processing.....	40
2.6.5. Model building and phase refinement	40
2.7. Chemical synthesis of aromatic substrate	41
3. Expression and characterization of 1,4-dihydroxy-2-naphthoate octaprenyltransferase (MenA) ...	42
3.1. Recombinant expression of EcMenA in <i>E. coli</i>	42
3.2. Solubilization of EcMenA protein.....	43
3.3. Enzymatic activity of the EcMenA-His membrane fraction	44
3.4. Purification of EcMenA protein.....	46
3.5. Secondary structure of purified EcMenA investigated using circular dichroism (CD)	49
3.6. Substrate Specificity	50
3.7. Inhibition of purified EcMenA	53
3.8. Discussion.....	55
4. Expression and characterization of a homolog of 4-hydroxybenzoate octaprenyltransferase (UbiA) from <i>Thermus thermophilus</i> (TtUbiA)	59
4.1. Identification of UbiA/ MenA homologs in <i>Thermus thermophilus</i>	59
4.2. Recombinant expression of <i>Thermus thermophilus</i> UbiA (TtUbiA) in <i>E. coli</i>	60
4.3. TtUbiA exhibits neither 4-hydroxybenzoate octaprenyltransferase (UbiA) nor 1,4-dihydroxy-2-naphthoic acid (MenA) activity	61
4.4. The lack of activity is not due to the membrane composition	63
4.4.1. Cloning, expression and activity assay of SIUbiA.....	64
4.4.2. Cloning, expression and activity assays of EcMenA in <i>S. lividans</i> TK24 cells.....	65
4.5. TtUbiA and SIUbiA belong to a distinct class of aromatic prenyltransferases associated with the futasolose pathway	66
4.5.1. TtUbiA and its mutants are unable to complement for EcMenA in <i>E. coli</i>	69
4.5.1.1. Expression of mutants in a <i>menA</i> ⁻ deletion strain	69
4.5.1.2. Activity assay of mutants	70
4.5.1.3. TtUbiA is unable to complement for MenA.....	71
4.6. Solubilization and purification of TtUbiA	72

4.7. Discussion.....	73
5. Crystal structure analysis of futasosine hydrolase from <i>Thermus Thermophilus</i> (TtMqnB).....	81
5.1. Recombinant expression of TtMqnB in <i>E. coli</i>	81
5.2. Purification of TtMqnB.....	82
5.3. TtMqnB is a dimer in solution	82
5.4. Crystallization of TtMqnB.....	83
5.5. Data collection, model building and structure of TtMqnB	84
5.6. Ligand-soaking experiments and the structure of Hypo-TtMqnB.....	86
5.7. Structural similarities between TtMqnB and 5'-methylthioadenosine nucleosidase (MTAN) .	88
5.8. Active-site of MqnB.....	93
5.10 Discussion.....	99
6. Summary.....	105
7. References.....	107
8. Appendix.....	i
9. Abbreviations	xiii
Resume.....	xv
Publications	xvi
Danksagung	xviii
Declaration	xix

1. Introduction

1.1. Isoprenoid quinones

Isoprenoid or terpenoid quinones are lipid-soluble molecules found in almost all organisms. In prokaryotic cells the isoprenoid quinones are found in the cell membrane, whereas in eukaryotic cells, most of the quinones are associated with the inner membranes of the mitochondria and also in the chloroplast (Hiraishi, 1999). Isoprenoid quinones are composed of a polar head group and also of a hydrophobic side chain that gives the molecules a lipid-soluble character and hold them in the lipid bilayer membrane (Nowicka and Kruk, 2010). The hydrophobic side chain varies depending on the species. Humans and plants have 10 isoprenoid moieties in the side chain, whereas the quinone in *E. coli* and *Saccharomyces cerevisiae* consist of 8 and 6 isoprenoid moieties, respectively (Søballe and Poole, 1999). An interesting property of the isoprenoid quinones is the ability of the quinone ring to undergo a two-step reversible reduction to form a quinol (Figure 1.1). This together with the presence of a lipid-soluble chain makes these molecules essential for the electron transport between protein complexes inside the membrane in the respiratory chains of prokaryotic and eukaryotic organisms (Hiraishi, 1999; Nowicka and Kruk, 2010).

Most of the biological isoprenoid quinones found in nature can be divided in two groups: 1) benzoquinones, which include ubiquinone and plastoquinone and 2) naphthoquinones, which include menaquinone and phyloquinone. The two groups differ from each other not only in the ring structure, but also in the length and degree of saturation of the hydrophobic side chain. Due to this wide structural diversity, these molecules can also be classified in different taxonomic groups, which have been used as taxonomic tools in order to isolate and characterized new molecules (Collins and Jones, 1981; Nowicka and Kruk, 2010; Søballe and Poole, 1999).

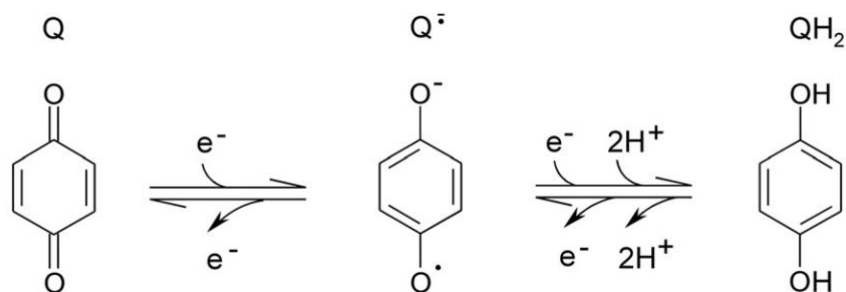


Figure 1.1. Redox reaction of the quinone ring. Q represents the oxidized form; Q^{•-} represents the unstable semi-quinone radical that can be stabilized by interaction with proteins; and QH₂ represents the stable and non-charged hydroquinone form (Nowicka and Kruk, 2010).

1.2. Ubiquinone (UQ)

Ubiquinone (UQ), also known as coenzyme Q (CoQ), belongs to the group of benzoquinones and it is found in aerobic Gram-negative bacteria as well as in eukaryotic cells (Nowicka and Kruk, 2010). UQ plays an essential role in the respiratory chain by transferring electrons from NADH dehydrogenase (complex I) to succinate dehydrogenase (complex II) and further to the bc1 complex (complex III) at the plasma membrane in prokaryotes or at the inner mitochondrial membrane in eukaryotes (Okada et al., 2004; Szkopińska, 2000). Reduction and oxidation processes of UQ involve the transfer of two electrons with addition or release of two H^+ to form ubiquinol (UQH) and UQ, respectively (Figure 1.1). Removal or transfer of just one electron and H^+ leads to the formation of a semiquinone radical that may be stabilized by binding with different proteins. In *E. coli*, a highly stabilized semiquinone radical is found to associate with two proteins, UQH₂ oxidase and cytochrome *bo'* (Søballe and Poole, 1999).

In humans, the most common ubiquinone form is known as coenzyme Q₁₀ (CoQ₁₀), which contains 10 isoprenoid units. Although CoQ₁₀ is found in all cells, high amounts of CoQ₁₀ are found in the heart and liver, since they contain the most amount of mitochondria per cell (Kurosu and Begari, 2010). The function of CoQ₁₀ as a component of the mitochondrial respiratory chain is well established (Meganathan, 2001a; Turunen et al., 2004), although, other functions such as antioxidant and membrane stabilizer have also been reported (Kagan et al., 1990; Turunen et al., 2004).

Deficiency of CoQ₁₀ has been associated with several diseases including cerebellar ataxia, a disease that causes problems with incoordination of movements and unsteadiness (Gempel et al., 2007; Quinzii et al., 2006) and heart failure (Folkers, 1993). Clinically, CoQ₁₀ has been used as a therapy against a wide of humans' diseases, mainly in the treatment of heart diseases (Turunen et al., 2004; Weant and Smith, 2005). Therapy based on CoQ₁₀ supplementation offers the advantage that the molecule is not toxic even at high concentrations and so far no side effects have been reported (Meganathan, 2001a). Recently, the studies with CoQ₁₀ gained importance since it was demonstrated through *in vitro* and *in vivo* experiments, beneficial effects after supplementation with CoQ₁₀ in patients with neurodegenerative disease such as Huntington's and Parkinson's diseases (Ferrante et al., 2002; Spindler et al., 2009; Turunen et al., 2004).

1.2.1 Biosynthesis of ubiquinone

The biosynthetic pathways of UQ in *E. coli* and *S. cerevisiae* have been widely studied (Meganathan, 2001b; Søballe and Poole, 1999). Although both pathways are very similar, they differ in some aspects such as the origin of the quinone nucleus, which in *E. coli* is only

derived from the shikimate pathway via chorismate, whereas in *S. cerevisiae* the quinone nucleus could also be derived from tyrosine (Meganathan, 2001b).

In *E. coli* the synthesis of the quinone starts with the conversion of chorismate (1) into 4-hydroxybenzoate (2) by chorismate pyruvate-lyase, an enzyme encoded by the *ubiC* gene (Figure 1.2). The importance of chorismate pyruvate-lyase was demonstrated through mutation, since *ubic* knock out mutants were unable to produce UQ and to grow under aerobic conditions on oxidizable substrate such as succinate (Meganathan, 2001b; Søballe and Poole, 1999). The second reaction is the prenylation of 4-hydroxybenzoate to 3-octaprenyl-4-hydroxybenzoate (3) carried out by the integral membrane enzyme 4-hydroxybenzoate octaprenyltransferase (UbiA) or CoQ2 in *S. cerevisiae*, encoded by the *ubiA* and *CoQ2* gene, respectively. Interestingly, the length of the isoprenoid side chain in UQ is determined by the polyprenyl diphosphate synthase present in the cells and not by the polyprenyltransferase. In *E. coli*, the octaprenyl diphosphate synthase, encoded by the *ispB* gene, is responsible for the eight isoprenoid moiety found in UQ-8 (Søballe and Poole, 1999). Next, the 3-octaprenyl-4-hydroxybenzoate (3) is decarboxylated to 2-octaprenylphenol (4) by the enzyme prenyl-4-hydroxybenzoate decarboxylase, also known as UbiD. In *E. coli* and in *Salmonella enterica* a second decarboxylase, encoded by the *ubiX* gene, was found and described to be responsible for this decarboxylation together with UbiD (Meganathan, 2001b; Søballe and Poole, 1999).

In the subsequent steps of the pathway, the 2-octaprenylphenol (4) is hydroxylated and methylated three times. The hydroxylation reactions occur at the position C6, C4 and C5 and are catalyzed by different enzymes: UbiI, UbiH and UbiF, respectively. Although it was originally believed that the UbiB enzyme was responsible for the initial hydroxylation, since *ubiB*⁻ mutants accumulated 2-octaprenylphenol, it was later demonstrated that the accumulation of 2-octaprenylphenol is not completely related with absence of *ubiB* because strains deficient in the methyltransferase (UbiG) also showed accumulation of 2-octaprenylphenol (Hsu et al., 1996). In addition, it was showed that the UbiB protein sequence contains conserved motifs found in a superfamily of kinases and not of hydroxylases (Lagier-Tourenne et al., 2008). The methylation reactions occur at position 6-OH, at the ring C-3 and at the 5-OH, respectively. The methylation at the ring C-3 is catalyzed by UbiE, whereas the both *O*-methylations are carried out by the same *O*-methyltransferase encoded by the *ubiG* gene, leading to the formation of UQ (10) (Meganathan, 2001b).

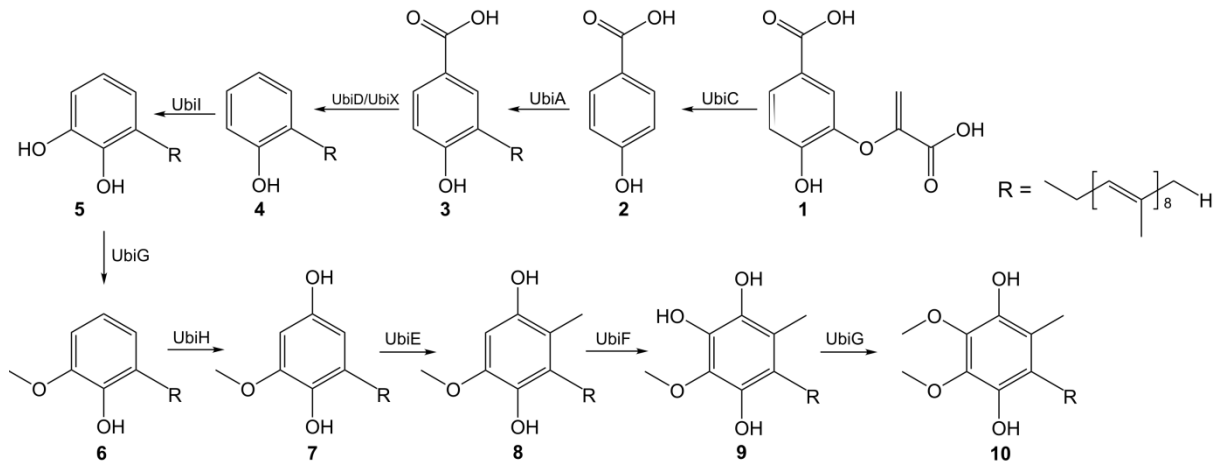


Figure 1.2. Biosynthesis of Ubiquinone in *E. coli*. The biosynthesis of UQ in *E. coli* is catalyzed by the nine named enzymes. The numbers indicate the intermediates; (1) chorismate; (2) 4-hydroxybenzoate; (3) 3-octaprenyl-4-hydroxybenzoate; (4) 2-octaprenylphenol; (5) 2-octaprenyl-6-hydroxyphenol; (6) 2-octaprenyl-6-methoxyphenol; (7) 2-octaprenyl-6-methoxy-1,4-benzoquinol; (8) 2-octaprenyl-3-methyl-6-methoxy-1,4-benzoquinol; (9) 2-octaprenyl-3-methyl-5-hydroxy-6-methoxy-1,4-benzoquinol; (10) Ubiquinol.

1.3. Vitamin K

Vitamin K is a lipid-soluble vitamin that works as a cofactor for γ -glutamyl carboxylase (GGCX), an enzyme responsible for converting specific glutamic acid residues to γ -carboxyglutamic acid (Gla) residues in several proteins (Cranenburg et al., 2007; Furie et al., 1999). Because Gla containing proteins are involved in many biological activities in humans such as blood coagulation and vascular repair, vitamin K is an essential molecule for humans (Benzakour and Kanthou, 2000; Furie et al., 1999). Vitamin K occurs in the nature in two forms: menaquinone found in bacteria, and phyloquinone (also known as vitamin K₁) found in plants, which acts as cofactor for photosystem I-mediate electrons (Gross et al., 2006; Kurosu and Begari, 2010). All forms of vitamin K possess a common 2-methyl-1,4-naphthoquinone ring structure; however, menaquinone and phyloquinone differ from each other in their hydrophobic side chain. At the 3-position of the ring phyloquinone contains a monounsaturated side chain with one isoprenoid moiety, whereas menaquinone contains an unsaturated side chain with different numbers of isoprenoid residues (Figure 1.3) (Kurosu and Begari, 2010; Nakagawa, 2010).

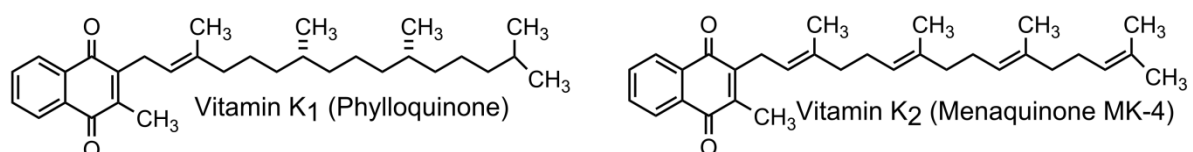


Figure 1.3. Natural forms of vitamin K. Representation of phyloquinone (PK), the natural form of vitamin K found in plants with a phytyl side chain and menaquinone, the vitamin K form found in bacteria with a prenyl side chain (Kurosu and Begari, 2010 – modified).

1.3.1. Menaquinone (MK)

Menaquinone (MK) or vitamin K₂ is the most ancient type of isoprenoid quinones and can be found in several Archea, Gram-positive bacteria, green sulfur bacteria and flavobacteria (Nowicka and Kruk, 2010). Due to its low midpoint redox potential ($E^{\circ} = -74$ mV) and the existence in early phase of evolution, MK is connected with earlier atmosphere conditions containing low oxygen concentration. The low midpoint redox potential allows that the reduced MK becomes rapidly and non-catalytically oxidized in the presence of oxygen, making this molecule inefficient to operate in an atmosphere containing oxygen (Schoepp-Cothenet et al., 2009).

The best known function of MK is its participation in prokaryotic respiration by transferring electrons from a donor to acceptor in an enzyme-dependent process. Figure 1.4 shows a schematic representation of the electron transfer mediated by MK in *M. tuberculosis*, where electrons are transported along the membrane via MK and a series of protein carries. At the same time, protons are transferred across the cell membrane from the cytoplasm to the periplasmic space, generating a proton gradient that is used by ATP-Synthase for the synthesis of ATP (Kurosu and Begari, 2010). In most anaerobic and all Gram-positive organisms, MK is the sole quinone in the respiratory chain, and therefore essential for their survival. Facultative organisms such as *E. coli* are able to synthesize UQ as well as MK, wherein UQ is used under aerobic conditions and MK under anaerobic conditions (Dairi et al., 2011; Jiang et al., 2007).

Menaquinone can be synthesized through two different pathways: the classical pathway, elucidated in *E. coli* in 1970s and 1980s (Bentley and Meganathan, 1982) and the futasolone pathway, an alternative pathway recently discovered, found in *Thermus thermophilus*, *Streptomyces coelicolor*, *Helicobacter pylori* and *Campylobacter jejuni* (Hiratsuka et al., 2008).

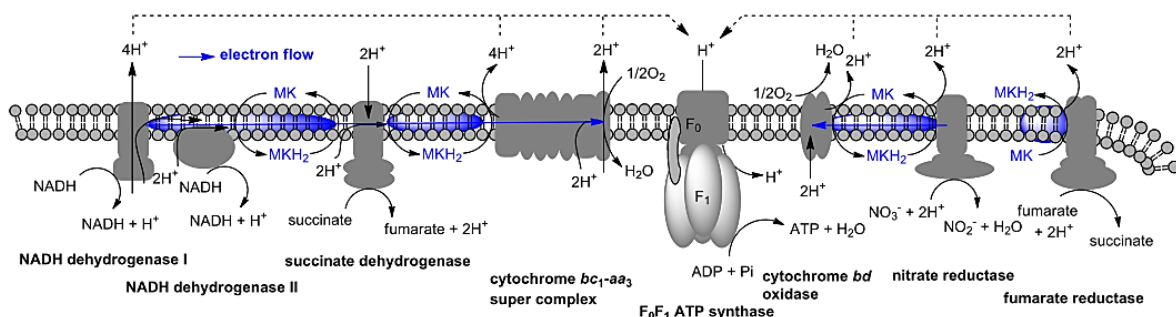


Figure 1.4. Electron transport chain of *M. tuberculosis*. Electron transfer mediated by menaquinone shown in blue (Kurosu and Begari, 2010 – modified).

1.3.1.1. Biosynthesis of menaquinone in microorganisms

The classical MK biosynthetic pathway has been studied extensively in *E. coli*, where nine enzymes (MenA-MenH and *yfbB*) are involved in the biosynthesis (Bentley and Meganathan, 1982; Meganathan, 2001a; Shineberg and Young, 1976). The biosynthesis starts with the conversion of chorismate (1) (derived from the shikimate pathway) into isochorismate (2) catalyzed by MenF, an isochorismate synthase (Figure 1.5). Isochorismate is converted into 2-succinyl-5-enolpyruvyl-6-hydroxy-3-cyclohexadiene-1-carboxylate (SEPHCHC) (3) by MenD in the presence of 2-ketoglutarate as a second substrate. In the following reactions, MenH eliminates the pyruvate moiety of (SEPHCHC) forming the 2-succinyl-6-hydroxy-2,4-cyclohexadiene-1-carboxylate (SHCHC) (4), which is then dehydrated by MenC to yield an aromatic compound, *o*-succinylbenzoate (5). In the next steps, MenE transfers a coenzyme CoA to *o*-succinylbenzoate yielding *o*-succinylbenzoate-CoA (6) that is converted into 1,4-dihydroxy-2-naphthoyl-CoA (7) by MenB followed by a hydrolysis reaction catalyzed by a thioesterase (*yfbB*) to generate 1,4-dihydroxy-2-naphthoate (DHNA-2) (8), the head group of MK. The last two steps of the pathway are synthesized by MenA and MenG/UbiE, which catalyze the prenylation and methylation of the head group, respectively, forming the menaquinone (10) (Dairi et al., 2011; Kurosu and Begari, 2010).

The first evidence of an alternative pathway for the synthesis of MK came after the determination of the complete genome sequence of *Streptomyces coelicolor* (Bentley et al., 2002). Bioinformatics analyses showed the absence of *menF*, *menD*, *menC*, *menE* and *menB* genes in its genome, although this strain is able to produce MK. Further investigations showed that *Thermus thermophilus* and some pathogenic organisms, including *Helicobacter pylori* and *Campylobacter jejuni* also lack orthologues *men* genes, suggesting that the naphthoquinone moiety can be synthesized via an alternative pathway (Dairi et al., 2011; Hiratsuka et al., 2008). The presence of the alternative pathway was confirmed through trace experiments using radiolabeled [U-¹³C₆] glucose to feed *Streptomyces ssp* as well as strains known to synthesize MK via the classical pathway.

Bioinformatic analyses starting with the genomes of organisms that likely possess the alternative pathway, such as *S. coelicolor*, *T. thermophilus*, *H. pylori* and *Campylobacter jejuni* revealed four potential enzymes supposed to be involved in the formation of the naphthoquinone ring, later proved by mutant strains. The alternative pathway was named futasoline pathway, after an intermediate that was identified (Dairi, 2009; Hiratsuka et al., 2008).

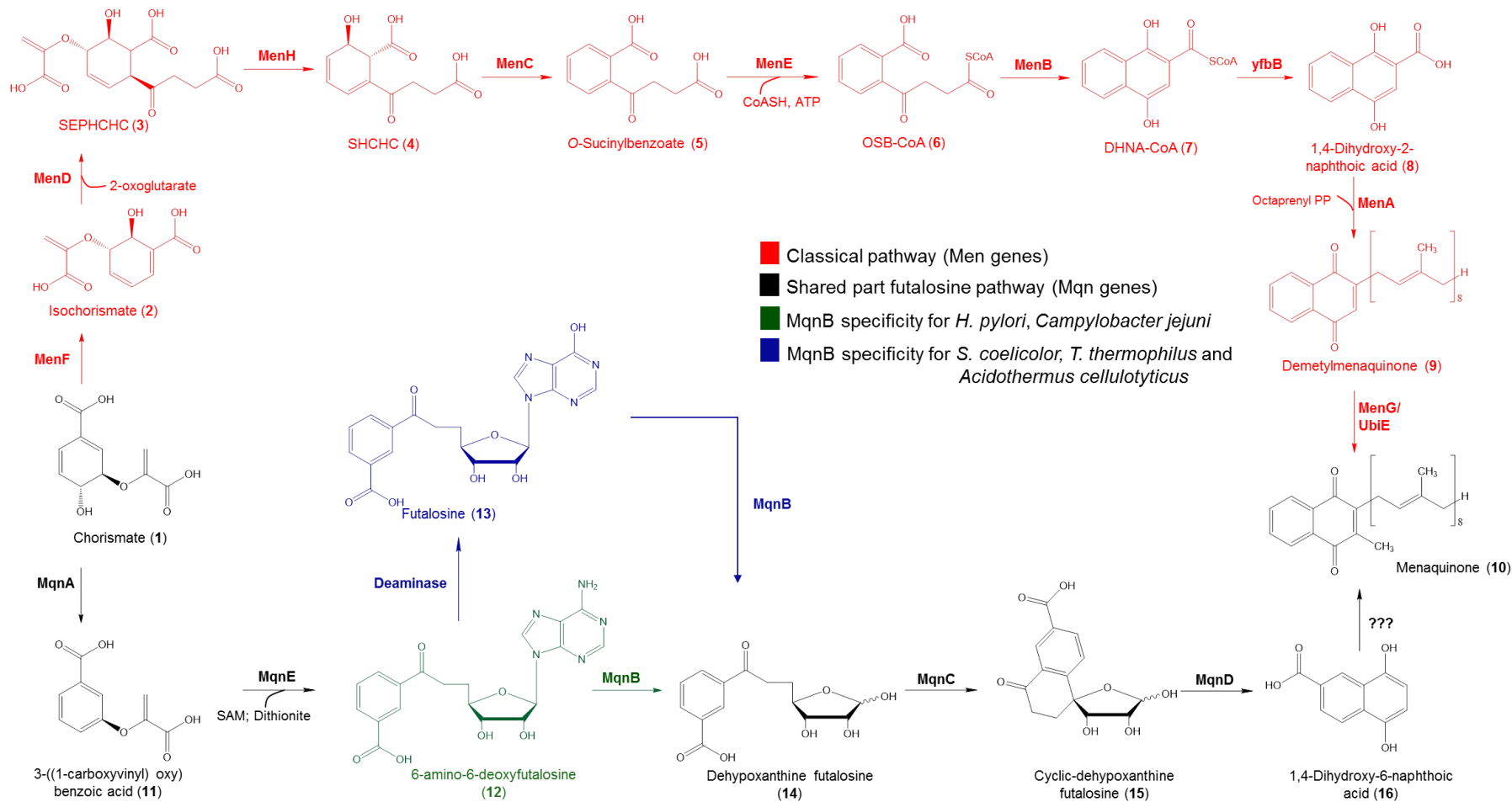


Figure 1.5. Biosynthesis of menaquinone. Scheme showing the biosynthesis of MK via the classical pathway (colored in red) and via the futilosine pathway (colored in black). A divergence has been observed in the futilosine pathway regarding the substrates of MqnB. In *H. pylori* and *C. jejuni*, MqnB orthologs hydrolyze directly the 6-amino-6-deoxyfutilosine (AFL) to form dehypoxanthine futilosine (shown in green), while in *S. coelicolor* and *T. thermophilus* AFL is converted into futilosine and then hydrolyzed by MqnB to form dehypoxanthine futilosine (shown in blue). SEPHCHC: 2-succinyl-5-enolpyruvyl-6-hydroxy-3-cyclohexene-1-carboxylic acid; SHCHC: 2-succinyl-6-hydroxy-2,4-cyclohexadiene-1-carboxylic acid (Kim et al., 2014 – modified).

In *T. thermophilus* and *S. coelicolor*, the biosynthesis of MK via fufalosine pathway starts with MqnA, an enzyme that catalyzes the condensation of chorismate (1), inosine and a C2 unit (probably derived from phosphoenolpyruvate) to form fufalosine (13). In the following step, MqnB (fufalosine hydrolase) splits off hypoxanthine to form dehypoxanthinylfufalosine (DHFL) (14), which is cyclized by MqnC to yield cyclic DHFL (15). The last reaction to generate the naphthoquinone ring is catalyzed by MqnD, which cleaves the cyclic DHFL to release 1,4-dihydroxy-6-naphthoate (DHNA-6) (16), which differs from the DHNA-2 (classical pathway) by the position of the carboxyl group. Although there is no direct evidence to confirm the synthetic process from DHNA-6 to MK, it is believed that prenylation, methylation and decarboxylation should be involved in the last steps of the fufalosine pathway (Hiratsuka et al., 2008).

Although the enzymes belonging to the fufalosine pathway have been identified and studied over the past years, some details of the pathway still remain unclear. Recently, it has been proposed that the first steps of fufalosine pathway are different in some organisms and that at least three different routes lead to formation of DHFL (Arakawa et al., 2011). The first route, found in *T. thermophilus*, suggests that fufalosine (FL) (13) is directly formed by MqnA and converted into DHFL by MqnB. The second route suggests that in *A. cellulolyticus* and *S. coelicolor*, the 6-amino-6-deoxyfufalosine (AFL) (12) is formed by MqnA, converted to FL (13) by a deaminase and then converted to DHFL (14) by MqnB. Finally, the last route, observed in *H. pylori*, showed that the AFL (12) was directly converted into DHFL (14) by MqnB (Arakawa et al., 2011). Furthermore, analyses of the intermediates of MK biosynthesis in *C. jejuni* strain showed that this organism produces MK through the same route described for *H. pylori* and that the AFL obtained from MqnA is hydrolyzed by MTAN (5'-methylthioadenosine nucleosidase), which acts as MqnB ortholog (Li et al., 2011).

In 2013 a new enzyme, MqnE, involved in the fufalosine pathway was identified in *T. thermophilus* that helped elucidate the first steps of this pathway. According to the new proposed route, MqnA just catalyzes the dehydration of chorismate to 3-((1-carboxyvinyl)oxy) benzoic acid (11), which is converted into 6-amino-6-deoxyfufalosine (12) by MqnE in the presence of S-adenosylmethionine and dithionite under anaerobic conditions (Mahanta et al., 2013). The presence of a MqnE homolog in *T. thermophilus* strains suggests that fufalosine is converted from 6-amino-6-deoxyfufalosine by a deaminase reaction and not directly from the chorismate via MqnA, as previously proposed. Hence, according to the new route, 6-amino-6-deoxyfufalosine is a common intermediate for all organisms. A scheme showing the biosynthesis of MK via classical pathway and the different routes found in fufalosine pathway is illustrated in Figure 1.5.

1.3.1.2. Menaquinone biosynthesis as a target for antibacterial drugs

It is estimated that one-third of the world population is infected with *M. tuberculosis* (Mtb), in particular HIV-AIDS patients that are more susceptible to tuberculosis infection due to their fragile immune-system (Amante and Ahemed, 2015). According to the Centre for Disease Control and Prevention (CDC), tuberculosis was responsible in 2013 for around 1.5 million deaths worldwide. In addition, the emergence of multidrug-resistant strains of Mtb has complicated the control and treatment of tuberculosis (Cohen, 2004). Thus, the development of new drugs against *M. tuberculosis* has become essential. In this context, the enzymes involved in the biosynthesis of MK have been highlighted, since MK is the sole quinone in the respiratory chain of Gram-positive bacteria and therefore essential for their survival. Moreover, the absence of this pathway in humans makes this pathway a target for novel antibacterial drug discovery (Kurosu and Begari, 2010; Lu et al., 2008). Recent studies have demonstrated that inhibition of MenA (1,4-dihydroxy-2-naphthoate prenyltransferase) resulted a significant growth inhibition of *Mycobacterium spp*, whereas no inhibitory effect was observed in facultative Gram-negative *E. coli* under aerobic conditions (Debnath et al., 2012; Kurosu and Crick, 2009; Kurosu et al., 2007).

Apart from MenA, others enzymes of the classical pathway, including MenB, MenD and MenE have been studied for the development of novel drugs against *M. tuberculosis*. Li et al., (2010) designed 1,4-benzoxazine derivatives that were able to inhibit the catalytic activity of MenB as well as the growth of *M. tuberculosis* H37Rv; some compounds also inhibited the growth of *E. coli* and *S. aureus*. Initial studies using a series of vinyl sulfonamides, based on the MenE substrate also showed promising results by inhibiting the activity of MenE at low concentrations (Lu et al., 2008).

Since the discovery of the futasine pathway in some pathogenic organisms (including *H. pylori* and *C. jejuni*), this pathway has also become a target for novel antibacterial drug discovery, since it is present neither in humans nor in bacteria from the gut (Dairi et al., 2011). The MqnB ortholog of *H. pylori* for instance has been widely studied in order to identify compounds able to inhibit the catalytic activity.

1.3.2. Futasine hydrolase (MqnB)

Futasine hydrolase or futasine nucleosidase (MqnB) (EC 3.2.2.26) catalyzes the most diverse step during the biosynthesis of menaquinone via futasine pathway. In *T. thermophilus* and *S. coelicolor*, MqnB hydrolyzes futasine (FL) in dehydropyrimidinofutasine (DHFL) to release hypoxanthine, while in *H. pylori* and *C. jejuni* the 6-amino-6-deoxyfutasine (AFL) is directly converted in DHFL by an MqnB ortholog releasing adenine (Figure 1.5) (Arakawa et al., 2011; Li et al., 2011; Mahanta et al., 2013). Interestingly, it has

been reported that the most similar MqnB ortholog present in *H. pylori* and *C. jejuni* is the 5'-methylthioadenosine/S-adenosylhomocysteine nucleosidase (MTAN) (EC 3.2.2.9) (Arakawa et al., 2011; Li et al., 2011), a multifunctional enzyme involved in the biosynthesis of purine and methionine salvage pathways (Ronning et al., 2010). Structural studies of MTAN homologs have suggested that the specificity of MTAN towards AFL encompasses the adenosine moiety.

The function of MqnB has been studied in *S. coelicolor* and in *T. thermophilus* (Dairi, 2009; Dairi et al., 2011). In *T. thermophilus*, MqnB (TtMqnB) contains 225 amino acids with a molecular mass of 23.81 kDa and is encoded by the gene *mqnB*. Biochemical characterization of TtMqnB has demonstrated that the enzyme is strictly specific towards futasalose and that no cofactor is required for enzymatic activity. In addition, due to its thermostability, a high level of activity of TtMqnB was reported at high temperatures (80 °C) with an optimal pH of 4.5 (Hiratsuka et al., 2009).

Although MqnB enzymes have been classified as an ortholog of MTAN enzymes and the structure and function of MTANs have been widely studied in different organisms (Haapalainen et al., 2013; Lee et al., 2003; Ronning et al., 2010) to date, there is no data concerning structural information of any MqnB homolog.

1.3.3. Vitamin K in humans

The best known role of vitamin K in humans is its function as cofactor for γ -glutamyl carboxylase (GGCX) (Cranenburg et al., 2007; Furie et al., 1999). The vitamin K-dependent GGCX enzymes catalyze the carboxylation of glutamate residues in a number of proteins (Gla containing proteins) related to blood coagulation (Cranenburg et al., 2007). For GGCX catalysis, the reduced form of vitamin K (hydroquinone) is necessary. During the enzymatic carboxylation to form the γ -carboxyglutamic acid (Gla) residue, vitamin K is oxidized to the vitamin K 2,3-epoxide form, which is afterwards reduced back to vitamin K by the action of two enzymes, vitamin K epoxide reductase (VKOR) and vitamin K reductase, respectively, completing the vitamin K cycle (Kurosu and Begari, 2010; Okano et al., 2008; Shearer and Newman, 2014).

In humans, vitamin K₁ (phyloquinone – PK) is found in all tissues, with high amounts in liver, heart and pancreas, although its concentration is relatively low compared with menaquinone 4 (MK-4) levels (Nakagawa, 2010). For several years it was believed that humans were not able to synthesize MK and that the MK-4 found in several tissues was either obtained from the diet or through the conversion of PK to MK-4 by bacteria present in the gut (Nakagawa, 2010; Thijssen et al., 1996). However, Nakagawa (2010) showed that mouse and human cells were able not only to convert PK to MK-4 directly, but also to convert PK to menadione (vitamin K₃) followed by prenylation in the presence of

geranylgeranyl pyrophosphate (GGPP) to form MK-4 independently of the gut bacteria. Further studies have demonstrated that UBIAD1, the *menA* homolog in humans, is responsible not only for the cleavage of the side chain of PK to produce menadione, but also for its prenylation in the presence of GGPP to generate MK-4 (Nakagawa et al., 2010).

1.4. Prenyltransferases

Prenylation of the aromatic ring is the key reaction for formation of quinones (Heide, 2009). Each of the biosynthetic routes contains an oligoprenyl transfer to an aromatic molecule catalyzed by a prenyltransferase. While in the biosynthesis of UQ the *para*-hydroxy benzoic acid (PHB) is prenylated by 4-hydroxybenzoate octaprenyltransferase (UbiA) in the initial steps, the 1,4-dihydroxy-2-naphthoic acid (DHNA-2) is prenylated during the biosynthesis of MK by another octaprenyltransferase (MenA) in the last steps (Meganathan, 2001a). The most likely precursor for prenylation in the fufalosine pathway is the 1,4-dihydroxy-6-naphthoate (DHNA-6); however, the enzyme responsible for its prenylation has not been identified (Seto et al., 2008; Zhi et al., 2014).

Prenyltransferases are enzymes that transfer a prenyl moiety to different acceptor molecules (isoprenoid groups, aromatic compounds, proteins, etc.) (Liang et al., 2002) The prenyl moiety is derived from allylic isoprenyl diphosphates, which includes dimethylallyl pyrophosphate (DMAPP), geranyl pyrophosphate (GPP) and farnesyl pyrophosphate (FPP) (Saleh et al., 2009). These enzymes are widely distributed in all organisms and they are involved in metabolic routes and production of carotenoids (Botta et al., 2005). Prenyltransferases have been the object of several studies, since a large variety of biological activities has been reported for prenylated molecules, particularly in polyphenol compounds (Botta et al., 2005; Yazaki et al., 2009).

In plants, prenyltransferases are essential for the synthesis of secondary metabolites such as prenylated polyphenols (phenylpropanoids, flavonoids, coumarins and xanthenes) and terpenoids, which are molecules involved in plant defense mechanism and also help against abiotic environmental stresses (Yazaki et al., 2002, 2009). Many plants used worldwide as medicinal plants contain different prenylated polyphenols that possess extensive biological activities, such as anti-tumor, anti-bacterial, anti-oxidant and prevention of osteoporosis (Shin et al., 2008; Yazaki et al., 2009).

Prenyltransferases can be divided in three different groups: 1) isoprenyl pyrophosphate synthases (IPPS); 2) protein prenyltransferases and 3) aromatic prenyltransferases (Brandt et al., 2009; Liang et al., 2002). Isoprenyl pyrophosphate synthases are soluble enzymes responsible for generating linear prenyl pyrophosphates with defined chain lengths by

elongating isoprenyl pyrophosphate (IPP). These proteins can be classified in cys-type and trans-type depending on the stereochemistry of the end product (Brandt et al., 2009; Liang et al., 2002). The amino acid sequence of IPPS showed two conserved aspartate-rich motifs (DDXXD) that are involved in substrate binding by chelating the diphosphate moiety with three magnesium ions (Brandt et al., 2009; Heide, 2009; Liang et al., 2002).

Protein prenyltransferases catalyze the transfer of isoprenyl pyrophosphate to a protein or peptide (Liang et al., 2002). These enzymes play crucial roles in post translation modifications of eukaryotic proteins and have been widely described as important drug targets (Casey and Seabra, 1996; Hast et al., 2011). Protein prenyltransferases can be divided in three members: farnesyltransferases (FTase), geranylgeranyltransferase type I (GGTase I) and Rab geranylgeranyltransferase or GGTase type II (Casey and Seabra, 1996). FTase and GGTase I are designated as CaaX prenyltransferases due to their ability to attach a farnesyl or geranylgeranyl group on proteins containing an invariant cysteine residue followed by mostly two aliphatic amino acids (CaaX) at the C-terminus. On the other hand, GGTases II are able to attach two geranylgeranyl groups to two C-terminal cysteine residues in motifs that terminate in Cys-Cys or Cys-X-Cys (where X is alanine, serine or glycine); GGTases II enzymes are unable to recognize the CaaX-motif (Casey and Seabra, 1996; Seabra et al., 1992). All three members of protein prenyltransferases depend on zinc, which coordinates the cysteine (anion) of the target enzyme (Brandt et al., 2009). Different from the isoprenyl pyrophosphate synthases, protein prenyltransferases lack the DDXXD conserved motifs (Heide, 2009).

1.4.1. Aromatic prenyltransferases

Aromatic prenyltransferases (PTases) are enzymes that catalyze the transfer of prenyl moieties to aromatic acceptor molecules, forming C-C bonds between C-1 or C-3 of the isoprenoid substance and one of the aromatic carbons of the acceptor substrate. The reaction catalyzed by aromatic PTases represents an electrophilic alkylation or a Friedel-Crafts alkylation of the aromatic ring (Heide, 2009; Saleh et al., 2009). In addition, the enzymatic reaction is a crucial coupling reaction of products of two important metabolic pathways: aromatic compounds, derived from the shikimate and acetate/malonate pathway, with isoprenoid diphosphate, derived from the mevalonate or the methylerythritol phosphate pathways (Haagen et al., 2007; Yazaki et al., 2009). The reactions catalyzed by aromatic PTases have been widely investigated not only because they give a huge diversity of secondary metabolites in plants, fungi and bacteria, but also because of the difficulties to achieve chemical synthesis of prenylated aromatic compounds with good yield and the appropriate regio and stereo specificity that is essential for biological activity (Botta et al., 2005; Haagen et al., 2007; Saleh et al., 2009).

Aromatic PTases can be divided in three different types: the ABBA family of aromatic prenyltransferases; the aromatic PTases of plant secondary metabolism, and the aromatic PTases of lipoquinone biosynthesis (Heide, 2009).

The proteins belonging to the ABBA family of PTases are soluble enzymes. The term ABBA prenyltransferases was designated after the crystal structure of NphB, which showed an arrangement of α/β barrel fold with antiparallel strands forming the α - β - β - α fold architecture (Saleh et al., 2009; Tello et al., 2008). None of these enzymes contain the conserved aspartate-rich motifs described to be essential for several prenyltransferases, and they do not require divalent cations for enzymatic activity, except NphB, which showed to be a Mg^{2+} -dependent enzyme (Bonitz et al., 2011; Heide, 2009; Saleh et al., 2009).

Some of these ABBA PTases are promiscuous enzymes and can recognize different substrates. For instance, NphB shows specificity towards 1,6-dihydroxynaphthalene, naringenin, 4-hydroxyphenylpyruvate and resveratrol. SCO7190 recognizes 1,6-dihydroxynaphthalene, 2,7-dihydroxynaphthalene, naringenin and isosakuranetin as aromatic substrates (Sugiyama et al., 2011). This promiscuity for different aromatic substrates is explained by the unusual large central cavity, which allows the accommodation of different aromatic compounds (Heide, 2009; Kumano et al., 2008). Due to the broad range of aromatic substrates, this type of aromatic prenyltransferase has become an important tool for the synthesis of bioactive compounds (Koehl, 2005).

The second type of enzymes, the aromatic PTases of plants secondary metabolism, are membrane-bound proteins that are classified in two groups: 1) homogentisate (HG) prenyltransferases, involved in the biosynthesis of vitamin E and 2) *p*-hydroxybenzoate (PHB) prenyltransferases involved in the biosynthesis of naphthoquinone. The HG prenyltransferases are localized in plastids and according to prediction programs they contain nine transmembrane helices (Sasaki et al., 2008). Protein sequence analysis showed the presence of the NQXXDXXXD-motif, important for prenyl diphosphate binding, and naringenin 8-dimethylallyl transferase has been showing to require Mg^{2+} ions as co-factor (Heide, 2009; Sasaki et al., 2008). On the other hand, the PHB prenyltransferases are commonly localized in the inner membrane of mitochondria, except the LePGT1 that is located in endoplasmic reticulum (Yazaki et al., 2009). The *Lithospermum erythrorhizon* *p*-hydroxybenzoate geranyltransferase (LePGT1) is one of the best-studied prenyltransferases from plants (Ohara et al., 2009, 2013). The reaction catalyzed by LePGT1 is identical to the reaction catalyzed by UbiA during the ubiquinone biosynthesis (Figure 1.2) and recent studies have demonstrated that the two conserved Asp-rich motifs NDXXDXXXD are essential for catalytic activity through coordination with Mg^{2+} ions (Ohara et al., 2009).

The final group of aromatic prenyltransferases proteins involves the enzymes involved in the biosynthesis of lipoquinones such as ubiquinone, menaquinone and plastoquinone. These

aromatic PTases are also membrane-bound proteins and catalyze the transfer of all-*trans* prenyl moieties to the aromatic acceptor (Figure 1.6). All prenyltransferases involved in lipoquinone biosynthesis contain two Asp-rich motifs DXXDXXXD for binding of prenyl diphosphate via Mg^{2+} , which is essential for enzymatic function (Heide, 2009). The best-studied examples are the UbiA and MenA enzymes, involved in the biosynthesis of ubiquinone and menaquinone, respectively, and topic of this thesis.

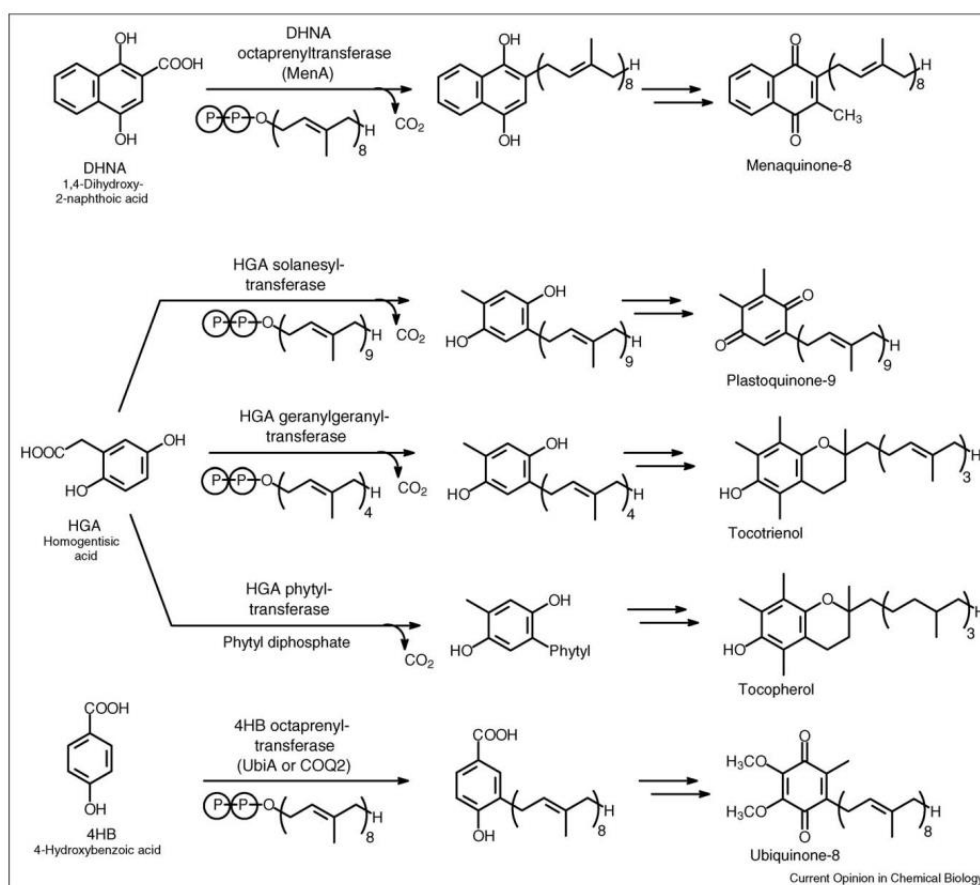


Figure 1.6. Aromatic prenyltransferases in lipoquinone biosynthesis. Prenyl transfer reactions catalyzed by aromatic prenyltransferases during lipoquinone biosynthesis (Heide, 2009).

1.4.2. 4-hydroxybenzoate octaprenyltransferase (UbiA)

The membrane-bound 4-hydroxybenzoate oligoprenyltransferase enzyme from *E. coli* (EcUbiA) consists of 290 amino acids with a molecular mass of 32.54 kDa and is encoded by the *ubiA* gene. In *T. thermophilus*, the UbiA homolog (TtUbiA) contains 285 amino acids with a molecular mass of 31.28 kDa and shares a sequence identity of 28% with EcUbiA. Melzer & Heide (1994) demonstrated that overexpressed UbiA present in isolated membrane fractions of *E. coli* was able to prenylate the 4-hydroxybenzoic acid (PHB) in the presence of geranyl pyrophosphate (GPP) and magnesium. The first evidence that UbiA is a functional homolog of the human 4-hydroxybenzoate polyprenyltransferase (*Coq2*) was demonstrated using

mutant strains. Suzuki and co-workers (Suzuki et al., 1994) reported that $\Delta ubiA$ cells unable to synthesize ubiquinone can recover their biosynthesis after complementation with the *coq2* gene from *S. cerevisiae*.

The prenyl transfer catalyzed by UbiA is an electrophilic substitution reaction. The reaction probably includes the formation of a carbocation and two similar mechanisms have been proposed by (Bräuer et al., 2004) and Meganathan (2001a). The prenylation of PHB has been shown to be regiospecific; however, studies demonstrated that UbiA recognize IPPs of different chain lengths such as GPP, farnesyl pyrophosphate (FPP) and solanesyl pyrophosphate (SPP) and also various aromatic molecules like 4-amino benzoic acid, 2,4 dihydroxy benzoic acid and 3,4-dihydroxy benzoic acid (Melzer and Heide, 1994; Wessjohann and Sontag, 1996).

UbiA enzymes are predicted to contain nine transmembrane helices (Yazaki et al., 2009) and until recently structural characterization has been a challenge, since the enzymes are membrane-bound and loss of activity is observed after solubilization with detergents (Melzer and Heide, 1994).

1.4.3. 1,4-dihydroxy-2-naphthoic acid octaprenyltransferase (MenA)

The 1,4-dihydroxy-2-naphthoic acid octaprenyltransferase from *E. coli* (EcMenA) consists of 308 amino acids with a molecular mass of 33.6 kDa and is encoded by the *menA* gene. In bacteria, MenA is a membrane-bound protein and catalyze the prenylation of 1,4-dihydroxy-2-naphthoic acid (DHNA-2) in a Mg^{2+} -dependent reaction during the biosynthesis of menaquinone (MK). The first evidence that MenA is involved in the prenylation step was demonstrated by Shineberg and Young (1976) using *E. coli menA*⁻ mutants, which showed accumulation of DHNA-2. Later Suvarna and co-workers (1998) reported that MK biosynthesis in *E. coli menA*⁻ mutants could be restored after complementation of the *menA* gene. Due to the fact that in *E. coli* the prenylation reactions play a key role during the menaquinone and ubiquinone biosynthesis, it was expected that the reactions catalyzed by MenA and UbiA are similar (Shineberg and Young, 1976). Indeed, both reactions are catalyzed by membrane-bound proteins that require magnesium for catalytic activity. Moreover, because the menaquinone and ubiquinone molecules contain 8 isoprenoid units in *E. coli* it is believed that both prenyltransferases utilize a common pool of octaprenyl pyrophosphate as natural polyisoprenoid substrate (Shineberg and Young, 1976; Suvarna et al., 1998). Despite the similarities, MenA and UbiA share 21% identity and genetic evidence indicates that the two prenyltransferases are distinct. The *ubiA* and *menA* genes are separated on the *E. coli* chromosome at 78 and 81 minutes, respectively, and mutation of one gene does not influence the expression of the other gene (Young, 1975; Young et al., 1972). Although both enzymes catalyze the prenylation of an isoprenoid moiety to an

aromatic compound, the MenA reaction involves an additional decarboxylation step (Bentley and Meganathan, 1982; Shineberg and Young, 1976). Initially, it was believed that two enzymes were involved in this step, since the conversion of DHNA-2 to demethylmenaquinone requires a decarboxylation and a prenylation. However, trace elements experiments demonstrated that 1,4-naphthoquinol is not an intermediate of the reaction and that *menA*⁻ mutants of *E. coli* accumulate DHNA-2 and not 1,4-naphthoquinol (Shineberg and Young, 1976; Young, 1975), suggesting that just MenA is involved in this step.

1.5. Aims of the work

Aromatic prenyltransferases catalyze the transfer of prenyl moieties to aromatic acceptor molecules through C–C bond formation. Prenylation of aromatic compounds has been widely investigated since this reaction leads to a variety of molecules with diverse biological activities. In addition, prenyltransferases have been used during organic chemical synthesis to improve the regio- and stereospecificity of prenylated aromatic compounds. In this context, the enzymes 4-hydroxybenzoate octaprenyltransferase (UbiA) and 1,4-dihydroxy-2-naphthoate octaprenyltransferase (MenA), both involved in the biosynthesis of ubiquinone and menaquinone, respectively, have been highlighted since they are able to recognize different isoprenoids moieties and different aromatic molecules as substrates (Melzer and Heide, 1994; Saito and Ogura, 1981; Wessjohann and Sontag, 1996).

The first chapter describes the biochemical characterization of MenA from *E. coli* (EcMenA). Although few studies have demonstrated that membrane fraction of *E. coli* containing MenA is able to prenylate DHNA-2 (Huang et al., 2014; Shineberg and Young, 1976), no data have been published to date reporting the enzymatic activity of MenA after detergent solubilization or purification. To evaluate the activity of MenA the *EcmenA* gene should be cloned into different vectors and EcMenA protein expressed in *E. coli* cells. In addition, a protocol for EcMenA purification, including membrane fraction preparation and detergent solubilization should be established. For *in vitro* enzymatic activity, the protein should be evaluated with distinct prenyl donors and acceptors.

Structural studies of membrane proteins are challenging in structural biology since these proteins exhibit low enzyme stability after removal from the membrane, leading to aggregation and loss of activity. In order to avoid the problems observed during the work with membrane proteins, the UbiA homolog from *Thermus thermophilus* (TtUbiA) was chosen, since the proteins from this organism are known to be thermostable and more resistance towards chemical agents (Cava et al., 2009). Thus, the second chapter of this work involves the cloning of the *TtubiA* gene in different vectors and the protein expression in *E. coli* cells. In addition, a purification protocol for this membrane protein should be established. *In vitro* enzymatic assays will be performed to investigate substrate specificity, and crystallization trials should be carried out.

The recent discovery of the futasoline pathway in some pathogenic organisms and its absence in *E. coli* and humans makes this pathway a target for novel antibacterial drug discovery (Dairi et al., 2011). As structural information of enzymes involved in this route are limited to date, the last chapter of this thesis describes the purification, crystallization and

structural characterization of the first futasine hydrolase (MqnB) homolog from *T. thermophilus* in the presence and absence of ligand.

2. Materials and Methods

2.1. Materials

2.1.1. Chemicals

1,4-dihydroxy-2-naphtoic acid	Sigma-Aldrich GmbH
1,4-dihydroxynaphthalene	Sigma-Aldrich GmbH
4-hydroxybenzoic acid	Sigma-Aldrich GmbH
6-Cyclohexyl-1-Hexyl- β -D-Maltoside (Cymal-6)	GLYCON Biochemical GmbH
Acetic acid	Carl Roth GmbH & Co. KG
Acetonitrile (ACN)	Carl Roth GmbH & Co. KG
Acrylamid (30%)	Carl Roth GmbH & Co. KG
ADA [N-(2-Acetamido) iminodiacetic acid, N-(Carbamoylmethyl) iminodiacetic acid]	Carl Roth GmbH & Co. KG
Agar-Agar	Carl Roth GmbH & Co. KG
Agarose	Carl Roth GmbH & Co. KG
Ammonium sulfate	AppliChem GmbH
Ampicillin	Carl Roth GmbH & Co. KG
Ammonium persulfate (APS)	Carl Roth GmbH & Co. KG
Bovine serum albumin (BSA)	Carl Roth GmbH & Co. KG
Bromophenol blue	Carl Roth GmbH & Co. KG
Calcium chloride	Carl Roth GmbH & Co. KG
Casamino acids	Becton Dickinson and Co.
CASO-Bouillon	Carl Roth GmbH & Co. KG
CHAPS	GLYCON Biochemical GmbH
Chloramphenicol	Carl Roth GmbH & Co. KG
Chloroform	Carl Roth GmbH & Co. KG
Coomassie-Brilliant blue G250	Carl Roth GmbH & Co. KG
Coumarin-3-Carboxylic acid	Sigma-Aldrich GmbH
n-Dodecyl- β -D-maltopyranoside (DDM)	GLYCON Biochemical GmbH
Dimethyl sulfoxide (DMSO)	Sigma-Aldrich GmbH
Disodium citrate	Carl Roth GmbH & Co. KG
Dithiothreitol (DTT)	AppliChem GmbH
n-Decyl- β -D-maltopyranoside (DM)	GLYCON Biochemical GmbH
Ethanol	Carl Roth GmbH & Co. KG
Ethidium bromide	Carl Roth GmbH & Co. KG

Ethylacetate	Sigma-Aldrich GmbH
Ethylenediamine tetraacetic acid (EDTA)	Merck KgaA
Ethylene glycol	Carl Roth GmbH & Co. KG
Farnesyl pyrophosphate (FPP)	Sigma-Aldrich GmbH
Formic acid	Carl Roth GmbH & Co. KG
Formycin B	Berry & Associates, Inc.
Geranyl pyrophosphate (GPP)	Sigma-Aldrich GmbH
Geranylgeranyl pyrophosphate (GGPP)	Sigma-Aldrich GmbH
Glucose	AppliChem GmbH
Glycerin	Sigma-Aldrich GmbH
Glycerol	Sigma-Aldrich GmbH
Glycine	AppliChem GmbH
Guanidinium hydrochloride	Carl Roth GmbH & Co. KG
Hexane	Carl Roth GmbH & Co KG
Hydrochloric acid	Carl Roth GmbH & Co. KG
Hydrogen peroxide	Merck KgaA
Hypoxanthine	Sigma-Aldrich GmbH
Imidazole	Merck KgaA
Inosine	Sigma-Aldrich GmbH
Isopropyl- β -D-thiogalactopyranoside (IPTG)	AppliChem GmbH
Kanamycin	Carl Roth GmbH & Co. KG
Lactose	AppliChem GmbH
LDAO	Affymetrix, Inc.
Luminol	Sigma-Aldrich GmbH
Magnesium Chloride	Merck KgaA
Magnesium Sulphate	Carl Roth GmbH & Co. KG
Maleic acid	Carl Roth GmbH & Co. KG
Menadione	Sigma-Aldrich GmbH
Mercaptoethanol	Merck KgaA
Methanol	Carl Roth GmbH & Co. KG
Milk powder	AppliChem GmbH
<i>n</i> -octyl- β -glucoside	GLYCON Biochemical GmbH
PEG (Polyethylene glycol) 1000	Sigma-Aldrich GmbH
PEG (Polyethylene glycol) 8000	Sigma-Aldrich GmbH
Phenylmethanesulfonyl fluoride (PMSF)	Sigma-Aldrich GmbH

<i>o</i> - Phosphoric acid (85%)	Carl Roth GmbH & Co. KG
Potassium chloride	AppliChem GmbH
Rotiphorese Gel 30	Carl Roth GmbH & Co. KG
Sodium chloride	Carl Roth GmbH & Co. KG
Sodium dodecyl sulfate (SDS)	Carl Roth GmbH & Co. KG
Sodium fumarate	Sigma-Aldrich GmbH
Sodium hydroxide	Carl Roth GmbH & Co. KG
Sucrose	Carl Roth GmbH & Co. KG
Tetramethylethylenediamine (TEMED)	Carl Roth GmbH & Co. KG
Thiamine	Sigma-Aldrich GmbH
Trifluoroacetic acid (TFA)	Carl Roth GmbH & Co. KG
Tris(hydroxymethyl)-aminomethane (TRIS)	Carl Roth GmbH & Co. KG
Trypton	AppliChem GmbH
Tween 20	Carl Roth GmbH & Co. KG
Yeast extract	AppliChem GmbH

2.1.2. Enzymes and Antibodies

Benzonase	Sigma-Aldrich GmbH
Calf Intestinal Alkaline Phosphatase (CIP)	New England Biolabs
<i>DpnI</i>	New England Biolabs
<i>EcoRI</i>	New England Biolabs
<i>NcoI</i>	New England Biolabs
<i>NdeI</i>	New England Biolabs
Phusion-DNA-Polymerase	New England Biolabs
T4-DNA-Ligase	New England Biolabs
<i>XhoI</i>	New England Biolabs
Mouse penta anti-his antibody	Qiagen
Goat anti-mouse IgG antibody, HPR conjugated	Millipore

2.1.3. Markers

BenchMark™ Fluorescent Protein Marker.	Invitrogen GmbH
BenchMark™ His-tagged Protein Marker.	Invitrogen GmbH
Broad Range Protein Ladder	Bio-Rad-Laboratories, Inc.
Spectra Multicolor Broad Range Protein Ladder	Thermo Fisher Scientific
Quick Load 1kb DNA Ladder	New England Biolabs

2.1.4. Kits

GeneJET™ Plasmid Miniprep Kit	Thermo Fisher Scientific
Illustra™ MicroSpin G25 Columns	GE Healthcare
PCR Purification kit	Qiagen
Phusion® High-Fidelity PCR Master Mix	New England Biolabs
QIAmp DNA Mini kit	Qiagen
Zymoclean™ Gel DNA Recovery kit	Zymo Research Corporation
Crystallization kits	Hamptom Research
	Molecular Dimensions
	Sigma Aldrich
	Jena Bioscience

2.1.5. Bacteria Strains and Plasmids

<i>Strains</i>	<i>Genotype</i>
<u>Plasmid amplification</u>	
<i>E. coli</i> XL1 (Stratagene)	<i>recA1, endA1, gyrA96, thi-1, hsdR17, supE44, relA1, [F' proAB lacI_q ZΔM15 Tn10 Tet^R]]</i>
<i>E. coli</i> TOP10 (Invitrogen)	<i>F, mcrA, Δ(mrr-hsdRMS-mcrBBC), Φ80lacZ ΔM15, ΔlacX74, recA1, deoR, araD139, Δ(ara-leu)7697, galU, galK, rpsL, (Str^R), endA1, nupG</i>
<i>E. coli</i> ET12567 (Methylation-deficient)	<i>dam-13::Tn9, dcm-6, hsdM, hsdS</i>
<u>Expression</u>	
BL21 (DE3) (Novagen)	<i>B F ompT hsdS_B (r_B⁻ m_B⁻) gal dcm (DE3)</i>
Rosetta (DE3) (Novagen)	<i>B F ompT hsdS_B (r_B⁻ m_B⁻) gal dcm pRARE (Cam^R) (DE3)</i>
NiCo21 (DE3) (New England Biolabs)	<i>can::CBD fhuA2 [lon] ompT gal (λ DE3) [dcm] arnA::CBD slyD::CBD glmS6Ala ΔhsdS λ DE3 = λ sBamHlo ΔEcoRI-B int::(lacI::PlacUV5::T7 gene1) i21 Δnin5</i>
C43 (DE3) (Lucigen)	<i>F⁻ ompT hsdSB (rB⁻ mB⁻) gal dcm (DE3)</i>
JW3901-1 Keio Collection (CGSC)	<i>F⁻, Δ(araD-araB)567, ΔlacZ4787(::rrnB-3),λ⁻, rph-1, Δ(rhaD-rhaB)568, ΔmenA789::kan, hsdR514.</i>
Rosetta-gami(DE3) pLysS ¹ (Novagen)	<i>Δ(ara-leu)7697 ΔlacX74 ΔphoA PvuII phoR araD139 ahpC galE galK rpsL (DE3) F'[lac⁺ lacI^R pro] gor522::Tn10 trxB pLysSRARE2 (Cam^R)</i>
<i>Streptomyces lividans</i> 66 TK24(Hopwood, 1985)	<i>SLP2⁻ SLP3⁻</i>

<i>Plasmid</i>	<i>Description</i>
pET15b-TEV (pET15b modified)	Expression vector, N-terminal His-tag, TEV cleavage site. Ampicillin resistance.
pET21a	Expression vector, C-terminal His-tag. Ampicillin resistance.
pNGFP-BC	Expression vector, N-terminal GFP and His-tag, thrombin cleavage site. Ampicillin resistance.
pCGFP-BC	Expression vector, C-terminal GFP and His-tag, thrombin cleavage site. Ampicillin resistance.
PUWL201PW	C-terminal 6x His-tag Bla ^r tsr P _{ermE} ColE1-ori pIJ101-ori (Doumith et al., 2000)

2.1.6. Oligonucleotides

The oligonucleotides were synthesized by Metabion International AG. The lyophilized oligonucleotides were resuspended in distilled water in a concentration of 100 pM and diluted 1:10 before use.

<i>Primers</i>	<i>Sequence (5' – 3')</i>	<i>Used for:</i>
TtUbiA_NdeI_fw	GGAATTCATATGATGAGGCGCCTCAGG	Cloning pET15b_TEV
TtUbiA_XhoI_rev	ATTCGACTCGAGTCAAGCCCCGCGGGCGAGG	
TtUbiA_NdeI_fw	GGAATTCATATGATGAGGCGCCTCAGG	Cloning pET21a
pCGFP_XhoI_rev	CCGCTCGAGAGCCCCGCGGGCGAGG	
pNGFP_EcoRI_fw	ATTCGGACTCCGAATTCATGAGGCGCCTCAG	Cloning pNGFP
pNGFP_XhoI_rev	CTGAGGCGCCTCATGAATTCGGAGTCCGAATT	
pCGFP_EcoRI_fw	CCGGAATTCATGAGGCGCCTCAGG	Cloning pCGFP
pCGFP_XhoI_rev	CCGCTCGAGAGCCCCGCGGGCGAGG	
TtUbiAR59D_fw	GCCATGGCCCTGAACGACCTCATTGACTGGGG	Mutation in TtUbiA
TtUbiAR59D_rev	CGCCAGTCAATGAGGTCGTTTCAAGGCCATGGC	
EcMenA_NdeI_fw	GGAATTCATATGATGACTGAACAAC	Cloning pET15b_TEV
EcMenA_XhoI_rev	CCGCTCGAGCGGTTATGCTGCCCACTGG	
EcMenAD65R_fw	CTAACCTCGCCAATCGTTACGGCGATGCGG	Mutation in EcMenA
EcMenAD65R_rev	CCGCATCGCCGTAACGATTGGCGAGGTTAG	

TtMqnB_KpnI_fw	ATTTAGGTACCATGTGGCTCCTCCTTTCCC	Cloning pET15b-TEV
TtMqnB_NdeI_rev	ATATTGTACATATGTCAGCCGGGGGCCTACG	
SIUbiAForwNdeI	GGAATTCCATATGATGACGTCCGCTTCCGCCG	Cloning PUWL201PW
SIUbiARevBamHI	CGCGGATCCTCAGACCGTGAGGCCCTTACGAGC	
SIUbiAR73D_fw	GCGATGGCGGTCAACGACATCATCGACCGCGAG	Mutation in SIUbiA
SIUbiAR73D_rev	CTCGCGGTTCGATGATGTCGTTGACCGCCATCGC	
hslU_forw	TGCACCGTTTCCACCAAACACG	PCR verification Transduction
rraA_rev	CCTGACGCACCGCGCCGTAAG	
T7_forw	TAATACGACTCACTATAGGG	PCR verification
T7_rev	CTAGTT ATTGCTCAGCGG	

2.2. Molecular Biology Methods

2.2.1. DNA Extraction

The DNA from *Thermus thermophilus* HB27 (DSMZ) used for amplification of *TtubiA* and *TtmqnB* genes was extracted according to QIAmp DNA Mini kit. The pellet of the bacteria was resuspended in ATL buffer (provided with the kit) and the extraction was performed according to the protocol.

For the extraction of *Escherichia coli* DNA used to amplify the *EcmenA* gene, *E. coli* XL1 cells were incubated in 4 mL LB-medium (1% (w/v) Trypton 0.5% (w/v) yeast extract, 1% (w/v) NaCl) overnight at 37 °C. After centrifugation, the supernatant was discarded and the pellet resuspended in ATL buffer according to the kit's protocol. DNA concentration was determined by absorption at 260 nm.

2.2.2. Polymerase Chain Reaction (PCR)

Amplification of the genes of interest was performed by PCR using the Phusion® High-Fidelity PCR Master Mix. The reactions were performed in 50 µL. For PCR reactions using DNA from *Thermus thermophilus* as template, GC buffer and DMSO were used due to GC-rich genome.

2.5 μ L	Reverse primer (10 pmol)
2.5 μ L	Forward primer (10 pmol)
5.0 μ L	Template
1.0 μ L	dNTP mix (200 μ M)
1.5 μ L	DMSO [3% (v/v)]
0.5 μ L	Phusion [®] -DNA-Polymerase (1 U)
10.0 μ L	Polymerase buffer (10X)
X μ L	ddH ₂ O (add for 50 μ L final volume)

All reactions were performed in a Thermocycler (Mastercycler Gradient, Eppendorf) using the following program:

Initialization	98.0 °C	5 min	
Denaturation	98.0 °C	30 sec	} 30X
Annealing	T _m	30 sec	
Elongation	72.0 °C	30 sec	
Final elongation	72.0 °C	7 min	
	12.0 °C	∞	

The PCR products were purified using QIAquick[®] PCR Purification Kit for *E. coli* and Illustra[™] MicroSpin G25 Columns for *T. thermophilus*. To check the presence of DNA bands, PCR purified products were analyzed by agarose gel.

For amplification of the *SlubiA* gene from *Streptomyces lividans*, the spore colony was used as template. The amplification was performed using the conditions used for *T. thermophilus*.

2.2.3. Agarose gel

All amplified PCR products were checked by 1% (w/v) agarose gel. 50.0 mg of agarose was dissolved in 50 mL TAE buffer (40 mM Tris, 20 mM acetic acid, 1 mM EDTA pH 8.0) and 2 drops of ethidium bromide (0.5 mg/mL) were added. The DNA samples were mixed with agarose loading buffer [49.95% (v/v) glycerine, 0.05% bromphenol blue, 50% (v/v) TAE-buffer] and loaded into the gel. The separation was performed in an electrophoresis chamber (Easy Cast B1A – Owl Separation System) at a potential of 90 V for 45 minutes. DNA bands were observed under UV-light.

2.2.4. Site-directed mutagenesis

The variants (TtUbiAR59D; EcMenAD65R and SIUbiAR73D) were generated through site-directed mutagenesis according to the Quick-Change® Site-Directed Mutagenesis Kit protocol using the appropriate pET15b-TEV and pWUL201PW constructs as templates. For 50 μ L reaction, the following preparation was used:

1.3 μ L	Reverse primer (125 ng)
1.3 μ L	Forward primer (125 ng)
3.0 μ L	Template (35 ng)
1.0 μ L	dNTP mix (200 μ M)
5.0 μ L	HF buffer (5X)
38.4 μ L	ddH ₂ O
1.0 μ L	Phusion®-DNA-Polymerase (1 U)

The PCR cycles were performed according to the desired mutation. For single amino acid change 16 cycles are indicated.

Initialization	98.0 °C	30 sec	} 16X
Denaturation	98.0 °C	30 sec	
Annealing	55.0 °C	60 sec	
Elongation	72.0 °C	x* min	
Final elongation	12.0 °C	∞	

* 1 min/kb of plasmid length

After the PCR reaction, the parental and methylated DNA were digested by *DpnI* endonuclease for 1 hour at 37 °C followed by chemical transformation into *E. coli* XL1 cells. Mutations were validated by sequencing (GATC – Biotech).

2.2.5. Digestion

Before the ligation step, the PCR products and vectors were digested with the desired restriction enzymes. For 50 μ L setup reaction, 40.5 μ L insert or vector, 5 μ L specific buffer, 2 μ L enzyme 1, 2 μ L enzyme 2 and 0.5 μ L BSA (100 μ g/mL) were incubated at 37 °C for 3 hours. The enzymes were inactivated at 65 °C for 20 minutes. The total volume was mixed with 10 μ L agarose loading buffer and loaded into the agarose gel. The bands corresponding to digested vector and insert were cut and purified according to the protocol of Zymoclean Kit.

2.2.6. Ligation

In order to insert the PCR product into the vector, both digested products were incubated at a ratio of 1:3 and 1:6 (vector: insert) in the presence of ligase buffer and T4 DNA ligase (1 U) for 1h at room temperature. One third of the volume was transformed into XL1/TOP 10 (Stratagene/Invitrogen) cells and the rest of the reaction was incubated overnight at 8°C for a second transformation if necessary.

2.2.7. Plasmid preparation

To isolate plasmid-DNA from *E. coli*, the cells were grown overnight in 4 mL LB-Medium containing the selecting antibiotic and after centrifugation the pellet was resuspended in a “Resuspension solution” according to GeneJET™ Plasmid Miniprep Kit. The extraction was performed according to the protocol. The DNA product was resuspended in 50 µL water. DNA concentration was determined by absorption at 260 nm.

2.3. Microbiology Methods

2.3.1. Preparation of chemically competent *E. coli* cells

For the preparation of chemically competent *E. coli* cells, the desired strain was incubated overnight at 37 °C in 4 mL LB medium containing the selecting antibiotic. 1 mL of this pre-culture was added into 50 mL LB medium and incubated at 37 °C until OD₆₀₀ reaches 0.3-0.6. The cells were incubated for 10 min on ice and after centrifugation (8.000 g, 15 min, 4 °C) the supernatant was discarded, the pellet resuspended in 20 mL of 0.1 M CaCl₂ and incubated for 5 min on ice. After a second centrifugation step (8.000 g, 15 min, 4 °C), the supernatant was discarded, the pellet resuspended in 1 mL of CaCl₂ (0.1 M) and incubated for 2 hours on ice. Afterwards, 1 mL of glycerine [50% (v/v)] was added to the solution and the cells stored at -80 °C in aliquots of 100 µL.

2.3.2. Heat shock transformation

The competent *E. coli* cells were thawed on ice and the plasmid or ligation product was added and incubated for 20 minutes on ice. The heat shock was performed at 42 °C for 70 seconds followed by cooling on ice for 2 minutes. 500 µL of SOC-medium [2 % (w/v) Tryptone, 0.5% (w/v) yeast extract, 10 mM NaCl, 2.5 mM KCl, 10 mM MgCl₂, 10 mM MgSO₄, 20 mM glucose] was added and the cells incubated for 1 h at 37 °C under gentle agitation. 100 µL of the cell mixture were plated on LB-agar plate containing the selection antibiotic and incubate overnight at 37 °C.

2.3.3. Gene expression of recombinant proteins in *E. coli*

In order to identify the best conditions to express the proteins of interest (EcMenA, TtUbiA and TtMqnB) several parameters such as temperature, IPTG concentration and cells strains were tested. Desired constructs were transformed in different strains and incubated overnight in 4 mL LB medium at 37 °C with the appropriate antibiotic. The pre-culture was centrifuged (10.000 g for 2 min) and the pellet was resuspended in 1 mL fresh LB medium. 100 µL were added in a 250 mL Erlenmeyer containing 50 mL LB-medium and antibiotic. The flasks were incubated at 37 °C under agitation (130 rpm) until the OD₆₀₀ reached 0.6-0.8. Afterwards, the gene expression was started with addition of IPTG and the cells incubated overnight at 30 °C.

Large scale expression was performed using the best conditions obtained from the test expression. For 6 L expression, Tunair® shake flasks (Sigma-Aldrich) were used. 50 mL of pre-culture was prepared and after overnight incubation it was centrifuged for 15 min at 4.500 rpm (Hettich Universal 320R). The pellet was resuspended in 6 mL fresh LB-medium and 1 mL was added into each Tunair flask containing 1 L LB-medium. The flasks were incubated at 37°C under agitation (150 rpm) until the OD₆₀₀ reached 0.6-0.8. After IPTG addition, the temperature was decreased to 30 °C and the flasks incubated overnight. The cells were harvested at 4 °C in a JLA 8.1000 rotor (Beckman/Avanti J-20) for 25 min at 4.300 rpm and stored at -20 °C.

2.3.4. Preparation of *Streptomyces lividans* TK24 protoplasts

The preparation of protoplasts from *S. lividans* TK24 was performed according to Babcock and Kendrick (Babcock and Kendrick, 1988). 5.0 µL of one spore culture of *S. lividans* TK24 cells were incubated in 20 mL TBS/PEG8000 medium (section 8.1). In the presence of a metal spiral to suppress cell clusters, the medium was incubated under agitation for 36-48 hours at 30 °C. The medium (2 x 20 mL) was centrifuged at 4 °C for 15 min (3.000 g). Pellet was washed twice with 30 mL of 10.3% (w/v) sucrose solution followed by centrifugation (4 °C, 15 min 3.000 g). The pellet was resuspended in 8 mL buffer P (section 8.1) containing lysozyme (1.0 mg/mL) and incubated at 37 °C under gentle agitation until the protoplasts were visible under the microscopy (5-6 h). Afterwards, 8 mL of buffer P (without lysozyme) was added and the protoplast suspension was filtrated. The suspension was then centrifuged for 20 min at 4 °C (3.000g) and the pellet was resuspended in 1 mL buffer P. 15% (v/v) glycerine solution was added and the protoplasts was aliquoted (100 µL) and stored at -80 °C.

2.3.5. Transformation in *Streptomyces lividans* TK24 protoplasts

For the protoplast transformation it is appropriate to use non-methylated DNA. Thus, the construct PUWL201PW_SIUbiA was transformed in *E. coli* ET12567 and the cells were incubated in LB medium for 24 h at 37 °C under agitation. After plasmid preparation (section 2.2.7), 5 – 10 µL of non-methylated DNA (3 µg – 10 µg) was mixed with one aliquot of *S. lividans* protoplast solution and 200 µL of buffer T/PEG1000 (section 8.1) and 1 mL of buffer P was gently added. The solution was plated in a SPMR-agar plate (section 8.1) and incubated at 30 °C. After 24 h incubation, 2 mL of antibiotic (20 µL thiostreptone solution [250 µg/mL] in DMSO and 1980 µL H₂O) was overlaid on the plate and incubated for further 2-3 days at 30 °C.

2.3.6. Gene expression of recombinant proteins in *Streptomyces lividans* TK24

The pre-culture was prepared by picking one spore-forming colony of *Streptomyces* from the SPMR-agar plate and incubating it in 4 tubes containing 20 mL of 3% (w/v) CASO-Bouillon media, thiostrepton (25 µg/mL) and a metal spiral. The pre-culture was incubated for 72 h at 30 °C under agitation (200 rpm).

For the large scale expression, 4 x 5 L Erlenmeyer flasks with four bottom baffles containing each 1 L of 3% (w/v) CASO-Bouillon media were used. In each Erlenmeyer 20 mL of pre-culture was added followed by 1 mL of thiostreptone (250 µg/mL), which works as antibiotic and inducer of expression. After incubation for 72 h at 30 °C under agitation (110 rpm) the cells were harvested at 4 °C in a JLA 8.1000 rotor (Beckman/Avanti J-20) for 25 min at 4.300 rpm and stored at -20°C.

2.3.7. Cell disruption

Frozen cell pellets of *E. coli* and *S. lividans* TK24 were thawed and resuspended in Tris buffer (50 mM Tris/HCl pH 8.5; 5mM EDTA). The cells were disrupted through high pressure with the use of FRENCHTM-PRESS (Gaulin APV Homogeniser GmbH) with the maximal pressure of 1200 bar. To eliminate the viscous DNA benzonase (1 U/mL) and MgCl₂ (3 mM) were added.

2.3.8. Generation of *menA* knockout cells by homologous recombination in bacteriophage P1

2.3.8.1. Preparation of P1 liquid lysate

P1 transduction was used to transfer the desired gene from one *E. coli* strain to another. A phage P1 liquid lysate was prepared according to (Thomason et al., 2007) with some

modifications. 4 mL of *E. coli* donor strain (JW3901-1) were incubated overnight at 37 °C with the appropriated antibiotic. 20 µL of this pre-culture was added into 2 mL of LB containing 5 mM CaCl₂ without antibiotic and incubated for 1 hour at 37 °C under agitation. Varying amounts of P1 (10 – 40 µL) were added into the solution and incubated under gentle agitation at 37 °C for 6 – 8 hours or until the lysate became clear. To kill the remaining *E. coli* cells, 100 µL of chloroform were added and after vortexing (10 – 30 seconds) the lysate was incubated at room temperature for 10 min followed by a centrifugation step (4.000 rpm for 15 min). The supernatant containing the new P1-lysate was separated and incubated at 4 °C.

2.3.8.2. P1 Transduction

5 mL of *E. coli* recipient strain [Rosetta-gami (DE3) pLysS] were incubated overnight at 37 °C without antibiotic. 5 mL of a solution containing 10 mM MgSO₄, 5 mM CaCl₂ were added to this pre-culture followed by incubation at 37 °C for 30 min under gentle agitation. Afterwards, the solution was aliquoted (1.5 mL) and centrifuged for 10 minutes at 8.000 rpm. The supernatant was discarded and the pellet resuspended in 100 µL of LB-medium with 0.4% (w/v) glucose. Different amounts of P1 lysate (50 – 100 µL) and 10 µL of CaCl₂ (0.1 M) were added. The cells were incubated for 30 minutes at 37 °C without shaking. As a control, cells and P1 lysate were incubated alone. After 30 minutes, 500 µL of LB-citrate-medium (0.5 M sodium citrate) was added and the cells incubated for 1 hour at 37 °C under gentle agitation. Finally, the cells were centrifuged (5 min, 13.000 rpm) and the pellet resuspended in 100 µL LB-citrate-medium and plated on LB-citrate-agar plate (20 mM sodium citrate) containing the appropriate antibiotic and incubated overnight at 37 °C. A single colony was picked from the plate and streaked on a new LB-citrate-plate. This procedure was performed twice in order to remove residual P1 phage. The mutation in the genome was confirmed by PCR and sequencing.

2.3.9. Complementation assay

The complementation assay of the *menA* gene with different constructs was performed according to (Suvarna et al., 1998). For anaerobic growth, M9-minimal medium (Sambrook et al., 1989) with 0.8% (v/v) glycerol as carbon source and fumarate as electron acceptor was used (Table 2.1). The medium was supplemented with 0.2% (w/v) casamino acids solution. The constructs were transformed in Rosetta-gami (DE3) pLysS and plated in M9-minimal medium agar plate containing 100 µg/mL of ampicillin, 30 µg/mL kanamycin and 30 µg/mL chloramphenicol and incubated overnight at aerobic conditions. Glycerine stocks of M9-minimal medium were prepared for each construct.

Complementation of the *menA* gene was performed in a Bellco glass hungate tubes with 14 mL M9-minimal medium, 14 µg/mL of ampicillin, 8.4 µg/mL kanamycin, 8.4 µg/mL chloramphenicol and 0.5 mM IPTG. The cultures were inoculated with 15 µL of glycerine stock and incubated at 37 °C without agitation. The OD₆₀₀ was measured after 72 h for each culture.

Table 2.1: Composition of M9-minimal medium (100 ml)

<i>Stock solution</i>	<i>Volume</i>
5 x M9 buffer *	20 mL
98% (v/v) glycerol	800 µL
1 M MgSO ₄	200 µL
1 M CaCl ₂	10 µL
0.1% (w/v) trace elements *	100 µL
0.01% (w/v) Thiamine	10 µL
10% (w/v) casamino acids	2 mL
1M Sodium Fumarate	2.5 mL

* Appendix (8.2)

2.4. Biochemical Methods

2.4.1. Polyacrylamide gel electrophoresis (SDS – PAGE)

The separation of proteins in a sample was performed through gel electrophoresis according to Laemmli (Laemmli, 1970). Acrylamide gels consisting of a stacking gel (6.5% acrylamide) and a resolving gel (12% acrylamide) were placed in an electrophoresis chamber (Amersham Bioscience) connected to a power source with a current of 25-30 mA per gel and a constant voltage of 300 V. The protein samples were mixed with SDS-loading buffer (175 mM Tris/HCl pH 6.8; 6% (w/v) glycerol; 5% (w/v) SDS; 20% (v/v) mercaptoethanol; 0.125% bromophenol blue). Membrane protein samples were incubated for 10-15 min at room temperature, whereas samples of soluble proteins were incubated for 5 min at 95 °C and loaded into the gel in the presence of running buffer (25 mM Tris; 200 mM glycine; 0.05 mM SDS). Gels were stained with Coomassie blue (Wong et al., 2000).

For analyses of proteins with GFP fusion, the GFP fluorescence was observed with a Fujifilm LAS-4000 Imager using a wavelength of 488 nm for excitation and 512 nm for emission.

Stacking gel: 0.5 M Tris/HCl pH 6.8, 0.61% (w/v) SDS

Resolving gel: 1.5M Tris/HCl pH 8.8, 0.31% (w/v) SDS

Running buffer: 25 mM Tris, 200 mM glycine, 0.3 mM SDS

2.4.2. Immunoblotting

Due to difficulties of identifying membrane proteins in SDS-PAGE gel, immunoblotting were performed to confirm the presence of the His-tagged proteins. The protein was transferred from the SDS-PAGE gel onto a PVDF membrane (BioRad) through a semi-dry procedure (TE 77PWR GE) and transfer buffer (25 mM Tris, 192 mM glycine, 20% (v/v) methanol) for 1 h with 1 mA/cm². Afterwards, the membrane was blocked for 1 h in blocking solution [3% (w/v) BSA in 12 mL TBS (0.01 M Tris/HCl pH 7.6, 0.15 M NaCl)] followed by incubation with the Mouse anti-His primary antibody in blocking solution (1:1.500) for 1 h at room temperature or overnight at 4 °C. After the incubation, the membrane was washed 3 x 6 min with TBST buffer (0.05% Tween 20 in TBS buffer). The second incubation with horseradish peroxidase-conjugated Goat anti-Mouse IgG secondary antibody was performed in 5% (w/v) milk powder in TBS buffer for 1 h at room temperature. The membrane was washed 3 x 6 min with TBST buffer and once at the end with TBS before detection. For the immune detection 1 mL of ECL1 (0.1 M Tris/HCl pH 8.5, 0.396 mM cumaric acid, 2.5 mM luminol) and 1 mL ECL2 (0.1 M Tris/HCl pH 8.5, 0.0096% (v/v) hydrogen peroxide) were mixed and applied on the membrane. The membrane and the film (Carestream® Kodak) were incubated in the dark in a western blot cassette film for some seconds and the film developed with developer and fixer solution (Carestream® Kodak).

2.4.3. Alignment

Multiple sequence alignments were carried out using the MUSCLE algorithm (Edgar, 2004) and optimized in Jalview (Waterhouse et al., 2009). For phylogenetic analyses the program MEGA6 was used (Tamura et al., 2013).

2.4.4. Membrane Proteins

2.4.4.1. Preparation of membrane fractions

After cell disruption (2.3.7), phenylmethanesulfonyl fluoride (PMSF) was added (1 mM) to the lysate, which was centrifuged in a JA 30.50 Ti rotor (Beckman/Avanti J-30I) at 10.000 g for 12 min at 4 °C. The pellet was discarded and the supernatant centrifuged at 100.000 g for 2 h at 4 °C. The resulting pellet was resuspended in homogenization buffer (50 mM Tris/HCl pH 8.5, 0.3 M KCl) using a Potter/Elvehjem PTFE pestle and glass tube. The membrane fraction was frozen with liquid nitrogen and stored at -20 °C.

2.4.4.2. Solubilization of membrane fraction

In order to identify the best detergent for the solubilization of membrane fraction, small scale solubilization tests were performed. In a final volume of 200 μ L, membrane fraction, homogenization buffer and detergent [10 x CMC (Critical Micelle Concentration)] were mixed and incubated at 4 °C for 1-2 h under agitation. The mixture was transferred into polycarbonate tubes and centrifuged in a TLA 100 Rotor (Beckman Coulter Optima™ Max-XP Ultracentrifuge) at 100.000 g for 1 h. The supernatant was analyzed by immunoblotting and catalytic activity was measured when possible. For large scale solubilization, the membrane fraction was mixed with detergent solution at 4 °C, and centrifuged in a JA 30.50 Ti rotor (Beckman/Avanti J-30I) at 100.000 g for 1 h.

2.4.5. Purification

2.4.5.1. Membrane proteins – TtUbiA and EcMenA

2.4.5.1.1. Immobilized metal ion affinity chromatography (IMAC) – Batch mode

Batch mode was performed according to (Drew et al., 2008). The solubilized membrane protein was incubated for 2 h or overnight with nickel-charged resin (Qiagen) at 4 °C under mild agitation with buffer A (50 mM Tris/HCl pH 8.5, 0.3 M KCl, 2 x cmc DM or DDM). The mixture was loaded into a Glass Econo-Column (Bio-Rad) and the flow through collected. The column was washed with 4% buffer B (buffer A, 0.5 M imidazole) followed by protein elution with 50% buffer B. A final elution step was performed with 500 mM imidazole. The samples were analyzed by SDS-PAGE and immunoblotting.

2.4.5.1.2. TEV digestion

Some constructs contained the TEV protease cleavage site which allowed the removal of the His₆-tag. After the affinity chromatography, the protein concentration of the elution fractions were determined by UV/Vis spectroscopy (2.5.1.2) and TEV protease solution (1.5 mg/mL) was mixed to a ratio of 1:50 TEV:protein and put into a dialysis bag (Spectra/Pore dialysis membrane MWCO 12.000-14.000). The digestion was performed overnight at 4 °C in the presence of dialysis buffer (50 mM Tris/HCl pH 8.5, 0.3 M KCl, 1 mM DTT). After incubation and cleavage of the His₆-tag, the sample was loaded into a 1 or 5 mL HisTrap HP column and the protein without His₆-tag was collected in the flow through fraction. TEV protease and His₆-tag was eluted with 50% buffer B. The fractions were analyzed by SDS-PAGE.

2.4.5.1.3. Size Exclusion Chromatography (SEC)

In order to remove aggregated protein, or to better separate the protein of interest or to exchange detergents, size exclusion chromatography was performed. A Superdex 200 10/300 (GE) was equilibrated with Tris buffer (50 mM Tris/HCl pH 8.5, 0.15 M KCl, 1 x CMC detergent). The protein was loaded onto the column through a loop (500 μ L) with a flow rate of 0.35 mL/min. The samples were collected and analyzed by SDS-PAGE and immunoblotting.

2.4.5.2. Futasine Hydrolase (TtMqnB)

2.4.5.2.1. Heat treatment

Due to the thermostability of TtMqnB, a heat treatment step was used as part of the purification strategy. Thus, after cell disruption and centrifugation (75.000 g, 40 min), the lysate was incubated for 20 min in a water-bath at 70 °C and cooled on ice for 10 min before pelleting. Afterwards, the lysate was centrifuged for 30 min at 4 °C (75.000 g) and the supernatant was purified by affinity chromatography.

2.4.5.2.2. Purification Co-NTA – 5 mL column Äkta system

After the heat precipitation step TtMqnB was purified with a 5 mL HisTrap HP column (GE) containing cobalt as metal chelate in an ÄKTA™ system (GE). The column was pre-equilibrated with buffer A (50 mM Tris/HCl pH 8.5, 0.15 M KCl) and the protein was loaded through a superloop with a flow rate of 0.8 mL/min. The column was washed with buffer A with flow rate of 1.0 mL/min until the absorbance at 280 nm reached the baseline. The protein elution was performed with 50% buffer B (buffer A, 0.5 M imidazole). The collected samples were analyzed by SDS-PAGE and immunoblot.

2.4.6. Prenyltransferase assays

Two different prenyltransferase assays were performed in order to evaluate the activity of UbiA and MenA enzymes.

2.4.6.1. UbiA prenyltransferase assays

UbiA assays were performed according to (Bräuer et al., 2008). Assay mixtures with 100 μ L final volume contained geranyl pyrophosphate (GPP) (2.46 mM, 10 μ L), 4-hydroxy benzoic acid (PHB) (2.46 mM, 10 μ L), MgCl₂ (10 mM, 10 μ L), 10 μ L DMSO, Tris/HCl pH 7.8 (50 mM; 10 μ L) and 50 μ L EcUbiA membrane fraction were incubated at 37 °C for 2 h under agitation

(600 rpm). The reaction was stopped by adding 2% formic acid and 500 μ L ethylacetate were used to extract the prenylated products. The mixture was centrifuged for phase separation and the organic phase was removed in vacuo. The pellet was resuspended in methanol before RP-HPLC analyses. The formation of 3-geranyl-4-hydrobenzoate (GHB) was analyzed by HPLC (MeOH:H₂O – 80:20; 0.2% formic acid; UV 254 nm) in a C18 column (300A; 250 x 4.6 nm; Phenomenex) with flow rate of 1.0 mL/min.

2.4.6.2. MenA prenyltransferase assays

MenA assays were conducted as described by (Debnath et al., 2012). The substrate 1,4-dihydroxy-2-naphthoic acid (DHNA-2) (10 mM; 20 μ L), MgCl₂ (10 mM; 20 μ L); CHAPS (0.1%; 20 μ L), Tris/HCl pH 8.5 (50 mM; 50 μ L), GPP (2.46 mM; 10 μ L) and EcMenA membrane fraction (100 μ L) were mixed and incubated for 1 h at 37 °C under agitation (600 rpm). The reaction was stopped by adding 100 μ L of acetic acid in methanol (0.1 M) and the extraction of the prenylated products was performed in the presence of hexane (600 μ L). After centrifugation for phase separation, the organic phase was removed in vacuo and the pellet resuspended in methanol. The formation of demethylmenaquinone (DMK) was analyzed by HPLC (CH₃CN:0.05% TFA in H₂O – 90:10; UV 254 nm) in a C18 column (300A; 250 x 4.6 nm; Phenomenex) with flow rate of 0.7 mL/min.

2.5. Biophysical Methods

2.5.1. Protein concentration determination

Two different techniques were used to determinate the protein concentration. For membrane fraction and solubilized protein, the RC DCTM Protein Assay Detergent compatible (Bio-Rad) was used. The absorption of the aromatics residues at 280 nm, (UV) spectroscopy was used for measurements after purification steps and for soluble proteins.

2.5.1.1. RC DCTM Protein assay

The colorimetric assay is similar to the Lowry assay (Lowry et al., 1951) with the advantage that the reaction reaches 90% of its maximum color within 15 min. For the assay copper tartrate and Folin reagent are necessary.

The assay is based on the reaction of the protein with copper tartrate in an alkaline medium leading to reduction of the Folin reagent by the copper-treated protein. The reduced species have a blue color with maximum absorbance at 750 nm. The samples were treated according to the protocol and known BSA concentrations were used to generate the calibration curve.

2.5.1.2. UV/Vis Spectroscopy

The protein concentration was measured under denaturing conditions using the absorption at 280 nm (A_{280}) according to the Lambert-Beer law.

$$A_{280 \text{ nm}} = c \cdot d \cdot \varepsilon \quad \text{equation 1}$$

Equation 1: Lambert-Beer law. A_{280} is the absorption measured at 280 nm, ε extinction coefficient ($\text{M}^{-1} \cdot \text{cm}^{-1}$), c molar concentration in M and d the path length (cm).

The extinction coefficient $\varepsilon_{280\text{nm}}$ can be calculated according to the amino acid sequence. In this work, the coefficient was determined using the ProtParam program from ExPASy Proteomics Server (Gasteiger et al., 2005) (Table 2.2).

Table 2.2: Molecular weight and extinction coefficient of proteins studied in this work.

Proteins	Molecular weight ($\text{g} \cdot \text{mol}^{-1}$)	$\varepsilon_{280\text{nm}}$ [$\text{M}^{-1} \cdot \text{cm}^{-1}$] denat. in 6 M GdnHCl*
TtUbiA-His ₆ -tag	33974.0	68870
TtUbiA	31762.7	67380
EcMenA-His ₆ -tag	36288.8	55920
EcMenA-GFP-His ₆ -tag	67009.0	77810
EcMenA	34077.5	54430
TtMqnB	26236.1	29450

* GdnHCl: Guanidinium Chloride

2.5.2. Circular Dichroism (CD) spectroscopy

Secondary structure of the proteins was analyzed under native and denatured (6 M guanidinium chloride) conditions. Far-UV CD spectroscopy was performed with a J-810 CD Spectrometer (Jasco) at 4 °C and/or 20 °C (Thermostat PTC-4235) with a glass cuvette of 0.1 mm (Hellma). The spectra were measured from 190-250 nm with a speed of 50 nm/min. 30 accumulations were performed in order to obtain a single spectrum. The protein concentration was 1.0 mg/mL in the presence of buffer containing detergent. All CD spectra were buffer corrected. The molar ellipticity per residue was calculated according to the followed equation:

$$[\Theta]_{MRW} = \frac{\theta \cdot M}{10 \cdot d \cdot c \cdot N} \quad \text{equation 2}$$

Equation 2: Molar ellipticity equation. $[\Theta]_{MRW}$: molar ellipticity per residue (in $\text{deg} \cdot \text{cm}^2 \cdot \text{dmol}^{-1}$), Θ : ellipticity in degree, M : protein molecular mass (g mol^{-1}), d : cuvette optical path (cm), c : protein concentration ($\text{mg} \cdot \text{mL}^{-1}$), N : number of amino acids.

2.5.3. Mass spectrometry

2.5.3.1. MALDI-TOF Mass spectrometry

Protein samples were analyzed after the last purification step. The SDS-PAGE was stained with Coomassie brilliant blue G-250 solution [0.25% (w/v) Coomassie brillante blue G-250 in 50% (v/v) ethanol, 10% (v/v) acetic acid] and de-stained with a solution containing ethanol, acetic acid and distilled water (2:1:2). Relevant bands were cut out of the gel and washed three times with water, twice with 10 mM $(\text{NH}_4)\text{HCO}_3$ followed by a final wash step with 10 mM $(\text{NH}_4)\text{HCO}_3$ in 50% of acetonitrile. The pieces of gel were dried and resuspended in a solution of 10 mM $(\text{NH}_4)\text{HCO}_3$. The digestion reaction was performed overnight at 37 °C with 1 μg of trypsin. The extracted peptides were injected into a CapLC (Micromass, Manchester, UK) and the MS/MS experiments were performed on a Q-TOF mass spectrometer. Data were analyzed by using MASCOT (Matrix Science) and MSDB protein sequence database.

MALDI-TOF Mass spectrometry measurements were carried out by Dr. Angelika Schierhorn (Institute of Biotechnology and Biochemistry – Martin Luther University).

2.5.3.2. ESI–Mass spectrometry

In order to verify the prenylation activity of the prenyltransferases, the samples were analysed by ESI–mass spectrometry. The analyses were carried out by Dr. Nadine Strehmel from Leibniz Institute of Plant Biochemistry (IPB) in Halle (Saale).

Samples (2.6 μL , full loop injection) were separated at 40°C on an Acquity UPLC platform (Waters, www.waters.com) equipped with a HSS T3 column (100 x 1.0 mm, particle size 1.8 μm , Waters) applying the following gradient at a flow rate of 150 $\mu\text{L}/\text{min}$: 0-1 min, isocratic 95% A [water/formic acid, 99.9/0.1 (v/v)], 5% B [acetonitrile/formic acid, 99.9/0.1 (v/v)]; 1-16 min, linear from 5 to 95% B; 16-18 min, isocratic 95% B; 18-20 min, isocratic 5% B.

Eluting compounds were detected from m/z 90–1000 using a MicroTOF–Q I hybrid quadrupole time-of-flight mass spectrometer equipped with an Apollo II electrospray ion source (Bruker Daltonics, www.bruker.com) in positive and negative ion mode using the

following instrument settings: nebulizer gas, nitrogen, 1.6 bar; dry gas, nitrogen, 6 L/min, 190°C; capillary, -5000 V (+4000 V); end plate offset, -500 V; funnel 1 RF, 200 V; funnel 2 RF, 200 V; in-source CID energy, 0 V; hexapole RF, 100 V; quadrupole ion energy, 3 eV (5 eV); collision gas, argon; collision energy, 3 eV (7 eV); collision RF 100/200 V (timing 50/50); transfer time, 70 μ s; pre pulse storage, 5 μ s; spectra rate, 3 Hz.

For the acquisition of CID mass spectra, appropriate precursor ions ($[M+H]^+$ or $[M-H]^-$) were selected by the first quadrupole using an isolation width of ± 3 m/z and fragmented inside the collision cell applying collision energies in the range of 5 to 30 eV. Argon was used as collision gas. Product ions were detected using the same parameter settings as described above.

All mass spectra were acquired in centroid mode. Recalibration of the m/z scale was performed for individual raw data files on lithium formate cluster ions obtained by automatic infusion of 20 μ L 10 mM lithium hydroxide in isopropanol/water/formic acid, 49.9/49.9/0.2 (v/v/v) at a gradient time of 18 min using a diverter valve.

DataAnalysis 4.0 (Bruker Daltonics) was used for the generation of extracted ion chromatograms, deconvolution of compound mass spectra and calculation of elemental compositions. For the relative quantification of compounds, extracted ion chromatograms of corresponding quantifier ions were integrated applying QuantAnalysis 2.0 (Bruker Daltonics).

2.5.4. Analytical Ultracentrifugation

Analytical ultracentrifugation is a powerful technique that gives information about the size and shape of macromolecules in solution (Cole et al., 2008). Two types of experiments are possible: 1) sedimentation velocity (SV) measurements, in which a high centrifugal force is applied and the time-course sedimentation process is analyzed; 2) sedimentation equilibrium (SE) measurements, where a low centrifugal force is applied allowing the analysis of the exponential concentration distribution in steady state of sedimentation and diffusion. The definition of sedimentation coefficient (S) of a macromolecule is defined by the Svedberg equation (Lebowitz et al., 2002):

$$S = \frac{u}{\omega^2 \cdot r} = \frac{M \cdot (1 - \bar{v} \cdot \rho)}{N_A \cdot f} \quad \text{equation 3}$$

Equation 3: Sedimentation coefficient equation: S is the Svedberg unit (10^{-13} sec); u is the observed radial velocity; $\omega^2 \cdot r$ the centrifugal field; M the molar mass; \bar{v} the partial specific volume; ρ the density of the solvent; N_A the Avogadro's number and f the frictional coefficient.

In sedimentation equilibrium, the centrifugal force is small enough to generate an equilibrium concentration distribution of the sample throughout the cell where sedimentation flux is balanced with the diffusion flux (Cole et al., 2008). At equilibrium, the mixture of non-interacting molecule is the measured signal as a function of radial position $a(r)$ (Lebowitz et al., 2002):

$$a(r) = \sum_n c_{n,o} \cdot \varepsilon_n \cdot d \cdot \exp \left[\left(\frac{M_n \cdot (1 - \bar{v} \cdot \rho) \cdot \omega^2}{2 \cdot R \cdot T} \right) \cdot (r^2 - r_0^2) \right] \quad \text{equation 4}$$

Equation 4: Exponential distribution at SE. $c_{n,o}$ is molar concentration of specie n at a reference position r_0 ; M_n the molar mass; \bar{v} the partial specific volume; ε_n the extinction coefficient; d the optical path length.

Several concentrations of TtMqnB (30 – 1000 $\mu\text{g}/\text{mL}$) in 15 mM Tris/HCl pH 8.5, 45 mM KCl buffer were used in the presence and absence of imidazole (75 mM). The centrifugations were carried out in an Optima XL-A ultracentrifuge (Beckman) with a An50Ti rotor at 20 °C. The sedimentation velocity experiments were performed for 3 hours at 40.000 rpm and monitored at $A_{280\text{nm}}$ each 10 min. The sedimentation equilibrium experiments were performed for 70 hours at 10.000 rpm.

All measurements and analyses were kindly carried out by Dr. Hauke Lilie (Institute of Biotechnology and Biochemistry – Martin Luther University).

2.6. Crystallography Methods

2.6.1. 96-well plate crystallization screening

The initial crystallization screening was carried out in a MRC-3-well sitting drop plate (SWISSCI) at 12 °C using a Microsys SQ robot (Cartesian). For each drop, 0.2 μL protein was mixed with 0.2 μL reservoir (from 50 μL). The drops were monitored using a Desktop Minstrel UV-Imager (Rigaku). For the initial screening, three different TtMqnB concentrations (3.0 mg/mL, 8.0 mg/mL and 12.0 mg/mL) in Tris buffer (15 mM Tris/HCl pH 8.5, 45 mM KCl and 75 mM imidazole) were tested with the following commercial crystallization kits: Morpheus (Molecular Dimensions), JBScreen classic 1-10 (Jena Bio-Science), JBScreen JCSG++ (Jena Bio-Science), Cryo crystallization kit (Sigma Aldrich), Low Ionic Strength crystallization kit (Sigma Aldrich) and Crystal screen 1+2 (Hampton Research).

2.6.2. 15-well plate fine screening

For fine screening, the 15 well-plate (EasyXtalTool, Qiagen) and hanging drop-method were used. To optimize the conditions and the crystal quality, precipitant and protein

concentration were varied. The plates were set up with 450 μL reservoir at 12 °C and each lid contained different ratio of protein and reservoir: i) 1 μL protein + 1 μL reservoir, ii) 1 μL protein + 2 μL reservoir and iii) 2 μL protein + 1 μL reservoir.

2.6.3. Ligand soaking

In order to gain further information about the catalytic center of TtMqnB and structural modifications in the presence of ligands, soaking experiments were performed with different substrate analogs. Hypoxanthine (5 mM), formycin B (5 mM and 15 mM) and inosine (10 mM) were solubilized in the reservoir solution: 1.1 M $(\text{NH}_4)_2\text{SO}_4$, 0.1 M ADA pH 6.5 in the presence of cryo-protectant (25% (v/v) ethylene glycol). Crystals were incubated in a 5 μL drop at 20 °C between 5 – 60 min, after which the diffraction of each crystal was measured either in-house or at SLS (Swiss Light Source).

2.6.4. Data collection and data processing

The data collection was performed using cryo-crystallography at -180 °C (100 K). For in-house measurements, the X-ray generator (MicroMax 007, $\lambda = 1.54182 \text{ \AA}$ -Rigaku) and the detector Saturn 944+ (Rigaku) were used. The distance between crystal and detector varied from 50 – 80 mm. The crystals were exposed to X-rays either for 60 or 90 sec.

Measurements were also kindly performed at SLS (Swiss Light Source) in the beamline X06DA and X06SA ($\lambda = 1.00 \text{ \AA}$) by Dr. Mikio Tanabe (HALOmem – Membrane protein structure & dynamics), Halle (Saale).

The collected data were processed (indexing and integration) using iMosflm (Battye et al., 2011) and scaled in Aimless (CCP4) program (Evans and Murshudov, 2013).

2.6.5. Model building and phase refinement

The initial phases for apo TtMqnB were obtained through molecular replacement using Phenix-Phaser (Adams et al., 2010). As model, the chain A of methylthioadenosine nucleosidase (MTAN, PDB: 4BMZ) from *Helicobacter pylori* was used (Kim et al., 2014). Due to the low amino acid sequence identity between the two proteins (27%), a poly-alanine (ALA) chain was used as search model. The new structure was firstly rebuilt through AutoBuild wizard – Phenix (Adams et al., 2010) followed by manual building based on $F_o - F_c$ and $2F_o - F_c$ difference maps in the Coot program (Emsley and Cowtan, 2004). Refinements were carried out through Refmac5 (CCP4) (Murshudov et al., 1997). All

structure figures were created using Pymol (The PyMOL Molecular Graphics System, Version 1.5.0.4 Schrödinger, LLC).

For solving the phases of hypoxanthine-TtMqnB crystals, a monomer from TtMqnB was used as search model for molecular replacement.

2.7. Chemical synthesis of aromatic substrate

In order to investigate the prenylation activity of TtUbiA and SlUbiA, different aromatic substrates were synthesized. 1,4-dihydroxy-6-naphthoic acid was synthesized according to (Sugishima et al., 1994) by Dr. Tula Beck Bisol from Leibniz Institute of Plant Biochemistry (IPB) in Halle (Saale).

The synthesis of 1,4-dihydroxy-3-methyl-naphthoic acid was performed in two steps: 1) synthesis of 2-ethoxycarbonyl-3-methyl-1,4-naphthoquinone by the method of (Sharma et al., 1978) followed by a reduction reaction in the presence of $\text{Na}_2\text{S}_2\text{O}_4$ to generate the corresponding hydroquinone; 2) saponification of the ester in the presence of NaOH and $\text{Na}_2\text{S}_2\text{O}_3$ according to Saito & Ogura (Saito and Ogura, 1981). The synthesis was monitored by ESI-MS measurements to check sub- and final products. For the generation of 1,4-dihydroxy-2-methylnaphthalene, menadione (K3) was reduced with 10% (w/v) $\text{Na}_2\text{S}_2\text{O}_4$ aqueous solution under nitrogen as described by (Suhara et al., 2011). Both syntheses were performed at Leibniz Institute of Plant Biochemistry (IPB) under the supervision of Dr. Ricardo W. Neves Filho.

3. Expression and characterization of 1,4-dihydroxy-2-naphthoate octaprenyltransferase (MenA)

3.1. Recombinant expression of EcMenA in *E. coli*

Two constructs were generated for the expression of EcMenA protein based on the prediction program TOPCONS (Bernsel et al., 2009). The topology of EcMenA was predicted to have the N-terminus localized in the bacteria cytoplasm and the C-terminus in the periplasm. Thus, *menA* was cloned into pET15b-TEV (N-terminal His₆-tag) and pNGFP-BC vector with His₆-tag and GFP protein at N-terminal (Kawate and Gouaux, 2006).

Various *E. coli* strains were used to find the best conditions for EcMenA protein expression. The presence of the protein after expression was analyzed by immunoblot for the pET15b-TEV construct and by in-gel fluorescence for the GFP-fusion. Curiously, the immunoblot detected protein bands around 25 kDa after EcMenA-His expression in BL21 (DE3), Rosetta (DE3) and C43 (DE3) cells, although the estimated molecular weight is 30 kDa (Figure 3.1A). Such behavior in SDS-PAGE gels has been described as typical for membrane proteins (Zheng and Trudeau, 2015), since they are not boiled before applied in the gel, leading to incomplete unfolding so that they do not run at their expected molecular weight. The same behavior was also observed for EcMenA-GFP fusion protein in the fluorescence gel. The predicted molecular weight for EcMenA-GFP fusion protein is 67 kDa, but the fluorescence bands were detected around 60 kDa (Figure 3.1B).

Although EcMenA-GFP fusion protein expression could be detected in BL21 (DE3) and Rosetta (DE3), no expression was observed in C43 (DE3) cells. For large scale expression BL21 (DE3) was used with 0.3 mM IPTG at 30 °C overnight.

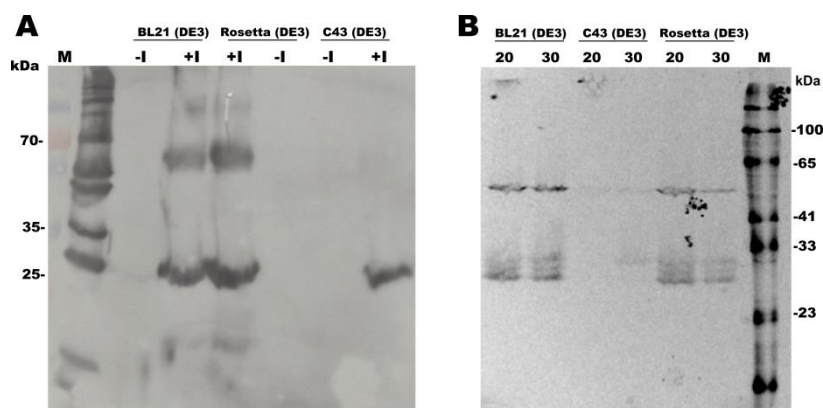


Figure 3.1. Expression of EcMenA in *E. coli* cells. (A) Immunoblotting analysis of EcMenA-His protein after expression in *E. coli*. Protein expression was detected in Rosetta (DE3), BL21 (DE3) and C43 (DE3). M: His-tag marker, -I indicates before expression and +I indicates after expression with 0.3 mM IPTG. Expressions were performed at 30 °C. **(B) in-gel fluorescence of EcMenA-GFP fusion protein expression.** Fluorescence bands were observed in BL21 (DE3) and Rosetta (DE3) cells. 20 and 30 indicates temperature of expression, M: fluorescence marker. Primary antibody: mouse anti-his; secondary antibody: goat anti-mouse (HRP).

3.2. Solubilization of EcMenA protein

The extraction of membrane proteins from the cell membrane is usually accomplished with the help of detergents. This step has been classified as crucial, as many membrane proteins are poorly stable and short-lived in such detergent solution. Thus, the best detergent should mimic the physiological properties of the cell membrane and maintain the protein integrity after solubilization (Privé, 2007).

In order to find which detergent is the most appropriate for future experiments, a variety of detergents that have been described as for crystallization of membrane proteins was tested: Lauryldimethylamine N-oxide (LDAO); *n*-Decyl- β -D-maltopyranoside (DM); *n*-Dodecyl- β -maltopyranoside (DDM); 6-Cyclohexyl-1-hexyl- β -D-maltopyranoside; *n*-octyl- β -D-glucoside (β -OG) and 3-[(3-cholamidopropyl) dimethylammonio]-1-propanesulfonate (CHAPS) (Privé, 2007). EcMenA-His was solubilized with 10-fold CMC (critical micelle concentration) of each detergent and analyzed by immunoblotting and protein concentration determined according to the Bio Rad DC method (2.5.1.1).

Although all tested detergents were able to solubilize EcMenA-His protein, β -OG and Cymal-6 detergents presented a higher effectiveness of solubilization, resulting in stronger bands in the immunoblotting and higher protein concentration (Figure 3.2). Although these results show that several detergents may be useful for the EcMenA-His solubilization, it does not provide any information about the long-term integrity of EcMenA.

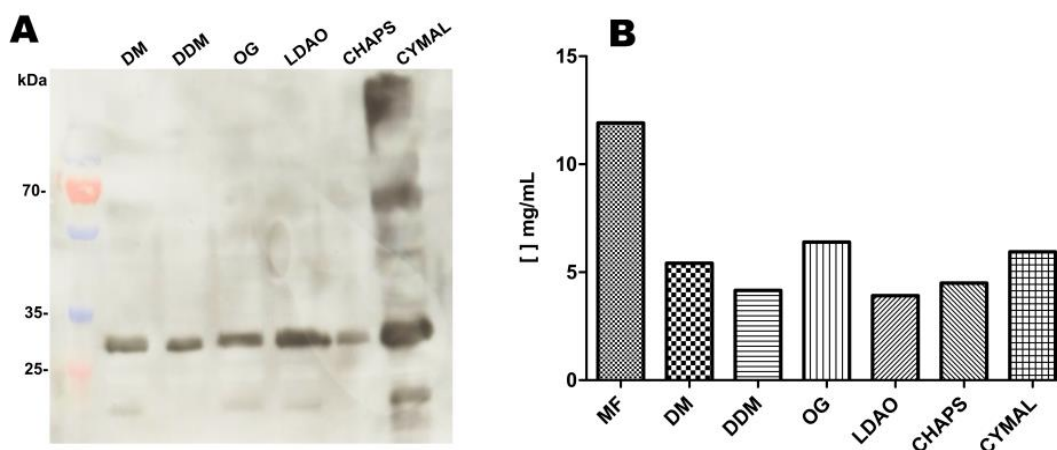


Figure 3.2. EcMenA-His solubilization in different detergents. (A) Immunoblotting of EcMenA after detergent solubilization. Solubilization was performed with 10-fold CMC of each detergent for 1h30 at 4 °C. EcMenA bands could be detected around 30 kDa. Primary antibody: mouse anti-his; secondary antibody: goat anti-mouse (HRP). **(B) RC DC Assay for detergent-compatible protein concentration determination.** After solubilization, the detergents *n*-octyl- β -D-glucoside (β OG) and Cymal-6 showed the highest level of solubilized protein. DM: *n*-Decyl- β -D-maltopyranoside; DDM: *n*-Dodecyl- β -D-maltopyranoside; β -OG: *n*-octyl- β -D-glucoside; LDAO: Lauryldimethylamine N-oxide; CHAPS: 3-[(3-cholamidopropyl) dimethylammonio]-1-propanesulfonate; Cymal-6: 6-Cyclohexyl-1-hexyl- β -D-maltopyranoside; MF: membrane fraction.

3.3. Enzymatic activity of the EcMenA-His membrane fraction

According to the classical pathway of menaquinone biosynthesis in *E. coli*, MenA catalyzes the prenylation of 1,4-dihydroxy-2-naphthoic acid (DHNA-2) at position C2 (Bentley and Meganathan, 1982), which has been demonstrated experimentally using the cells extract of *E. coli* and membrane fraction of *Micrococcus luteus* (Saito and Ogura, 1981; Shineberg and Young, 1976).

In order to investigate the enzymatic activity of EcMenA-His, activity assays were carried out according to Debnath et al., (2012) and analyzed by RP-HPLC. The membrane fraction of *E. coli* containing overexpressed his-tagged EcMenA was incubated with DHNA-2 and geranyl pyrophosphates (GPP) in the presence of magnesium. The same setup without GPP was used as negative control. After 1 hour incubation, the organic phase was extracted with hexane and dried using vacuum speed. The samples were analyzed in a C18 column with a wavelength of 254 nm. The RP-HPLC result for the sample containing DHNA-2 and GPP showed a peak after 6 minutes, which was not observed in the negative control (Figure 3.3A). To verify whether this peak corresponds to the demethylmenaquinone-2 (DMK-2) product, samples were collected and analyzed by ESI-MS. The result confirmed that the observed product corresponds to the prenylated form of DHNA-2 in the oxidized state with a molecular weight of 295.17 g.mol⁻¹ (Figure 3.3B).

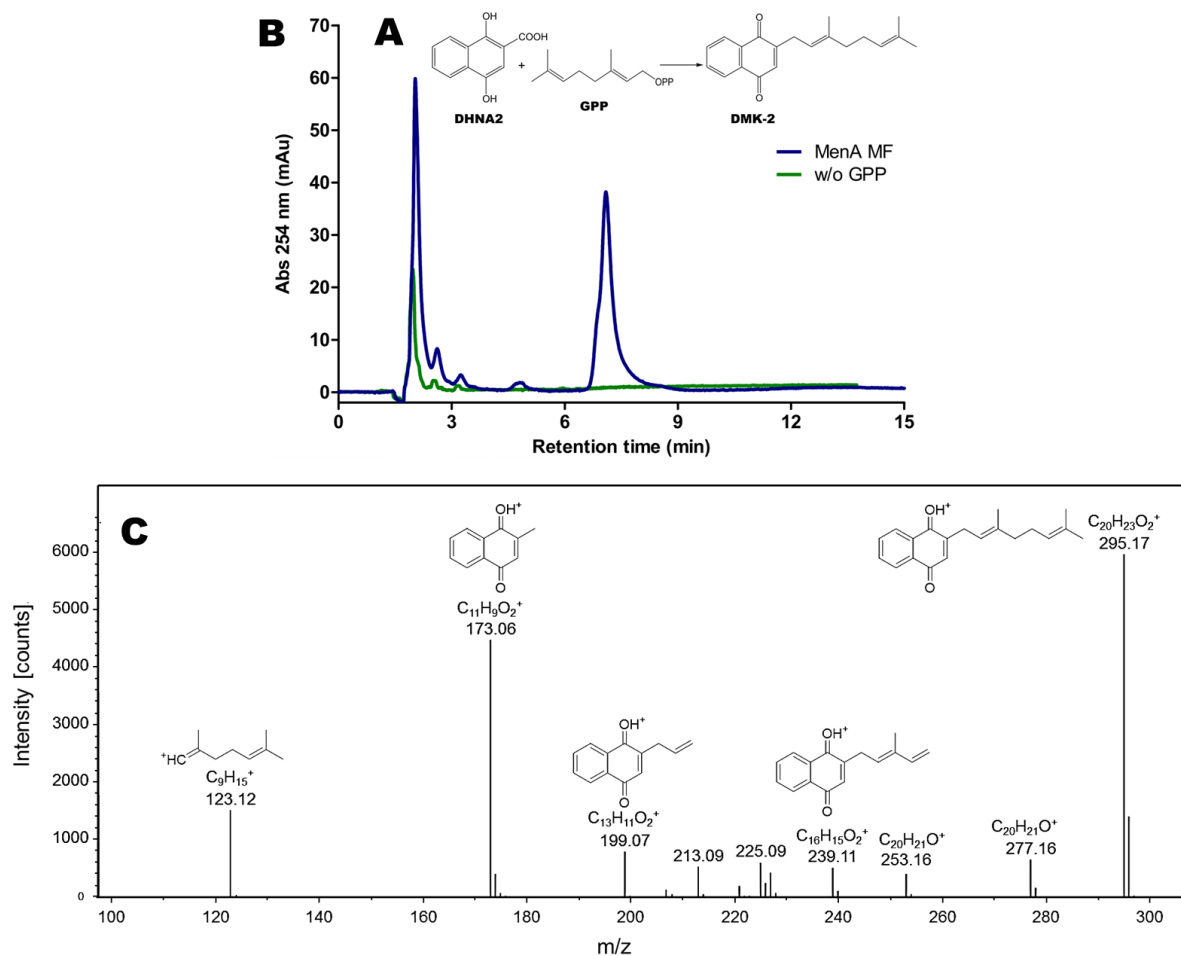


Figure 3.3. EcMenA-membrane fraction activity assay (A) Enzymatic reaction scheme. DHNA-2 is prenylated by MenA in the presence of GPP and Mg^{2+} . The formed product (DMK-2) is analyzed by HPLC. **(B) HPLC profile from EcMenA-His membrane fraction.** Blue line shows the assay profile in the presence of both substrates. The peak indicates the formation of DMK-2; green line shows the assay profile in the absence of GPP (negative control). Assays were carried out at 37 °C. HPLC flow rate: 1.0 mL/min. **(C) Mass spectrum of the EcMenA reaction product.** The last peak corresponds to the DMK-2 in the positive ionization mode with molecular weight of 295.17 $g \cdot mol^{-1}$.

The observed activity of EcMenA in the membrane fraction of *E. coli* demonstrates that the protein is correctly folded and functional in the cell membrane. As demonstrated above (Figure 3.2), EcMenA could be effectively solubilized in all detergents tested, so that detergent-solubilized EcMenA was assayed under the same conditions as membrane fraction in order to find the most appropriate detergent. Significantly different activity levels were observed with the various detergents (Figure 3.4A).

Although CHAPS and DM were able to support EcMenA-His activity after solubilization, the peak areas showed that more than 65% of the activity was lost in comparison to the membrane fraction. In contrast, only around 20% EcMenA-His activity was lost when solubilized with DDM. Interestingly, the detergents that showed the best solubilization

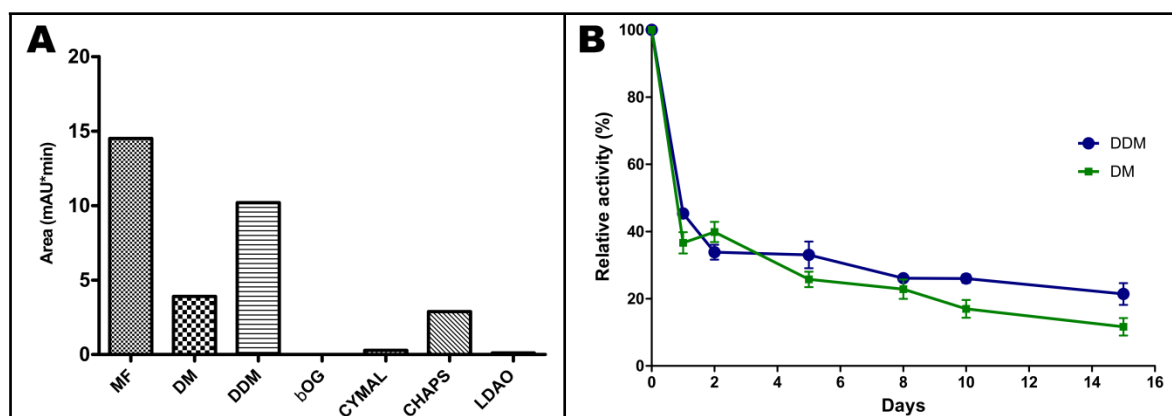


Figure 3.4. (A) Detergent-solubilized EcMenA-His activity assay. Enzymatic assays were performed using the same volume of membrane fraction and solubilized samples (100 μ L). The area of each peak showed different activity levels among the detergents. **(B) EcMenA stability within detergent solution.** Time-dependent activity assays (shown in days) of EcMenA after solubilization in 10-fold CMC of DM (green line) and DDM (blue line) detergents to determine the long-term protein stability. The curves showed a decrease in EcMenA relative activity with time. Relative activity was calculated using the area of 4-PP (internal standard) and the samples. All tests were carried out using DHNA-2 and GPP as substrates

properties and highest proteins concentration (β -OG and Cymal-6, Figure 3.2B) were associated with little or no enzymatic activity (Figure 3.4A).

The long-term stability of EcMenA in DM and DDM detergents was also evaluated by activity assays. After solubilization, the samples were stored at 4 $^{\circ}$ C for several days and aliquots were analyzed by their ability to form DMK-2 using 4-phenylphenol (4-PP) as internal standard in the RP-HPLC. Figure 3.4B shows the relative activity of EcMenA-His after 15 days in 10-fold CMC of DM and DDM solutions. The results demonstrate that after the first day, the detergent-solubilized enzyme loses more than 50% of its activity in both detergent solutions. Interestingly, the activity level does not decrease drastically between day 2 and 15 and detectable activity levels were also observed after 15 days. This is an important result for enzyme purification, since this step usually requires several days.

3.4. Purification of EcMenA protein

The first strategy used to purify EcMenA-His (using the pET15b-TEV construct) consisted of three purification steps: Immobilized metal ion affinity chromatography (IMAC) utilizing the His₆-tag from the vector, ionic exchange chromatography (IEC), and size exclusion chromatography (SEC). All steps were monitored by Coomassie-stained SDS gels and immunoblotting. Although bands of the expected size of EcMenA-His were observed after SEC using Coomassie-stained gels, no signal was detected by immunoblotting (data not shown). To check whether the observed band was EcMenA-His, it was cut out of the SDS-PAGE gel and analyzed by mass spectrometry (2.5.3.1) revealing the presence of the peptidyl

prolyl *cis-trans* isomerase SlyD. SlyD is a soluble *E.coli* protein with chaperone and peptidyl-prolyl *cis-trans* isomerase (PPIase) domains, and has been cited as the most frequent IMAC contamination due to its histidine rich domain (Parsy et al., 2007). Although it exhibits a molecular weight of 21 kDa, SlyD migrates at an apparent molecular mass of 27 kDa (Robichon et al., 2011). Since the size of SlyD and EcMenA are quite similar, they run at the same molecular weight and a separation by SEC is not possible. Robichon and co-workers (2011) released a new BL21 (DE3) derivative strain (the so-called NiCO21 (DE3) strain, New England Biolabs) which expresses SlyD as a fusion protein with a chitin binding domain (SlyD-CBD). With this methodology, the SlyD-CBD fusion protein can be immobilized on a chitin column and separated from the IMAC elution fraction. Attempts to express and purify EcMenA using this strain were not successful (data not shown).

The second strategy applied was the utilization of the GFP-EcMenA fusion protein using two purification steps (IMAC and SEC). GFP-EcMenA fusion has a molecular weight of 67 kDa allowing separation from SlyD by SEC. For the IMAC step, GFP-EcMenA was incubated with nickel-agarose beads as described in 2.4.5.1.1. After elution with buffer containing high imidazole concentration (50 mM Tris pH 8.5; 0.3M KCl; 0.36 mM DDM; 500 mM imidazole), the sample was concentrated and purified by SEC. Although the SEC profile showed the presence of a single protein peak, the protein was eluted in the void volume of the column, suggesting that the protein is aggregated or is not stable in the buffer (Figure 3.5A). Coomassie-stained gels and in-gel fluorescence showed that the observed peak corresponds to the GFP-EcMenA fusion protein. Free GFP could also be found, probably due to the action of proteases (Figure 3.5B). Newby and co-workers (Newby et al., 2009) have reported that membrane proteins tend to elute in the void volume of SEC columns either due to low protein stability in the buffer solution (leading to aggregates) or due to micelle formation (resulting different oligomeric states). Nevertheless, SlyD protein was not detected using this methodology. Despite purifying GFP-EcMenA in only two steps, proteins yields were very low at just 0.38 mg/L culture.

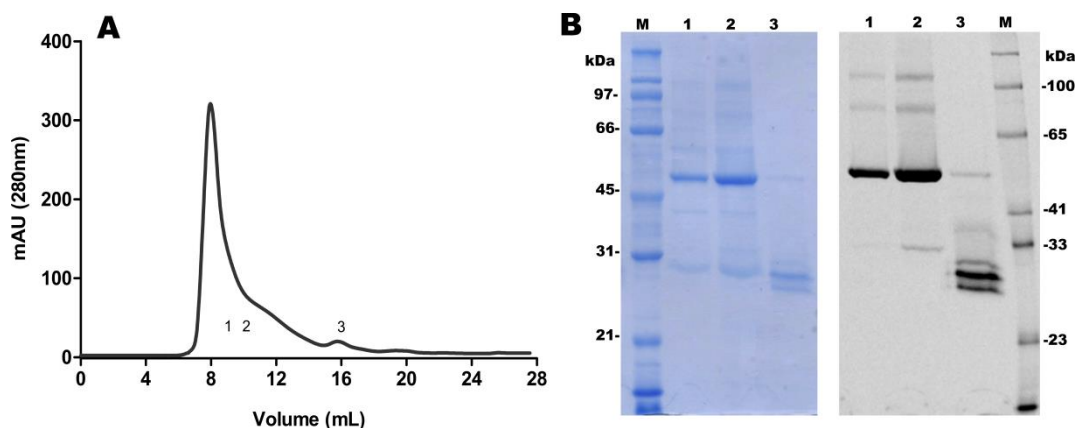


Figure 3.5. Purification of GFP-EcMenA fusion protein (A) Äkta profile from size exclusion chromatography (SEC). GFP-EcMenA was purified in a Superdex 200 (10/300 GL) column at 4 °C in buffer containing DDM. **(B) Coomassie-stained gel and in-gel fluorescence of GFP-EcMenA.** Gels show the fractions (numbered in A) obtained after SEC, lanes 1 and 2 indicate fractions of GFP-EcMenA fusion and lane 3 indicates free GFP.

The third methodology used to purify EcMenA was also based on two chromatographic steps: IMAC of GFP-EcMenA, GFP removal using TEV protease cleavage and a second IMAC step. The removal of GFP via TEV protease cleavage is not a trivial step when working with membrane proteins. Mohaty and co-workers (Mohanty et al., 2003) have demonstrated that some detergents such as β -OG and LDAO should be avoided during TEV digestion of membrane proteins since the TEV activity is reduced. Although there are no reports on the effect of DDM on TEV activity, their results showed that DM allows TEV protease activity.

Thus, after the first IMAC, the elution fraction was incubated overnight with excess of TEV protease at 4 °C in 50 mM Tris/HCl pH 8.5; 300 mM KCl; 0.17 mM DDM; 1mM DTT. After TEV protease digestion, GFP-EcMenA was loaded on a 5 mL Ni²⁺ column and the flow-through containing free EcMenA was collected. The elution fraction (250 mM imidazole) containing GFP and TEV protease was also collected and analyzed by SDS-PAGE. Figure 3.6 shows an overview of the purification of GFP-EcMenA with samples before and after IPTG induction, membrane fraction and after solubilization with DDM (lanes 1 – 4, respectively). The results show that TEV protease digestion was successful in the presence of DDM, since no band correspondent to the GFP-EcMenA molecular mass (60 kDa) was detected in the in-gel fluorescence (lane 6). Mass spectrometry analysis of EcMenA after TEV cleavage showed the presence of EcMenA and GFP peptides with no SlyD peptides detected. Despite the fact that just two purification steps were used as strategy, the yields of EcMenA after GFP removal remained low (0.1 – 0.3 mg/L culture). This purification procedure was used for further characterization steps. Application of a third chromatographic step (SEC, Superdex 200 column) after the second IMAC gave no improvement in purification. Furthermore, the protein yield at end was even lower and for this reason SEC was not used further.

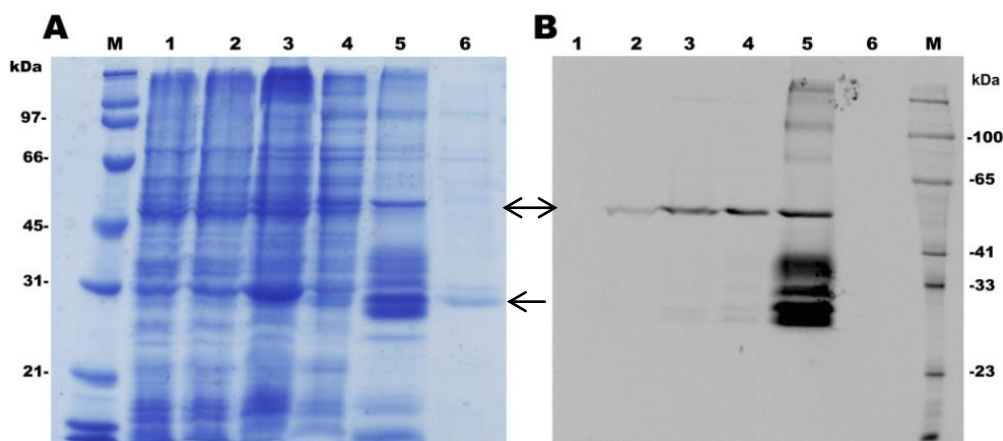


Figure 3.6. Overview of EcMenA purification. (A) Coomassie-stained gel. (B) in-gel fluorescence. 1: before induction; 2: after induction with 0.3 mM IPTG, the band around 60 kDa indicates GFP-EcMenA fusion protein; 3: membrane fraction; 4: after solubilization with 10-fold CMC DDM; 5: after first IMAC showing the elution fraction containing the fusion protein (60 kDa) and free GFP (27 kDa), 6: second IMAC after TEV protease cleavage. Double-headed arrow indicates GFP-EcMenA fusion protein and the single arrow indicates EcMenA with a molecular mass of 30 kDa after GFP removal.

3.5. Secondary structure of purified EcMenA investigated using circular dichroism (CD)

The far-UV CD spectra of GFP-EcMenA fusion protein and EcMenA after GFP removal were measured between 190 and 250 nm. Measurements were performed in buffer containing detergent (20 mM Tris pH 8.5; 60 mM KCl; 0.36 mM DDM) at 4 °C. It was observed that the CD spectrum of GFP-EcMenA exhibited a typical α -helical signal with two minima at 222 nm and 208 nm (Figure 3.7A). This result was expected, as the EcMenA is predicted to have 9 transmembrane helices, which corroborates with the recent crystal structure of AfUbiA (Huang et al., 2014). However, the secondary structure of GFP seems to influence the CD spectrum in the positive signal. GFP contains high β -sheet content ($60\% \pm 8\%$) and its CD spectrum shows a negative band between 210 and 220 nm and a positive band between 195 and 200 nm (Visser et al., 2002). Although the spectrum of GFP-EcMenA showed the two negative bands correspondent to α -helices, the positive band detected between 195 nm and 200 nm is probably influenced by the GFP secondary structure, since after GFP removal the positive band switched to values around 190 nm (characteristic for typical α -helical signals) (Figure 3.7). GFP removal did not cause major changes in the EcMenA CD spectrum (Figure 3.7B), suggesting that the protein remains folded following cleavage. The CD spectrum of EcMenA recorded under denaturing conditions with 6M guanidinium chloride supports this assumption.

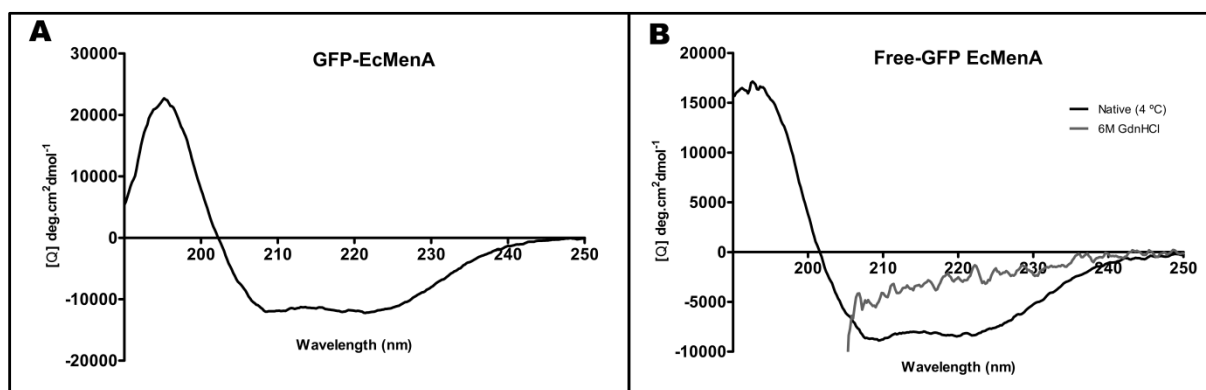


Figure 3.7. (A) Experimental far-UV CD spectrum of GFP-EcMenA. The spectrum shows two negative bands at 222 nm and 208 nm and a positive band between 195 nm and 200 nm. Protein conc.: 1.0 mg/mL. **(B) Experimental far-UV CD spectra of EcMenA after GFP removal.** The spectrum shows two negative bands at 222 nm and 208 nm, however, the positive band switched to 190 nm. The difference observed in the positive band can be attributed to the β -barrel structure of GFP. Protein conc. 0.745 mg/mL. Black spectrum corresponds to native protein and grey spectrum corresponds to denatured EcMenA. Measurements were performed at 4 °C.

CD analyses of membrane proteins have been considered problematic due to the (i) small database of membrane protein structures, (ii) the different spectra arising from soluble and membrane proteins and (iii) the inadequacy of using existing soluble proteins as reference set (Park et al., 1992; Wallace et al., 2003). On the other hand, other studies have demonstrated that data analysis using soluble proteins as reference is reliable when membrane proteins are included in the dataset (Abdul-Gader et al., 2011; Sreerama and Woody, 2004). In addition, it has been observed that the position of the positive band varies between 192 and 196 nm in CD spectra of α -rich membrane proteins, a range similar to that for soluble proteins (192-195 nm) (Sreerama and Woody, 2004).

3.6. Substrate specificity

Saito & Ogura (1981) demonstrated that membrane fractions of *Micrococcus luteus* containing MenA are able to catalyse prenyltransferases using different aromatic and pyrophosphate substrates. Yazaki and co-workers (2009) have also shown that LePTG1, an aromatic prenyltransferase of plants, is also able to accept different substrates molecules. On the other hand, Karamat and co-workers (2014) demonstrated that a prenyltransferases isolated from parsley is strictly specific towards umbelliferone and dimethylallyl pyrophosphate (DMAPP) as prenyl acceptor and donor, respectively. Although the current work has shown that EcMenA is capable of catalyzing the prenylation of DHNA-2 in the presence of magnesium using GPP as pyrophosphate substrate (section 3.3), it remains unknown whether EcMenA can accept other substrates.

In order to investigate specificity for prenyl-donor substrates, the membrane fraction containing overexpressed EcMenA-His was incubated with DHNA-2 and prenyl-donor substrates containing different chain lengths: dimethylallyl pyrophosphate (DMAPP, with one isoprenoid moiety C5), geranyl pyrophosphate (GPP, with two isoprenoid moieties C10), farnesyl pyrophosphate (FPP, with three moieties C15), geranylgeranyl pyrophosphate (GGPP, with four moieties C20) and geranylgeranyl pyrophosphate (GFPP, with five moieties C25) (Figure 3.8A). As negative control, a membrane fraction preparation from cells containing the empty vector was used.

EcMenA-His recognizes all substrates except the DMAPP, with highest activity levels observed with GPP and FPP. For calculation of EcMenA-His relative activity, the ratio between the highest product area and internal standard area was set up as 100% of activity (Table 3.1).

Table 3.1: Activity of EcMenA towards different prenyl-donating substrate.

Prenyl Substrate	AUC*	Relative activity (%)
DMAPP	0	0
GPP	2 931 388	73.0
FPP	4 017 949	100
GGPP	295 065	7.33
GFPP	360 663	8.95

*AUC: area under a curve

Substrate specificity was also evaluated with respect to the aromatic substrate – prenyl acceptor. Using GPP as prenyl donor, various molecules containing the naphthoquinone ring and also 4-hydroxybenzoic acid, the substrate for UbiA and LePTG1 were tested (Figure 3.8B). In contrast to the broad range of acceptable isoprenyl pyrophosphate substrate, EcMenA showed a narrow specificity towards 1,4-dihydroxy-2-naphthoic acid and no others peaks correspondent to prenylated product were observed in the RP-HPLC using the other aromatic compounds (data not shown). Therefore, the results showed that in contrast to other aromatic prenyltransferases, EcMenA-His recognizes just DHNA-2 as prenyl acceptor.

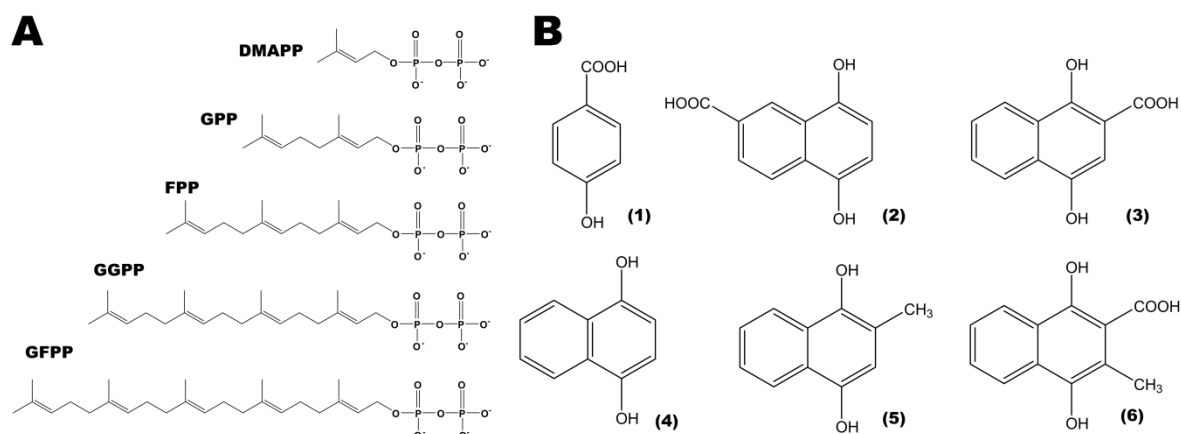


Figure 3.8. Substrates tested with EcMenA. (A) Prenyl-donor substrates. DMAPP with one isoprenoid moiety (C5), GPP with two isoprenoid moieties (C10), FPP with three isoprenoid moieties (C15), GGPP with four moieties (C20) and GFPP with five moieties (C25). **(B) Aromatic substrates.** (1) 4-hydroxybenzoic acid (PHB); (2) 1,4-dihydroxy-2-naphthoic acid (DHNA-2); (3) 1,4-dihydroxy-6-naphthoic acid (DHNA-6); (4) 1,4-dihydroxynaphthalene; (5) 1,4-dihydroxy-2-methylnaphthalene; (6) 1,4-dihydroxy-3-methyl-2-naphthoic acid.

Activity assays were also performed using purified EcMenA (after GFP removal). Purified EcMenA (37.0 μg) was incubated with DHNA-2 as prenyl acceptor and GPP/FPP as prenyl donor. As observed in the activity assays using membrane fraction, the prenylated products from DHNA-2 and GPP (Figure 3.9A, B) or FPP (Figure 3.9C, D) were detected in the RP-HPLC. HPLC product peaks obtained with purified protein showed the same retention time as from the EcMenA-His membrane fraction, indicating that EcMenA remains active after purification.

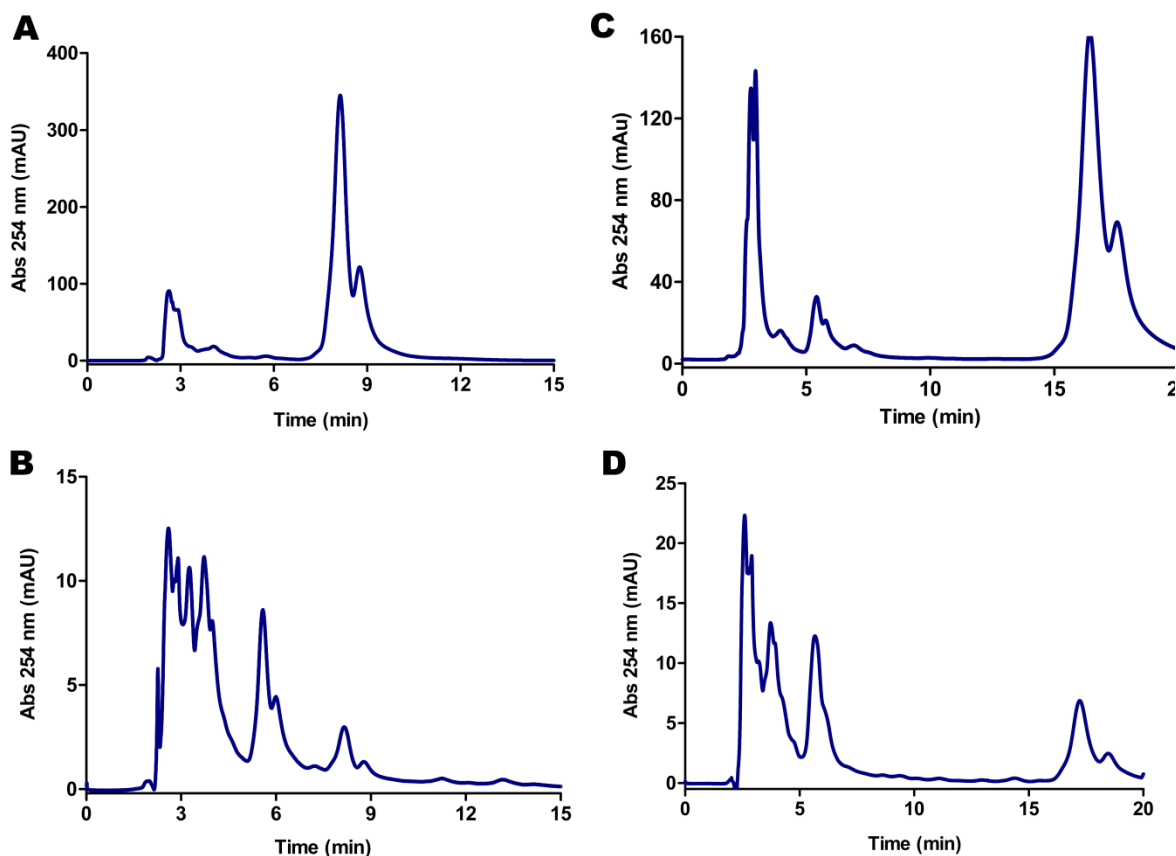


Figure 3.9. HPLC profiles of EcMenA activity assays. DHNA-2 was used as prenyl acceptor. **(A)** GFP-EcMenA membrane fraction using GPP as prenyl donor. **(B)** purified free-GFP EcMenA (37.0 μ g) with GPP. The peaks after 7 min in samples A and B indicate the formation of DMK-2 **(C)** GFP-EcMenA membrane fraction with FPP as prenyl donor. **(D)** purified free-GFP EcMenA (37.0 μ g) with FPP. The peaks after 15 min in samples C and D indicate the formation of DMK-3 that due to the longer hydrophobic chain is eluted later than DMK-2. HPLC flow rate: 0.8 mL/min

3.7. Inhibition of purified EcMenA

Ohara and co-workers (2013) demonstrated that LePTG1 is strongly inhibited by phenolic compounds that have a similar structure to its substrate, 4-hydroxybenzoic acid. The DHNA-2-prenylating activity of DDM-solubilized EcMenA was assayed in the presence of 1,4-dihydroxynaphthalene, 1,4-dihydroxy-6-naphthoic acid and 1,4-dihydroxy-2-methhlynaphthalene in a similar concentration of DHNA-2 (1.0 mM DHNA-2 and 0.85 mM potential inhibitor). As observed in figure 3.10, the naphthoquinone compounds have only slight influence on the activity of EcMenA, with 1,4-dihydroxynaphthalene and 1,4-dihydroxy-6-naphthoic acid reducing the activity by around 15 %.

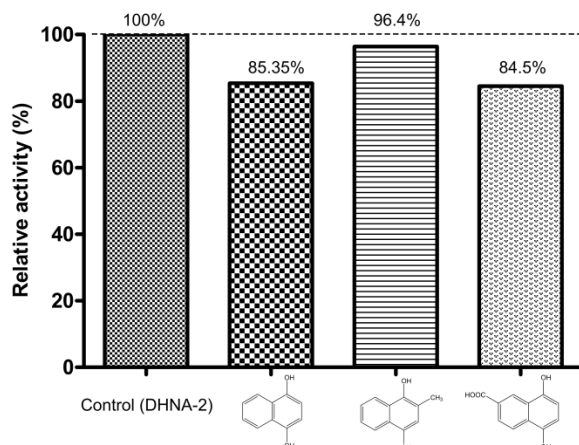


Figure 3.10. Influence of naphthoquinone compounds on EcMenA activity. Assays were performed using DHNA-2 as prenyl acceptor and GPP as prenyl donor. First bar shows the control with only DHNA-2. Second bar: 1,4-dihydroxynaphthalene, third bar: 1,4-dihydroxy-2-methylnaphthalene, fourth bar: in the presence of 1,4-dihydroxy-6-naphthoic acid.

The results demonstrate that purified EcMenA is able to catalyze the prenylation of DHNA-2. However, a significant reduction of activity was detected after the first IMAC step (data not shown). The only obvious difference after the first purification step is the high concentration of imidazole used to elute the protein. To test whether imidazole influences the activity of EcMenA, assays were carried out using samples collected during the purification (flow through, washing fraction and elution fraction). EcMenA activity is abolished in the presence of 250 mM imidazole, even though strong bands corresponding to protein were observed using immunoblotting (Figure 3.11A, B). Testing activity of EcMenA in the presence of different concentrations of imidazole (0, 20, 50, 100, 200, 250 and 500 mM) suggests that imidazole inhibits EcMenA activity with an IC_{50} of 10-20 mM (Figure 3.11C), indicating that a new strategy for purification is needed. Although purification of His-tagged proteins is usually performed in the presence of imidazole, elution with low pH or with high concentrations of EDTA is also possible (although this may strip Ni^{2+} ions from the column). Both alternative methodologies were tested to avoid the use of imidazole, but they proved ineffective for EcMenA purification (data not shown).

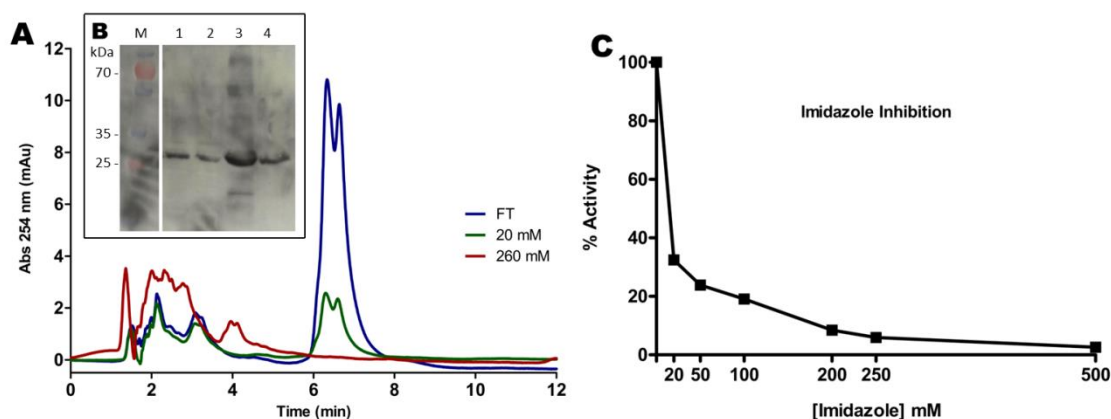


Figure 3.11. Influence of imidazole concentration on EcMenA activity. (A) HPLC profile of EcMenA activity in different fractions during the first IMAC. FT: Flow through (blue line), 20 mM imidazole (green line) and 260 mM imidazole (red line). **(B) Immunoblotting after first IMAC** shows the presence of EcMenA in all fractions. 1: Flow through, 2: washing step with 20 mM imidazole, 3: elution step with 260 mM imidazole, 4: elution step with 500 mM imidazole. Primary antibody: mouse anti-his; secondary antibody: goat anti-mouse (HRP). **(C) Imidazole concentration-dependent inhibition** demonstrates that imidazole inhibits EcMenA activity with an IC_{50} of ca. 10 mM.

3.8. Discussion

In this part of the project, methodologies for functional expression, solubilization and effective purification of EcMenA were established.

The extraction out of the membrane is considered the first challenge in the work with membrane proteins. Their removal from the lipid layer can be accomplished using either organic solvents or detergents, with the latter being the most used. Although the solubilization of membrane proteins using detergents is considered a milder method, it is a crucial step concerning the protein stability, since the solubilization may result in inactive proteins or irreversible aggregation (Arnold and Linke, 2008; Garavito and Ferguson-Miller, 2001). Due to different properties between membrane proteins, the choice of the optimal detergent to obtain stable solubilized protein is empirically determined (Ren et al., 2009). Detergent screening for EcMenA was performed with six different detergents and all of them were able to extract the protein from the membrane (Figure 3.2). Three out of the six detergents supported a detectable level of activity: DM, DDM and CHAPS. In addition, EcMenA showed to be stable in DM and DDM solution, with good activity levels observed after 15 days post-solubilization.

Purification of EcMenA (from the pET15b-TEV construct) showed significant amounts of peptidyl prolyl *cis-trans* isomerase SlyD protein as contaminant. One of the possible reasons for this contamination is the low yield of EcMenA. According to Andersen and co-workers (2013), SlyD competes for binding on Ni^{2+} and Co^{2+} resins in bacterial expression systems that yield only 0.1 – 1 mg/L of target protein, being co-purified in equivalent or higher

amounts than the target protein. Although the contamination of SlyD during the purification of recombinant proteins has been widely reported (Andersen et al., 2013; Parsy et al., 2007; Robichon et al., 2011), the presence of this protein during EcMenA preparation was unexpected, since the procedure to isolate membrane fraction through centrifugation exclude soluble proteins. However, SlyD exhibits isomerase and chaperone activities that could lead to unwanted interactions or reactions with the target protein (Parsy et al., 2007). Because of the similar molecular weights of EcMenA and SlyD, size exclusion chromatography (SEC) was not effective to separate both proteins. To circumvent this, the construct carrying the GFP protein fused with EcMenA was used. This construct provides not only a fusion protein with high molecular weight and therefore better chances to remove SlyD by chromatography, but also an indication whether SlyD interacts with by acting as a chaperone. Mass spectroscopy showed that SlyD was not found after SEC of GFP-EcMenA. In addition, CD analyses from GFP-EcMenA and EcMenA after GFP removal indicated that the protein is correctly folded. Altogether, the results suggest that SlyD does not play any role in EcMenA folding and that its presence is just a purification artifact.

Purification of EcMenA using the GFP construct was effective, even though with very low yield (0.1 – 0.3 mg/L). Low yields have been reported for several membrane proteins and has been considered the second challenge during the work with these proteins. Eshaghi and co-workers (Eshaghi et al., 2005) have classified the expression of membrane proteins in three types based on their purification yield after SEC: high expression (with yields from 3–5 mg/L culture); medium expression (with yields from 1–3 mg/L) and low expression (with yields from 0.2–1 mg/L). These amounts are approximately 1000 times less than the yields for overexpression of soluble protein (Wuu and Swartz, 2008). Despite the low yield after purification, some characterization using purified EcMenA could be carried out.

CD measurements with GFP-MenA fusion protein and after GFP removal, showed a typical α -helices behaviour, despite the known problems involving membrane proteins and CD analyses, such as choice of ideal detergent with low absorption in the far-UV and few nm shifts in the wavelength of absorption bands (Kelly et al., 2005). The results are consistent with predictions analysis and with the recent protein structures of ApUbiA and AfUbiA that showed the presence of nine transmembrane helices (Cheng and Li, 2014; Huang et al., 2014).

Earlier studies on the catalytic activity of MenA demonstrated that cell-free extracts of *E. coli* were able to convert DHNA-2 in MK-3 and/or DMK-3 in the presence of farnesyl pyrophosphate and magnesium (Bentley, 1975; Shineberg and Young, 1976). Saito & Ogura

(1981) showed, using the membrane fraction of *Micrococcus luteus* that MenA was able to accept prenyl-donor with different chain length, but was specific regarding to the aromatic substrate, since just naphthoquinones with a carboxyl group at position 2 were recognized, with better results for the DHNA-2. Purified EcMenA showed high specificity for DHNA-2 with no activity towards 1,4 dihydroxy-3-methyl-2-naphthoic acid, in contrast to the results observed for MenA from *Micrococcus luteus*.

Several pathogenic organisms such as *Mycobacterium tuberculosis* (Mtb), responsible for tuberculosis disease, use menaquinone for respiration. According to the Center for Disease Control and Prevention (CDC), tuberculosis was responsible for around 1.5 million deaths worldwide in 2013. Thus, the development of new drugs is urgent and the importance of MenA inhibitors has been highlighted in the last years. Kurosu and co-workers (2007) demonstrated that new antimycobacterial molecules were able to inhibit MenA activity, leading to bacterial death of Mtb by blocking the electron flow during the respiration. Further studies have demonstrated that the topology of the nitrogen (N) atom in the inhibitor molecules play an important role for MenA selectivity (Debnath et al., 2012). These molecules were designed with tertiary or secondary amine or hydrazine (Figure 3.12) and it is believed that the amino moiety would interact directly with Asp residues or through the divalent cations in the active site (Kurosu and Crick, 2009; Kurosu et al., 2007).

Ohara and co-workers (2013) demonstrated that several compounds containing the benzoquinone ring are able to inhibit the activity of a plant prenyltransferase LePTG1. However, similar analysis showed that no significant inhibition of EcMenA was observed in the presence of other naphthoquinone molecules. On the other hand, 20 mM of imidazole inhibited more than 50% the activity of EcMenA (Figure 3.11). A possible explanation for this inhibition could be the presence of secondary amines in the structure of imidazole (Figure 3.12), that, according to Kurosu et al., (2007), could interact with Asp residues or magnesium ions involved in the enzymatic activity. In addition, Rosenberg, 2013 reported that, although the complex formation between imidazole and magnesium is weak, high imidazole concentration is able to destabilize the protein-metal complex.

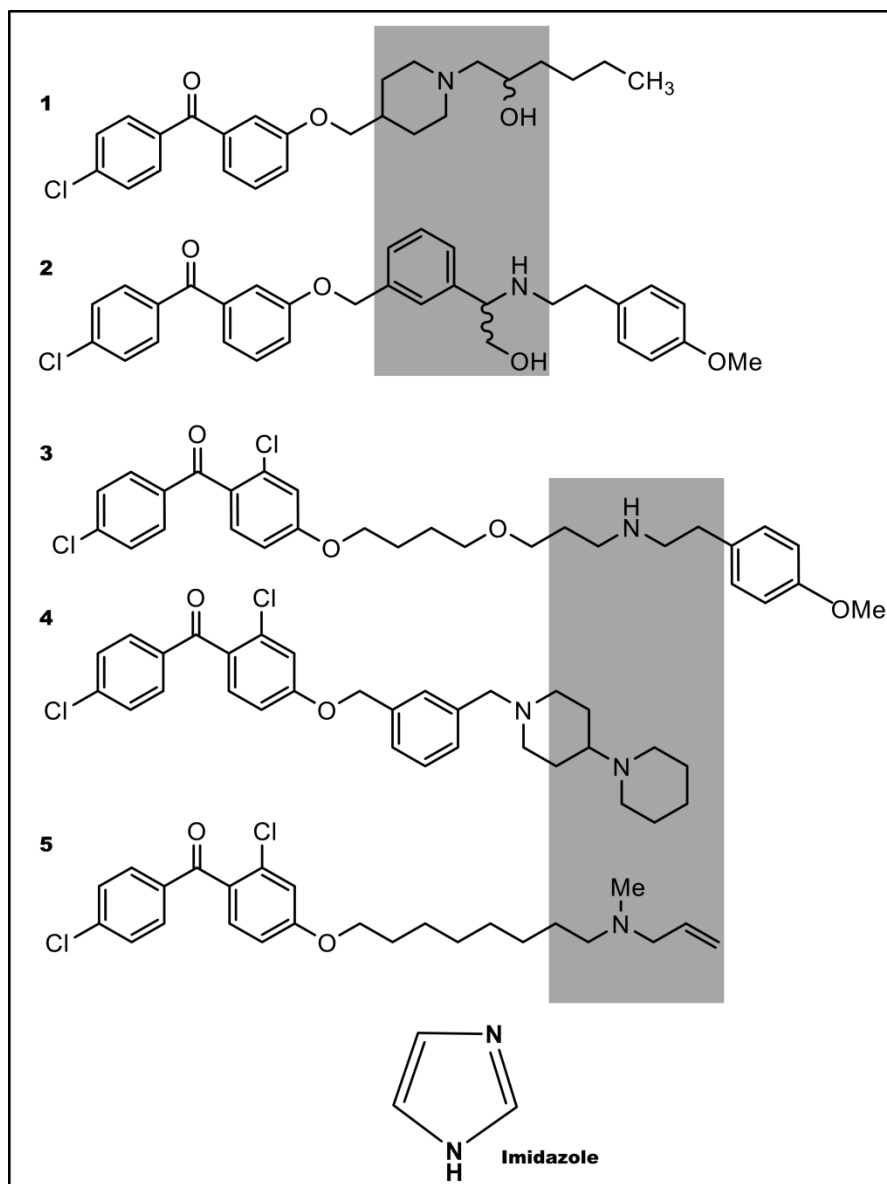


Figure 3.12. MenA inhibitors designed by Debnath et al., 2012. The topology of the nitrogen atom in the inhibitor (shown in gray) plays a role in bactericidal activities. Molecules 1 and 2 inhibit *M. tuberculosis* growth and molecules 3-5 inhibit *M. tuberculosis* and *S. aureus* growth (Debnath et al., 2012, modified). Imidazole molecule showing the presence of secondary amines.

4. Expression and characterization of a homolog of 4-hydroxybenzoate octaprenyltransferase (UbiA) from *Thermus thermophilus* (TtUbiA)

4.1. Identification of UbiA/ MenA homologs in *Thermus thermophilus*

Different to the Gram-negative organisms, which possess ubiquinone (UQ) as mobile electron carrier in the electron transport chain, *Thermus thermophilus* contains just menaquinone (MK) as the sole quinone (Cava et al., 2008; Mooser et al., 2006). In agreement with this, a BLAST sequence search (Altschul et al., 1990) revealed that important genes involved in the biosynthesis of ubiquinone (such as *ubiC*) are absent in this strain. Furthermore, genome analyses showed that *T. thermophilus* does not have the *men* genes important for the formation of MK via classical pathway (Hiratsuka et al., 2008, 2009). Instead, an alternative pathway for the biosynthesis of menaquinone, the futasoline pathway, is utilized, involving products of the *mqn* genes (Hiratsuka et al., 2008; Li et al., 2011).

As prenylation is a crucial step in ubiquinone and menaquinone biosynthesis, it is expected that a prenyltransferase related to MenA/UbiA should be present in the futasoline pathway. In order to identify a possible enzyme in *Thermus thermophilus*, BLAST searches were performed using MenA sequences from *Escherichia coli*, *Bacillus subtilis* as well as *Mycobacterium tuberculosis*. However, no significant similarities could be found, indicating the absence of a MenA homolog in this strain. In contrast, BLAST searches performed using the UbiA sequence from *E. coli* (EcUbiA) resulted in two hits in *T. thermophilus*: a putative protoheme IX farnesyltransferase (Q72H22) and a putative 4-hydroxybenzoate polyprenyltransferase (Q72L23). The former sequence, which corresponds to a protein of 608 amino acids (section 8.3), appears to be a genetic fusion of two integral membrane proteins: CtaA and CtaB (*Bacillus subtilis* nomenclature) that are both essential in the biosynthesis of heme A, the prosthetic group of respiratory oxidases (Svensson et al., 1993). Thus, the 285 amino acid putative 4-hydroxybenzoate polyprenyltransferase (TtUbiA) (section 8.3) was chosen for further studies as a potential aromatic prenyltransferases in *Thermus thermophilus*.

4.2. Recombinant expression of *Thermus thermophilus* UbiA (TtUbiA) in *E. coli*

The gene for expression of TtUbiA in *E. coli* cells was inserted in four plasmids: pET15b-TEV and pET21a with N-terminal and C-terminal His₆-tag, respectively, and pNGFP-BC and pCGFP-BC for expression of a fusion protein with GFP and His₆-tag at N-terminal and C-terminal, respectively (Kawate and Gouaux, 2006). Expression levels were tested in small scale (50 mL) in different strains – BL21 (DE3), Rosetta (DE3), C43 (DE3) and Tuner (DE3) cells. Initial results showed low level or no expression in constructs using pET21a and pCGFP-BC vectors. The predicted topology of TtUbiA (Figure 4.1) suggests that the N-terminus is localized in the bacteria cytoplasm and the C-terminus in the periplasm, which could be a possible explanation for the low expression of TtUbiA in these constructs. Expression of TtUbiA using the pNGFP-BC vector showed a reasonable small scale expression level; however this was not reproducible in large scale (6 L). Good expression levels using the pET15b-TEV vector were obtained in BL21 (DE3) and Rosetta (DE3) strains, although a decrease was also observed when expressed in 6 L (data not shown).

Analysis of the codon usage (Figure 8.4) showed that the amount of AGG, a codon that codifies arginine in TtUbiA, is below 10% in several *E. coli* strains (Fuhrmann et al., 2004). The pRARE vector, a chloramphenicol resistance vector found in Rosetta (DE3) strains, encodes tRNA genes for the most common rarely used codons encoding Arg, Ile, Gly, Leu and Pro and is compatible with pET expression vectors (Novy et al., 2001). Large scale expressions of TtUbiA were therefore carried out in Rosetta (DE3) strains containing the pRARE vector in the presence of ampicillin (100 µg/mL) and chloramphenicol (30 µg/mL).

Figure 4.2 shows the results of overnight expression of TtUbiA at 30 °C. The immunoblotting detected a protein band around 25 kDa, although the estimated molecular mass of TtUbiA is 33 kDa. This behavior has been described for membrane proteins in SDS-PAGE gels and was also observed for EcMenA (section 3.1).

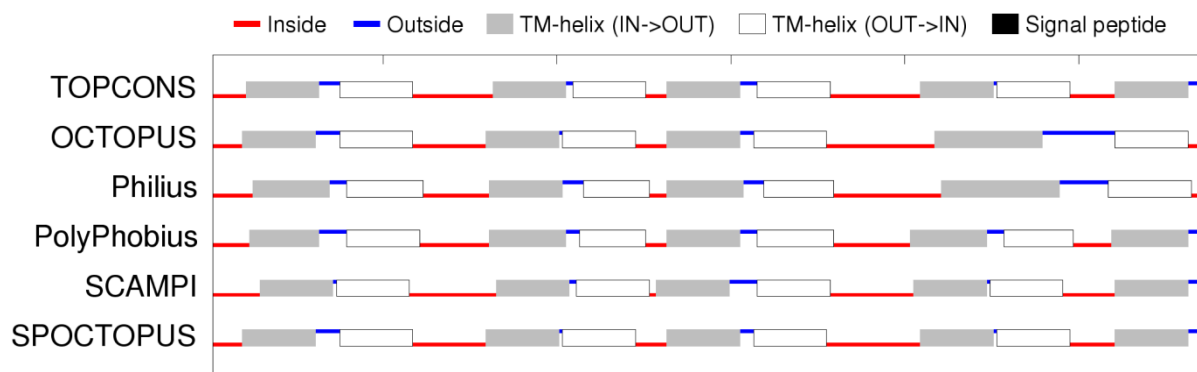


Figure 4.1. Predicted topology of TtUbiA. Topology prediction programs suggest the presence of eight to nine transmembrane helices. The consensus topology (according to the TOPCONS program (Bernsel et al., 2009)) suggests nine helices, with the N-terminus localized in the cytoplasm (shown in red) and the C-terminus in the periplasm (shown in blue).

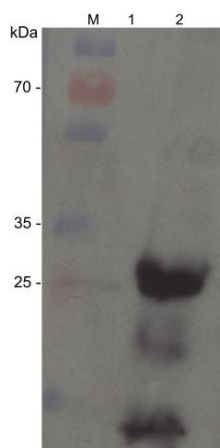


Figure 4.2. Immunoblotting analysis of His-tagged TtUbiA after large scale expression in Rosetta (DE3). M: Spectra multicolor broad range protein marker, 1: before induction, 2: after overnight expression with 0.3 mM IPTG at 30 °C. The band indicates expression of TtUbiA (~ 25 kDa). Primary antibody: mouse anti-his; secondary antibody: goat anti-mouse (HRP).

4.3. TtUbiA exhibits neither 4-hydroxybenzoate octaprenyltransferase (UbiA) nor 1,4-dihydroxy-2-naphthoic acid (MenA) activity

The gene for TtUbiA is annotated as a 4-hydroxybenzoic acid prenyltransferase. The prenylation of 4-hydroxybenzoic acid (PHB) by EcUbiA in the presence of magnesium and geranyl pyrophosphate (GPP) and farnesyl pyrophosphate (FPP) as prenyl-donors has been reported (Bräuer et al., 2008; Melzer and Heide, 1994).

The initial activity of the TtUbiA membrane fraction was investigated as described in 2.4.6.1, using an EcUbiA membrane fraction, kindly provided by Dr. Annett Weidner, as positive control. Assays were carried out using PHB and GPP as prenyl-acceptor and prenyl-donor, respectively. The product of the reaction (3-geranyl-4-hydroxybenzoate) was followed by RP-HPLC using 4-phenylphenol (4PP) as internal standard. Initial HPLC results from the reaction using EcUbiA showed the presence of a peak after 6 minutes, indicating the formation of a prenylated product (Figure 4.3A), which was confirmed by mass spectrometry (Figure 8.5). Using the same conditions to evaluate the activity of TtUbiA, no peak or prenylated product was observed in the HPLC profile (Figure 4.3A). As *T. thermophilus* cells grow at high temperatures, it might be that TtUbiA is not active at 37 °C and that higher temperatures are necessary for activity assays. Although appropriate temperatures for *T. thermophilus* enzymes vary between 80 °C - 90 °C, experiments at such high temperatures are not suitable for the cell membrane of *E. coli*. As a compromise, assays at temperatures up to 60 °C were carried out. No peak could be detected in the HPLC chromatogram after 6 minutes (data not shown), suggesting that TtUbiA might not be active in the *E. coli* cell membrane.

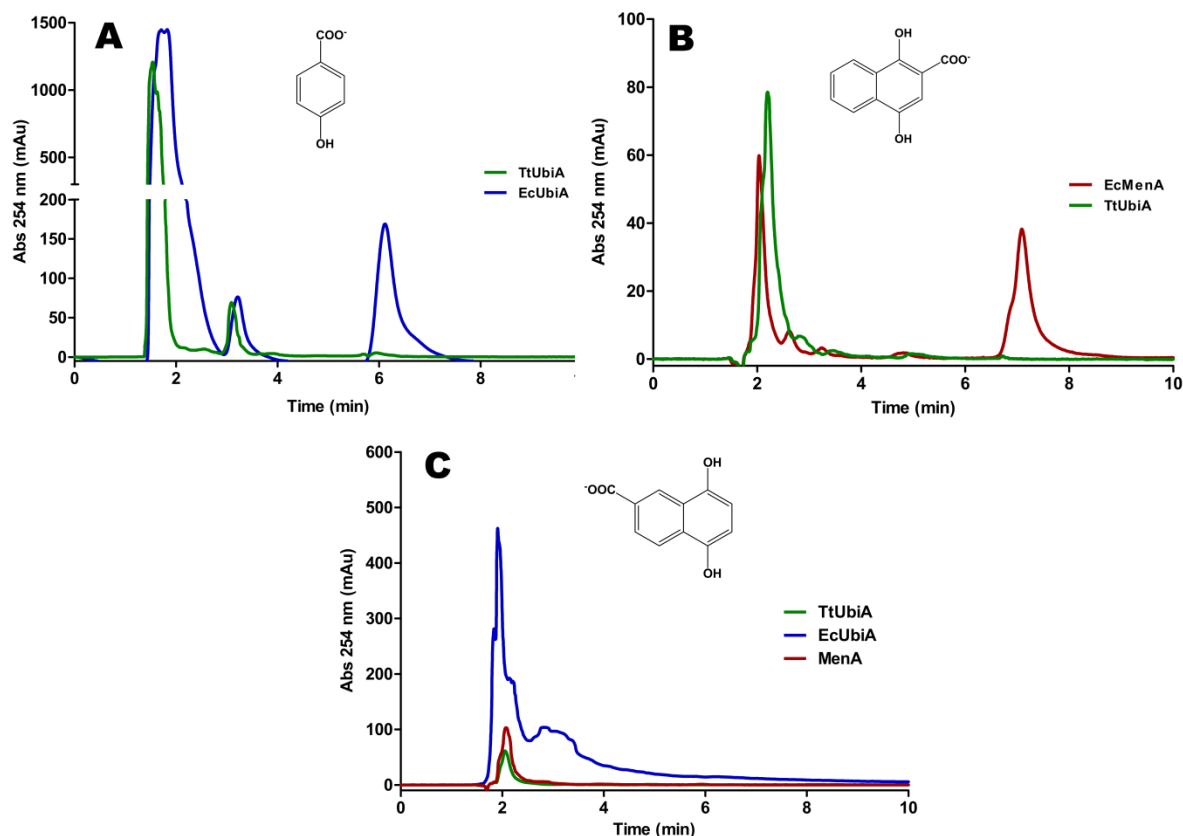


Figure 4.3. HPLC profiles of the reaction catalyzed by UbiA and MenA enzymes. (A) HPLC profile of UbiA assay conditions using PHB as aromatic substrate. Blue line shows the result obtained after reaction using EcUbiA membrane fraction. The peak observed after 6 min corresponds to 3-geranyl-4-hydroxybenzoate, the prenylated form of PHB. Green line shows the result using TtUbiA membrane fraction. No product peak was detected. **(B) HPLC profile of MenA assay conditions using DHNA-2 as aromatic substrate.** Red line shows the result after reaction with EcMenA membrane fraction. The peak observed around 7 min corresponds to demethylmenaquinone-2 (DMK-2). Green line shows the result after reaction using TtUbiA membrane fraction. **(C) HPLC profile using DHNA-6 as aromatic substrate.** Green line corresponds to TtUbiA membrane fraction, blue line to EcUbiA membrane fraction and red line to EcMenA membrane fraction. All assays were performed at 37 °C using GPP as prenyl-donor. HPLC flow rate: 1.0 mL/min.

As *T. thermophilus* uses menaquinone in the respiratory chain, the MenA substrate 1-4-dihydroxy-2-naphthoic acid (DHNA-2) was also tested as described in section 2.4.6.2. In contrast to the positive control (EcMenA), no prenylation of DHNA-2 by TtUbiA was observed (Figure 4.3B). Inspection of the futasolone pathway suggests that 1,4-dihydroxy-6-naphthoic acid (DHNA-6) as a potential more suitable substrate for TtUbiA; once again, however no activity could be measured (Figure 4.3C).

Not all enzymes necessary for formation of MK via futasolone pathway have been identified, nor the reaction sequence is completely clear. MqnD catalyzes the conversion of cyclic dehypoxanthine futasolone into 1,4-dihydroxy-6-naphthoate (DHNA-6), which is then thought to undergo prenylation, methylation and decarboxylation (Arai et al., 2009; Hiratsuka et al., 2008). As DHNA-6 does not appear to be a substrate for TtUbiA, three additional compounds

were tested (Figure 3.8B): 1,4-dihydroxynaphthalene (on the assumption that a decarboxylation reaction might take place first), 1,4-dihydroxy-2-methylnaphthalene (assuming that a methylation and decarboxylation might occur prior to prenylation) and 1,4-dihydroxy-3-methyl-naphthoic acid (assuming that methylation takes place first). TtUbiA activity was tested towards all the molecules using different prenyl-donors (Figure 3.8A), but no prenylated products could be observed (data not shown).

4.4. The lack of activity is not due to the membrane composition

E. coli and *T. thermophilus* possess very different membrane compositions. The cell membrane of *T. thermophilus* contains a special type of carotenoid (thermozeaxanthin) that to date has been exclusively found in *Thermus ssp* (Hara et al., 1999; Tian and Hua, 2010; Yokoyama et al., 1995). Thermozeaxanthin is an ester of zeaxanthin with a glucose moiety esterified to fatty acids. The carotenoid is anchored in the membrane, with the zeaxanthin moiety located in the hydrophobic core of the lipid bilayers, the glucose moiety anchored in the hydrophilic head group region and the branched fatty acids moieties curling back into the lipid bilayer, creating a “hook” as illustrated in Figure 4.4 (Hara et al., 1999). The presence of such carotenoids in the membrane of *T. thermophilus* leads to a decrease in the membrane fluidity and an increase in stability, which is necessary for membrane function at high temperatures (Hara et al., 1999, 2008). The presence of thermozeaxanthin in the cell membrane could therefore increase the stability of membrane proteins and thereby influence their activities at high temperatures (Tian and Hua, 2010).

Although the production of carotenoids in *E. coli* cells has been described, this is not trivial, as more than five genes are involved in their biosynthesis (Lemuth et al., 2011; Ruther et al., 1997). Moreover, although the production of zeaxanthin has been successful described in

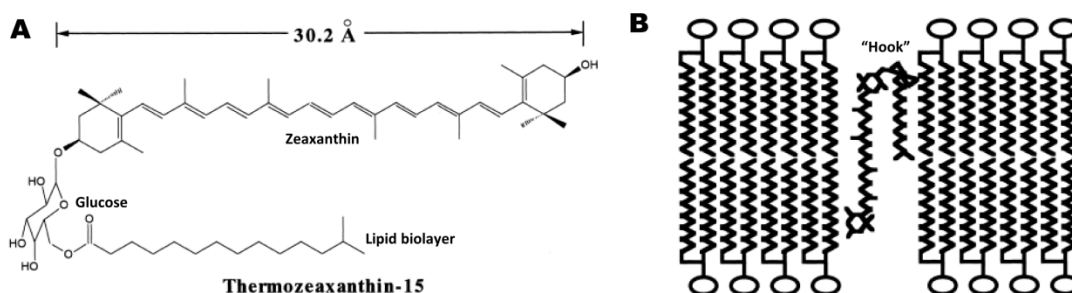


Figure 4.4. Carotenoid thermozeaxanthin found in *Thermus ssp*. (A) Structure of thermozeaxanthin, including the zeaxanthin, the monoglucose ester and the branched fatty acids moieties. (B) Schematic representation of thermozeaxanthin incorporated in the cell membrane. The zeaxanthin moiety is located in the core of the lipid bilayer, whereas the glucose moiety is oriented to the hydrophilic region and the branched fatty acids moiety curves back into the membrane forming a hook (Hara et al., 1999).

E. coli, the production of thermozeaxanthin has not been reported (Misawa and Shimada, 1997; Ruther et al., 1997). In order to test whether the membrane architecture plays a role in the activity of TtUbiA expressed in *E. coli*, the putative UbiA homolog from *Streptomyces lividans* (SIUbiA) was chosen for cloning and expression in *S. lividans* cells.

4.4.1. Cloning, expression and activity assay of SIUbiA

Streptomyces spp are Gram-positive bacteria that use MK for the transport of electrons. Several studies have demonstrated that *Streptomyces spp* synthesize MK via the futasolone pathway (Dairi, 2012; Hiratsuka et al., 2008; Seto et al., 2008). BLAST results using the UbiA homologs from *E. coli* and *T. thermophilus* found the putative 4-hydroxybenzoate polyprenyltransferase (UbiA) as the probable aromatic prenyltransferase involved in the biosynthesis of quinone in this organisms. The gene from *S. lividans* (SIUbiA) shares 47% sequence identity with TtUbiA and just 25% with EcUbiA. Thus, expression of SIUbiA in *S. lividans* TK24 cells allows the evaluation of prenyltransferases activity in the corresponding cell membrane.

SIUbiA was cloned into the pUWL201-PW vector (Figure 8.6) using the restriction enzymes *Bam*HI and *Nde*I. The pUWL201-PW vector contains a C-terminal His₆-tag and uses thiostrepton as antibiotic as well as protein inducer (Doumith et al., 2000). For large scale (4L) expression, Erlenmeyer flasks with four baffles were used to improve the aeration, yielding around 20-22 g of biomass. Since optical density (OD) measurements of *S. lividans* culture were not possible due to the spore suspension, expression levels were checked by immunoblotting of the membrane fraction. The membrane fraction was prepared as described in 2.4.4.1 and resuspended in Tris buffer (50 mM Tris/HCl pH 8.5; 150 mM KCl). As shown in Figure 4.5A, immunoblotting detected bands around 32 kDa, the expected molecular mass of SIUbiA.

Activity of the SIUbiA membrane fraction was first assayed using PHB and GPP as prenyl-acceptor and prenyl-donor respectively, under UbiA assay conditions (2.4.6.1). Figure 4.5B shows that no product could be detected, as observed for the TtUbiA activity assays. Further assays were performed using DHNA-2 and DHNA-6 as prenyl-acceptors and different prenyl-donors with longer side chain (GGPP and GFPP) under MenA assay conditions. However, the enzyme did not prenylate DNHA-2 or DHNA-6 (Figure 4.5C, D) with any prenyl-donor. The lack of activity of SIUbiA expressed in *S. lividans* cells suggests that the difference in membrane composition in *E. coli* and *T.thermophilus* is not responsible for the lack of activity

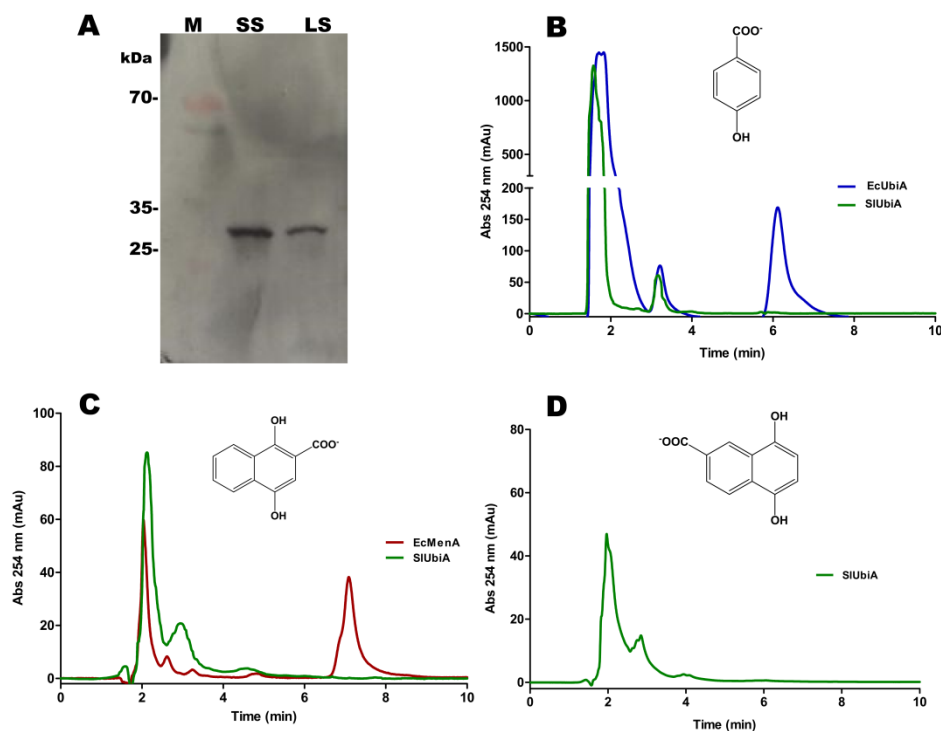


Figure 4.5. Expression and activity assay of SIUbiA. (A) Immunoblotting of SIUbiA after expression in *S. lividans* cells. M: Marker; SS: Small scale expression was carried out in 20 mL, whereas LS: large scale expression was carried out in 4 L. Expressions were performed for 3 days at 30 °C. Bands of SIUbiA were detected with molecular weight of 30 kDa. Primary antibody: mouse anti-his; secondary antibody: goat anti-mouse (HRP). **(B) HPLC profile of SIUbiA activity under UbiA assay condition.** Blue line corresponds to EcUbiA, which was used as positive control and green line corresponds to SIUbiA. The peak observed after 6 min corresponds to the prenylated product of PHB. **(C) HPLC profile of SIUbiA activity under MenA assay conditions using DHNA-2 as aromatic substrate.** Green line corresponds to SIUbiA and red line to EcMenA (positive control). The peak after 7 min corresponds to DMK-2, the prenylated form of DHNA-2. **(D) HPLC profile of SIUbiA activity under MenA assay conditions using DHNA-6 as aromatic substrate.** All assays were carried out at 37 °C. HPLC flow rate: 1.0 mL/min.

of TtUbiA. To check whether prenyltransferase activity is compatible with the membrane of *S. lividans*, EcMenA was cloned and expressed in *S. lividans* cells and its catalytic activity towards DHNA-2 was tested.

4.4.2. Cloning, expression and activity assays of EcMenA in *S. lividans* TK24 cells

The EcMenA gene was isolated from the pET15b-TEV vector with *Bam*HI and *Nde*I enzymes and ligated into the previously digested pUWL201-PW vector. Small scale expression was carried out in 3% (w/v) CASO-Bouillon media for 3 days and the membrane fraction prepared as previously described (section 2.4.4.1). The expression of EcMenA in *S. lividans* cells was similar to that observed in *E. coli* cells (Figure 4.6A). Activity assays using the membrane fraction were performed in the presence of DHNA-2 and GPP as substrates, using EcMenA expressed in *E. coli* as positive control. RP-HPLC analysis of EcMenA expressed in *S. lividans*

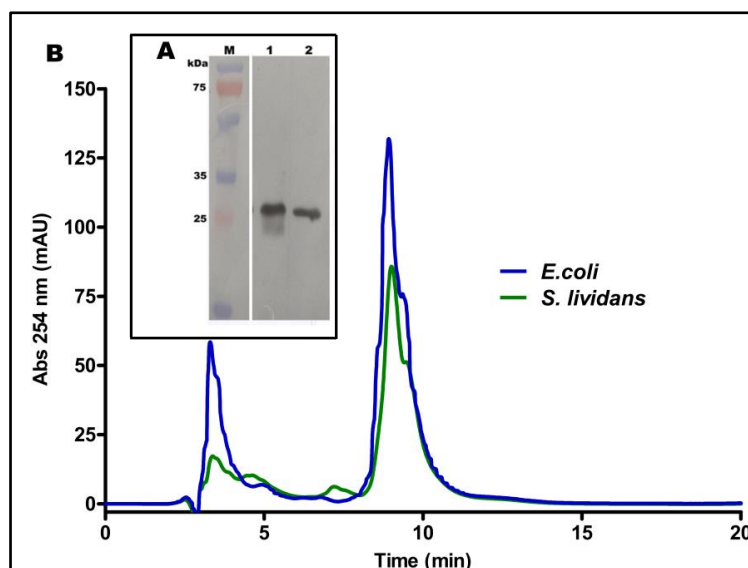


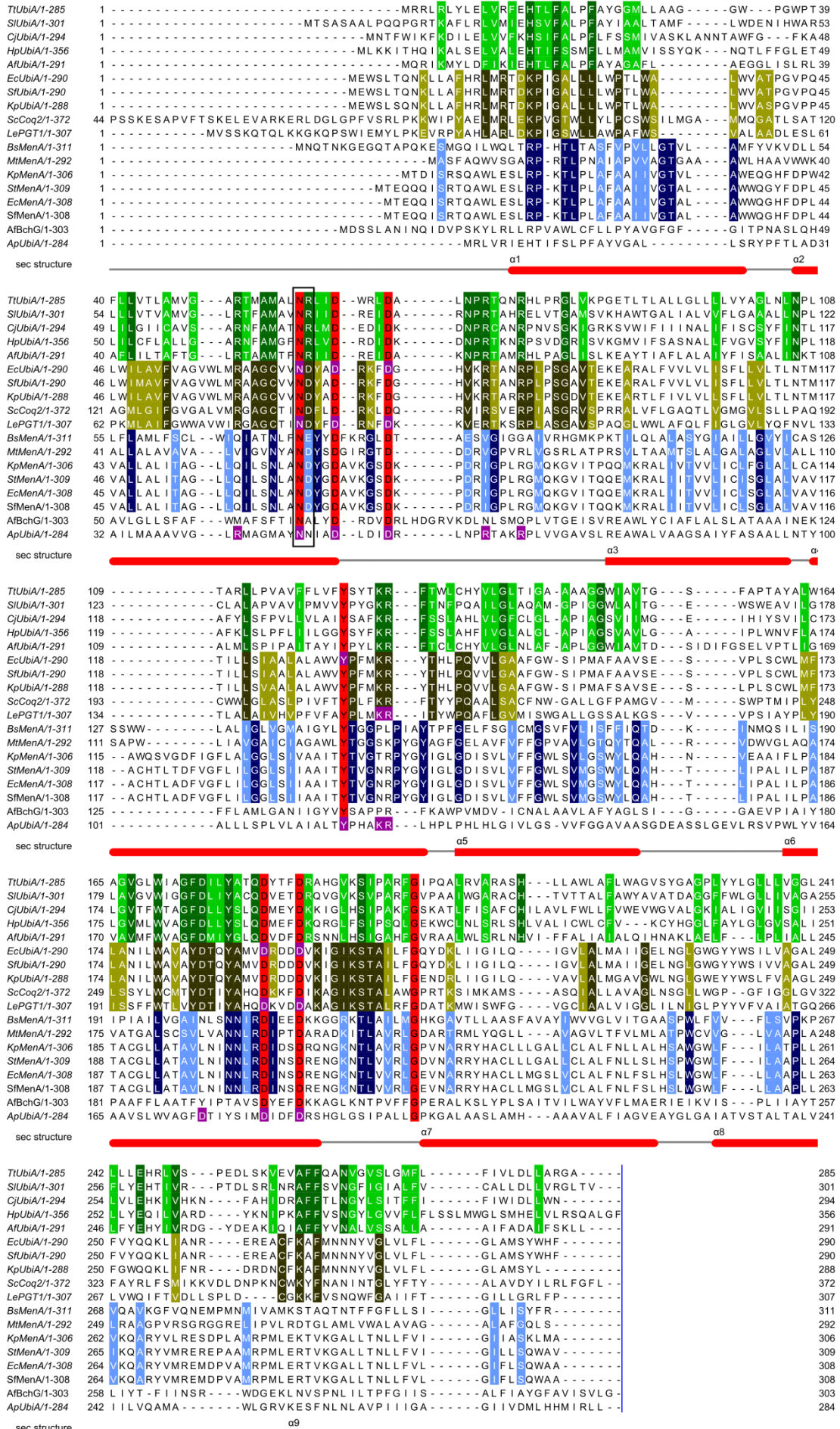
Figure 4.6. Expression and activity assay of EcMenA expressed in *Streptomyces lividans* TK 24 cells. (A) Immunoblotting showing the expression of EcMenA. M: Spectra multicolor broad range protein marker, 1: membrane fraction of *S. lividans* TK24 cells containing EcMenA, 2: membrane fraction of *E. coli* cells containing EcMenA. Primary antibody: mouse anti-his; secondary antibody: goat anti-mouse (HRP) (B) HPLC profile of EcMenA activity assay. Assays were performed at 37 °C. Blue line corresponds to EcMenA expressed in *E. coli* and green line corresponds to EcMenA expressed in *S. lividans* cells. The presence of a peak after 9 min using both membrane fractions indicates product formation. HPLC flow rate: 0.7 mL/min.

showed the presence of a peak after 9 minutes, the same retention time as the peak observed for EcMenA expressed in *E. coli* (Figure 4.6B), indicating formation of the prenylated form of DHNA-2. The results show that the cell membrane of *S. lividans* is able to support prenyltransferase activity, demonstrating that the lack of activity of SIUbiA expressed in *S. lividans* (or TtUbiA expressed in *E. coli*) is not due to different membrane composition.

4.5. TtUbiA and SIUbiA belong to a distinct class of aromatic prenyltransferases associated with the futasolone pathway

Although the catalytic mechanism for the UbiA superfamily prenyltransferases remains unclear, it is known that several regions are conserved, such as the two aspartate-rich motifs (DDXXD) that are thought to chelate magnesium ions and bind the substrate (Heide, 2009; Yazaki et al., 2009). Ohara and co-workers (2009) have identified several amino acids important for the catalytic activity of prenyltransferases using LePGT1, an aromatic prenyltransferase found in plants. These amino acids are also conserved in TtUbiA and SIUbiA (Figure 4.7, shown in purple) with the exception of Arg59 in TtUbiA and Arg73 in SIUbiA, where the 4-hydroxybenzoate octaprenyltransferases (*bona fide* UbiA) and MenA homologs have an aspartate. Further analyses showed that all “UbiAs” associated with the futasolone pathway have an arginine at this position. Mutation of the corresponding Asp84 in

Chapter 4: TtUbiA - a novel prenyltransferase associated with the futasoline pathway



Chapter 4: TtUbiA - a novel prenyltransferase associated with the futasoline pathway

Figure 4.7. Sequence alignment of three classes of prenyltransferases. Protein were aligned by MUSCLE (Edgar, 2004) and optimized in Jalview (Waterhouse et al., 2009). Green color shows the conserved residues in UbiAs associated with the futasoline pathway. Brown color shows the residues conserved in *bona fide* UbiAs. Blue color shows the conserved residues in MenA homologs. In red are shown the residues conserved in all prenyltransferases. Secondary structure is shown based on the crystal structure of ApUbiA. The aligned sequences from top to bottom are: UbiA from *Thermus thermophilus* (TtUbiA) (Q72L23), UbiA from *Streptomyces lividans* (SIUbiA) (D6EGY8), UbiA from *Campylobacter jejuni* (CjUbiA) (Q0PBX3), UbiA from *Helicobacter pylori* (HpUbiA) (JQ362), UbiA from *Archaeoglobus fulgidus* (AfUbiA) (O28106), UbiA from *Escherichia coli* (EcUbiA) (P0AGK1), UbiA from *Shigella flexneri* (SfUbiA) (Q83IP7), UbiA from *Klebsiella pneumoniae* (KpUbiA) (A6TGU9), COQ2 from *Saccharomyces cerevisiae* (ScCoq2) (P32378), LePTG1 from *Lithospermum erythrorhizon* (Q8W405), MenA from *Bacillus subtilis* (BsMenA) (P39582), MenA from *Mycobacterium tuberculosis* (MtMenA) (P9WIP3), MenA from *Klebsiella pneumonia* (KpMenA) (R4Y411) MenA from *Salmonella typhi* (StMenA) (Q8Z2Y9), MenA from *Escherichia coli* (EcMenA) (P32166), MenA from *Shigella flexneri* (SfMenA) (Q83PD5), bacteriochlorophyll synthase from *Archaeoglobus fulgidus* (AfBchG) (O28625) and UbiA from *Aeropyrum pernix* (ApUbiA) (Q9YBM8). Box shows the position of R59 (TtUbiA); D65 (EcMenA) and N51 (ApUbiA).

LePTG1 to alanine or glutamine leads to loss of catalytic activity, whereas a high level of activity was detected after mutation to glutamate, suggesting that an acidic amino acid is essential at this position (Ohara et al., 2009). Thus, the lack of activity for TtUbiA and SIUbiA may be due to the presence of this basic amino that is common to prenyltransferases associated with the futasoline pathway. The recent X-ray structures of ApUbiA and AfUbiA (Cheng and Li, 2014; Huang et al., 2014) show that this residue is located near the binding pocket, so that it could influence substrate binding (Figure 4.8). In order to evaluate whether the change from aspartate to arginine at this position affects the activity of TtUbiA and SIUbiA, mutants were generated by site-direct mutagenesis (TtUbiAR59D and SIUbiAR73D). Conversely, the mutation aspartate to arginine was made in EcMenA (EcMenAD65R) to investigate the influence of this amino acid on the activity of MenA homologs. To avoid possible endogenous activity of MenA, *menA* knockout cells were produced by P1 transduction for further activity assays.

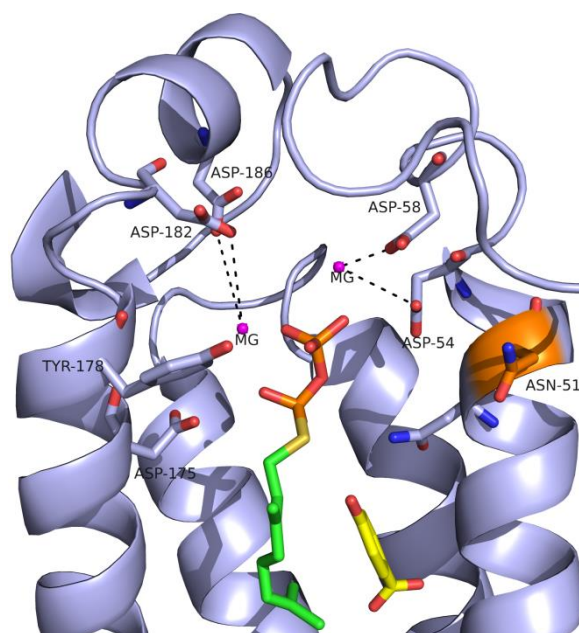


Figure 4.8. Binding pocket of ApUbiA. The structure of ApUbiA (PDB: 4OD5) shows the presence of two Mg^{2+} ions (magenta spheres) bound to the two DDXXD motifs, geranyl S-thiolodiphosphate (GSPP) molecule (green and orange sticks) and modeled PHB (yellow sticks). Asn51 (orange) localized nearby the catalytic pocket indicates the position of the amino acid corresponding to Arg59 in TtUbiA characteristic of “UbiA”s associated with the futasoline pathway.

4.5.1. TtUbiA and its mutants are unable to complement for EcMenA in *E. coli*

4.5.1.1. Expression of mutants in a *menA*⁻ deletion strain

For P1 transduction, the *E. coli* strain JW3901-1 (a Keio strain with the *menA* gene replaced by the kanamycin cassette (Baba et al., 2006)) was used as donor strain and Rosetta-gami (DE3) pLysS as receptor strain. Transduction was performed as described in 2.3.8 and confirmed by PCR and sequencing. The new Rosetta-gami (DE3) pLysS $\Delta menA$ knockout strain was able to grow in the presence of chloramphenicol and kanamycin, and expression tests carried out in LB media confirmed the expression of TtUbiA, EcMenA and their mutants in the Rosetta (DE3) pLysS $\Delta menA$ cells (Figure 4.9). In addition, SIUbiAR73D could be expressed in *S. lividans* cells (Figure 4.9C).

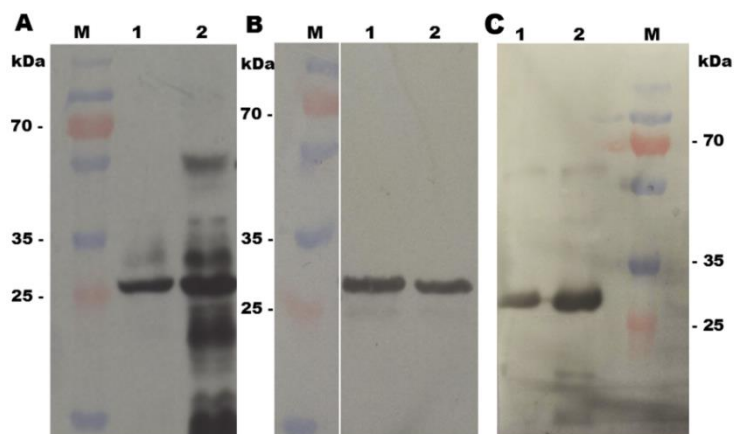


Figure 4.9. Immunoblotting showing the expression of mutant proteins. (A) Expression of TtUbiA and TtUbiAR59D after overnight expression in Rosetta gami (DE3) pLySs $\Delta menA$ cells. Lane 1 shows the expression of TtUbiA and lane 2 shows the expression of TtUbiAR59D. **(B) Expression of EcMenA and EcMenAD65R** after overnight expression in Rosetta gami (DE3) pLySs $\Delta menA$ cells. Lane 1 corresponds to EcMenA and lane 2 corresponds to EcMenAD65R. Expressions were carried out at 30 °C in the presence of 0.3 mM IPTG. **(C) Expression of SIUbiA and SIUbiAR73D** in *S. lividans* TK24 cells. Lane 1 corresponds to SIUbiA and lane 2 corresponds to SIUbiAR73D. Expression was performed in the presence of thiostrepton (25 μ g/mL) at 30 °C for three days. Primary antibody: mouse anti-his; secondary antibody: goat anti-mouse (HRP)

4.5.1.2. Activity assay of mutants

Activity assays using membrane fraction from Rosetta (DE3) pLySs $\Delta menA$ cells overexpressing TtUbiA, EcMenA or their variants were carried out according to section 2.4.6.2 using DHNA-2 and GPP as substrates. The HPLC profile from $\Delta menA$ cells expressing wild type EcMenA confirmed the activity of the recombinant enzyme (Figure 4.10), whereas the variant EcMenAD65R is inactive, indicating that Asp65 is essential for the catalytic activity of MenA prenyltransferases in agreement with the results observed in LePTG1 (Ohara et al., 2009). No activity could be observed for TtUbiAR59D or SIUbiAR73D against any of the potential substrates shown in Figure 3.8B (data not shown).

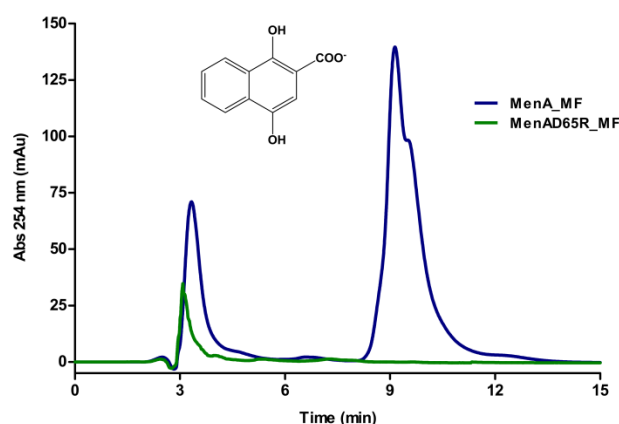


Figure 4.10. HPLC profiles of the reaction catalyzed by the EcMenA enzyme. Assays were performed using membrane fractions containing proteins overexpressed in Rosetta (DE3) pLySs $\Delta menA$ cells. Using DHNA-2 and GPP as substrates, the presence of a peak after 9 minutes corresponding to the prenylated product confirms the activity of wild type EcMenA (blue line). The variant EcMenAD65R (green line) is inactive.

4.5.1.3. TtUbiA is unable to complement for MenA

E. coli cells have a highly versatile respiratory chain that allows them to adapt to altering conditions of oxygen concentration and redox state (Bekker et al., 2007; Portnoy et al., 2010). Under aerobic conditions, electrons are transferred from NADH to oxygen by ubiquinone (UQ), whereas under anaerobic conditions, electrons are transferred from NADH to succinate via menaquinone (MK) (Portnoy et al., 2010). Thus, deletion of the *menA* gene in Rosetta gami (DE3) pLySs should result in disruption of MK biosynthesis leading to compromised bacterial growth under anaerobic conditions.

Genetic complementation assays were performed using transformation of pET15b-TEV-TtUbiA, pET15b-TEV-TtUbiAR59D, pNGFP-BC-EcMenA and pET15b-TEV-EcMenAD65R to Rosetta (DE3) pLySs $\Delta menA$. Under aerobic conditions in M9 minimal medium, all proteins were expressed in the presence of IPTG (Figure 8.7). Cells harboring the *TtubiA*, *TtubiAR59D*, *EcMenA* and *EcmenAD65R* genes were incubated for 72 h under anaerobic conditions in M9 minimal medium using glycerol and fumarate as electron donor and acceptor, respectively. Although cells containing the wild type Rosetta gami (DE3) pLySs were able to grow under anaerobic conditions (Figure 4.11), this was not possible after deletion of *menA* gene. This could be complemented in the presence of the pNGFP-BC-MenA construct, where cell growth was observed. On the other hand, cells containing the TtUbiA and TtUbiAR59D constructs failed to grow, indicating that these enzymes are not able to rescue the biosynthesis of MK. The same result was observed for the EcMenAD65R mutant, where the mutation from aspartate to arginine also inhibits the formation of MK *in vivo*.

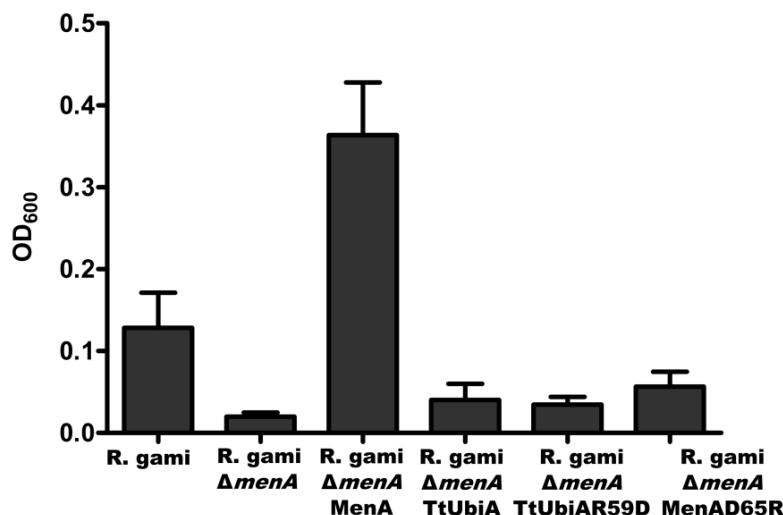


Figure 4.11. *In vivo* complementation assays. Cells were incubated in M9-minimal media with 0.5 mM IPTG under anaerobic conditions for 72 h using glycerol and fumarate as electron donor and acceptor, respectively. R. gami corresponds to Rosetta gami wild type; $\Delta menA$ corresponds to Rosetta gami cells after *menA* deletion. The presence of TtUbiA, TtUbiAR59D and EcMenAD65R in the pET15b-TEV vector and EcMenA in the pNGFP-BC vector were evaluated with respect to their ability to complement deletion of *menA* gene.

4.6. Solubilization and purification of TtUbiA

TtUbiA was extracted from the cell membrane as described in 2.4.4.2 in the presence of various detergents (DM, DDM, β -OG, CHAPS, LDAO and Cymal-6). The immunoblotting showed that DM, DDM, β -OG and Cymal-6 were able to solubilize TtUbiA, whereas no bands were detected after solubilization using CHAPS and LDAO (Figure 4.12A). Protein concentration measurements using the RC-DC (reducing agent and detergent compatible) Bio-Rad kit showed that the highest protein concentration was found using CHAPS (Figure 4.12B), although no band corresponding to TtUbiA was observed in the immunoblotting after solubilization with this detergent. DDM and Cymal-6 also resulted in suitable amounts of protein after solubilization, although a more intense band was detected using Cymal-6. Since DDM is the detergent most indicated for crystallization of membrane proteins (Newstead et al., 2008), Cymal-6 was exchanged to DDM during the purification for further crystallization attempts.

A two step purification protocol was evaluated to purify TtUbiA. As observed after the purification of EcMenA (section 3.4), the purified fraction of TtUbiA also showed a high degree of SlyD protein contamination. Several methodologies were tested to eliminate SlyD from the purified protein: expression and purification using NiCO (DE3) strains (Robichon et al., 2011), heat precipitation with solubilized TtUbiA or an additional ion exchange chromatography step, but none of these proved successful (data not shown). Improved purity was obtained using Immobilized metal ion affinity chromatography (IMAC) with Ni²⁺ beads, His₆-tag removal through TEV protease cleavage, followed by a second IMAC step. After solubilization with Cymal-6, TtUbiA was incubated with Ni²⁺-agarose beads and eluted

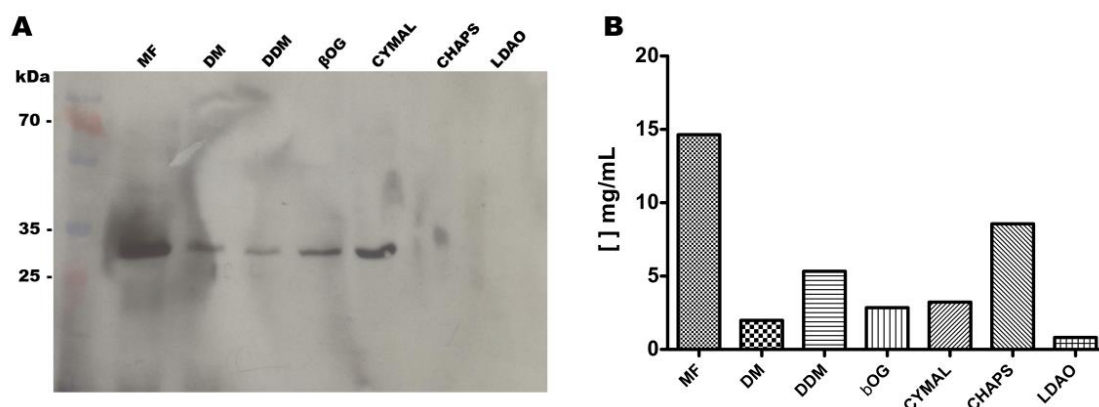


Figure 4.12. TtUbiA solubilization using different detergents. (A) Immunoblotting of the solubilized membrane fraction. Solubilization was performed with 10-fold CMC of each detergent for 1h30 at 4 °C. TtUbiA bands are observed around 30 kDa. Primary antibody: mouse anti-his; secondary antibody: goat anti-mouse (HRP). **(B) RC DC Assay for detergent-compatible protein concentration determination.** DDM and CHAPS showed the highest protein concentration. MF: membrane fraction; DM: *n*-Decyl- β -D-maltopyranoside; DDM: *n*-Dodecyl- β -D-maltopyranoside; β -OG: *n*-octyl- β -D-glucoside; Cymal-6: 6-Cyclohexyl-1-hexyl- β -D-maltopyranoside; CHAPS: 3-[(3-cholamidopropyl) dimethylammonio]-1-propanesulfonate; LDAO: Lauryldimethylamine N-oxide.

with buffer containing 250 mM imidazole. During the first IMAC, Cymal-6 was replaced with DDM, which is better suited to TEV protease cleavage (performed with excess protease due to the presence of detergents) and crystallization. After dialysis, the sample was loaded in a HisTrap™HP-Ni²⁺ (5 mL) column and the flow-through containing TtUbiA collected. Figure 4.13A shows the overview of TtUbiA purification during the first IMAC step, whereas Figure 4.13B shows the Coomassie-stained gel of the second IMAC after His₆-tag removal by TEV protease cleavage. Lanes 1 and 2, containing the flow-through fraction with TtUbiA, showed the presence of two bands at the expected molecular weight of TtUbiA (30 kDa). MALDI-TOF spectrometry identified both bands as TtUbiA, although low amounts of SlyD were also detected. The band from lane 3 (wash fraction) also contained peptides from TtUbiA, but higher amounts of SlyD were detected and for this reason this fraction was not used for further assays. Although this strategy enabled a good separation from SlyD, purification of TtUbiA showed low yields, with values among 0.1 – 0.25 mg/L culture. This material was subjected to crystallization trials using lipid cubic phase (LCP), but no protein crystals could be obtained as yet (data not shown).

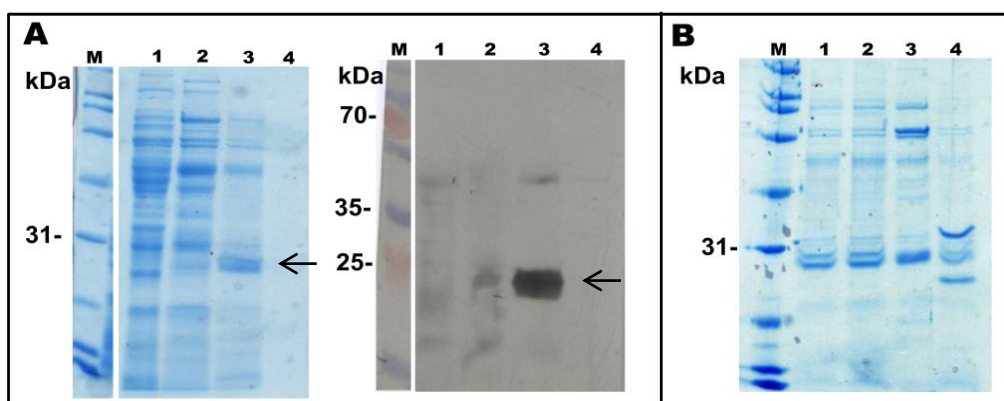


Figure 4.13. Overview of TtUbiA purification. (A) Coomassie-stained gel and immunoblotting after first IMAC step. M: marker, lane 1: flow through; lane 2: wash fraction with 20 mM imidazole; lane 3: elution fraction with 250 mM imidazole; lane 4: elution fraction with 500 mM imidazole. Band in lane 3 around 30 kDa indicates His₆-tagged TtUbiA (shown with arrow); Primary antibody: mouse anti-his; secondary antibody: goat anti-mouse (HRP). **(B) Coomassie-stained gel of the second IMAC step after TEV protease cleavage.** Lanes 1 and 2: Flow through fraction containing TtUbiA without His₆-tag and low amounts of SlyD; lane 3: wash fraction with 20 mM imidazole containing high amounts of SlyD; lane 4: elution fraction with 250 mM imidazole containing TEV protease (27 kDa).

4.7. Discussion

The thermophilic organism *Thermus thermophilus* has become an excellent laboratory model, since its enzymes and proteins are not only thermostable but also resistant to denaturing chemical agents and easier to purify, manipulate and to crystallize than those from mesophiles (Cava et al., 2009). *T. thermophilus* utilizes the electron carrier menaquinone (MK) (Mooser et al., 2006), which is synthesized via the futasoline pathway

Chapter 4: TtUbiA - a novel prenyltransferase associated with the futasolone pathway

(Dairi et al., 2011; Kurosu and Begari, 2010). As no aromatic prenyltransferase has been identified in this pathway, a BLAST search using the sequence for 4-hydroxybenzoate oligoprenyltransferase (UbiA) from *E. coli* was carried out. Two hits proteins were found: Protoheme IX farnesyltransferase (CTaB) and a protein assigned as 4-hydroxybenzoate polyprenyltransferase (UbiA). CTaB probably plays a role in heme prosthetic group synthesis for cytochrome C oxidase (Throne-Holst and Hederstedt, 2000) and it is not involved in the biosynthesis of quinones. Thus, UbiA is likely to be the aromatic prenyltransferase in *T. thermophilus* involved in the synthesis of menaquinone.

Initial attempts at heterologous expression of TtUbiA in *E. coli* resulted in low yields; previous studies (Ishida and Oshima, 1994; Ishida et al., 2002) have attributed similar behavior to (i) the high CG content in the genomic DNA of *Thermus* species (61 – 70%), which can create stable hairpin structures that may suppress translation at 37 °C in *E. coli* and (ii) the frequent presence of codons such as AGG, AGA (arginine) and AUA (isoleucine) that are rare in *E. coli*. TtUbiA has seven arginines that are coded by AGG; using Rosetta (DE3) containing the pRARE vector (Novy et al., 2001), better results could be obtained, similar to what observed for *E. coli*.

TtUbiA could only be purified in low yield and with significant SlyD contamination. For EcMenA, better separation from SlyD was observed during purification with GFP fusion; however, such methodology was not applicable for TtUbiA, since good levels of expression were not observed using GFP constructs.

Recently, the structures of UbiA homologs from *Aeropyrum pernix* (ApUbiA) and *Archaeoglobus fulgidus* (AfUbiA) were published (Cheng and Li, 2014; Huang et al., 2014) at resolutions of 3.3 Å and 2.5 Å, respectively. Despite being termed as UbiA enzymes, no 4-hydroxybenzoate oligoprenyltransferase activity could be observed in either case. Moreover, BLAST and Uniprot analyses showed that there are four prenyltransferases in *Archaeoglobus fulgidus* associated with the membrane (section 8.8): the first one assigned as 4-hydroxybenzoate octaprenyltransferase (AfUbiA) (O28106), likely involved in the biosynthesis of respiratory quinones, a second one named as putative 4-hydroxybenzoate octaprenyltransferase-2 (AfUbiA-2) (O29843), shown to be a geranylgeranylgeranyl phosphate synthase (GGGSP) or UbiA-2 homolog, described to be involved in the biosynthesis of archaeal ether-linked membrane lipids (Hemmi et al., 2004), a third one assigned as putative 1,4-dihydroxy-2-naphthoate octaprenyltransferase (AfMenA) (A0A075WDC0), which function is still unknown and the last one, described by Huang et al., (2014), assigned as bacteriochlorophyll synthase (AfBchG) (O28625). The function of BchG in

Chapter 4: TtUbiA - a novel prenyltransferase associated with the futasine pathway

archaea is not well understood, but it was suggested that this protein might be involved in the biosynthesis of membrane lipids, since it is thought that archaea do not require bacteriochlorophyll molecules (Hemmi et al., 2004; Meng et al., 2009). Nevertheless, all homologs are members of the UbiA prenyltransferases family and except the GGGPS subfamily, exhibit similar structures that are probably representative for membrane-bound aromatic prenyltransferases.

The overall structure of both crystallized proteins shows nine transmembrane helices (TM) arranged counterclockwise in a U shape with the N-terminal oriented to the cytoplasm and the C-terminal oriented to the extracellular side. The central cavity of ApUbiA is surrounded by TM1, TM2 and TM9 at the front and TM5 and TM6 from the back. It also contains a basic pocket, likely involved in aromatic substrate recognition, a hydrophobic wall for binding of the isoprenyl chain and a lateral portal accessible to the membrane that could accommodate the isoprenyl chain. In addition, helix/loop regions (HL) HL2-3, HL4-5 and HL6-7 located in the cytoplasm form a cap over the central cavity, generating a polar pocket responsible for pyrophosphate binding (Figure 4.14A). The central cavity of AfUbiA is formed by polar and charged residues and by a hydrophobic tunnel that extends deeper into the transmembrane region and opens into the bilayer, which could potentially accommodate longer polyprenyl chains (Figure 4.14C). Both structures contain two conserved Asp-rich motifs (DDXXD) localized in HL2-3 and HL6-7, respectively, that are important for the prenylation reaction (Heide, 2009; Yazaki et al., 2009), probably via diphosphate substrate stabilization by binding with Mg^{2+} ions (Figure 4.14B, D).

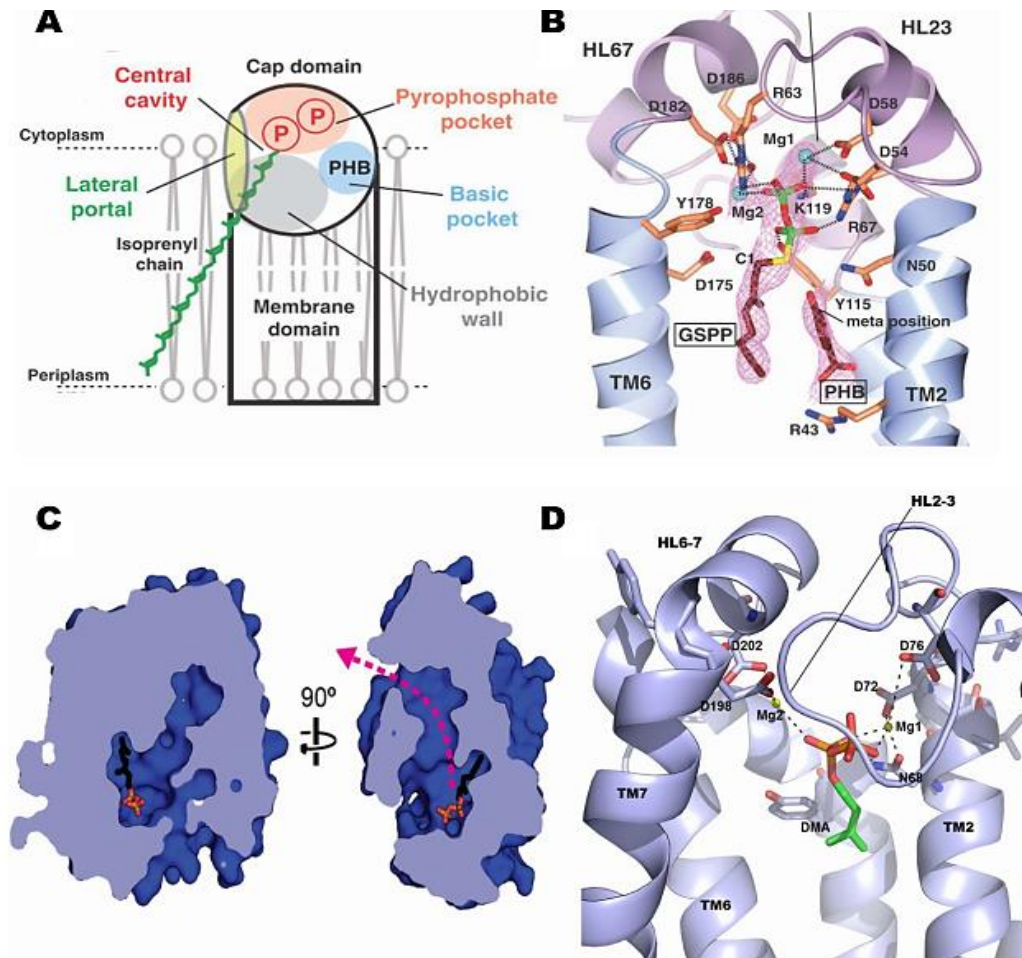


Figure 4.14. Structure of ApUbiA and AfUbiA. (A) Cartoon representation of the active site of ApUbiA. The central cavity contains a polar pocket (red) for pyrophosphate binding, a lateral portal buried in the membrane (yellow), a hydrophobic wall (gray) important for the isoprenyl chain stabilization and a basic pocket (blue) probably important for aromatic substrate binding. **(B) Substrate binding pocket of ApUbiA.** The structure of ApUbiA shows the putative complex formation between Mg^{2+} ions (blue spheres), geranyl-S-thiolodiphosphate (GSPP) (green and dark red sticks) and the two Asp-rich motifs (HL2-3 and HL6-7). Modeled 4-hydroxybenzoic acid (PHB) (red sticks) is likely bound in the basic pocket. TM: transmembrane helix (Cheng and Li 2014, modified). **(C) Cartoon representation of the central cavity of AfUbiA.** Cutaway view of the central cavity showing the hydrophobic tunnel (pink arrow) that likely accommodates the isoprenyl chain. GPP (geranyl pyrophosphate) is shown as sticks (Huang et al., 2014 modified). **(D) Substrate binding pocket of AfUbiA.** The structure of AfUbiA (PDB code: 4QT4) shows the putative complex formation between Mg^{2+} ions (yellow spheres), dimethylallyl diphosphate (DMA) (green and orange sticks) and the two Asp-rich motifs (HL2-3 and HL6-7). TM: transmembrane helix.

First evidence that such motifs are involved in the catalytic activity was demonstrated by Ohara and co-workers (2009) using LePTG1. Point mutations in these residues to alanine decreased strongly the catalytic activity of the enzyme. These results corroborate with the structure of ApUbiA and AfUbiA containing Mg^{2+} ions, which demonstrate that the two cations coordinate aspartates from both motifs (Cheng and Li, 2014; Huang et al., 2014). The structure of AfUbiA showed that the first Mg^{2+} is coordinated by Asp68 and Asp72 from the first motif, whereas the second is coordinated by Asp198 and Asp202 from the second motif. Similar arrangement was also observed for ApUbiA (Figure 4.15).

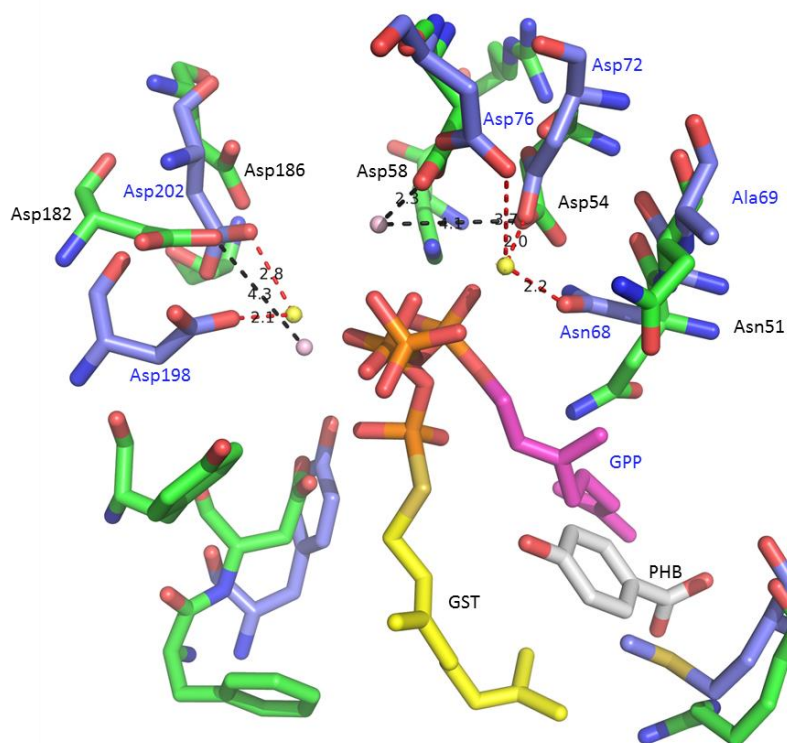


Figure 4.15. Active site of ApUbiA and AfUbiA. Structural comparison between ApUbiA (green residues) and AfUbiA (blue residues) shows the coordination with Mg^{2+} ions. The first Mg^{2+} from the AfUbiA structure (yellow sphere) binds to Asn68 and Asp72 through hydrogen bonds (red dotted lines) with 2.2 Å and 2.0 Å, respectively. Asp76 is 3.2 Å distant from Mg^{2+} and probably bound to it through one water molecule. The second Mg^{2+} (yellow sphere) are coordinate by Asp198 and Asp202. The first Mg^{2+} ion of ApUbiA (white spheres) is coordinated directly by Asp58 and through water molecule by Asp54, due to the 4.1 Å distance. The second Mg^{2+} ion (white sphere) is > 3.4 Å away from both Asp182 and Asp186 and may bind to these residues through water molecules. Geranyl S-thiolodiphosphate (GST) was soaked in ApUbiA and geranyl pyrophosphate (GPP) soaked in AfUbiA. 4-hydroxybenzoic acid (PHB) was modeled in ApUbiA. Note the vicinity of ApUbiAAsn51 / AfUbiAAla69 to the aromatic substrate binding site. Figure was prepared with PyMOL.

Bona fide UbiA prenyltransferases catalyze the prenylation of isoprenoid moieties to 4-hydroxybenzoic acid (PHB) in the presence of magnesium (Bräuer et al., 2008; Melzer and Heide, 1994). “UbiA” from *Thermus thermophilus* shares a sequence identity of 28% with EcUbiA and is also predicted to have 9 transmembrane helices. The results presented in this thesis demonstrate that TtUbiA does not recognize PHB. As *T. thermophilus* utilizes MK for electron transport, the MenA substrate DHNA-2 was also tested. TtUbiA is however also unable to prenylate DHNA-2, suggesting that TtUbiA is neither UbiA nor MenA homologs. A closer look at the futasoline pathway (Arakawa et al., 2011; Dairi, 2012; Zhi et al., 2014) suggested that 1,4-dihydroxy-6-naphthoic acid (DHNA-6) might be the substrate that is prenylated by TtUbiA; once again, however, no product could be detected.

Several studies have demonstrated that *Streptomyces* strains synthesize MK via futasoline pathway (Dairi, 2012; Hiratsuka et al., 2008; Seto et al., 2008). As the UbiA homologs found in these strains are more similar to TtUbiA than to EcUbiA (47% identity with TtUbiA against

Chapter 4: TtUbiA - a novel prenyltransferase associated with the futasoline pathway

25% with EcUbiA) (Figure 8.9), we reasoned that the UbiA homolog from *S. lividans* (SIUbiA) could be expressed in *S. lividans* cells at room temperature, providing a natural environment for the membrane protein. Nevertheless, SIUbiA is not able to prenylate PHB, DHNA-2 or DHNA-6. On the other hand, expression of EcMenA in *S. lividans* cells resulted in activity towards the DHNA-2, showing that the cell membrane of *S. lividans* is able to support such activity if present. Thus, the membrane composition in *E. coli* or *S. lividans* is not responsible for the lack of activity, in turn suggesting that TtUbiA and SIUbiA possess undetermined substrate specificity.

Sequence alignments of UbiA, MenA and TtUbiA/SIUbiA enzymes (Figure 4.7) reveal a crucial difference in the neighborhood of the first conserved aspartate-rich motif N[R/D]XXD[XX]XXD. Whereas TtUbiA / SIUbiA possess an arginyl residue (in position Arg59 / Arg73, respectively) that is conserved in UbiA homologs associated with the futasoline pathway, the corresponding amino acid is an Asp in EcUbiA (Asp68) and EcMenA (Asp65) as well as other confirmed UbiA and MenA enzymes. Interestingly, this position is occupied by Ala69 in AfUbiA and Asn51 in ApUbiA (Figure 4.15). Although this residue is not directly involved with Mg²⁺ coordination, Ohara and co-workers (2009) demonstrated that the presence of an acidic amino acid at this position is essential for the activity of LePGT1, another 4-hydroxybenzoate prenyltransferases. Mutations of the corresponding residues in EcMenAD65R abolished MenA activity completely, suggesting that Asp65 plays a role in aromatic substrate recognition, supported by the *in vivo* complementation assay in $\Delta menA$ cells that showed that EcMenAD65R cells were not able to grow under anaerobic conditions (Figure 4.11).

The lack of activity observed for TtUbiA, SIUbiA, TtUbiAR59D and SIUbiAR73D against the potential aromatic substrates PHB, DHNA-2 or DHNA-6 is likely involved to an incorrect aromatic substrate. Because the futasoline pathway was only recently discovered, the complete enzyme sequence for the formation of MK is still unclear. Five enzymes have been identified to date that are involved in the formation of 1,4-dihydroxy-6-naphtoate, which is thought to be subsequently prenylated, methylated and carboxylated in unknown sequence to yield the final product (Arai et al., 2009; Hiratsuka et al., 2008). Activity assays using substrates that mimic possible intermediates have however, failed to identify the correct aromatic substrate for TtUbiA and SIUbiA until now, suggesting a high substrate specificity, as observed for the membrane-bound prenyltransferase from parsley, that among 17 different prenyl acceptor substrates and the three prenyl donors substrate was able to metabolize just one prenyl acceptor in the presence of DMAPP (Karamat et al., 2014).

Chapter 4: TtUbiA - a novel prenyltransferase associated with the fufalosine pathway

Phylogenetic analyses of the UbiA prenyltransferases superfamily members (Figure 4.16) demonstrate that these two enzymes represent a novel class of aromatic prenyltransferase associated with the fufalosine pathway (which we would like to term MqnF) that can be differentiated from UbiA and MenA enzymes. Interestingly, (Nagata et al., 2010) demonstrated that the MenA substrate DHNA-2 is toxic for some organisms that synthesize MK via the fufalosine pathway, such as *Helicobacter pylori* and *Campylobacter jejuni*, but no inhibitory effect was observed for *E. coli* and *Bacillus subtilis*.

Sequence analyses (Figure 4.7) demonstrate that the motifs NRXXD (helix α -2) and NPR (loop 2) are conserved in the MqnF enzymes, whereas the regions AGCXXN (helix 2), YDTXYA (helix α -6) and GIKSTA (loop 6) are highly conserved in *bone fide* UbiA sequences and the region NNXRDI (helix α -6) is conserved in MenA homologs. ApUbiA possesses the loop 2 NPR, helix α -1 HTLIFS and helix α -6 GFDTI signatures found in fufalosine aromatic prenyltransferases, although it lacks the arginyl residue identified here. Studies have demonstrated that *Aeropyrum pernix* uses MK and DMK for electron transport (Nishida et al., 1999). Moreover, the presence of *mqn* genes strongly suggest that MK/DMK is synthesized via fufalosine pathway (Zhi et al., 2014). Analysis of the prenyltransferases existing in *A. pernix* shows the presence of two membrane bound prenyltransferases: a probable (S)-2,3-Di-O-farnesylgeranylgeranyl synthase (Q9YFU1) and the putative 4-hydroxybenzoate octaprenyltransferase (ApUbiA) (Q9YBM8). The former sequence corresponds to a protein of 282 amino acids (section 8.10) that contains the motif NDXXD (helix α -2) absent in MqnF homologs and potentially involved in the biosynthesis of MK. BLAST analyses indicate however, that this protein is an UbiA-2 or GGGPS homolog, sharing a similarity of 29% with the characterized GGGPS/UbiA-2 from *Sulfolobus solfataricus* (Hemmi et al., 2004). Thus, one can assume that ApUbiA is potentially involved with the biosynthesis of MK and belongs, together with TtUbiA and SIUbiA, to the novel MqnF subclass.

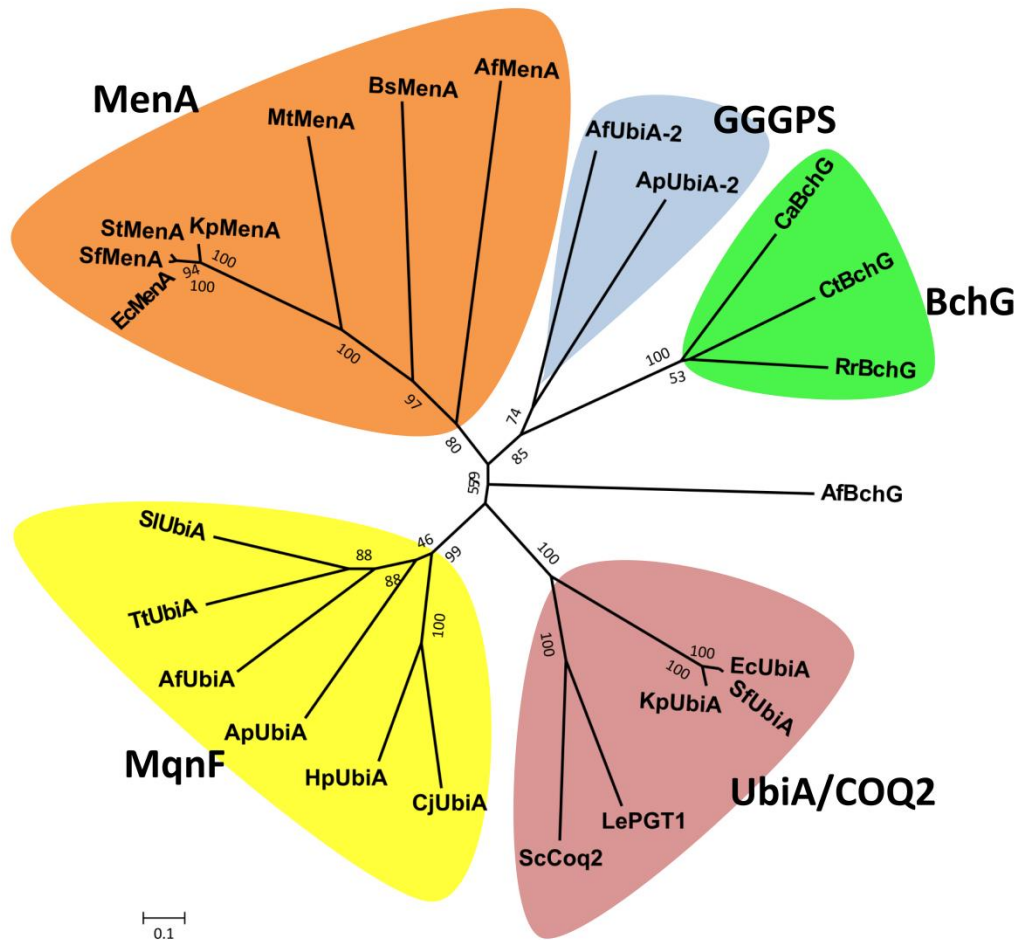


Figure 4.16. Phylogenetic tree of UbiA prenyltransferases family proteins. Branches were classified in different organisms. The bootstrap value is above each node. These values indicate the bootstrap replicates that support this node out of 1000 samples. MEGA6 program was used for the analyses. The colored areas represent different clusters of subfamilies: MenA (orange), geranylgeranyl glyceryl phosphate synthase (GGGPS) (light blue), BchG (green), UbiA/COQ2 (pink) and the novel proposed MqnF subfamily (yellow) associated with the futasolone pathway. Abbreviations and accession number of each protein are as follows: BsMenA, MenA from *Bacillus subtilis* (P39582); MtMenA, MenA from *Mycobacterium tuberculosis* (P9WIP3); KpMenA, MenA from *Klebsiella pneumoniae* (R4Y411); StMenA, MenA from *Salmonella typhi* (Q8Z2Y9); EcMenA, MenA from *Escherichia coli* (P32166); SfMenA, MenA from *Shigella flexneri* (Q83PD5); AfMenA, MenA from *Archaeoglobus fulgidus* (A0A075WDC0); AfUbiA-2, GGGPS from *Archaeoglobus fulgidus* annotated as putative 4-hydroxybenzoate octaprenyltransferase (O29843); ApUbiA-2, GGGPS from *Aeropyrum pernix* annotated as probable (S)-2,3-Di-O-farnesylgeranyl glyceryl synthase (Q9YFU1); CaBchG, bacteriochlorophyll synthase from *Chloroflexus aurantiacus* (P33326); CtBchG, bacteriochlorophyll synthase from *Chlorobium tepidum* (H2VFJ6); RrBchG, geranylgeranyl-bacteriochlorophyll synthase from *Rhodospirillum rubrum* (Q936J7); AfBchG, bacteriochlorophyll synthase from *Archaeoglobus fulgidus* (O28625); EcUbiA, UbiA from *Escherichia coli* (P0AGK1); SfUbiA, UbiA from *Shigella flexneri* (Q83IP7); KpUbiA, UbiA from *Klebsiella pneumoniae* (A6TGU9); ScCoq2, COQ2 from *Saccharomyces cerevisiae* (P32378); LePTG1 from *Lithospermum erythrorhizon* (Q8W405); TtUbiA, UbiA from *Thermus thermophilus* (Q72L23); SIUbiA, UbiA from *Streptomyces lividans* (D6EGY8); CjUbiA, UbiA from *Campylobacter jejuni* (Q0PBX3); HpUbiA, UbiA from *Helicobacter pylori* (J0Q362); ApUbiA, UbiA from *Archaeoglobus fulgidus* (O28106); ApUbiA, UbiA from *Aeropyrum pernix* (ApUbiA) (Q9YBM8).

5. Crystal structure analysis of futasoline hydrolase from *Thermus Thermophilus* (TtMqnB)

5.1. Recombinant expression of TtMqnB in *E. coli*

Futasoline hydrolase from *Thermus thermophilus* (TtMqnB) was cloned into pET15b-TEV vector and kindly provided by Dr. Ulrike Bräuer. Because TtMqnB contains six arginines which are codified by AGG codon and seven codified by CGG, both codons rarely used codons in several *E. coli* strains (Figure 8.11) (Fuhrmann et al., 2004), Rosetta (DE3) cells were used to express TtMqnB. As already described (section 4.2), this strain contains the pRARE vector that encodes tRNA genes for rare codons encoding Arg, Ile, Gly, Leu and Pro (Novy et al., 2001). Expression tests carried out varying IPTG concentration, temperature and time of incubation showed that a band around 26 kDa (the calculated molecular weight of TtMqnB) was observed in all conditions (Figure 5.1). Although good TtMqnB expression was achieved after 4 h at 37 °C, Rosetta (DE3) cells grew very slowly in large scale (6 L), so that the expression was carried out overnight at 30 °C in the presence of 0.3 mM IPTG.

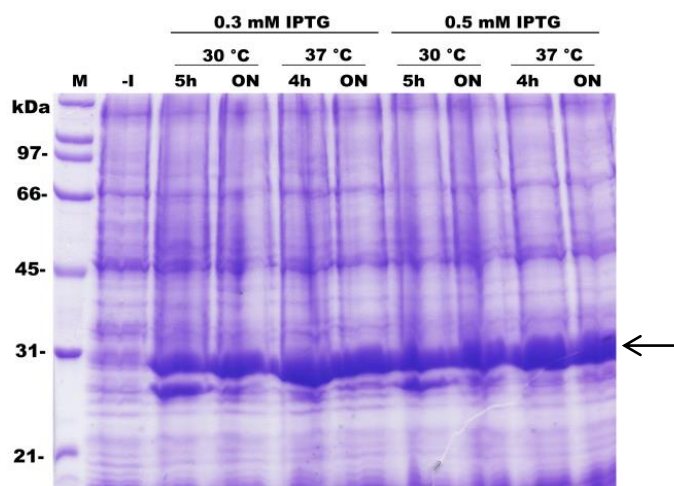


Figure 5.1. Expression of TtMqnB in Rosetta (DE3) cells. Coomassie-stained gel shows the expression of TtMqnB at different IPTG concentrations, temperatures and time of incubation. Good expression levels were observed for all conditions. M: marker, -I: before induction, 5h: after 5 h induction, ON: overnight induction, 4h: after 4 h induction. The arrow indicates the expected molecular weight of TtMqnB (~ 26.0 kDa).

5.2. Purification of TtMqnB

Exploiting the thermostability of TtMqnB, a heat treatment was very effective in removing impurities during the purification (Figure 5.2A). Subsequent Co^{2+} affinity chromatography resulted in highly pure protein (Figure 5.2B) with yields of 8.7 mg – 9.5 mg per liter.

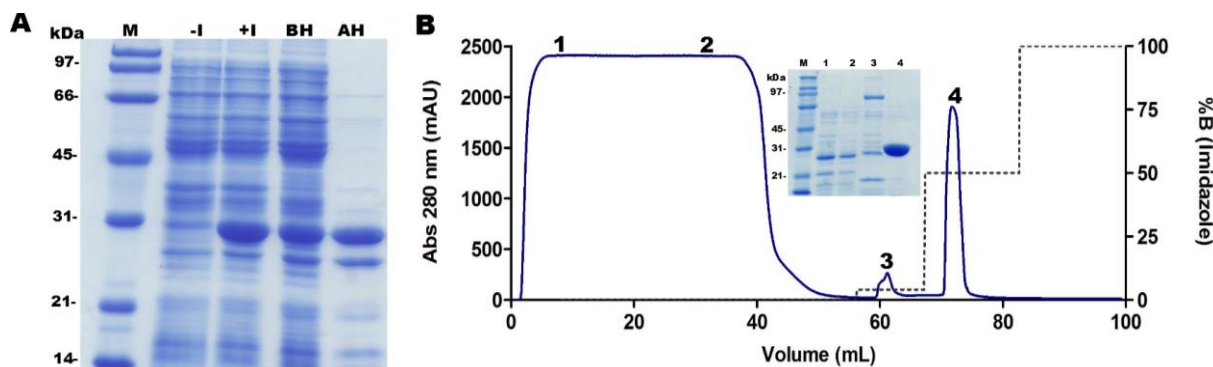


Figure 5.2. Purification of TtMqnB. (A) Overview of TtMqnB purification. Coomassie-stained gel shows the purification overview of TtMqnB. M: Marker; -I: before expression; +I: after expression with 0.3 mM IPTG; BH: before heat treatment; AH: after heat treatment at 70°C for 20 min. **(B) Chromatogram profile of a 5 mL HisTrap HP column containing cobalt as metal chelate.** After the heat treatment, TtMqnB was loaded in an equilibrated column containing buffer A (50 mM Tris/HCl pH 8.5, 0.15 M KCl) and eluted with 50% of buffer B (buffer A + 0.5 M imidazole). The fractions were analyzed by SDS-PAGE.

5.3. TtMqnB is a dimer in solution

The oligomeric state of TtMqnB was evaluated by analytical centrifugation. The sedimentation velocity, measured using different protein concentrations, as described in section 2.5.4, showed the presence of a symmetric peak, corresponding to a homogenous protein solution with a sedimentation coefficient (s) of 3.3 S (Figure 5.3A). To calculate the apparent molecular weight (MW_{app}), sedimentation equilibrium (Figure 5.3B) was analyzed at 5.000 rpm and determined by a regression of the data using the Svedberg equation. The MW_{app} of 47.6 ± 3.2 kDa is in agreement with TtMqnB existing as a dimer in solution, since the theoretical molecular mass of the His₆-tagged TtMqnB is the 26.6 kDa.

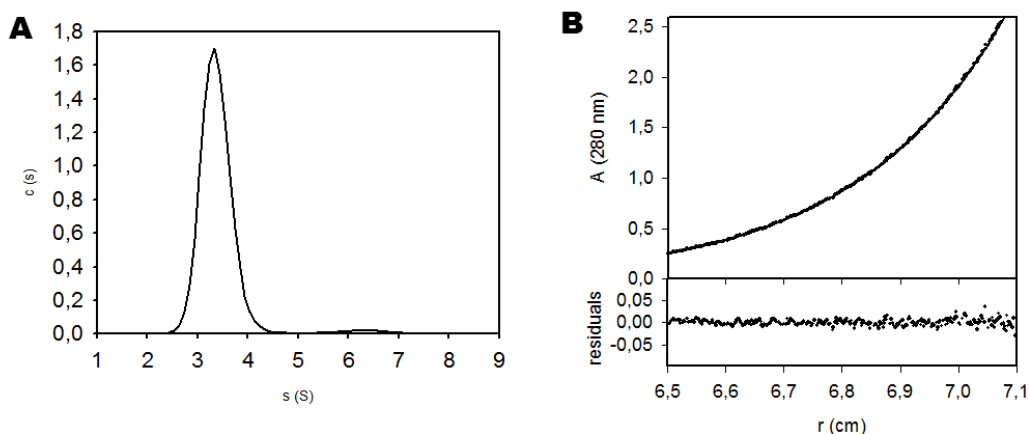


Figure 5.3. Analytical ultracentrifugation of TtMqnB indicates that the protein forms a dimer in solution. (A) sedimentation velocity of TtMqnB. Protein concentration was 1.0 mg/mL. Data were analyzed with the time derivative method providing a sedimentation coefficient of 3.3 S. **(B) Sedimentation equilibrium.** Upper panel: original data. Lower panel: deviations from the fit. The MWapp generated from the data regression was 47.6 ± 3.2 kDa.

5.4. Crystallization of TtMqnB

For initial screening (96-well plate), TtMqnB was concentrated up to 12 mg/mL in tris buffer containing imidazole (15 mM Tris/HCl pH 8.5, 45 mM KCl, 75 mM imidazole) and three different protein concentrations (3.0 mg/mL, 8.0 mg/mL and 12 mg/mL) were used to set up nine kits, which corresponds to 864 different conditions. After seven days, crystals were observed in one of the conditions [1M $(\text{NH}_4)_2\text{SO}_4$, 0.1 M ADA pH 6.5] with protein concentrations of 8.0 mg/mL and 12 mg/mL (Figure 5.4A). Fine screening (15-well plate) was carried out by varying the protein concentration (5.0 mg/mL, 6.5 mg/mL and 8.0 mg/mL), precipitant concentration (from 0.8 M to 1.1 M $(\text{NH}_4)_2\text{SO}_4$) and drop ratio concerning the protein and precipitant volume. The plates were set up as described in 2.6.2 and stored at 12 °C. After five months, bigger and separated crystals were observed in several conditions (Figure 5.4B, C, D).

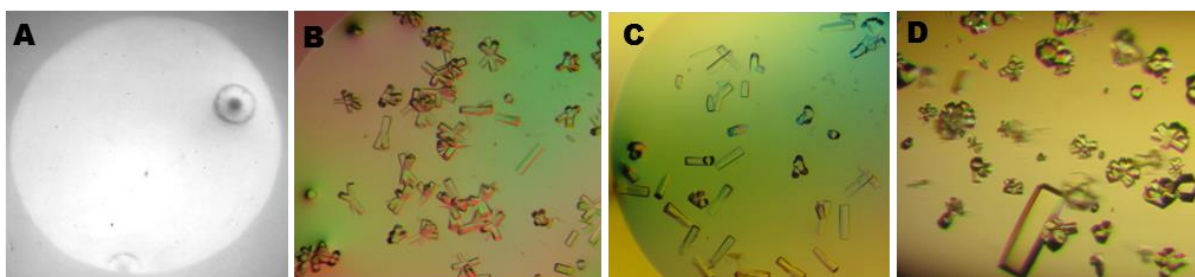


Figure 5.4. Crystals of TtMqnB (A) Initial screening in 96-well plate. Condition: 1 M $(\text{NH}_4)_2\text{SO}_4$, 0.1 M ADA pH 6.5. Protein conc.: 8.0 mg/mL. **(B) Fine screening in 15-well plate.** Condition: 0.8M $(\text{NH}_4)_2\text{SO}_4$, 0.1 M ADA pH 6.5 Protein conc.: 6.5 mg/mL, drop ratio: 2.0 μL protein + 1.0 μL reservoir. **(C) 15-well plate.** Condition: 0.9 M $(\text{NH}_4)_2\text{SO}_4$, 0.1 M ADA pH 6.5 Protein conc.: 5.0 mg/mL, drop ratio: 1.0 μL protein + 1.0 μL reservoir. **(D) 15-well plate.** Condition: 1.1 M $(\text{NH}_4)_2\text{SO}_4$, 0.1 M ADA pH 6.5 Protein conc.: 8.0 mg/mL, drop ratio: 2.0 μL protein + 1.0 μL reservoir.

5.5. Data collection, model building and structure of TtMqnB

Data collection was carried out at the SLS (Swiss Light Source beamline X06SA) at a wavelength of 1.00 Å. TtMqnB crystallized in the trigonal space group $P3_112$ with unit cell parameters $a = b = 94.73$ Å, $c = 237.32$ Å, $\alpha = \beta = 90^\circ$, $\gamma = 120^\circ$ and the highest resolution was 2.2 Å. In order to obtain initial phases, the molecular replacement method (MR) was used.

BLAST analyses against the Protein Data Bank (PDB) were performed in order to find possible structures to be used as search models for MR. Analysis revealed several hits, among them the structure of 5'-methylthioadenosine/S-adenosylhomocysteine nucleosidase (MTAN) from *Helicobacter pylori* (PDB code: 3NM4 – Ronning et al., 2010) and a futasoline hydrolase/MTAN mutant from *Helicobacter pylori* (PDB code: 4BMZ – Kim et al., 2014), both share sequences identity of 28% with TtMqnB. Despite the low sequence identity, the futasoline hydrolase mutant from *Helicobacter pylori* (PDB code: 4BMZ, chain A) was used as the search model for MR using Phaser (McCoy et al., 2007). Although no solution was found using the full model, the phase problem could be solved using the Poly-ALA chain as search model. The structure was built manually and improved based on $F_o - F_c$ and $2F_o - F_c$ maps to give final R-work and R-free values of 18.21% and 21.36%, respectively. Data-processing and refinement statistics are shown in (Table 5.1).

The crystals of TtMqnB contain four protein molecules per asymmetric unit (monomer A – monomer D) (Figure 5.5A) forming a tetramer, 10 molecules of ethylene glycol from the cryoprotectant solution and 276 solvent molecules. The enzyme was crystallized with an N-terminal His₆-tag and TEV cleavage site which added 22 residues to the chain and could partly be seen in the electron-density map in chain A (ENLYFQGGT). The last 8 residues from the C-terminus (218-225) were not built in any of the chains due to absence of electron-density. The loop region from residues Lys93 to Ala103 and from Gly107 to Phe112 showed poor electron density and for this reason these residues were not built in the monomers A, B and D.

Each monomer contains a mix of helices and slightly curved β -strands as a core surrounded by five α -helices and one 3_{10} helix. Altogether, there are 11 β -strands, six helices and two 3_{10} helices (Figure 5.5C).

The asymmetric unit containing four monomers shows a possible dimer formation between monomers A and D and between monomers B and C. The dimer interface is formed by four helices, two from each monomer (helix α -1 and helix α -5) and a single loop (from Gly91 to Gly100) that forms a cap covering part of the active site of the opposing monomer (Figure 5.5B). Comparison between the two dimers based on C α atoms resulted a RMSD value of 0.168 Å.

Chapter 5: Crystal structure of the futasolase TtMqnB

Table 5.1: Data-processing and refinement statistics from TtMqnB and hypo-TtMqnB

	MqnB	MqnB+Hypoxanthine
Data collection		
Radiation Source	X06SA (SLS*)	X06DA (SLS*)
Wavelength (Å)	1.00	1.00
Space group	P3 ₁ 12	P3 ₂ 21
Cell Dimensions		
a, b, c (Å)	94.73, 94.73, 237.32	94.89, 94.89, 121.88
angles (°)	90, 90, 120	90, 90, 120
Resolution range merged (Å)	82.0 – 2.20	48.9 – 2.30
Highest resolution shell (Å)	2.32 – 2.20	2.44 – 2.30
Rmerge	9.1 (70.8)	8.8 (82.4)
I/σ(I)	13.9 (3.1)	15.07 (2.06)
Completeness (%)	100 (100)	99.9 (99.4)
Multiplicity	8.9 (9.1)	5.32 (5.41)
Solvent content/ molecules in ASU	59.51% / 4	60.7% / 2
Model used for MR	4BMZ (Chain A)	MqnB monomer (Chain C)
Refinement		
No. reflections (work/test)	60421 (3116)	27209 (1403)
R _{work} / R _{free} (%)	18.21/21.36	18.08/20.79
No. atoms		
Protein	6337	3252
Ligand/ion	40	52
Solvent	273	127
B-factors		
Protein	48.83	47.03
Ligand/ion	57.99	49.01
Solvent	48.10	45.93
R.m.s deviations		
Bond lengths (Å)	0.002	0.002
Bond angles (°)	0.732	0.705
Ramachandran plot:		
Favored (%)	97.83	98.14
Outliers (%)	0.0	0.0
MolProbity clashscore	2.40	2.24

*Swiss Light Source – Detector: Pilatus 6M.

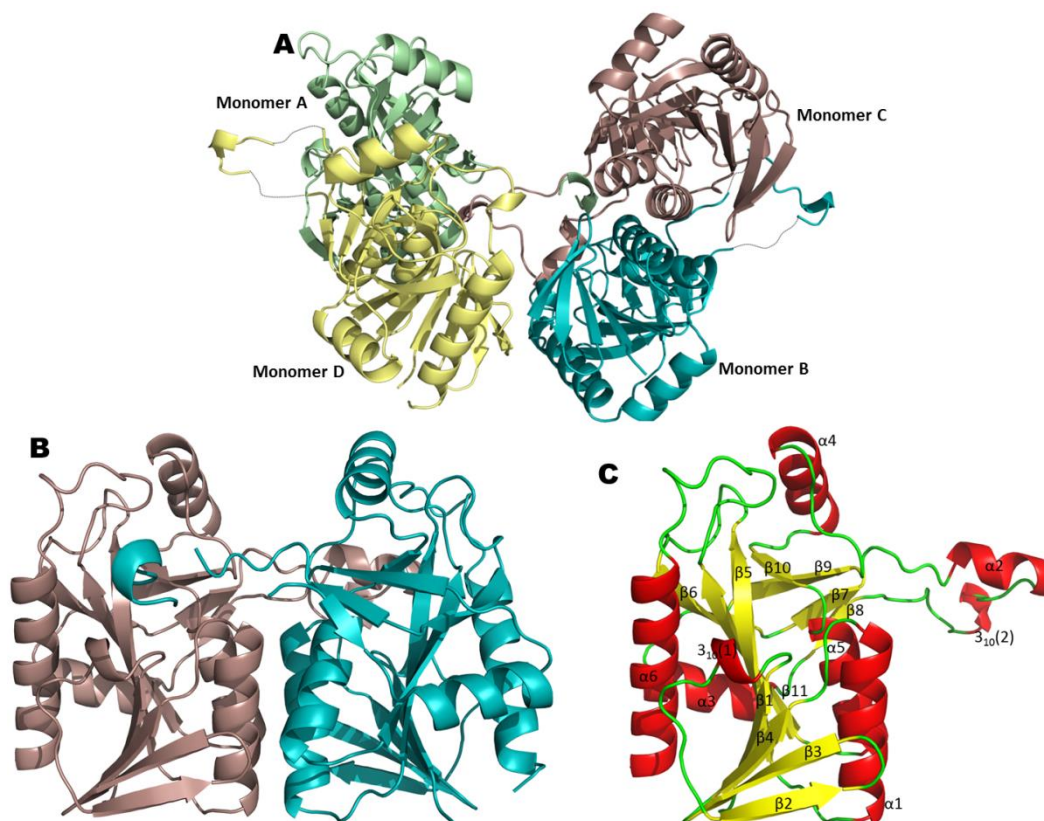


Figure 5.5. The overall structure of TtMqnB. (A) Four monomers were found per asymmetric unit. The arrangement suggests the formation of two dimers, the first one between monomers A and D and the second between monomers B and C. **(B) Likely dimer structure between monomers B and C.** Dimer interface formed by a cluster of four central helices and a loop that interacts with the active site of the other molecule **(C) View of monomer C showing the mixture of α + β structures.** β -sheets are shown in yellow, α -helices in red and random coil structures are shown in green. Figures were produced using Pymol.

The protein interface and assemblies (PISA) server (Krissinel and Henrick, 2007), used to assess potential modes of oligomerization (Figure 8.12), indicated potential interfaces between monomers A-D and monomers B-C with high interface areas of 1102.3 \AA^2 and 1607.4 \AA^2 , respectively and a complexation significance score (CSS) of 1.0, suggesting that the interfaces play an essential role in complexation. On the other hand, interfaces between monomers A-B; B-C; B-D; C-D showed interface areas below 600 \AA^2 with CSS values of 0.0, while the interface between monomers A-C showed an area of 769.1 \AA^2 and 10 potential hydrogen bonds across the interface with a CSS of 0.0, indicating that these interfaces are not relevant for complex formation.

5.6. Ligand-soaking experiments and the structure of Hypo-TtMqnB

In order to gain further insights about the substrate binding site, TtMqnB crystals were soaked with analogs of futasolase (Figure 5.6). Crystals incubated with inosine (10 mM) for 45 minutes showed no additional density. Soaking experiments were also performed using formycin B, a molecule very similar to inosine in which the N9–C1 bond is replaced by C9–C1.

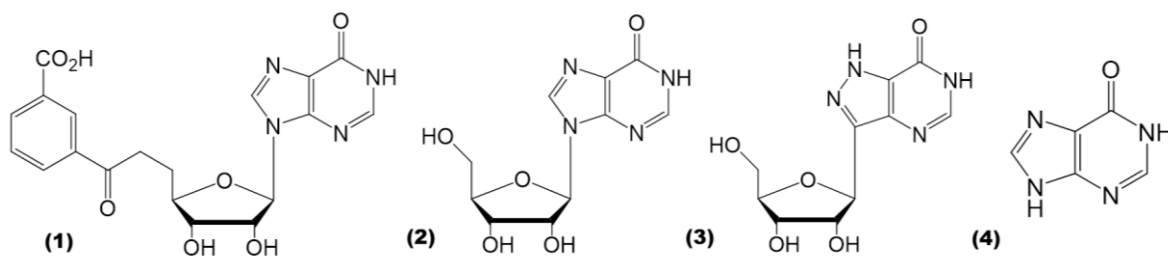


Figure 5.6. Futasosine and analogs used for soaking experiments. (1) futasosine, the substrate for MqnB enzymes, (2) inosine, (3) formycin B, and (4) hypoxanthine. TtMqnB crystals were incubated with inosine (10 mM) and hypoxanthine (5 mM) for 45 minutes. Crystals dissolved in buffer containing formycin B.

Concentrations of formycin B, between 5.0 and 15.0 mM, were tested, but the crystals dissolved after a few minutes in all the solutions. The last molecule tested was the purine base hypoxanthine. Data were collected in-house after 45 min of incubation and processed to a resolution of 2.6 Å. Data were also collected at SLS (beamline X06DA, $\lambda = 1.00$ Å) with highest resolution of 2.3 Å. For solving the phases, one apo-TtMqnB monomer was used as search model for MR.

Curiously, TtMqnB crystals soaked with hypoxanthine (TtMqnB-hypo) exhibited a different space group ($P3_221$) and unit cell parameters $a = b = 94.89$ Å, $c = 121.88$ Å, $\alpha = \beta = 90^\circ$, $\gamma = 120^\circ$ to the apo-TtMqnB crystals (Table 5.1). The length of the c axis was cut in half and consequently just two monomers were found in the asymmetric unit forming a dimer (Figure 5.7). In addition, two molecules of hypoxanthine (one in the active site of each monomer) and eight molecules of ethylene glycol were found in the structure. The last 8 residues from the C-terminus (218-225) were not built in either of the monomers due to absence of electron-density. Different from the apo-TtMqnB structure, electron-density was sufficient to build all the loop regions in both monomers. Superposition of the $C\alpha$ atoms of monomers C of apo-TtMqnB with monomers A and B of hypo-TtMqnB showed RMSD values of 0.158 Å and 0.144 Å, respectively.

Although the soaking methodology has been described as a technique that unlikely induces changes in unit cell and symmetry, such effects have been observed (Ladd and Palmer, 2013). Variations in unit cells dimensions caused by introduction of ligands are either attributed to conformational modifications or to variation of some components such as cryoprotectants (Iyengar and Hildebrandt, 2002). Ronning and co-workers (2010) have reported the same changes in the space group and in the unit cells parameters in the crystal structure of HpMTAN (PDB code: 3NM4) after co-crystallization with adenine. However, crystal packing analyses of HpMTAN structures showed that although different space groups were observed, both crystals exhibited identical packing. Crystal packing analyses of apo-TtMqnB and hypo-TtMqnB structures showed that the axis c of the apo-TtMqnB unit cell is twice as long as the hypo-TtMqnB and consequently the crystal structure of TtMqnB-apo has

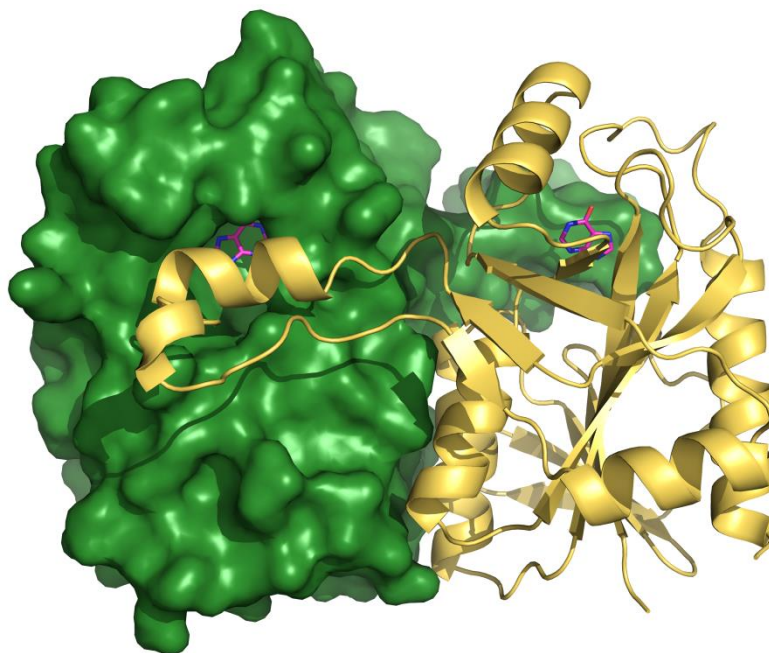


Figure 5.7. Dimer structure of TtMqnB-hypo. Monomer A (green) represented as surface showing part of the enzyme binding pocket and monomer B (yellow) represented as cartoon showing a single loop that forms a cap covering the active site of the monomer A. After soaking experiments with hypoxanthine, TtMqnB presented just two molecules in the asymmetric unit in a dimer conformation. Two molecules of hypoxanthine (magenta) were observed in the active site of each monomer.

four molecules in the asymmetric unit whereas hypo-TtMqnB just two. In addition, although the crystal packing of both structures is very similar, it is not the identical as observed for the HpMTAN (Figure 8.13)

5.7. Structural similarities between TtMqnB and 5'-methylthioadenosine nucleosidase (MTAN)

In order to identify functionally characterized proteins that are similar with TtMqnB, the DALI server (Holm et al., 2008) was used to search structural homology against the PDB database. The search resulted in hundred hit proteins that are classified either as 5'-methylthioadenosine nucleosidase (MTAN) or aminodeoxyfutasoline nucleosidase. The top 5 hit proteins are listed in table 5.2. All the structures align to TtMqnB with RMSD values lower than 2.30 Å and Z-Score between 25.5 and 26.4 indicating that the overall topology of TtMqnB is very similar with the MTAN fold.

MTAN is a multifunctional enzyme involved in different pathways in bacterial cells such as biosynthesis of methionine and polyamine. It has been shown that these enzymes catalyze the hydrolysis of the *N*-ribosidic bond of 5'-methylthioadenosine (MTA), *S*-adenosyl-L-homocysteine (SAH) and 5'-deoxyadenosine (5'-DOA) (Mishra and Ronning, 2012). Recently, Li and coworkers (2011) showed that the *Campylobacter jejuni* and *Helicobacter pylori* MTAN

Table 5.2: DALI homology of TtMqnB structural homology

TOP 5 DALI score					
Protein name	Z-score ^a	RMSD	lali/nres ^b	Identity (%) ^c	PDB code
MTAN <i>H. pylori</i> Strain 26695	26.4	2.3	205/230	22%	4BMZ
MTAN <i>H. pylori</i>	26.4	2.3	205/229	22%	3NM6
MTAN <i>Francisella philomiragia</i>	26.3	2.3	204/230	22%	4JOS
MTAN <i>Staphylococcus aureus</i>	26.2	2.2	203/230	19%	3BL6
MTAN <i>Bacillus Anthracis</i>	25.5	2.3	202/223	23%	4QEZ

^aStatistical significance of the similarity between protein of interest and other neighborhood proteins. Z-scores higher than 8.0 indicate that the two structures are most likely homologous

^blali: the number of structurally equivalent residues; nres: the total number of amino acids in the hit protein.

^cpercentage of identical amino acids over structurally equivalent residues.

is also able to hydrolyze 6-amino-6-deoxyfulalose (AFL) during the biosynthesis of menaquinone via futasalose pathway.

Structural studies have shown that MTAN enzymes possess a dimeric form and have either an “open” or “close” conformation (Haapalainen et al., 2013; Lee et al., 2003; Ronning et al., 2010). The open conformation, observed in the absence of ligand or in the presence of adenine, is defined by a larger and more solvent accessible purine, whereas the close conformation has been observed in the presence of larger ligands such as 5'-methylthiotubercidin (MTT) and formycin A (FMA) (Lee et al., 2005). Ronning and co-workers (2010) reported that the monomer A of MTAN from *H. pylori* (HpMTAN, PDB code: 3NM4) containing one molecule of tris[hydroxymethyl]aminomethane (tris) in the active site crystallized in the closed conformation while the monomer B, containing a single molecule of ethylene glycol in the active site, showed an open conformation. The most significant differences between the open and close conformation occurred near the active site. Superposition of both HpMTAN monomers showed clear modifications in helices α -1 and α -6 (Figure 5.8A). The modification in the first helix involves residues 10-21. The transition to close conformation breaks the hydrogen bond between the backbone carbonyl of Arg11 and the backbone amide of Ile14 and forms a new bond between the carbonyl of Arg11 and the backbone amide of Thr15. These changes add an additional turn to the N-terminus of α -1 and move the Glu13 toward the active site (Figure 5.9A), enabling a through-water hydrogen bonded network between the side chains of Glu13 and Arg194.

The other significant conformational change involves residues 198-224 of helix α -6, particularly residues 200-208 that in the open form are disordered but form a loop

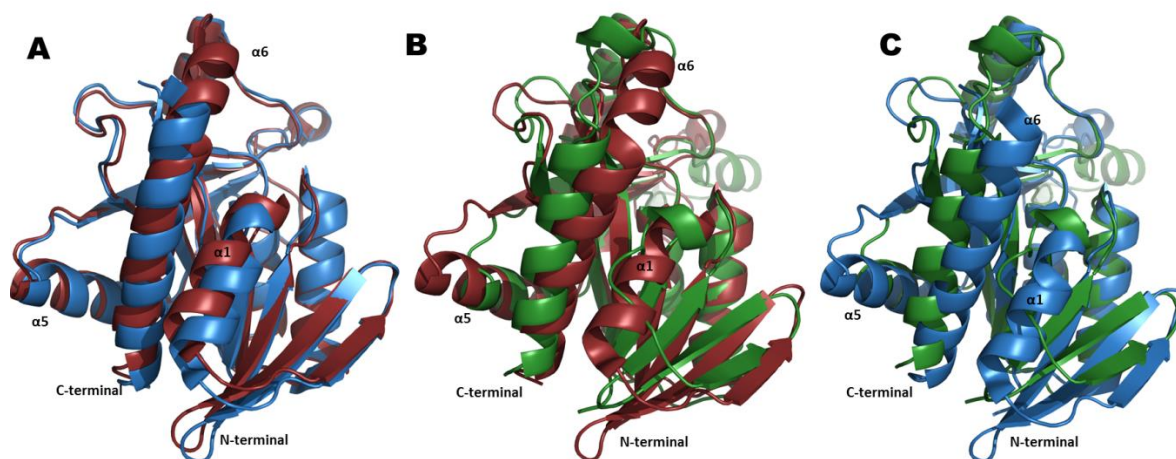


Figure 5.8. (A) Superposition of monomers A and B of HpMTAN. Brown color shows the monomer A in close conformation and blue color shows the monomer B in open conformation. The superposition clearly exhibits changes in helices α -1 and α -6 (PDB-code: 3NM4). **(B) Superposition of monomer A of hypo-TtMqnB with monomer A of HpMTAN.** TtMqnB monomer is shown in green and monomer A of HpMTAN, corresponding to the close conformation is shown in brown. RMSD value of 1.32 Å **(C) Superposition of monomer A of hypo-TtMqnB with monomer B of HpMTAN** (shown in blue) corresponding to the open form. RMSD value of 1.21 Å.

connecting β -11 to α -6 closing the active site. This conformational modification also induces a change in the position of Asp198 allowing it to form hydrogen bonding interactions with adenine moiety and to donate protons to N7 in order to start the catalysis (Figure 5.9D). Superposition of apo-TtMqnB with hypo-TtMqnB monomers showed no significant conformational changes after hypoxanthine binding (Figure 8.14). Structural superposition of both monomers of HpMTAN with hypo-TtMqnB (Figure 5.8B, C) showed RMSD values of 1.21 Å and 1.32 Å for open and close conformation, respectively, suggesting that hypo-TtMqnB was crystallized in an open conformation. However, analyses in helices α -1 and α -6 of TtMqnB showed that the residues involved in the conformational changes assume the orientation corresponding to the close form of MTAN. Figures 5.9B/C show that although Glu11 and Arg183 do not suffer any conformational change after hypoxanthine binding, they are already orientated in the position required for the catalysis (close conformation). The same was observed for Asn187 (Asp198 in HpMTAN). Whereas MTANs dislocate Asp198 closer to adenine moiety in the active site in order to allow hydrogen bonds, Asn187 is already orientated as Asp198 in the close form in both structures (apo-TtMqnB and hypo-TtMqnB), showing a short distance from hypoxanthine for hydrogen bonds (Figure 5.9E, F). Therefore, these observations suggest that similar conformational changes might not be required for MqnB catalysis.

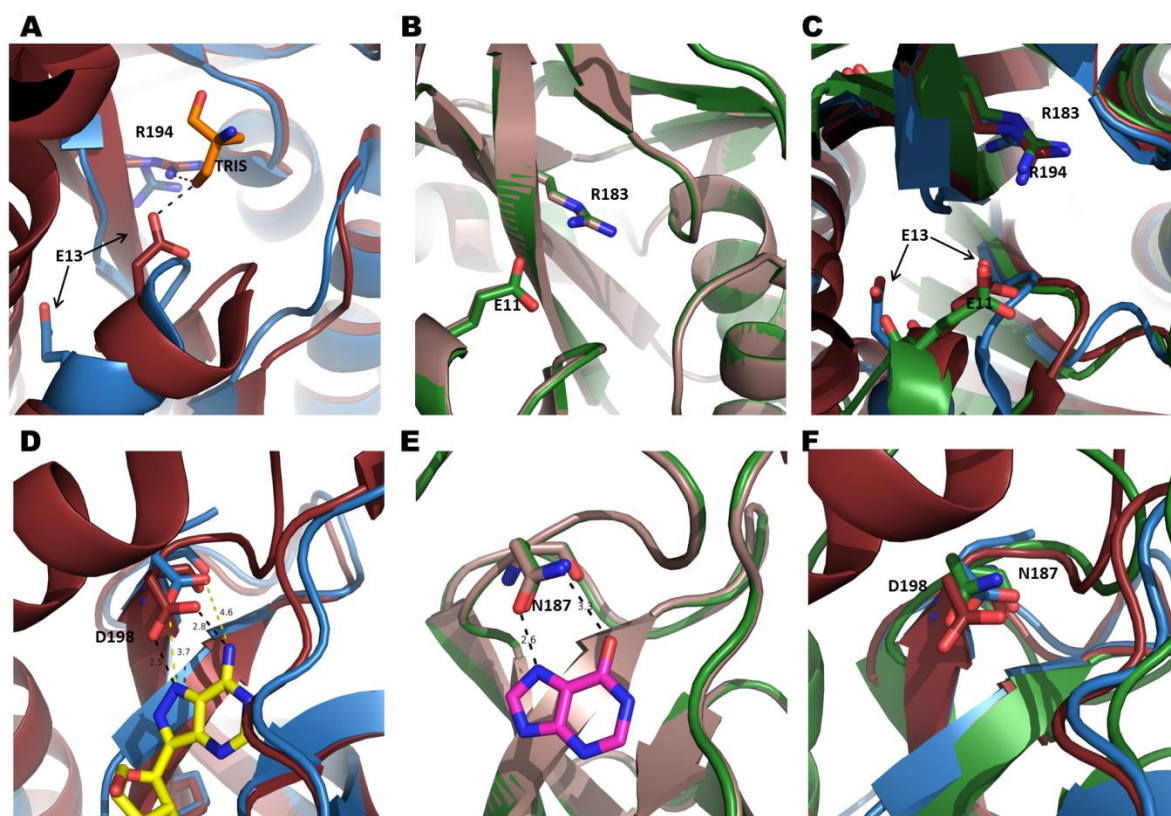


Figure 5.9. (A) Conformational change in helix α -1 of HpMTAN after ligand binding. Blue color corresponds to HpMTAN monomer in an open form and brown color to HpMTAN (close form) containing TRIS in the active site. After TRIS binding, Glu13 shifts towards the active site and together with Arg194 helps the stabilization of the ligand (PDB-code: 3NM4). **(B) Superposition of hypo-TtMqnB with apo-TtMqnB.** Brown structure corresponds to apo-TtMqnB. No changes in Glu11 and Arg183 are observed after hypoxanthine binding (green structure). **(C) Superposition of hypo-TtMqnB with HpMTAN** shows that Glu11 and Arg183 assume the conformation corresponding to the close form of HpMTAN. **(D) Conformational change in helix α -6 of HpMTAN.** The presence of ligand shifts Asp198 to a position closer to the adenine moiety (yellow sticks) in order to allow hydrogen bonds. Yellow dashes show that in an open form, Asp198 is far from adenine with distances of 4.6 Å and 3.7 Å for directly hydrogen bonds. **(E) Superposition of Asn187 in hypo-TtMqnB and apo-TtMqnB.** No conformational change is observed in Asn187 of TtMqnB after ligand binding. Directly hydrogen bonds (black dashes) are possible between hypoxanthine (magenta sticks) and the side chain of Asn187. **(F) Superposition of Asn187 of hypo-TtMqnB with Asp198 of HpMTAN** shows that Asn187 assumes a conformation more similar to the close form of HpMTAN.

The overall structure of TtMqnB is very similar with the other MTANs whose structures have been solved. Each monomer possess a mixed $\alpha+\beta$ fold with a central β -sheet surrounded by five α -helices (Barta et al., 2014; Haapalainen et al., 2013; Lee et al., 2003; Ronning et al., 2010). However, three main structural differences are observed between TtMqnB and MTAN. In MTAN enzymes, helix α -1 involves usually 4 turns, however, this helix is absent in TtMqnB and a 3_{10} helix and random coil structure is found instead (region 1 in Figure 5.10). Another interesting difference concerns the loop involved in the dimerization (region 2 in Figure 5.10). In several MTAN structures this loop contains just random coil structures and a 3_{10} helix formed by five residues, however, in TtMqnB this loop contains a helix with 3 turns (helix α -2) and a 3_{10} helix formed by three residues. In addition, the loop of TtMqnB is longer

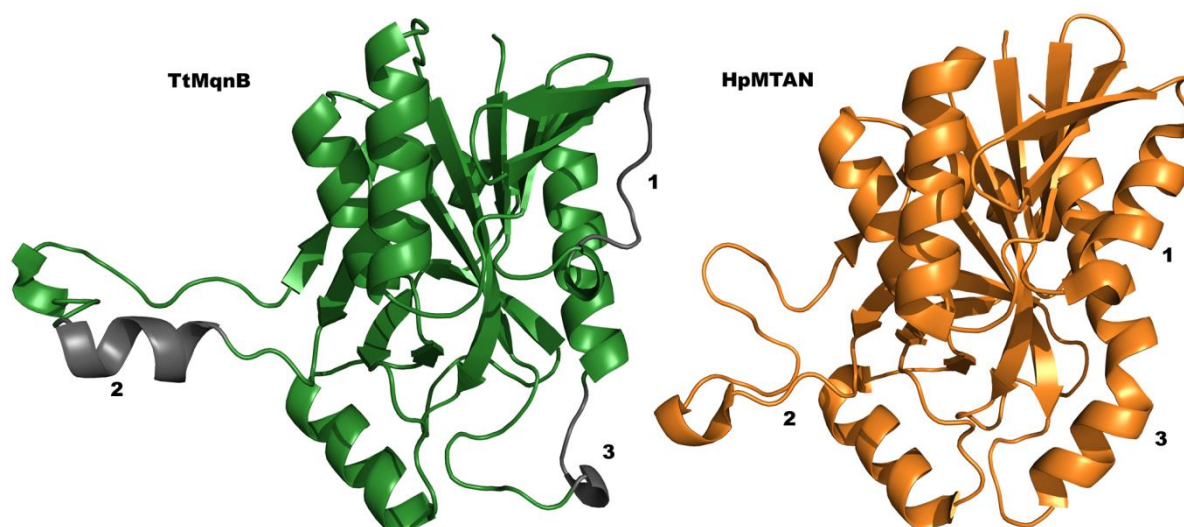


Figure 5.10. Structural conservation of TtMqnB and MTAN enzymes. Structural superposition of monomer A of hypo-TtMqnB (green) and monomer A of MTAN from *H. pylori* (PDB code: 3NM5, orange). Structural differences are highlighted in grey (TtMqnB) and numbered in both structures.

than the one found in MTAN enzymes. The last difference concerns helix α -6, which suffers conformational changes in the presence of ligand. In MTAN enzymes the helix α -6 involves six or seven turns and shows a slight kink oriented to the active site, but in TtMqnB the helix α -6 involves just five turns and the other two turns found in MTAN structures are replaced by random coil and 3_{10} helix structures in monomer A (region 3 in Figure 5.10).

Regarding the homodimeric structure, the biggest structural difference is observed in the loop involved in the dimerization. As previously described, the loop of MTAN contains a 3_{10} helix structure whereas the loop of TtMqnB contains one helix (α -2) and one 3_{10} helix structures. Superposition analysis showed that the helix α -2 of TtMqnB loop partially aligns with 3_{10} helix structure of MTAN while the 3_{10} helix of TtMqnB is completely oriented to outside the molecule and does not make any contact with the opposing monomer (Figure 5.11A, B). In addition, the analysis showed that in MTAN structures, the loop residues interact with the active site of the opposing monomer, but leave it visible and uncovered allowing the ligands to orient themselves to outside the binding pocket (Figure 5.11D). Interestingly, due to the longer loop of TtMqnB, the binding pocket is completely covered, so that the ligands cannot orient themselves to outside the active site (Figure 5.11C). These observations suggest that the MqnB substrate might adopt different conformations than the one described for MTANs.

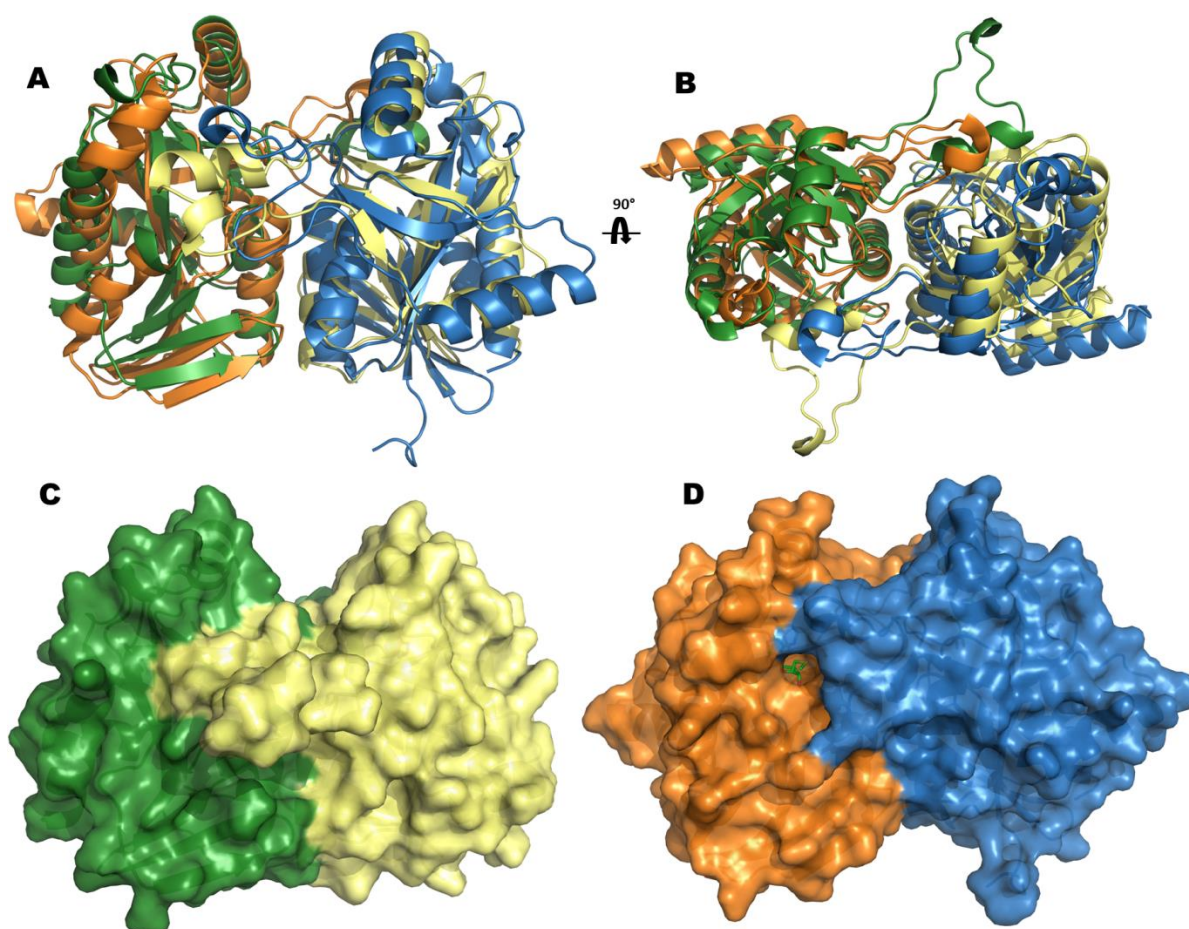


Figure 5.11. Structural comparison between TtMqnB and HpMTAN. (A) Structural superposition of TtMqnB-hypo dimer with monomers represented in green and yellow and HpMTAN dimer (PDB code: 4BMZ) with monomers represented in orange and blue. (B) View after rotation of 90° showing the difference between the loops regions. (C) Surface representation of TtMqnB dimer. The loop of the monomer B (yellow) covers the active site of the monomer A (green) and the binding pocket is not visible. (D) Surface representation of HpMTAN. The loop of the monomer B (blue) interacts with residues from the active site of the monomer A (orange), but leave it uncovered allowing the substrate (green sticks) to orient itself to outside the binding pocket.

5.8. Active-site of MqnB

In contrast to the MTAN enzymes, which have been characterized as multifunctional enzymes, MqnBs appear to be very specific towards the futilosine through replacement of Asp187 to Asn187, which allows the binding with hypoxanthine instead of adenine (Hiratsuka et al., 2009). Interestingly, BLAST searches showed that the genome of *Thermus thermophilus* contains a MTAN homolog (TtMTAN in the alignment, Figure 5.12) which shares 32% and 34% sequence similarities with EcMTAN and HpMTAN, respectively. TtMTAN shares 34% identity with TtMqnB and possess an aspartate residue at position 187 instead of asparagine, indicating that this enzyme likely accepts substrates containing the adenine moiety rather than hypoxanthine. Thus, the presence of TtMTAN and TtMqnB suggests separation of purine biosynthesis and futilosine pathway.

Chapter 5: Crystal structure of the futasolase TtMqnB

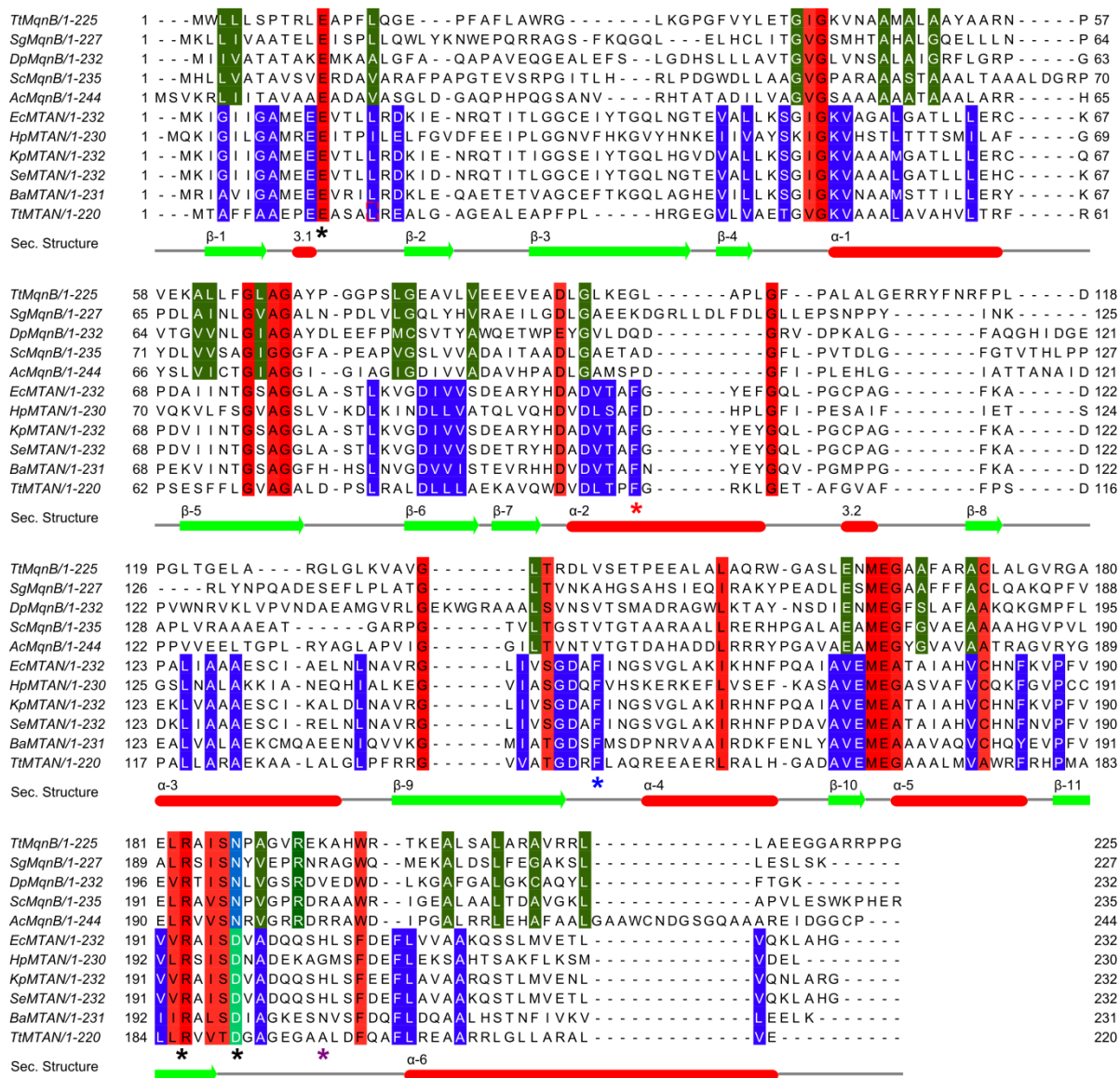


Figure 5.12. Protein sequences alignment of MqnB and MTAN enzymes. Protein were aligned by MUSCLE (Edgar 2004) and optimized in Jalview (Waterhouse et al., 2009). Green color shows the conserved residues in MqnB enzymes and blue color shows the conserved residues in MTAN enzymes. The conserved residues in all sequences are shown in red. Black asterisks (*) indicate the amino acids involved in the catalytic triad. Secondary structure is shown based on the crystal structure of TtMqnB. β -sheets and α -helices are shown in green and red, respectively. 3_{10} -Helix structures are represented as 3.1 and 3.2. The aligned sequences from top to bottom are: MqnB from *Thermus thermophilus* (TtMqnB) (Q72L73), MqnB from *Saprosira grandis* (SgMqnB) (J0XUB6), MqnB from *Desulfovibrio piezophilus* (DpMqnB) (M1WSJ0), MqnB from *Streptomyces coelicolor* (ScMqnB) (Q9KXN0), MqnB from *Acidothermus cellulolyticus* (AcMqnB) (A0LR22), MTAN from *E. coli* (EcMTAN) (POAF12), MTAN from *Helicobacter pylori* (HpMTAN) (Q9ZMY2), MTAN from *Klebsiella pneumoniae* (KpMTAN) (A6T4W3), MTAN from *Salmonella enterica* (SeMTAN) (A0A0J9WZM1), MTAN from *Bacillus anthracis* (BaMTAN) (Q81LL4) and MTAN from *Thermus thermophilus* (TtMTAN) (Q72IE7).

The crystal structure of TtMqnB soaked with hypoxanthine showed that the molecule is stabilized by hydrogen bonds between the oxygen of hypoxanthine (O6) and the ND2 of Asn187 (Figure 5.13) as well as the backbone oxygen of Ser143 (through a water molecule). The OD1 atom of Asn187 forms a hydrogen bond with the nitrogen N7 of

hypoxanthine (2.7 Å) and the side chain of Glu161 forms a hydrogen bond with nitrogen N1. In addition, the nitrogen N9 of hypoxanthine makes hydrogen bonds with ethylene glycol molecule (3.1 Å) in monomer A (Figure 5.13).

The active site of MTAN has been extensively studied and can be divided into three regions: 1) the adenine, 2) the ribose, and 3) the 5'-alkylthio-binding sites (Lee et al., 2003, 2005). The adenine-binding site of HpMTAN consists of residues Val154, Phe153, Ser197, Asp198 and Ala200. In the binding pocket of HpMTAN containing formycin A (FMA), the main chain carbonyl oxygen and the amide nitrogen of Val154 form hydrogen bonds with the amino group N6 and N1 of the adenine base, respectively. In addition, OD1 and OD2 of Asp198 also form hydrogen bonds with N6 and N7 of the adenine base, respectively. Ser197 and Ala200 do not interact directly with the adenine moiety but orient the side chain of Asp198 through hydrogen bonds with OD2 and OD1, respectively (Figure 5.14A). This region of the binding pocket of TtMqnB shows a similar arrangement with HpMTAN with slight changes. The first one is the substitution of Val154 for Ser143. Although the main chain carbonyl oxygen of Ser143 is far from hypoxanthine to directly bind, this residue helps the ligand stabilization

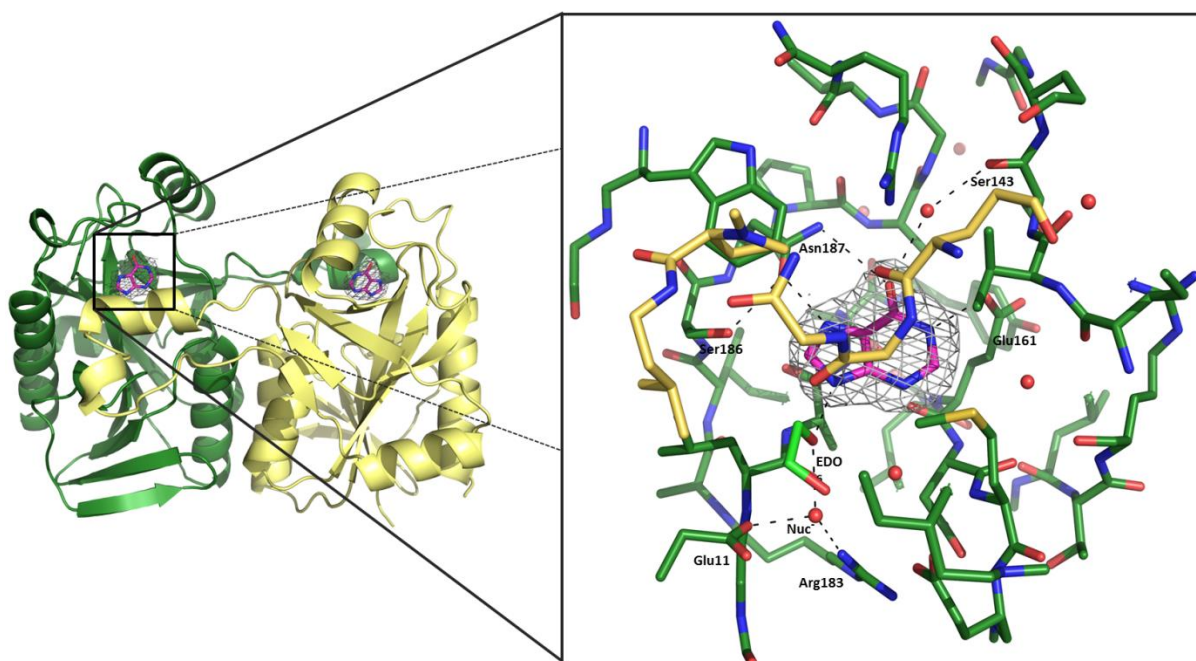


Figure 5.13. Substrate binding and active site of TtMqnB. Active site of monomer A is shown in detail. Hypoxanthine (magenta sticks) is stabilized by hydrogen bonds (dashed lines) with residues Asn187 and Ser143 through coordination with a water molecule. Ethylene glycol (EDO) also contributes for hypoxanthine stabilization in monomer A; this interaction is not found in monomer B. Nucleophilic water (Nuc⁻) is coordinate by Glu11 and Arg183. The grey mesh corresponds to $2F_o - F_c$ electron density (contoured at 1.0 σ). Water molecules are shown in red spheres.

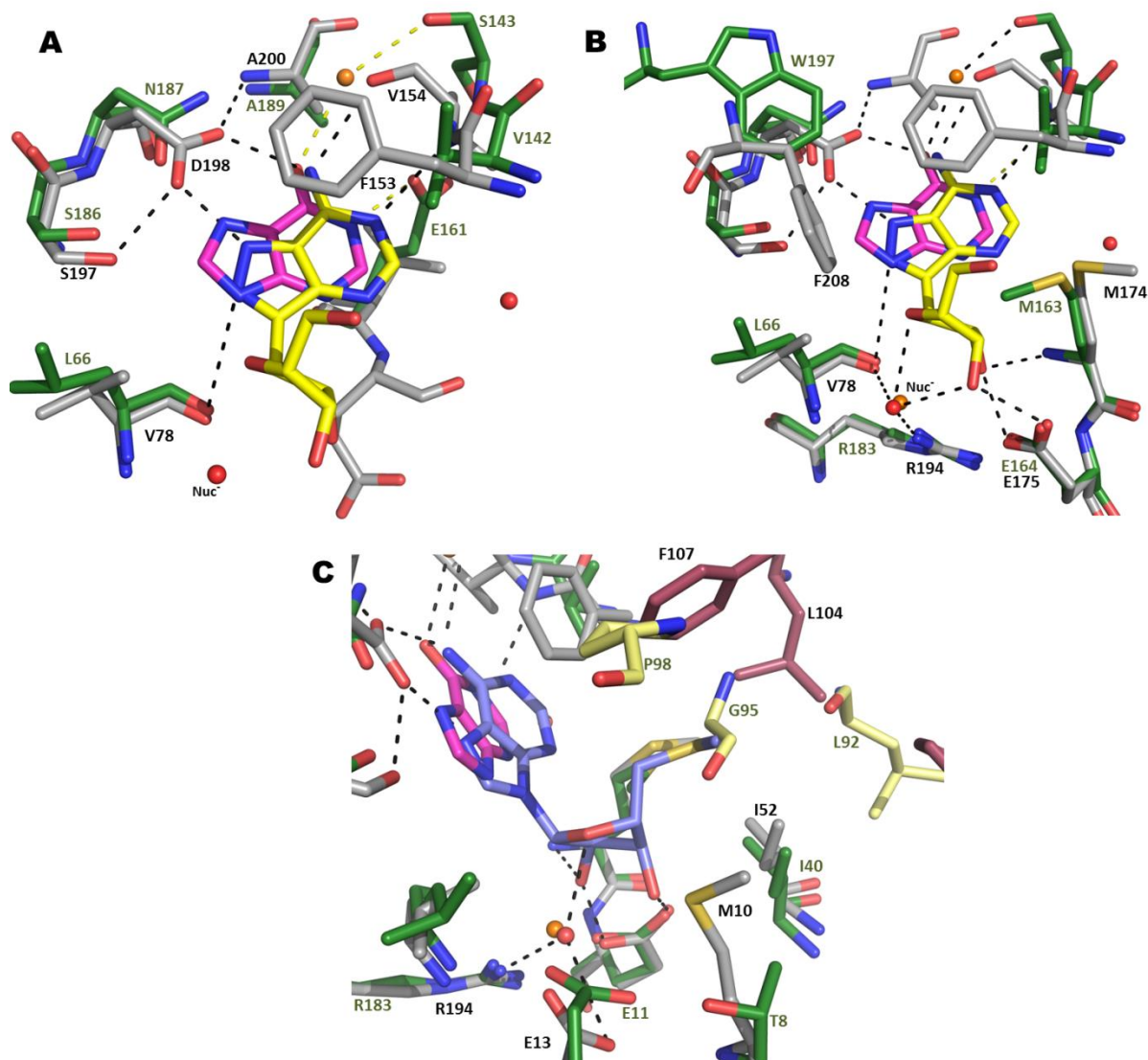


Figure 5.14. Structural comparison of the TtMqnB and HpMTAN active site. (A) Adenine-binding site. Residues important for adenine/hypoxanthine moiety are shown. HpMTAN (PDB code: 3NM5) residues are shown in gray and labeled in black while TtMqnB residues are shown in green and labeled in green. Superposition of both structures shows that hypoxanthine (magenta sticks) superposes with the adenine moiety of formycin A (yellow sticks). Black dashes indicate the hydrogen bonds present in both structures and yellow dashes indicate hydrogen bonds found just in TtMqnB. Red and orange spheres correspond to water molecules from HpMTAN and TtMqnB, respectively. **(B) Ribose-binding site.** The residues for the ribose stabilization are highly conserved in both structures. Nucleophilic water (Nuc⁻) plays also an important role in ribose stabilization through hydrogen bonds between L66/V78, R183/R194 with oxygen O4' of the ribose. **(C) 5'-Alkylthio-binding site.** Manual modeling of 5'-methiothioadenosine (purple sticks) shows that in HpMTAN the homocysteine moiety is stabilized by L104 and by the aromatic side chain of F107 from the neighboring monomer (sticks shown in pink). TtMqnB neighboring monomer has a glycine (G95, shown in yellow) instead of F107 at the same position and the structure shows that G95 is orientated in front of the homocysteine moiety and hence collides with it.

by forming hydrogen bonds through a water molecule with O6 of the hypoxanthine (Figure 5.14A, shown in yellow). Another difference is the presence of hydrogen bond between the oxygen OE2 of Glu161 and N1 of hypoxanthine (Figure 5.14A, shown in yellow). This residue is highly conserved in MqnB enzymes, suggesting its importance for substrate binding. In MTAN enzymes, however, this residue is substituted by valine (from the AVE motif) (Figure

5.12, β -10) and although the AVE motif is conserved in MTANs, no interaction with the adenine moiety has been observed. The last difference is the presence of Phe153 in MTAN enzymes. According to Lee et al., (2003), an aromatic residue (Phe or Tyr) is structurally conserved in MTA/Ado/Hcy nucleosidases and helps the stabilization of the adenine ring by base-stacking interaction (Figure 5.12, asterisks shown in blue). Such interaction, however, is not observed in MqnB enzymes, since they contain a valine, Val142, (or alanine in SgMqnB) at this position (Figure 5.14A).

The ribose-binding site of HpMTAN consists of residues Val78, Met174, Glu175, Arg194 and Phe208, which anchor the ribose moiety by both hydrogen bonds and van der Waals contacts (Lee et al., 2003) and is probably equivalent in TtMqnB (Figure 5.14B). Two water-mediated hydrogen bonds are observed between the main chain carbonyl oxygen of Val78 (Leu66 in TtMqnB) and O4' of the ribose and between the amide group NH1 of Arg194 (Arg183 in TtMqnB) with O4' of the ribose. Two additional hydrogen bonds are made by OE1 and OE2 of Glu175 (Glu164 in TtMqnB) to O2' and O3' hydroxyls of the ribose, respectively. Finally, the last hydrogen bond is made between the backbone amide hydrogen of Met174 (Met163 in TtMqnB) with the O2' of the ribose. Lee et al., (2003) also showed that Phe207 (Trp197 in TtMqnB) contributes for the sugar moiety stabilization through van der Waals contact with C4' of the ribose. Although an aromatic residue is conserved at this position, Trp197 of TtMqnB is too far from the ribose to make van der Waals contact and unlikely helps the stabilization of the sugar moiety. However, the possible role of this residue in the active site will be discussed later.

The 5'-alkylthio-binding sites of MTAN and TtMqnB show the greatest difference. Lee et al., (2003) reported that the 5' substituents of the ligands are stabilized by hydrophobic interactions. In HpMTAN, the hydrophobic pocket consists mainly of Ile52, Met10, Leu104 and Phe107, with Leu104 and Phe107 donated from the neighboring monomer. These residues (except Ile52) are not conserved in MqnBs (Figure 5.14C). Met10 is replaced by Thr8 in TtMqnB that is far for hydrophobic interactions. Leu104 corresponds to Leu92 in TtMqnB, but this residue is not conserved in MqnBs and the side of chain of Leu92 is orientated in the opposite of Leu104. In other words, Leu92 is unlikely involved with stabilization of the 3-keto benzoic acid moiety of futasosine (corresponding to the homocysteine moiety). Phe107 is conserved in MTANs enzymes and described to play a role in stabilization of the 5'-alkylthio group through van der Waals interaction (Lee et al., 2003; Mishra and Ronning, 2012). MqnB enzymes do not have any aromatic residue conserved at this position (Figure 5.12, asterisk shown in red); TtMqnB has, for instance, a glycine (Glu95) at this position that would collides with the homocysteine moiety. All together, these observations suggest that the keto benzoic acid moiety of futasosine might adopt a different conformation to the 5'-alkylthio group (Figure 5.14C).

MTANs from *E. coli* and from *H. pylori* have been well studied in the last decade (Kim et al., 2014; Lee et al., 2005; Ronning et al., 2010). According to the proposed mechanism (Figure 5.15), catalysis starts by proton transfer from Asp198 to the N7 atom of the substrate generating a delocalized positive charge on the adenine moiety, which leads to the rupture of the bond between N9 of the adenine and the C1 of the ribose group. This produces a carbocation that is attacked by a nucleophilic water molecule coordinated in the active site by Glu13 and Arg194. Mutations on these amino acids (D198N, D198A and E13Q, E13A) abolished the activity of HpMTAN, indicating the importance of this catalytic triad for MTAN enzymes (Kim et al., 2014). In TtMqnB, two out of the three residues of the catalytic triad are conserved (Glu11 and Arg183), but as already mentioned, asparagine (Asp187) is found in place of Asp198. Interestingly, Kim and co-workers (2014) showed, using structural studies, that the HpMTAN mutant D198N (corresponding to MqnB enzymes) is able to bind MTA; however, the asparagine is unable to bind the adenine tight enough to hydrolyze the ligand. These findings, along with the structure of TtMqnB with the hypoxanthine molecule strongly suggest that this substitution is essential for futasosine recognition and hydrolysis, since the ND2 of Asn187 would be able to donate protons to O6 of the hypoxanthine.

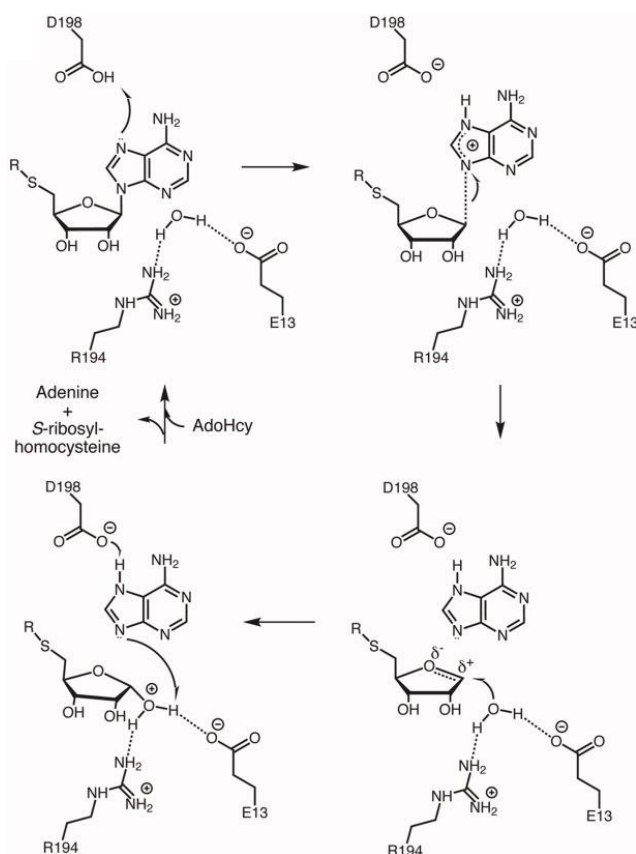


Figure 5.15. Proposed enzymatic mechanism for MTAN enzymes with the catalytic triad. The side chain of Asp198 donates a proton to the adenine moiety generating a delocalized positive charge. The delocalized charge makes the bond between N9 and C1 of the ribose more susceptible to nucleophilic attack by a water molecule that is coordinate by Glu13 and Arg 194 (Ronning et al., 2010). In TtMqnB Glu11, Arg183 and Asn187 are likely involved in the catalytic triad.

5.10 Discussion

Here we described the first crystal structures of an MqnB homolog from *Thermus thermophilus* in the presence and absence of hypoxanthine. The structure of TtMqnB displays a high level of structural similarities with the MTAN enzymes, although some structural differences were observed. The biggest difference concerns the two different enzyme conformations. Crystal structures of MTAN enzymes have revealed that these proteins assume a close conformation, induced by a ligand in the active site, and an open conformation, when the active site is empty (Kim et al., 2014; Lee et al., 2003; Ronning et al., 2010). Comparison between both forms showed that the presence of ligands in the active site induces conformational changes mainly in the helix α -1 by changing the orientation of Glu13 towards the binding pocket, and in the helix α -6 by (i) causing structural rearrangement in Asp198 that allows it to form hydrogen bonding interactions with the adenine moiety and (ii) forming a cap over the substrate binding site closing it (Figure 5.9) (Ronning et al., 2010). The current results showed that no conformational changes were observed in the structure of TtMqnB after binding of hypoxanthine. Structural superposition of TtMqnB with HpMTAN monomers corresponding to open and close formation showed RMSD values of 1.21 Å and 1.32 Å, respectively, suggesting that TtMqnB is more similar with the open form. However, analyses on helices α -1 and α -6 showed that although no conformational changes are observed in TtMqnB after hypoxanthine binding and that the residues involved in the conformational changes and important for catalysis (Glu11, Arg183 and Asn187) assume similar orientation to the close form of HpMTAN (Figure 5.9).

The conformational changes in MTAN enzymes have been described as essential for substrate binding and enzymatic activity (Lee et al., 2003, 2005; Ronning et al., 2010). In studies with MTAN from *Salmonella enterica* (SeMTAN), Haapalainen and co-workers (2013) have suggested that just a molecule of adenine alone is not sufficient to change the protein conformation from open to close form. Indeed, structural analyses of others MTANs in the close form showed that adenine is not the only ligand present in the active site. The structure of MTAN from *Klebsiella pneumoniae* (KpMTAN), for instance, contains an S-adenosyl-L-homocysteine (SAH) molecule in the active site in addition to the adenine molecule (PDB code: 4G89). Another example is the structure of MTAN from *Helicobacter pylori*, which contains one adenine and one tris molecule that occupies the ribose subsite (PDB code: 4BMX). On the other hand, structures that just contain adenine in the active site have not shown any conformational change when compared with the apo structure, as observed in the structure of CT263 (MTAN) from *Chlamydia trachomatis* (CtMTAN) (PDB code: 4QAR and 4QAQ) (Barta et al., 2014). The structure of MTAN from *E. coli* containing just one molecule of adenine in the active site showed an open form (PDB code: 1JYS);

however, the structure changed to the close form when a molecule of 2-(4-amino-pyrorrolo[2,3-D]pyrimidin-7-YL)-5-methylsulfanylmethyl-tetrahydro-furan-3,4-diol (MTH) was bound in the active site (PDB code: 1NC1), suggesting that the adenine molecule is too small to induce conformational changes (Lee et al., 2003, 2005). Based on this finding, that just adenine is not enough to induce conformational changes, it would be expected some conformational modification in the monomer A of hypo-TtMqnB structure, since the active site of this monomer contains not only hypoxanthine, but also a molecule of ethylene glycol (EDO) (Figure 5.13).

Superposition of TtMqnB monomer A with HpMTAN (PDB code: 3NM5) containing formycin A (FMA) and 5'-methiothioadenosine (MTA) in the active site showed that the EDO molecule occupies partially the subsite of the ribose moiety. In addition, the position of EDO is almost the same occupied by the tris molecule that was able to cause conformational changes in the structure of HpMTNA (PDB code: 3NM4). According to Ronning and co-workers (2010) the tris molecule was able to stabilize the close conformation due to hydrogen bonding interactions between residues Glu13, Glu175 and Arg194. Thus, it was suggested that any molecule able to interact with this three residues simultaneously would be sufficient to stabilize the close conformation. In fact, the most molecules that were able to change the enzyme conformation from open to close form showed such hydrogen bonding interactions. The KpMTAN structure containing adenine and SAH molecule in the active site showed that the ribose moiety of the SAH forms a hydrogen bonded network with residues Glu12, Glu174 and Arg193 with distances of 4.0 Å, 2.6 Å and 3.4 Å, respectively. However, analyses of the crystal structure of SeMTAN (PDB code: 4F1W) containing adenine and triethylene glycol (PGE) molecules showed that the presence of both ligands were sufficient to change the enzyme conformation to the close form, although the PGE molecule is quite far from the Glu12, Glu174 and Arg193 residues with distances of 4.9 Å, 5.7 Å and 7.0 Å, respectively, to form stable hydrogen bonds. On the other hand, the EDO molecule in the active site of TtMqnB-hypo monomer A forms a hydrogen bond with the Glu11 with distance of 3.2 Å, but it is also far from to the Glu164 and Arg183 to form hydrogen bonding interactions, with length of 4.3 Å and 5.1 Å, respectively. The fact that PGE was able to induce conformational changes in SeMTAN even without directly contacts with Glu12, Glu174 and Arg193 suggests that EDO would also be able to induce changes in the structure of TtMqnB. However, the first structural insights of TtMqnB showed that the residues important for catalysis assume already an orientation similar to the close form. All together, the results strongly suggest that the conformational changes induced by ligands observed in MTANs might not be a feature of the MqnB enzymes. Nevertheless, to conclude such observation other soaking or co-crystallization experiments with TtMqnB using larger molecules are necessary.

The binding site of TtMqnB showed several similarities with the binding site of MTAN enzymes. As observed for MTANs, the active site of TtMqnB can be divided into three regions: 1) adenine/hypoxanthine, 2) ribose, and 3) 5'-alkylthio/keto benzoic acid-binding site. Whereas the adenine/hypoxanthine and the ribose binding site showed high similarities, the 5'-alkylthio or keto benzoic acid-binding site was the region that most distinguish from each other, likely because this moiety is responsible for the diversity of the substrates accepted by MTAN enzymes. In MTANs this part of the binding site is occupied by the homocysteine moiety which is stabilized by hydrophobic interactions (Lee et al., 2003). In the active site of HpMTAN, two residues play an important role in the interaction between the homocysteine moiety and the 5'-alkylthio binding site: Phe107 and Asp209 (Mishra and Ronning, 2012). Asp209 is located near the N-terminus of the helix α -6 and also undergoes ligand-induced conformational change. Due to elongation of the helix α -6, Asp209 shifts towards the active site (5.2 Å) and helps substrate stabilization in two different ways, depending of the substrate. When MTA is the substrate, the stabilization is by solvent interactions through hydrogen bonds between Asp209-water-water. When SAH is the substrate, the stabilization is through a water-mediated hydrogen bond between Asp209 and the α -amino moiety of the SAH (Mishra and Ronning, 2012). Phe107, from the opposing molecule, does not undergo conformational changes after ligand binding and helps the stabilization by van der Waals-type interactions with the 5'-alkylthio group. Both residues (Asp209 and Phe107) are highly conserved in more than 85% of the MTAN enzymes and mutations of these residues to alanine showed decrease in the catalytic activity (Mishra and Ronning, 2012). Kim and co-workers (2014) also suggested, using a futasoline molecule modeled in the active site of HpMTAN, that Phe107 could help the stabilization of the substrate by interacting with the aromatic ring of the benzoic acid group, since this moiety would be likely orientated to outside the binding pocket. However, analysis of the binding pocket of TtMqnB showed that the 3-keto benzoic acid moiety likely assume a different conformation to the 5'-alkylthio group in MTAN (Figure 5.11).

MqnB enzymes have neither a conserved Asp/ Glu residue corresponding to Asp209 nor a conserved aromatic residue corresponding to Phe107 (Figure 5.12, asterisk shown in red), suggesting that the substrate recognition must be different. Other evidence that supports a different ligand conformation is the lack of sufficient volume in the active site of TtMqnB to accommodate the 3-keto benzoic acid moiety as the 5'-alkylthio group (Figure 5.17). A closer look in the binding pocket of both enzymes show that the TtMqnB possess a longer and more open binding pocket that extends to the left side of the pocket, which likely allows the

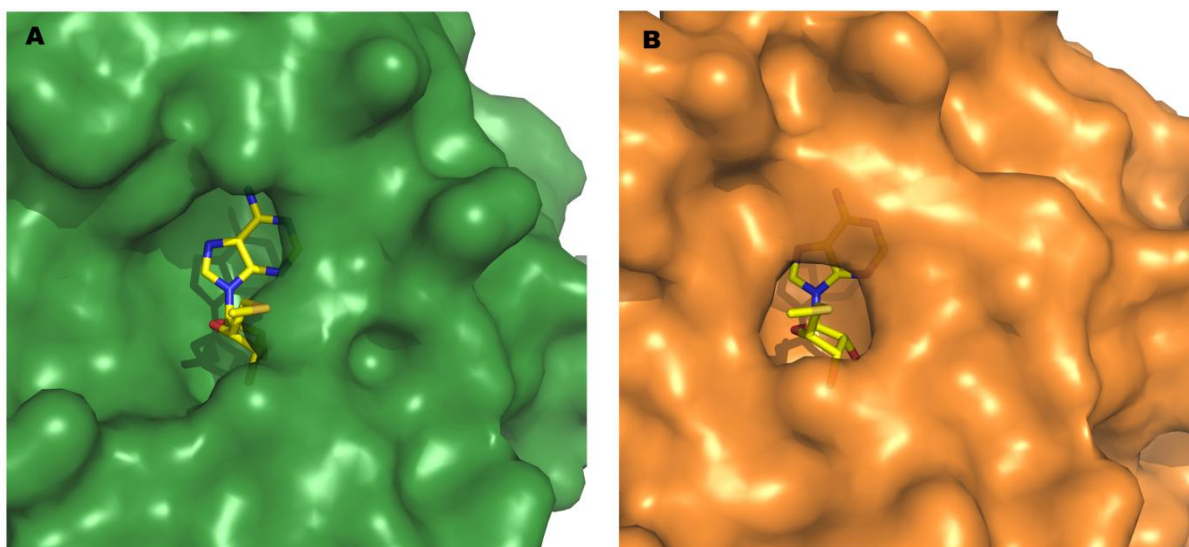


Figure 5.17. Difference in the binding pocket of TtMqnB and HpMTAN. (A) Binding pocket of TtMqnB. Surface representation of TtMqnB-hypo structure (monomer A) with the presence of MTA molecule (yellow sticks) in the active site. **(B) Binding pocket of HpMTAN.** Surface representation of HpHMTAN (PDB code: 3NM4) with the presence of MTA (yellow sticks) in the active site. While the binding pocket of HpMTAN is smaller than the TtMqnB and orients the substrate to outside the pocket, the binding site of TtMqnB extends to left side, suggesting different substrate conformation.

binding of the 3-keto benzoic acid moiety. In addition, the left side-surface that extends from the binding pocket present a hydrophobic region that could help the stabilization of substrate by hydrophobic interactions. To get more insights about these possible interactions, fufalosine was modeling in the active site using the AutoDock Vina program (Trott and Olson, 2010). The solutions are shown in Figure 8.15. The best score, with affinity of -9.3 kcal/mol, shows that different to the possible interactions suggested when fufalosine was modeled in the structure of HpMTAN (Kim et al., 2014), the aromatic ring of the benzoic acid is likely stabilized by hydrogen bonds and hydrophobic interactions (Figure 5.18A). The carboxyl group of the benzoic acid forms two hydrogen bonds with the side chains of Arg192 and Lys194, respectively (Figure 5.18B). Alignment of MqnBs sequences shows that MqnB homologs contain a basic amino acid conserved at position 194 (except the sequence of DpMqnB) (Figure 5.12, asterisk shown in purple) and that Arg192 is conserved in all homologs but not in MTAN enzymes, suggesting the importance of these amino acids in the binding pocket. The aromatic ring of the benzoic acid is likely stabilized (i) by hydrophobic interactions with the side chain of Trp197 (also conserved in all MqnB homologs) (Figure 5.18B) and (ii) by interactions between the hydrophobic wall as well as the hydrophobic region of the loop that cover the binding pocket of the opposing molecule.

Although the interactions using fufalosine are speculative, it provides some hints about possible residues involved in the 3-keto benzoic acid moiety stabilization and points to other differences between MqnB and MTAN enzymes.

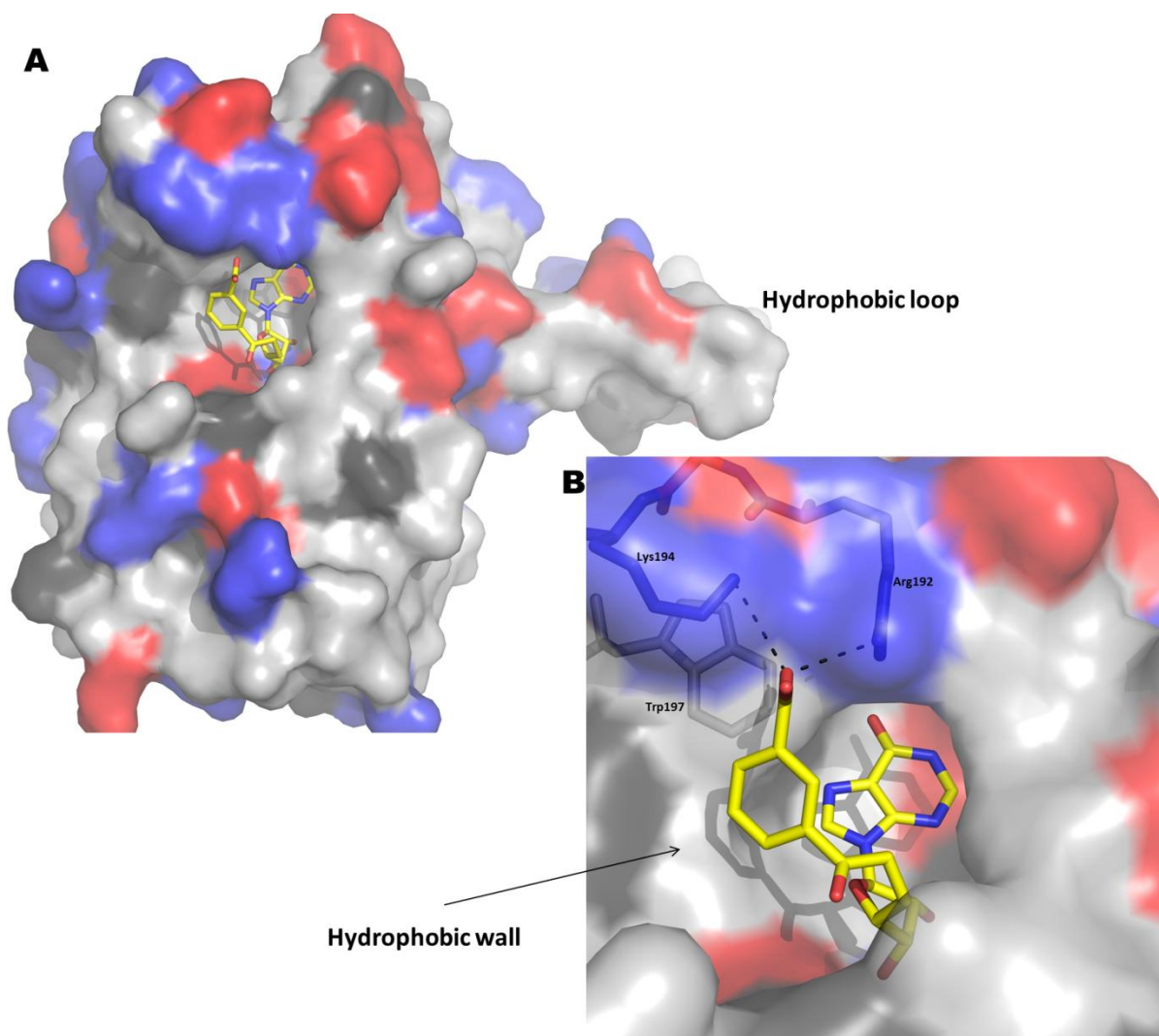


Figure 5.18. (A) Surface representation of electrostatic potential of TtMqnB. Color scheme represents regions of negative charged (red), positive charged (blue), hydrophobic (light grey) and polar (dark grey). Futasoline molecule (yellow sticks) was modeled in the active site using the AutoDock Vina program. **(B) Binding pocket of TtMqnB.** Proposed interactions for stabilization of the 3-keto benzoic acid moiety of futasoline. The carboxyl group likely forms hydrogen bonds with Arg192 and Lys194, whereas the benzene ring might be stabilized by the hydrophobic wall that extends through the left-side of the binding pocket and by hydrophobic interactions with Trp197 side chain. The hydrophobic loop of the opposite molecule might also help the stabilization of futasoline.

Enzymes essential for bacterial respiratory pathway represent attractive drug targets. In this context, the enzymes belonging to the menaquinone pathway have been highlighted, since this pathway is present in Gram-positive bacteria and absent in humans (Kurosu *et al* 2010). Inhibition of MenA (1,4-dihydroxy-2-naphthoate prenyltransferase) inhibits the growth of *Mycobacterium tuberculosis* (Mtb) with no effect in Gram-negative bacteria (Debnath *et al.*, 2012; Kurosu and Crick, 2009). MenB, MenD and MenE enzymes have also recently been studied for the development of novel antibacterial drugs (Fang *et al.*, 2010; Li *et al.*, 2010; Lu *et al.*, 2008). The discovery that the futasoline pathway is absent in *E. coli* and in humans

allows a new route for the development of new drug targets against pathogenic bacteria such as *H. pylori* and *Campylobacter jejuni*.

Structure-based inhibitor design has been described as a helpful tool in this field by providing information about catalytic mechanisms and enzyme binding sites that leads to the development of inhibitors (Lee et al., 2003; Mishra and Ronning, 2012; Ronning et al., 2010). Haapalainen and co-workers (2013) developed, for instance, MTAN inhibitors that are able to bind with low inhibitory constant (K_i) of 1.5 and 5.0 pM in the 5'-alkylthio-binding subsite of SeMTAN. Thus, the structural information of the first MqnB homolog described in this work can be used with fragment-based design methodology to generate compounds that could target the active site. The differences observed in the binding pocket of TtMqnB and the putative residues involved in the stabilization of the 3-keto benzoic acid moiety could lead to new potential drugs for this enzyme that could be used in the treatment of pathogenic strains of *Streptomyces ssp.*

6. Summary

The first part of this work describes the cloning, expression, purification and characterization of EcMenA, the enzyme responsible for the prenylation step during the menaquinone (MK) biosynthesis in *E. coli*. The results showed that during the purification of EcMenA (cloned in the pET15b-TEV vector) a high amount of SlyD protein was detected. The contaminant protein could be eliminated by changing the cloning (using a GFP-fusion vector) and purification strategies.

Membrane fraction containing overexpressed EcMenA was able to prenylate DHNA-2 using prenyl-donors with different side length (GPP, FPP, GGPP and GFPP); however, the enzyme showed a high specificity towards DHNA-2 as prenyl-acceptor. Enzymatic assays demonstrated that EcMenA activity remains not only after solubilization in DM and DDM, but also after purification. A decrease of the activity level was observed during the protein purification due to presence of imidazole, which likely binds to Mg²⁺ and/or Asp situated in the active site.

Mutation on Asp65 to Arg65 in EcMenA abolishes the enzymatic activity and the cells growth at anaerobic conditions, indicating the importance of this residue for MK biosynthesis.

The current results show good stability of EcMenA after detergent solubilization and purification. However, the low yield of pure protein achieved after purification was the limiting factor for crystallization setups. Although the structures of two aromatic prenyltransferases have recently been released, both enzymes did not show enzymatic activity, what makes EcMenA an interesting target for structural studies.

The second part of the work describes the cloning, expression, purification and classification of TtUbiA and SIUbiA in a novel class of aromatic prenyltransferase. Initial BLAST analyses suggested that TtUbiA was the UbiA homolog in *T. thermophilus* and likely involved in the ubiquinone biosynthesis; however, enzymatic assays showed that TtUbiA does not recognize PHB as aromatic substrate. The main reason for the lack of activity towards PHB was attributed to the fact that *T. thermophilus* has just menaquinone as the sole quinone for the electron transport during the respiratory chain. *T. thermophilus* synthesizes MK via futasolose pathway, which leads to DHNA-6 as a potential substrate. However, activity assays using this aromatic compound resulted in no prenylated compound. Activity assays using DHNA-2 also failed.

Different approaches were used in order to figure out possible reasons for the lack of activity of TtUbiA: (i) expression of *Streptomyces lividans* UbiA (SIUbiA) in *Streptomyces lividans* cells, to analyze the effect of different membrane composition, (ii) generation of mutant proteins, TtUbiAR59D and SIUbiAR73D, and (iii) different molecules to mimick the possible substrate.

The enzymatic assays results using the SIUbiA expressed in *S. lividans* showed that this enzyme also does not recognize PHB or DHNA-2 or DHNA-6 as substrate. On the other hand, EcMenA expressed in *S. lividans* cells was able to prenylate DHNA-2, showing that the cell membrane of this strain is able to support prenyltransferases activity. Therefore, the results suggest that the membrane composition plays not a crucial role in the lack of activity of TtUbiA expressed in *E. coli*. Enzymatic assays using the mutants (TtUbiAR59D and SIUbiAR73D) and PHB, DHNA-2 and DHNA-6 also resulted in non-prenylated products, suggesting that TtUbiA and SIUbiA have neither UbiA nor MenA activities. Alignment and phylogenetic analyses indicates that these enzymes belong to a different class of aromatic prenyltransferases (called in this work as MqnF) and recognize a different substrate, still unknown to date.

The last part of the work describes the first crystal structure of an MqnB homolog from *T. thermophilus* (TtMqnB). The crystal structures of TtMqnB suggested a dimer in solution, which was confirmed by analytical ultracentrifugation (AUC).

TtMqnB structure shows high structural similarities with the 5'-Methylthioadenosine Nucleosidase (MTAN) enzymes, but some differences in the loop region and ligand-induced conformation changes were observed. TtMqnB does not seem to undergo the same conformational changes induced by ligand, as described for MTANs. Comparison of apo and hypo-TtMqnB structures shows that the residues likely involved in catalytic triad are already oriented to the active site, similarly to the close (or ligand-bound) conformation of MTAN. However, others conformational changes cannot be discarded in the presence of futasine or bigger ligands. Soaking experiments of TtMqnB crystals with hypoxanthine also showed that Asn187 (conserved in all MqnB homologs) is essential for substrate recognition and stabilization.

Another difference observed between the two enzymes is the orientation of the homocysteine moiety. Docking analysis of TtMqnB with futasine suggests that the keto benzoic acid moiety is stabilized by hydrogen bonds between the carboxyl group of the benzoic ring with Arg192 and Lys194 (conserved in MqnB homologs) and by hydrophobic interactions with the side chain of Trp197 and with the loop of the neighbor molecule that cover the active site.

The results show a good overview of the MqnB structure and its active site, but due to the difficulties to obtain futasine, activity assays were not performed. However, once the substrate is available one could perform enzymatic activities with the wild type and generate mutants to obtain more insights about important residues involved in the catalytic activity.

7. References

- Abdul-Gader, A., Miles, A.J., and Wallace, B.A. (2011). A reference dataset for the analyses of membrane protein secondary structures and transmembrane residues using circular dichroism spectroscopy. *Bioinformatics* 27, 1630–1636.
- Adams, P.D., Afonine, P. V., Bunkóczi, G., Chen, V.B., Davis, I.W., Echols, N., Headd, J.J., Hung, L.-W., Kapral, G.J., Grosse-Kunstleve, R.W., et al. (2010). PHENIX: a comprehensive Python-based system for macromolecular structure solution. *Acta Crystallogr. D. Biol. Crystallogr.* 66, 213–221.
- Altschul, S.F., Gish, W., Miller, W., Myers, E.W., and Lipman, D.J. (1990). Basic local alignment search tool. *J. Mol. Biol.* 215, 403–410.
- Amante, T.D., and Ahemed, T.A. (2015). Risk factors for unsuccessful tuberculosis treatment outcome (failure, default and death) in public health institutions, Eastern Ethiopia. *Pan Afr. Med. J.* 20, 247.
- Andersen, K.R., Leksa, N.C., and Schwartz, T.U. (2013). Optimized *E. coli* expression strain LOBSTR eliminates common contaminants from His-tag purification. *Proteins* 81, 1857–1861.
- Arai, R., Murayama, K., Uchikubo-Kamo, T., Nishimoto, M., Toyama, M., Kuramitsu, S., Terada, T., Shirouzu, M., and Yokoyama, S. (2009). Crystal structure of MqnD (TTHA1568), a menaquinone biosynthetic enzyme from *Thermus thermophilus* HB8. *J. Struct. Biol.* 168, 575–581.
- Arakawa, C., Kuratsu, M., Furihata, K., Hiratsuka, T., Itoh, N., Seto, H., and Dairi, T. (2011). Diversity of the early step of the futasine pathway. *Antimicrob. Agents Chemother.* 55, 913–916.
- Arnold, T., and Linke, D. (2008). The use of detergents to purify membrane proteins. *Curr. Protoc. Protein Sci.* Editor. Board John E Coligan AI *Chapter 4*, Unit 4.8.1–4.8.30.
- Baba, T., Ara, T., Hasegawa, M., Takai, Y., Okumura, Y., Baba, M., Datsenko, K.A., Tomita, M., Wanner, B.L., and Mori, H. (2006). Construction of *Escherichia coli* K-12 in-frame, single-gene knockout mutants: the Keio collection. *Mol. Syst. Biol.* 2, 2006.0008.
- Babcock, M.J., and Kendrick, K.E. (1988). Cloning of DNA involved in sporulation of *Streptomyces griseus*. *J. Bacteriol.* 170, 2802–2808.
- Barta, M.L., Thomas, K., Yuan, H., Lovell, S., Battaile, K.P., Schramm, V.L., and Hefty, P.S. (2014). Structural and biochemical characterization of *Chlamydia trachomatis* hypothetical protein CT263 supports that menaquinone synthesis occurs through the futasine pathway. *J. Biol. Chem.* 289, 32214–32229.
- Battye, T.G.G., Kontogiannis, L., Johnson, O., Powell, H.R., and Leslie, A.G.W. (2011). iMOSFLM: a new graphical interface for diffraction-image processing with MOSFLM. *Acta Crystallogr. D. Biol. Crystallogr.* 67, 271–281.
- Bekker, M., Kramer, G., Hartog, A.F., Wagner, M.J., de Koster, C.G., Hellingwerf, K.J., and de Mattos, M.J.T. (2007). Changes in the redox state and composition of the quinone pool of *Escherichia coli* during aerobic batch-culture growth. *Microbiology* 153, 1974–1980.
- Bentley, R. (1975). Biosynthesis of vitamin K and other natural naphthoquinones. *Pure Appl. Chem.* 41.
- Bentley, R., and Meganathan, R. (1982). Biosynthesis of vitamin K (menaquinone) in bacteria. *Microbiol. Rev.* 46, 241–280.
- Bentley, S.D., Chater, K.F., Cerdeño-Tárraga, A.-M., Challis, G.L., Thomson, N.R., James, K.D., Harris, D.E., Quail, M.A., Kieser, H., Harper, D., et al. (2002). Complete genome sequence of the model actinomycete *Streptomyces coelicolor* A3(2). *Nature* 417, 141–147.
- Benzakour, O., and Kanthou, C. (2000). The anticoagulant factor, protein S, is produced by cultured human vascular smooth muscle cells and its expression is up-regulated by thrombin. *Blood* 95, 2008–2014.

- Bernsel, A., Viklund, H., Hennerdal, A., and Elofsson, A. (2009). TOPCONS: consensus prediction of membrane protein topology. *Nucleic Acids Res.* *37*, W465–W468.
- Bonitz, T., Alva, V., Saleh, O., Lupas, A.N., and Heide, L. (2011). Evolutionary relationships of microbial aromatic prenyltransferases. *PLoS One* *6*, e27336.
- Botta, B., Vitali, A., Menendez, P., Misiti, D., and Delle Monache, G. (2005). Prenylated flavonoids: pharmacology and biotechnology. *Curr. Med. Chem.* *12*, 717–739.
- Brandt, W., Bräuer, L., Günnewich, N., Kufka, J., Rausch, F., Schulze, D., Schulze, E., Weber, R., Zakharova, S., and Wessjohann, L. (2009). Molecular and structural basis of metabolic diversity mediated by prenyldiphosphate converting enzymes. *Phytochemistry* *70*, 1758–1775.
- Bräuer, L., Brandt, W., and Wessjohann, L.A. (2004). Modeling the *E. coli* 4-hydroxybenzoic acid oligoprenyltransferase (ubiA transferase) and characterization of potential active sites. *J. Mol. Model.* *10*, 317–327.
- Bräuer, L., Brandt, W., Schulze, D., Zakharova, S., and Wessjohann, L. (2008). A structural model of the membrane-bound aromatic prenyltransferase UbiA from *E. coli*. *Chembiochem* *9*, 982–992.
- Casey, P.J., and Seabra, M.C. (1996). Protein Prenyltransferases. *J. Biol. Chem.* *271*, 5289–5292.
- Cava, F., Zafra, O., da Costa, M.S., and Berenguer, J. (2008). The role of the nitrate respiration element of *Thermus thermophilus* in the control and activity of the denitrification apparatus. *Environ. Microbiol.* *10*, 522–533.
- Cava, F., Hidalgo, A., and Berenguer, J. (2009). *Thermus thermophilus* as biological model. *Extremophiles* *13*, 213–231.
- Cheng, W., and Li, W. (2014). Structural Insights into Ubiquinone Biosynthesis in Membranes. *Science* (80-.). *343*, 878–881.
- Cohen, J. (2004). Medicine. New TB drug promises shorter, simpler treatment. *Science* *306*, 1872.
- Cole, J.L., Lary, J.W., P Moody, T., and Laue, T.M. (2008). Analytical ultracentrifugation: sedimentation velocity and sedimentation equilibrium. *Methods Cell Biol.* *84*, 143–179.
- Collins, M.D., and Jones, D. (1981). Distribution of isoprenoid quinone structural types in bacteria and their taxonomic implication. *Microbiol. Rev.* *45*, 316–354.
- Cranenburg, E.C.M., Schurgers, L.J., and Vermeer, C. (2007). Vitamin K: the coagulation vitamin that became omnipotent. *Thromb. Haemost.* *98*, 120–125.
- Dairi, T. (2009). An alternative menaquinone biosynthetic pathway operating in microorganisms: an attractive target for drug discovery to pathogenic *Helicobacter* and *Chlamydia* strains. *J. Antibiot.* (Tokyo). *62*, 347–352.
- Dairi, T. (2012). Menaquinone biosyntheses in microorganisms. (Elsevier Inc.).
- Dairi, T., Kuzuyama, T., Nishiyama, M., and Fujii, I. (2011). Convergent strategies in biosynthesis. *Nat. Prod. Rep.* *28*, 1054–1086.
- Debnath, J., Siricilla, S., Wan, B., Crick, D.C., Lenaerts, A.J., Franzblau, S.G., and Kurosu, M. (2012). Discovery of selective menaquinone biosynthesis inhibitors against *Mycobacterium tuberculosis*. *J. Med. Chem.* *55*, 3739–3755.
- Doumith, M., Weingarten, P., Wehmeier, U.F., Salah-Bey, K., Benhamou, B., Capdevila, C., Michel, J.M., Piepersberg, W., and Raynal, M.C. (2000). Analysis of genes involved in 6-deoxyhexose biosynthesis and transfer in *Saccharopolyspora erythraea*. *Mol. Gen. Genet.* *264*, 477–485.
- Drew, D., Newstead, S., Sonoda, Y., Kim, H., von Heijne, G., and Iwata, S. (2008). GFP-based optimization scheme for the overexpression and purification of eukaryotic membrane proteins in *Saccharomyces cerevisiae*. *Nat. Protoc.* *3*, 784–798.
- Edgar, R.C. (2004). MUSCLE: multiple sequence alignment with high accuracy and high throughput.

Nucleic Acids Res. *32*, 1792–1797.

Emsley, P., and Cowtan, K. (2004). Coot: model-building tools for molecular graphics. *Acta Crystallogr. D. Biol. Crystallogr.* *60*, 2126–2132.

Eshaghi, S., Hedrén, M., Nasser, M.I.A., Hammarberg, T., Thornell, A., and Nordlund, P. (2005). An efficient strategy for high-throughput expression screening of recombinant integral membrane proteins. *Protein Sci.* *14*, 676–683.

Evans, P.R., and Murshudov, G.N. (2013). How good are my data and what is the resolution? *Acta Crystallogr. D. Biol. Crystallogr.* *69*, 1204–1214.

Fang, M., Toogood, R.D., Macova, A., Ho, K., Franzblau, S.G., McNeil, M.R., Sanders, D.A.R., and Palmer, D.R.J. (2010). Succinylphosphonate esters are competitive inhibitors of MenD that show active-site discrimination between homologous alpha-ketoglutarate-decarboxylating enzymes. *Biochemistry* *49*, 2672–2679.

Ferrante, R.J., Andreassen, O.A., Dedeoglu, A., Ferrante, K.L., Jenkins, B.G., Hersch, S.M., and Beal, M.F. (2002). Therapeutic effects of coenzyme Q10 and remacemide in transgenic mouse models of Huntington's disease. *J. Neurosci.* *22*, 1592–1599.

Folkers, K. (1993). Heart failure is a dominant deficiency of coenzyme Q10 and challenges for future clinical research on CoQ10. *Clin. Investig.* *71*, S51–S54.

Fuhrmann, M., Hausherr, A., Ferbitz, L., Schödl, T., Heitzer, M., and Hegemann, P. (2004). Monitoring dynamic expression of nuclear genes in *Chlamydomonas reinhardtii* by using a synthetic luciferase reporter gene. *Plant Mol. Biol.* *55*, 869–881.

Furie, B., Bouchard, B.A., and Furie, B.C. (1999). Vitamin K-dependent biosynthesis of gamma-carboxyglutamic acid. *Blood* *93*, 1798–1808.

Garavito, R.M., and Ferguson-Miller, S. (2001). Detergents as tools in membrane biochemistry. *J. Biol. Chem.* *276*, 32403–32406.

Gasteiger, E., Hoogland, C., Gattiker, A., Duvaud, S., Wilkins, M., Appel, R., and Bairoch, A. (2005). Protein Identification and Analysis Tools on the ExPASy Server. In *The Proteomics Protocols Handbook*, pp. 571–607.

Gempel, K., Topaloglu, H., Talim, B., Schneiderat, P., Schoser, B.G.H., Hans, V.H., Pálmafy, B., Kale, G., Tokatli, A., Quinzii, C., et al. (2007). The myopathic form of coenzyme Q10 deficiency is caused by mutations in the electron-transferring-flavoprotein dehydrogenase (ETFDH) gene. *Brain* *130*, 2037–2044.

Gross, J., Cho, W.K., Lezhneva, L., Falk, J., Krupinska, K., Shinozaki, K., Seki, M., Herrmann, R.G., and Meurer, J. (2006). A plant locus essential for phyloquinone (vitamin K1) biosynthesis originated from a fusion of four eubacterial genes. *J. Biol. Chem.* *281*, 17189–17196.

Haagen, Y., Unsöld, I., Westrich, L., Gust, B., Richard, S.B., Noel, J.P., and Heide, L. (2007). A soluble, magnesium-independent prenyltransferase catalyzes reverse and regular C-prenylations and O-prenylations of aromatic substrates. *FEBS Lett.* *581*, 2889–2893.

Haapalainen, A.M., Thomas, K., Tyler, P.C., Evans, G.B., Almo, S.C., and Schramm, V.L. (2013). *Salmonella enterica* MTAN at 1.36 Å resolution: a structure-based design of tailored transition state analogs. *Structure* *21*, 963–974.

Hara, M., Yuan, H., Yang, Q., Hoshino, T., Yokoyama, A., and Miyake, J. (1999). Stabilization of liposomal membranes by thermozeaxanthins: carotenoid-glucoside esters. *Biochim. Biophys. Acta - Biomembr.* *1461*, 147–154.

Hara, M., Yamano, Y., Sakai, Y., Kodama, E., Hoshino, T., Ito, M., and Miyake, J. (2008). Stabilization of liposomal membranes by carotenoids: Zeaxanthin, zeaxanthin glucoside and thermozeaxanthin. *Mater. Sci. Eng. C* *28*, 274–279.

- Hast, M.A., Nichols, C.B., Armstrong, S.M., Kelly, S.M., Hellinga, H.W., Alspaugh, J.A., and Beese, L.S. (2011). Structures of *Cryptococcus neoformans* protein farnesyltransferase reveal strategies for developing inhibitors that target fungal pathogens. *J. Biol. Chem.* *286*, 35149–35162.
- Heide, L. (2009). Prenyl transfer to aromatic substrates: genetics and enzymology. *Curr. Opin. Chem. Biol.* *13*, 171–179.
- Hemmi, H., Shibuya, K., Takahashi, Y., Nakayama, T., and Nishino, T. (2004). (S)-2,3-Di-O-geranylgeranylgeranyl glyceryl Phosphate Synthase from the Thermoacidophilic Archaeon *Sulfolobus solfataricus*. *J. Biol. Chem.* *279*, 50197–50203.
- Hiraishi, A. (1999). Isoprenoid quinones as biomarkers of microbial populations in the environment. *J. Biosci. Bioeng.* *88*, 449–460.
- Hiratsuka, T., Furihata, K., Ishikawa, J., Yamashita, H., Itoh, N., Seto, H., and Dairi, T. (2008). An alternative menaquinone biosynthetic pathway operating in microorganisms. *Science* *321*, 1670–1673.
- Hiratsuka, T., Itoh, N., Seto, H., and Dairi, T. (2009). Enzymatic Properties of Futalosine Hydrolase, an Enzyme Essential to a Newly Identified Menaquinone Biosynthetic Pathway. *Biosci. Biotechnol. Biochem.* *73*, 1137–1141.
- Holm, L., Kaariainen, S., Rosenstrom, P., and Schenkel, A. (2008). Searching protein structure databases with DaliLite v.3. *Bioinformatics* *24*, 2780–2781.
- Hopwood, D.A. (1985). Genetic manipulation of *Streptomyces*: a laboratory manual (John Innes Foundation).
- Hsu, A.Y., Poon, W.W., Shepherd, J.A., Myles, D.C., and Clarke, C.F. (1996). Complementation of coq3 mutant yeast by mitochondrial targeting of the *Escherichia coli* UbiG polypeptide: evidence that UbiG catalyzes both O-methylation steps in ubiquinone biosynthesis. *Biochemistry* *35*, 9797–9806.
- Huang, H., Levin, E.J., Liu, S., Bai, Y., Lockless, S.W., and Zhou, M. (2014). Structure of a Membrane-Embedded Prenyltransferase Homologous to UBIAD1. *PLoS Biol.* *12*, 1–11.
- Ishida, M., and Oshima, T. (1994). Overexpression of genes of an extreme thermophile *Thermus thermophilus*, in *Escherichia coli* cells. *J. Bacteriol.* *176*, 2767–2770.
- Ishida, M., Oshima, T., and Yutani, K. (2002). Overexpression in *Escherichia coli* of the AT-rich trpA and trpB genes from the hyperthermophilic archaeon *Pyrococcus furiosus*. *FEMS Microbiol. Lett.* *216*, 179–183.
- Iyengar, R., and Hildebrandt, J.D. (2002). G Protein Pathways: Effector mechanisms, Part 3 (Academic Press).
- Jiang, M., Cao, Y., Guo, Z.-F., Chen, M., Chen, X., and Guo, Z. (2007). Menaquinone biosynthesis in *Escherichia coli*: identification of 2-succinyl-5-enolpyruvyl-6-hydroxy-3-cyclohexene-1-carboxylate as a novel intermediate and re-evaluation of MenD activity. *Biochemistry* *46*, 10979–10989.
- Kagan, V., Serbinova, E., and Packer, L. (1990). Antioxidant effects of ubiquinones in microsomes and mitochondria are mediated by tocopherol recycling. *Biochem. Biophys. Res. Commun.* *169*, 851–857.
- Karamat, F., Olry, A., Munakata, R., Koeduka, T., Sugiyama, A., Paris, C., Hehn, A., Bourgaud, F., and Yazaki, K. (2014). A coumarin-specific prenyltransferase catalyzes the crucial biosynthetic reaction for furanocoumarin formation in parsley. *Plant J.* *77*, 627–638.
- Kawate, T., and Gouaux, E. (2006). Fluorescence-detection size-exclusion chromatography for precrystallization screening of integral membrane proteins. *Structure* *14*, 673–681.
- Kelly, S.M., Jess, T.J., and Price, N.C. (2005). How to study proteins by circular dichroism. *Biochim. Biophys. Acta* *1751*, 119–139.
- Kim, R.Q., Offen, W.A., Davies, G.J., and Stubbs, K.A. (2014). Structural enzymology of *Helicobacter pylori* methylthioadenosine nucleosidase in the futalosine pathway. *Acta Crystallogr. D. Biol.*

- Crystallogr. *70*, 177–185.
- Koehl, P. (2005). Relaxed specificity in aromatic prenyltransferases. *Nat. Chem. Biol.* *1*, 71–72.
- Krissinel, E., and Henrick, K. (2007). Inference of macromolecular assemblies from crystalline state. *J. Mol. Biol.* *372*, 774–797.
- Kumano, T., Richard, S.B., Noel, J.P., Nishiyama, M., and Kuzuyama, T. (2008). Chemoenzymatic syntheses of prenylated aromatic small molecules using *Streptomyces* prenyltransferases with relaxed substrate specificities. *Bioorg. Med. Chem.* *16*, 8117–8126.
- Kurosu, M., and Begari, E. (2010). Vitamin K2 in electron transport system: are enzymes involved in vitamin K2 biosynthesis promising drug targets? *Molecules* *15*, 1531–1553.
- Kurosu, M., and Crick, D.C. (2009). MenA is a promising drug target for developing novel lead molecules to combat *Mycobacterium tuberculosis*. *Med. Chem.* *5*, 197–207.
- Kurosu, M., Narayanasamy, P., Biswas, K., Dhiman, R., and Crick, D.C. (2007). Discovery of 1,4-dihydroxy-2-naphthoate prenyltransferase inhibitors: new drug leads for multidrug-resistant gram-positive pathogens. *J. Med. Chem.* *50*, 3973–3975.
- Ladd, M., and Palmer, R. (2013). *Structure Determination by X-ray Crystallography: Analysis by X-rays and Neutrons* (Springer Science & Business Media).
- Laemmli, U.K. (1970). Cleavage of Structural Proteins during the Assembly of the Head of Bacteriophage T4. *Nature* *227*, 680–685.
- Lagier-Tourenne, C., Tazir, M., López, L.C., Quinzii, C.M., Assoum, M., Drouot, N., Busso, C., Makri, S., Ali-Pacha, L., Benhassine, T., et al. (2008). ADCK3, an ancestral kinase, is mutated in a form of recessive ataxia associated with coenzyme Q10 deficiency. *Am. J. Hum. Genet.* *82*, 661–672.
- Lebowitz, J., Lewis, M.S., and Schuck, P. (2002). Modern analytical ultracentrifugation in protein science: A tutorial review. *Protein Sci.* *11*, 2067–2079.
- Lee, J.E., Cornell, K.A., Riscoe, M.K., and Howell, P.L. (2003). Structure of *Escherichia coli* 5'-methylthioadenosine/ S-adenosylhomocysteine nucleosidase inhibitor complexes provide insight into the conformational changes required for substrate binding and catalysis. *J. Biol. Chem.* *278*, 8761–8770.
- Lee, J.E., Smith, G.D., Horvatin, C., Huang, D.J.T., Cornell, K.A., Riscoe, M.K., and Howell, P.L. (2005). Structural snapshots of MTA/AdoHcy nucleosidase along the reaction coordinate provide insights into enzyme and nucleoside flexibility during catalysis. *J. Mol. Biol.* *352*, 559–574.
- Lemuth, K., Steuer, K., and Albermann, C. (2011). Engineering of a plasmid-free *Escherichia coli* strain for improved in vivo biosynthesis of astaxanthin. *Microb. Cell Fact.* *10*, 29.
- Li, X., Liu, N., Zhang, H., Knudson, S.E., Slayden, R.A., and Tonge, P.J. (2010). Synthesis and SAR studies of 1,4-benzoxazine MenB inhibitors: novel antibacterial agents against *Mycobacterium tuberculosis*. *Bioorg. Med. Chem. Lett.* *20*, 6306–6309.
- Li, X., Apel, D., Gaynor, E.C., and Tanner, M.E. (2011). 5'-methylthioadenosine nucleosidase is implicated in playing a key role in a modified futasoline pathway for menaquinone biosynthesis in *Campylobacter jejuni*. *J. Biol. Chem.* *286*, 19392–19398.
- Liang, P.-H., Ko, T.-P., and Wang, A.H.-J. (2002). Structure, mechanism and function of prenyltransferases. *Eur. J. Biochem.* *269*, 3339–3354.
- Lowry, O.H., Rosebrough, N.J., Farr, A.L., and Randall, R.J. (1951). Protein measurement with the Folin phenol reagent. *J. Biol. Chem.* *193*, 265–275.
- Lu, X., Zhang, H., Tonge, P.J., and Tan, D.S. (2008). Mechanism-based inhibitors of MenE, an acyl-CoA synthetase involved in bacterial menaquinone biosynthesis. *Bioorg. Med. Chem. Lett.* *18*, 5963–5966.
- Mahanta, N., Fedoseyenko, D., Dairi, T., and Begley, T.P. (2013). Menaquinone biosynthesis: formation of aminofutasoline requires a unique radical SAM enzyme. *J. Am. Chem. Soc.* *135*, 15318–

15321.

McCoy, A.J., Grosse-Kunstleve, R.W., Adams, P.D., Winn, M.D., Storoni, L.C., and Read, R.J. (2007). Phaser crystallographic software. *J. Appl. Crystallogr.* *40*, 658–674.

Meganathan, R. (2001a). Biosynthesis of menaquinone (vitamin K2) and ubiquinone (coenzyme Q): a perspective on enzymatic mechanisms. *Vitam. Horm.* *61*, 173–218.

Meganathan, R. (2001b). Ubiquinone biosynthesis in microorganisms. *FEMS Microbiol. Lett.* *203*, 131–139.

Melzer, M., and Heide, L. (1994). Characterization of polyprenyldiphosphate: 4-hydroxybenzoate polyprenyltransferase from *Escherichia coli*. *Biochim. Biophys. Acta* *1212*, 93–102.

Meng, J., Wang, F., Wang, F., Zheng, Y., Peng, X., Zhou, H., and Xiao, X. (2009). An uncultivated crenarchaeota contains functional bacteriochlorophyll a synthase. *ISME J.* *3*, 106–116.

Misawa, N., and Shimada, H. (1997). Metabolic engineering for the production of carotenoids in non-carotenogenic bacteria and yeasts. *J. Biotechnol.* *59*, 169–181.

Mishra, V., and Ronning, D.R. (2012). Crystal structures of the *Helicobacter pylori* MTAN enzyme reveal specific interactions between S-adenosylhomocysteine and the 5'-alkylthio binding subsite. *Biochemistry* *51*, 9763–9772.

Mohanty, A.K., Simmons, C.R., and Wiener, M.C. (2003). Inhibition of tobacco etch virus protease activity by detergents. *Protein Expr. Purif.* *27*, 109–114.

Mooser, D., Maneg, O., MacMillan, F., Malatesta, F., Soulimane, T., and Ludwig, B. (2006). The menaquinol-oxidizing cytochrome bc complex from *Thermus thermophilus*: Protein domains and subunits. *Biochim. Biophys. Acta - Bioenerg.* *1757*, 1084–1095.

Murshudov, G.N., Vagin, A.A., and Dodson, E.J. (1997). Refinement of macromolecular structures by the maximum-likelihood method. *Acta Crystallogr. D. Biol. Crystallogr.* *53*, 240–255.

Nagata, K., Inatsu, S., Tanaka, M., Sato, H., Kouya, T., Taniguchi, M., and Fukuda, Y. (2010). The bifidogenic growth stimulator inhibits the growth and respiration of *Helicobacter pylori*. *Helicobacter* *15*, 422–429.

Nakagawa, K. (2010). New Developments in Research on Vitamin K Biosynthesis. *Journal Heal. Sci.* *56*, 623–631.

Nakagawa, K., Hirota, Y., Sawada, N., Yuge, N., Watanabe, M., Uchino, Y., Okuda, N., Shimomura, Y., Suhara, Y., and Okano, T. (2010). Identification of UBIAD1 as a novel human menaquinone-4 biosynthetic enzyme. *Nature* *468*, 117–121.

Newby, Z.E.R., O'Connell, J.D., Gruswitz, F., Hays, F.A., Harries, W.E.C., Harwood, I.M., Ho, J.D., Lee, J.K., Savage, D.F., Miercke, L.J.W., et al. (2009). A general protocol for the crystallization of membrane proteins for X-ray structural investigation. *Nat. Protoc.* *4*, 619–637.

Newstead, S., Ferrandon, S., and Iwata, S. (2008). Rationalizing alpha-helical membrane protein crystallization. *Protein Sci.* *17*, 466–472.

Nishida, F., Nishijima, M., Mochida, K., Sano, H., Nomura, N., Sako, Y., and Maruyama, T. (1999). Isoprenoid quinones in an aerobic hyperthermophilic archaeon, *Aeropyrum pernix*. *FEMS Microbiol. Lett.* *174*, 339–346.

Noboru Sugishima, Noriaki Ikeda, Yasushi Fujii, Ryuji Aoki, Y.H. (1994). Process for preparation of 2-substituted 1,4-naphthoquinone.

Novy, R., Drott, D., Yaeger, K., and Mierendorf, R. (2001). Overcoming the codon bias of *E. coli* for enhanced protein expression. *News. Novagen, INC • Adv. Prod. Protoc. Mol. Biol. Res.* *12*, 1–3.

Nowicka, B., and Kruk, J. (2010). Occurrence, biosynthesis and function of isoprenoid quinones. *Biochim. Biophys. Acta* *1797*, 1587–1605.

- Ohara, K., Muroya, A., Fukushima, N., and Yazaki, K. (2009). Functional characterization of LePGT1, a membrane-bound prenyltransferase involved in the geranylation of p-hydroxybenzoic acid. *Biochem. J.* *421*, 231–241.
- Ohara, K., Mito, K., and Yazaki, K. (2013). Homogeneous purification and characterization of LePGT1-- a membrane-bound aromatic substrate prenyltransferase involved in secondary metabolism of *Lithospermum erythrorhizon*. *FEBS J.* *280*, 2572–2580.
- Okada, K., Ohara, K., Yazaki, K., Nozaki, K., Uchida, N., Kawamukai, M., Nojiri, H., and Yamane, H. (2004). The AtPPT1 gene encoding 4-hydroxybenzoate polyprenyl diphosphate transferase in ubiquinone biosynthesis is required for embryo development in *Arabidopsis thaliana*. *Plant Mol. Biol.* *55*, 567–577.
- Okano, T., Shimomura, Y., Yamane, M., Suhara, Y., Kamao, M., Sugiura, M., and Nakagawa, K. (2008). Conversion of phylloquinone (Vitamin K1) into menaquinone-4 (Vitamin K2) in mice: two possible routes for menaquinone-4 accumulation in cerebra of mice. *J. Biol. Chem.* *283*, 11270–11279.
- Park, K., Perczel, A., and Fasman, G.D. (1992). Differentiation between transmembrane helices and peripheral helices by the deconvolution of circular dichroism spectra of membrane proteins. *Protein Sci.* *1*, 1032–1049.
- Parsy, C.B., Chapman, C.J., Barnes, A.C., Robertson, J.F., and Murray, A. (2007). Two-step method to isolate target recombinant protein from co-purified bacterial contaminant SlyD after immobilised metal affinity chromatography. *J. Chromatogr. B. Analyt. Technol. Biomed. Life Sci.* *853*, 314–319.
- Portnoy, V.A., Scott, D.A., Lewis, N.E., Tarasova, Y., Osterman, A.L., and Palsson, B.Ø. (2010). Deletion of genes encoding cytochrome oxidases and quinol monooxygenase blocks the aerobic-anaerobic shift in *Escherichia coli* K-12 MG1655. *Appl. Environ. Microbiol.* *76*, 6529–6540.
- Privé, G.G. (2007). Detergents for the stabilization and crystallization of membrane proteins. *Methods* *41*, 388–397.
- Quinzii, C., Naini, A., Salviati, L., Trevisson, E., Navas, P., Dimauro, S., and Hirano, M. (2006). A mutation in para-hydroxybenzoate-polyprenyl transferase (COQ2) causes primary coenzyme Q10 deficiency. *Am. J. Hum. Genet.* *78*, 345–349.
- Ren, H., Yu, D., Ge, B., Cook, B., Xu, Z., and Zhang, S. (2009). High-level production, solubilization and purification of synthetic human GPCR chemokine receptors CCR5, CCR3, CXCR4 and CX3CR1. *PLoS One* *4*, e4509.
- Robichon, C., Luo, J., Causey, T.B., Benner, J.S., and Samuelson, J.C. (2011). Engineering *Escherichia coli* BL21(DE3) derivative strains to minimize E. coli protein contamination after purification by immobilized metal affinity chromatography. *Appl. Environ. Microbiol.* *77*, 4634–4646.
- Ronning, D.R., Iacopelli, N.M., and Mishra, V. (2010). Enzyme-ligand interactions that drive active site rearrangements in the *Helicobacter pylori* 5'-methylthioadenosine/S-adenosylhomocysteine nucleosidase. *Protein Sci.* *19*, 2498–2510.
- Rosenberg, I.M. (2013). *Protein Analysis and Purification: Benchtop Techniques* (Springer Science & Business Media).
- Ruther, A., Misawa, N., Böger, P., and Sandmann, G. (1997). Production of zeaxanthin in *Escherichia coli* transformed with different carotenogenic plasmids. *Appl. Microbiol. Biotechnol.* *48*, 162–167.
- Saito, Y., and Ogura, K. (1981). Biosynthesis of menaquinones. Enzymatic prenylation of 1,4-dihydroxy-2-naphthoate by *Micrococcus luteus* membrane fractions. *J. Biochem.* *89*, 1445–1452.
- Saleh, O., Haagen, Y., Seeger, K., and Heide, L. (2009). Prenyl transfer to aromatic substrates in the biosynthesis of aminocoumarins, meroterpenoids and phenazines: the ABBA prenyltransferase family. *Phytochemistry* *70*, 1728–1738.
- Sambrook, J., Fritsche, E. und Maniatis, T. (1989). *Cloning Techniques Molecular Cloning: A Laboratory Manual T.* (New York : Cold Spring Harbor Laboratory Press, 2nd edition).

- Sasaki, K., Mito, K., Ohara, K., Yamamoto, H., and Yazaki, K. (2008). Cloning and characterization of naringenin 8-prenyltransferase, a flavonoid-specific prenyltransferase of *Sophora flavescens*. *Plant Physiol.* *146*, 1075–1084.
- Schoepp-Cothenet, B., Lieutaud, C., Baymann, F., Verméglio, A., Friedrich, T., Kramer, D.M., and Nitschke, W. (2009). Menaquinone as pool quinone in a purple bacterium. *Proc. Natl. Acad. Sci. U. S. A.* *106*, 8549–8554.
- Seabra, M.C., Goldstein, J.L., Südhof, T.C., and Brown, M.S. (1992). Rab geranylgeranyl transferase. A multisubunit enzyme that prenylates GTP-binding proteins terminating in Cys-X-Cys or Cys-Cys. *J. Biol. Chem.* *267*, 14497–14503.
- Seto, H., Jinnai, Y., Hiratsuka, T., and Fukawa, M. (2008). Studies on A New Biosynthetic Pathway for Menaquinone. 5614–5615.
- Sharma, S.C., Torssell, K., Undheim, K., Enzell, C.R., and Matsuno, T. (1978). Alkoxyacylation of Quinones. A Route to Naphthacene Quinones. Reversibility in Homolytic Substitution. *Acta Chem. Scand.* *32b*, 347–353.
- Shearer, M.J., and Newman, P. (2014). Recent trends in the metabolism and cell biology of vitamin K with special reference to vitamin K cycling and MK-4 biosynthesis. *J. Lipid Res.* *55*, 345–362.
- Shin, E.M., Zhou, H.Y., Guo, L.Y., Kim, J.A., Lee, S.H., Merfort, I., Kang, S.S., Kim, H.S., Kim, S., and Kim, Y.S. (2008). Anti-inflammatory effects of glycyrol isolated from *Glycyrrhiza uralensis* in LPS-stimulated RAW264.7 macrophages. *Int. Immunopharmacol.* *8*, 1524–1532.
- Shineberg, B., and Young, I.G. (1976). Biosynthesis of bacterial menaquinones: the membrane-associated 1,4-dihydroxy-2-naphthoate octaprenyltransferase of *Escherichia coli*. *Biochemistry* *15*, 2754–2758.
- Søballe, B., and Poole, R.K. (1999). Microbial ubiquinones: multiple roles in respiration, gene regulation and oxidative stress management. *Microbiology* *145 (Pt 8)*, 1817–1830.
- Spindler, M., Beal, M.F., and Henchcliffe, C. (2009). Coenzyme Q10 effects in neurodegenerative disease. *Neuropsychiatr. Dis. Treat.* *5*, 597–610.
- Sreerama, N., and Woody, R.W. (2004). On the analysis of membrane protein circular dichroism spectra. *Protein Sci.* *13*, 100–112.
- Sugiyama, A., Linley, P.J., Sasaki, K., Kumano, T., Yamamoto, H., Shitan, N., Ohara, K., Takanashi, K., Harada, E., Hasegawa, H., et al. (2011). Metabolic engineering for the production of prenylated polyphenols in transgenic legume plants using bacterial and plant prenyltransferases. *Metab. Eng.* *13*, 629–637.
- Suhara, Y., Watanabe, M., Nakagawa, K., Wada, A., Ito, Y., Takeda, K., Takahashi, K., and Okano, T. (2011). Synthesis of novel vitamin K2 analogues with modification at the Ω -terminal position and their biological evaluation as potent steroid and xenobiotic receptor (SXR) agonists. *J. Med. Chem.* *54*, 4269–4273.
- Suvarna, K., Stevenson, D., Meganathan, R., and Hudspeth, M.E. (1998). Menaquinone (vitamin K2) biosynthesis: localization and characterization of the menA gene from *Escherichia coli*. *J. Bacteriol.* *180*, 2782–2787.
- Suzuki, K., Ueda, M., Yuasa, M., Nakagawa, T., Kawamukai, M., and Matsuda, H. (1994). Evidence that *Escherichia coli* ubiA product is a functional homolog of yeast COQ2, and the regulation of ubiA gene expression. *Biosci. Biotechnol. Biochem.* *58*, 1814–1819.
- Svensson, B., Lübben, M., and Hederstedt, L. (1993). *Bacillus subtilis* CtaA and CtaB function in haem A biosynthesis. *Mol. Microbiol.* *10*, 193–201.
- Szkopińska, A. (2000). Ubiquinone. Biosynthesis of quinone ring and its isoprenoid side chain. Intracellular localization. *Acta Biochim. Pol.* *47*, 469–480.

- Tamura, K., Stecher, G., Peterson, D., FilipSKI, A., and Kumar, S. (2013). MEGA6: Molecular Evolutionary Genetics Analysis version 6.0. *Mol. Biol. Evol.* *30*, 2725–2729.
- Tello, M., Kuzuyama, T., Heide, L., Noel, J.P., and Richard, S.B. (2008). The ABBA family of aromatic prenyltransferases: broadening natural product diversity. *Cell. Mol. Life Sci.* *65*, 1459–1463.
- Thijssen, H.H., Driittij-Reijnders, M.J., and Fischer, M.A. (1996). Phylloquinone and menaquinone-4 distribution in rats: synthesis rather than uptake determines menaquinone-4 organ concentrations. *J. Nutr.* *126*, 537–543.
- Thomason, L.C., Costantino, N., and Court, D.L. (2007). *E. coli* genome manipulation by P1 transduction. *Curr. Protoc. Mol. Biol. Chapter 1*, Unit 1.17.
- Throne-Holst, M., and Hederstedt, L. (2000). The *Bacillus subtilis* ctaB paralogue, yjdK, can complement the heme A synthesis deficiency of a CtaB-deficient mutant. *FEMS Microbiol. Lett.* *183*, 247–251.
- Tian, B., and Hua, Y. (2010). Carotenoid biosynthesis in extremophilic *Deinococcus-Thermus* bacteria. *Trends Microbiol.* *18*, 512–520.
- Trott, O., and Olson, A.J. (2010). AutoDock Vina: improving the speed and accuracy of docking with a new scoring function, efficient optimization, and multithreading. *J. Comput. Chem.* *31*, 455–461.
- Turunen, M., Olsson, J., and Dallner, G. (2004). Metabolism and function of coenzyme Q. *Biochim. Biophys. Acta* *1660*, 171–199.
- Visser, N. V., Hink, M.A., Borst, J.W., van der Krogt, G.N., and Visser, A.J.W.. (2002). Circular dichroism spectroscopy of fluorescent proteins. *FEBS Lett.* *521*, 31–35.
- Wallace, B.A., Lees, J.G., Orry, A.J.W., Loble, A., and Janes, R.W. (2003). Analyses of circular dichroism spectra of membrane proteins. *Protein Sci.* *12*, 875–884.
- Waterhouse, A.M., Procter, J.B., Martin, D.M.A., Clamp, M., and Barton, G.J. (2009). Jalview Version 2--a multiple sequence alignment editor and analysis workbench. *Bioinformatics* *25*, 1189–1191.
- Weant, K.A., and Smith, K.M. (2005). The role of coenzyme Q10 in heart failure. *Ann. Pharmacother.* *39*, 1522–1526.
- Wessjohann, L.A., and Sontag, B. (1996). Prenylation of Benzoic Acid Derivatives. *Angew. Chem. Int. Ed. Engl.* *35*, 1697–1699.
- Wong, C., Sridhara, S., Bardwell, J.C., and Jakob, U. (2000). Heating greatly speeds Coomassie blue staining and destaining. *Biotechniques* *28*, 426–428, 430, 432.
- Wuu, J.J., and Swartz, J.R. (2008). High yield cell-free production of integral membrane proteins without refolding or detergents. *Biochim. Biophys. Acta* *1778*, 1237–1250.
- Yazaki, K., KuniHisa, M., Fujisaki, T., and Sato, F. (2002). Geranyl diphosphate:4-hydroxybenzoate geranyltransferase from *Lithospermum erythrorhizon*. Cloning and characterization of a ket enzyme in shikonin biosynthesis. *J. Biol. Chem.* *277*, 6240–6246.
- Yazaki, K., Sasaki, K., and Tsurumaru, Y. (2009). Prenylation of aromatic compounds, a key diversification of plant secondary metabolites. *Phytochemistry* *70*, 1739–1745.
- Yokoyama, A., Sandmann, G., Hoshino, T., Adachi, K., Sakai, M., and Shizuri, Y. (1995). Thermozeaxanthins, new carotenoid-glycoside-esters from thermophilic eubacterium *Thermus thermophilus*. *Tetrahedron Lett.* *36*, 4901–4904.
- Young, I.G. (1975). Biosynthesis of bacterial menaquinones. Menaquinone mutants of *Escherichia coli*. *Biochemistry* *14*, 399–406.
- Young, I.G., Leppik, R.A., Hamilton, J.A., and Gibson, F. (1972). Biochemical and genetic studies on ubiquinone biosynthesis in *Escherichia coli* K-12:4-hydroxybenzoate octaprenyltransferase. *J. Bacteriol.* *110*, 18–25.

Zheng, J., and Trudeau, M.C. (2015). Handbook of Ion Channels (CRC Press).

Zhi, X.-Y., Yao, J.-C., Tang, S.-K., Huang, Y., Li, H.-W., and Li, W.-J. (2014). The futasine pathway played an important role in menaquinone biosynthesis during early prokaryote evolution. *Genome Biol. Evol.* 6, 149–160.

8. Appendix

8.1. Buffer for Protoplast preparation and expression of *Streptomyces lividans*.

SPMR-agar plate

10.3% (w/v) sucrose
 0.5% (w/v) D-glucose
 0.5% (w/v) yeast extract
 1.0% (w/v) MgCl₂
 2.0% (v/v) 1M TES (NaOH) pH 7.6
 0.2% (v/v) trace elements
 2.0% (w/v) agar
 After autoclaving
 0.2% (v/v) CaCl₂ (5M)

Trace elements

0.1% (w/v) ZnSO₄
 0.1% (w/v) FeSO₄
 0.1% (w/v) MnCl₂
 0.2% (v/v) CaCl₂ (5M)

TBS/PEG 8000 medium

0.3% (w/v) Trypton Soja Broth
 0.5% (w/v) PEG 8000
 After autoclave
 0.5% (w/v) glycine
 5 mM MgCl₂

Buffer P

10.3% (w/v) sucrose
 0.025% (w/v) K₂SO₄
 0.202% (w/v) MgCl₂
 0.2% (v/v) trace elements
 800 mL H₂O
 After autoclaving, in the following order:
 0.4% (v/v) 100 mM KH₂PO₄
 5.0% (v/v) 5.0 M CaCl₂
 10% (v/v) TES pH 7.2
 Complete the final volume (1L) with H₂O

Buffer T

25% (v/v) 10.3% sucrose
 1.45% (v/v) 100 mM K₂SO₄
 0.2% (v/v) trace elements
 Add 100 mL and after autoclave:
 2.0 mL CaCl₂ (5M)
 5.0 mL TM buffer (1M tris pH 8.0 – with maleic acid)

PEG 1000/Buffer T

1.0 g PEG 1000
 1.0 mL Buffer T

8.2. M9 – Minimal medium components.**5 x M9 salts**

Na ₂ HPO ₄	238 mM
KH ₂ PO ₄	110 mM
NaCl	42.2 mM
NH ₄ Cl	93 mM

Trace elements

HCL – 25% (v/v)	10 mL
FeCl ₂ x 4 H ₂ O	1.5 g
ZnCl ₂	0.07 g
MnCl ₂ x 4 H ₂ O	0.1 g
H ₃ BO ₄	0.006 g
CoCl ₂ x 6 H ₂ O	0.19 g
CuCl ₂ x 2 H ₂ O	0.002 g
NiCl ₂ x 2 H ₂ O	0.024 g
Na ₂ MoO ₄ x 2 H ₂ O	0.036 g
Na ₂ WO ₄ x 2 H ₂ O	0.033g
Na ₂ SeO ₃	0.171 g
Na ₂ VO ₃ x 2 H ₂ O	0.014 g
H ₂ O	Add 1.0 L

8.3. Proteins of *T. thermophilus* found after BLAST search using EcUbiA sequence:

-|Q72H22| Protoheme IX farnesyltransferase, OS=Thermus thermophilus (strain HB27)

```

      10      20      30      40      50      60
MKTPAWSRLA GYAWGVLLWN VLVALFGAYV RATGSGAGCG AHWPTCNGEV IPRAPQVETL

      70      80      90     100     110     120
IEFTHRATSG LAFLSVLALF LWALRAFPKG HPARFGAGLA LFFMVTESLV GASLVLFGWT

      130     140     150     160     170     180
ADNVSREAVV VQMVHLANTY FLLAALALTA WWASGGGPLR LRGQGAVGLA LFLGLLALLF

      190     200     210     220     230     240
LGMSGAVTAL GDLLFPVGST LEALERSLTP GEHFLVRLRV LHPLIAVSVG LYVVFAGYLV

      250     260     270     280     290     300
AHLRPSPLTR RLAQGLAYLY GAQLLAGLIN VALKAPVWMQ ILHLLLAYAV WLLFVFLATS

      310     320     330     340     350     360
ALERGAKRVE LGEGGEAVHR GTGGATWRDY LALTKPRVIS LLLFTALFGA LIAAKGWPGI

      370     380     390     400     410     420
GVFLAVALGG YMMAGAANA I NMVVDRIDA RMKRTAKRPT VTQRVSSRDA LLFAFALAVL

      430     440     450     460     470     480
GFAVLWGAN LLAATLALMG LIWYVLVYTL YLKRRTWHNI VIGGAAGAFP PLVGWAAVTC

      490     500     510     520     530     540
ELSLFAWYLF ALIFFWTPVH FWALALMIQD DYRAVGVPMI PVVLGERATV IQIALYALLT

      550     560     570     580     590     600
ALISLMPILL GELGLLYLAA SLLLNALLLI KSLALYRRPE RRTAVSLYKY SMLYLALLFA

AMAVDRAV

```

-|Q72L23| 4-hydroxybenzoate oligoprenyltransferase, OS=Thermus thermophilus (strain HB27)

```

      10      20      30      40      50      60
MRRRLRYLEL VRFEHTLFAL PFAYGGMLIA AGGWPGWPTF LLVTLAMVGA RTMAMALNRL

      70      80      90     100     110     120
IDWRDLALNP RTQNRHLPRG LVKPGETLTL ALLGLLLLLYV AGLNLNPLTA RLLPVAVFFL

      130     140     150     160     170     180
VFYSYTKRFT WLCHYVLGLT IGAAAAGGWI AVTGSFAPTA YALWAGVGLW IAGFDILYAT

      190     200     210     220     230     240
QDYTFDRAHG VKSIPARFGI PQALRVARAS HLLAWLAFLW AGVSYGAGPL YYLGLLLVGG

      250     260     270     280
LLLLLEHRLVS PEDLSKVEVA FFQANVGVSL GMFLFIVLDL LARGA

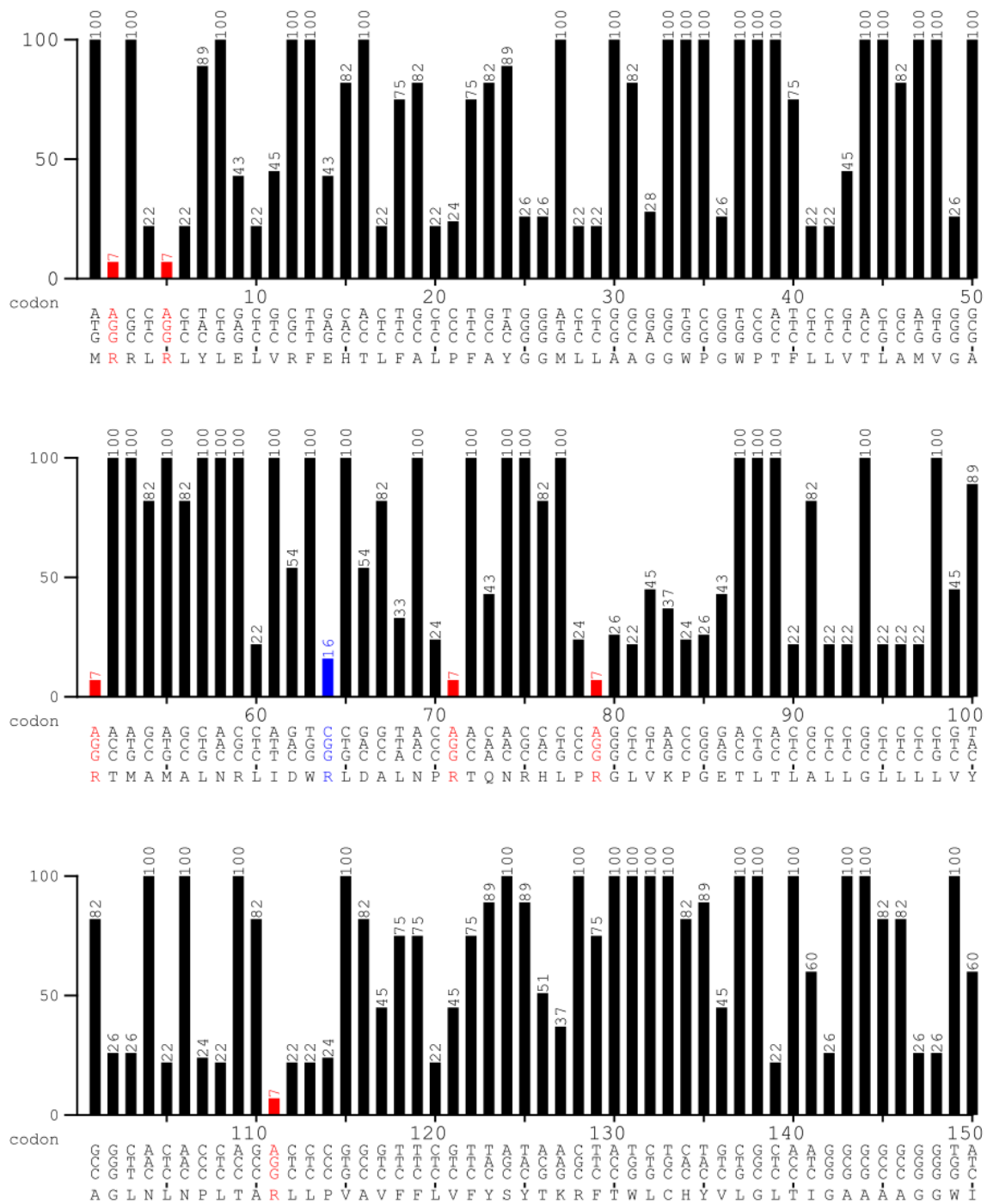
```

Figure 8.4. Codon-usage analysis of TtUbiA in *E. coli* cells.

TtUbiA
sequence derived from *Thermus thermophilus*

Codontable:
*Escherichia coli*_K12

Ordinate (y-axis): relative adaptiveness <20% <10%



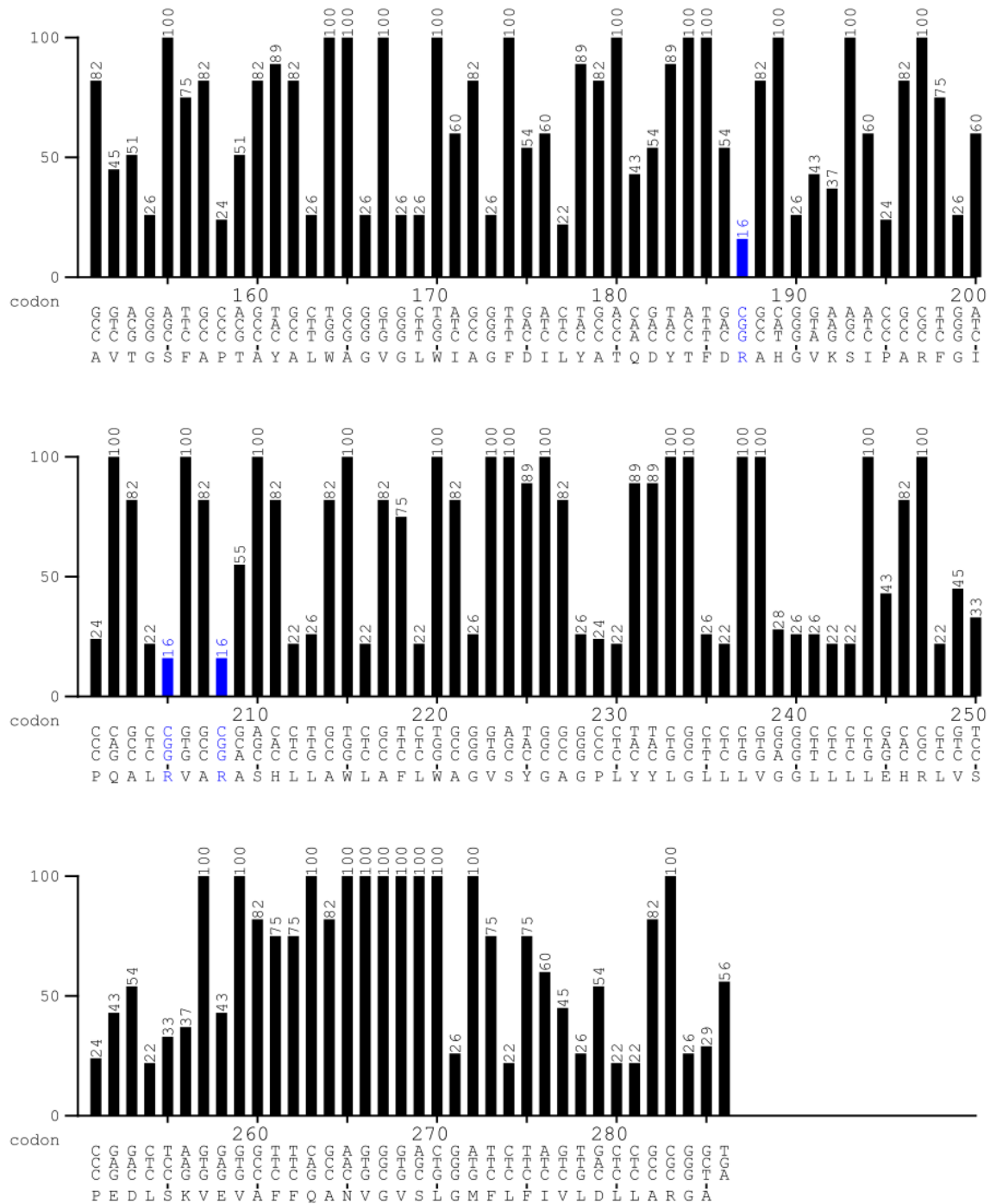


Figure 8.4. Graphical codon-usage analysis. Comparison of the codons of TtUbiA with their use in *E. coli* K-12 strains. The y-axis shows the relative adaptability of each codon. The most frequently used triplet is set to 100%. Blue and red bars show the codons, which the relative adaptability is lower than 20% and 10%, respectively (Fuhrmann *et al.*, 2004).

Figure 8.5. Mass spectroscopy of EcUbiA product

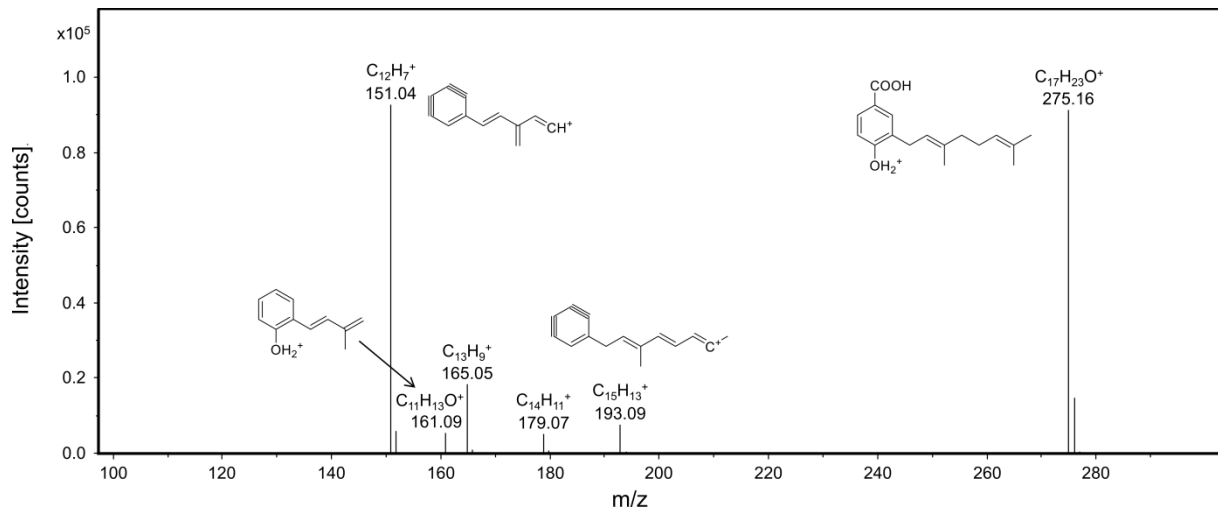


Figure 8.5. ESI-MS analysis. The product peak of EcUbiA was analysed by ES-MS. The prenylated product 3-geranyl-4-hydroxybenzoate (GHB) was identified in the positive mode with molecular weight of 275.16 g.mol⁻¹.

Figure 8.6. Map of pUWL201PW plasmid.

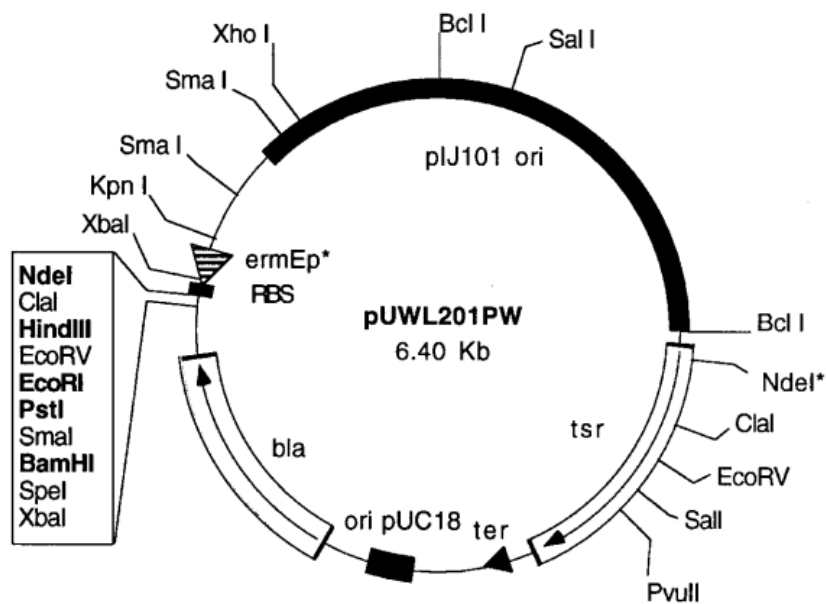


Figure 8.6. Map of pUWL201PW plasmid. Plasmid used for expression of SIUbiA and EcMenA in *Streptomyces lividans* TK24 strains. (Doumith *et al.*, 2000).

Figure 8.7. Expression of TtUbiA and EcMenA in M9-minimal medium.

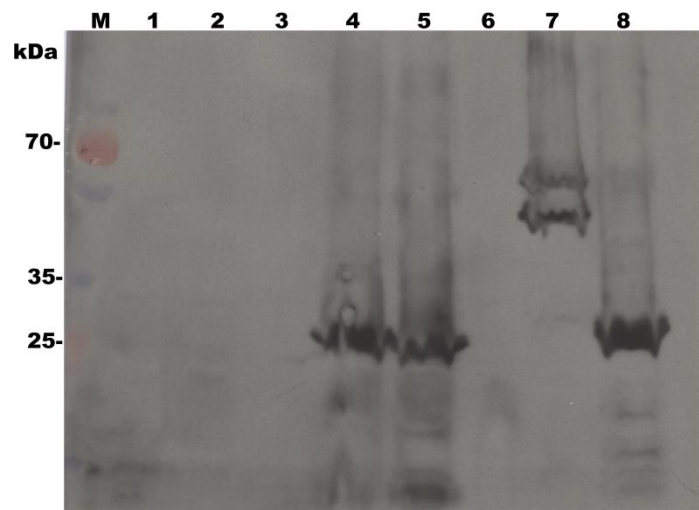


Figure 8.7. Immunoblotting analysis of TtUbiA and EcMenA proteins after expression in M9-minimal medium. Protein expression was tested in M9-minimal medium under aerobic conditions before complementation assays. Proteins were expressed overnight in Rosetta gami (DE3) pLySs $\Delta menA$ cells under aerobic conditions in the presence of 0.3 mM IPTG at 30 °C. **M:** Marker; **1:** Rosetta gami (DE3) pLySs without plasmid; **2:** Rosetta gami (DE3) pLySs $\Delta menA$ without plasmid; **3:** Rosetta gami (DE3) pLySs $\Delta menA$ + pET15b-TtUbiA before induction; **4:** Rosetta gami (DE3) pLySs $\Delta menA$ + pET15b-TtUbiA after induction; **5:** Rosetta gami (DE3) pLySs $\Delta menA$ + pET15b-TtUbiAR59D after induction; **6:** Rosetta gami (DE3) pLySs $\Delta menA$ + pNGFP-EcMenA before induction; **7:** Rosetta gami (DE3) pLySs $\Delta menA$ + pNGFP-EcMenA after induction; **8:** Rosetta gami (DE3) pLySs $\Delta menA$ + pET15b-EcMenAD65R after induction.

8.8. Membrane-bound prenyltransferases found in *Archaeoglobus fulgidus*

-|O28106| 4-hydroxybenzoate octaprenyltransferase (UbiA); strain DSM 4304

```

10      20      30      40      50      60
MQRIMKMYLDF IKIEHTLFAĻ PFAYAGAFLĀ EGGLISLRLĀ FLILTAFTGĻ RTAAMTFNRI

70      80      90      100     110     120
IDREIDAKNFĀ RTAMRHLPAĠ LISLKEAYTIĀ AFLALAIYFIĀ SAALINKTAĻ MLSPIPAITAĀ

130     140     150     160     170     180
YIYPYLKRFTĀ CLCHYVLGLNĀ LAFAPLGGWĪ AVTDSIDIFIĠ SELVPTLIGVĀ AVMFVWAGFĀ

190     200     210     220     230     240
MIYGLQDVDFĀ DRSNNLHSIGĀ AHFGVRAALWĀ LSRLNHVIFĀ ALIAIALQIHĀ NAKLAELFLPĀ

250     260     270     280     290
LIALLLFYEHĀ YIVRDGYDEĀ KIQIAFFYVNĀ ALVSSALLAĀ IFADAIFFSKĻ L

```

-|O29843| 4-hydroxybenzoate octaprenyltransferase, putative; strain DSM 4304 – named in this thesis as GGGPS or UbiA-2

```

10      20      30      40      50      60
MRRVSMRSLKĀ RYLKAIWDLĻ RLEHGLMYGFĀ GVVIGIYVSDĀ PFFSDLWKLĻ LGYLTAVFLQĀ

70      80      90      100     110     120
ASTFALNDYFĀ DYEVDLVNNRĀ TDRPLVRGDĻ SRRIALALAIĀ ALMPPGFVAAĀ YLISPLAFIFĀ

130     140     150     160     170     180
AFAVSVLACLĀ YDYKLKELGFĀ AGNVYIAFTMĀ AAPFLFGSIĀ SSGWITEKTAĀ LLASMAFLTGĀ

190     200     210     220     230     240
VGREIMKGIĒ DVEGDALRDVĀ RSLARTMGERĀ KAASIASLFYĀ LTAVVISPIĀ LFLLEPEFLFĀ

250     260     270     280     290
LKYAVPVSVTĀ DVLLIYVALRĀ LVGDYERESĀ RKYRKVTLVĀ MVLGLVGFĀ GAF

```

-|A0A075WDC0| 1,4-dihydroxy-2-naphthoate octaprenyltransferase; strain DSM 8774

```

10      20      30      40      50      60
MIFEIIKIGISĀ QPINFAYPIĀ LLSLLAFMLSĀ GSGYNELIISĀ YIFAFSFFTAĀ ANLWNHLNDAĀ

70      80      90      100     110     120
EDDLNAGRNYĀ ARFLIEHRKIĀ VTEFVVAFYFĀ VSFLLIFFISĀ KSKEIALLLTĀ GLSVVLTWLŸĀ

130     140     150     160     170     180
SDKIFIGKITĀ RRFKEDYKTEĀ VFTYILCSFSĀ FPLSFWTIFĀ EISQVGVVFTĀ LATGFTYLSGĀ

190     200     210     220     230     240
FFLKDLKDISĀ ADIKSGYRTLĀ AVVLSPTLLĀ IISVMLFIASĀ TFVVIFSSLĀ DVTPTSSLLVĀ

250     260     270     280
LTVYPPILFAĀ IYKFHKEKWKĀ ITKNIISLĀ IYTYSYLGFLĀ IAFAIGCKL

```

-|O28625| bacteriochlorophyll synthase, 33 kDa subunit; strain DSM 4304

```

10      20      30      40      50      60
MDSSLANINQĀ IDVPSKYLRĻ LRPVAWLCFĻ LPYAVGFGFGĀ ITPNASLQHĀ VLGLLSFAFVĀ

70      80      90      100     110     120
MAFSFTINALĀ YDRDVDRLHDĀ GRVKDLNLSMĀ QPLVTGEISVĀ REAWLYCIAFĀ LALSLATAAAĀ

130     140     150     160     170     180
INEKFFLAMĻ GANIIGYVYSĀ APPRFKAWPVĀ MDVICNALAAĀ VLAFYAGLSĪ GGAEVPIAIIĀ

190     200     210     220     230     240
PAAFFLAATFĀ YIPTAVSDYEĀ FDKKAGLKNTĀ PVFFGPERALĀ KSLYPLSAITĀ VILWAYVFLMĀ

250     260     270     280     290     300
AERIEIKVISĀ PLIIAYTLIŸĀ TFIINSRWDCĀ EKLVNVPNLĪ LTPFGIISAĻ FIAYGFAVISĀ VLG

```

Figure 8.9. Evolutionary genetic distance

	1	2	3	4	5	6	7	8	9	10	11	12	13	14	15	17	17	18
(1) TtUbiA	0.747																	
(2) SlUbiA	1.007	1.018																
(3) CjUbiA	0.985	1.052	0.673															
(4) HpUbiA	0.902	0.845	1.161	1.087														
(5) AfUbiA	1.343	1.359	1.492	1.510	1.440													
(6) EcUbiA	1.359	1.374	1.492	1.510	1.440	0.008												
(7) SfUbiA	1.313	1.343	1.492	1.457	1.440	0.101	0.106											
(8) KpUbiA	1.528	1.440	1.711	1.547	1.646	1.040	1.052	1.075										
(9) ScCoq2	1.440	1.343	1.566	1.547	1.626	1.052	1.063	1.099	0.873									
(10) LePTG	1.934	1.854	1.934	1.907	2.052	1.780	1.804	1.829	1.756	1.907								
(11) BsMenA	1.804	1.756	2.116	2.222	1.854	1.991	1.962	1.907	1.962	1.907	1.374							
(12) MttMenA	1.711	1.804	1.991	1.962	1.733	1.492	1.528	1.492	1.804	1.756	1.423	0.996						
(13) KpMenA	1.689	1.780	2.021	1.991	1.711	1.547	1.586	1.547	1.829	1.829	1.423	1.029	0.138					
(14) StMenA	1.667	1.756	2.083	1.934	1.689	1.528	1.566	1.474	1.829	1.880	1.440	1.018	0.142	0.033				
(15) EcMenA	1.689	1.756	2.083	1.934	1.711	1.547	1.586	1.492	1.829	1.880	1.440	1.018	0.142	0.037	0.004			
(16) SfMenA	1.040	1.029	1.123	1.123	0.883	1.187	1.174	1.187	1.423	1.528	1.780	1.907	1.626	1.646	1.667	1.689		
(17) ApUbiA	1.756	1.646	1.605	1.510	1.457	1.689	1.711	1.689	1.646	1.711	1.733	1.907	1.854	1.829	1.804	1.829	1.492	
(18) AfBchG																		

Figure 8.9. Estimates of evolutionary divergence between the sequences analyzed in Figure 4.7. The numbers of amino acid substitutions per site between the sequences are shown. Evolutionary analyses were conducted in MEGA6.

8.10. GGGPS/UbiA-2 homolog in *Aeropyrum pernix*

-|Q9YFU1| probable (S)-2,3-Di-O-farnesylgeranylgeranyl synthase

```

      10      20      30      40      50      60
MKA AIEITRP VNSLMVSLAI ILSLGIASRW SFQGFTPIDL MAVVVAGYCL SSVAMITNDI

      70      80      90     100     110     120
IDLEIDRINA PHRPLPAGKV STVEATILSI FLAALGFLAA ISVDLITTA F YLGG LALSLL

     130     140     150     160     170     180
YNTLLKRTGL PGNIVVAALV SAPFMYASLE AGGLGGPMSV FSTMVFLAVL GREVAKGVPD

     190     200     210     220     230     240
VEGDKAAGVR TVAVVFGKKT AAVASALYL ASAALGYIPL IYGYVDPLIY TPFILLLTLL

     250     260     270     280
VLREALLIVK RPTRENVLAH KNRVLGYMLI GLIAFALGTL GI

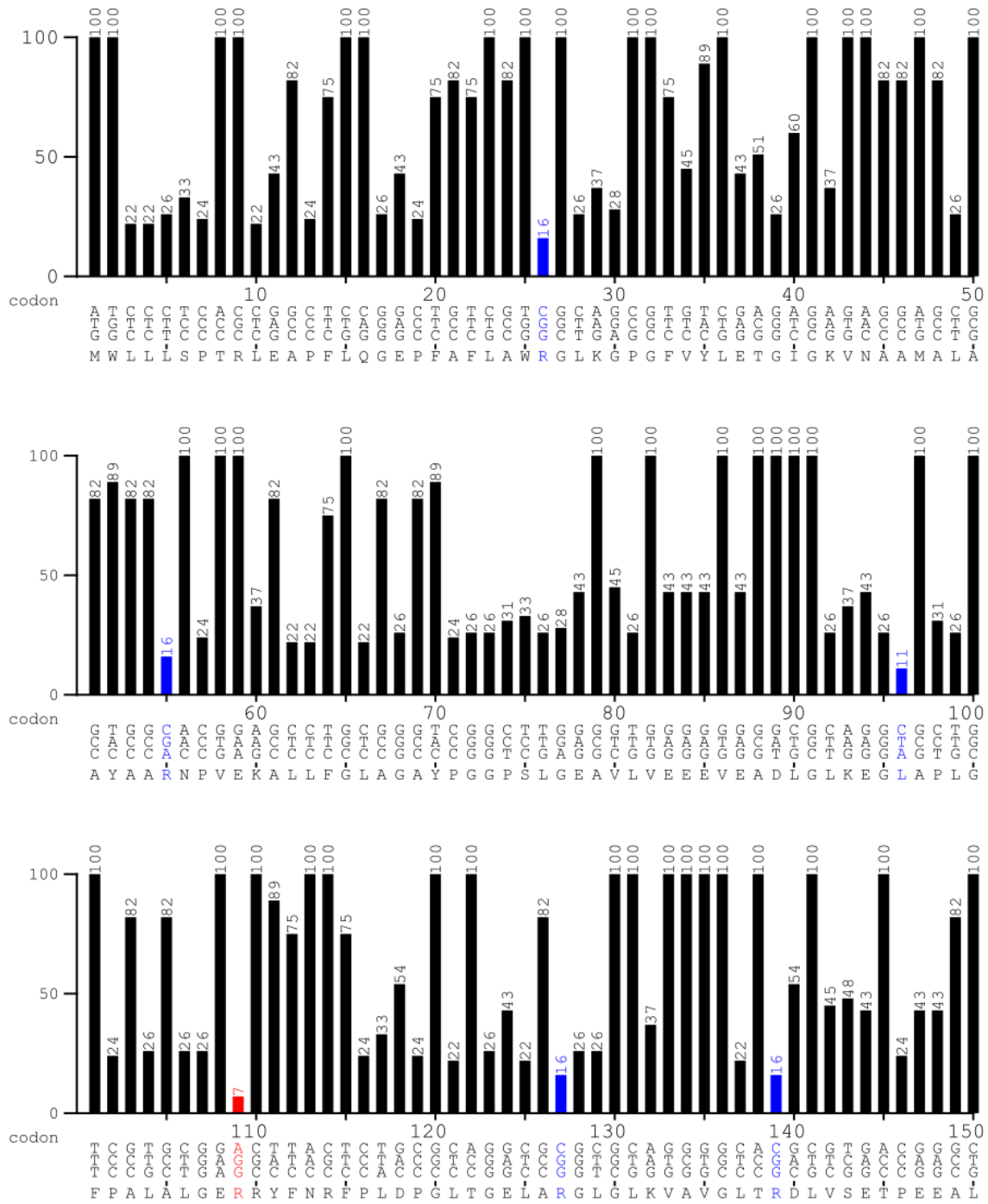
```

Figure 8.11. Codon-usage analysis of TtMqnB in *E. coli* cells.

TtMqnB
sequence derived from *Thermus thermophilus*

Codontable:
Escherichia coli K12

Ordinate (y-axis): relative adaptiveness <20% <10%



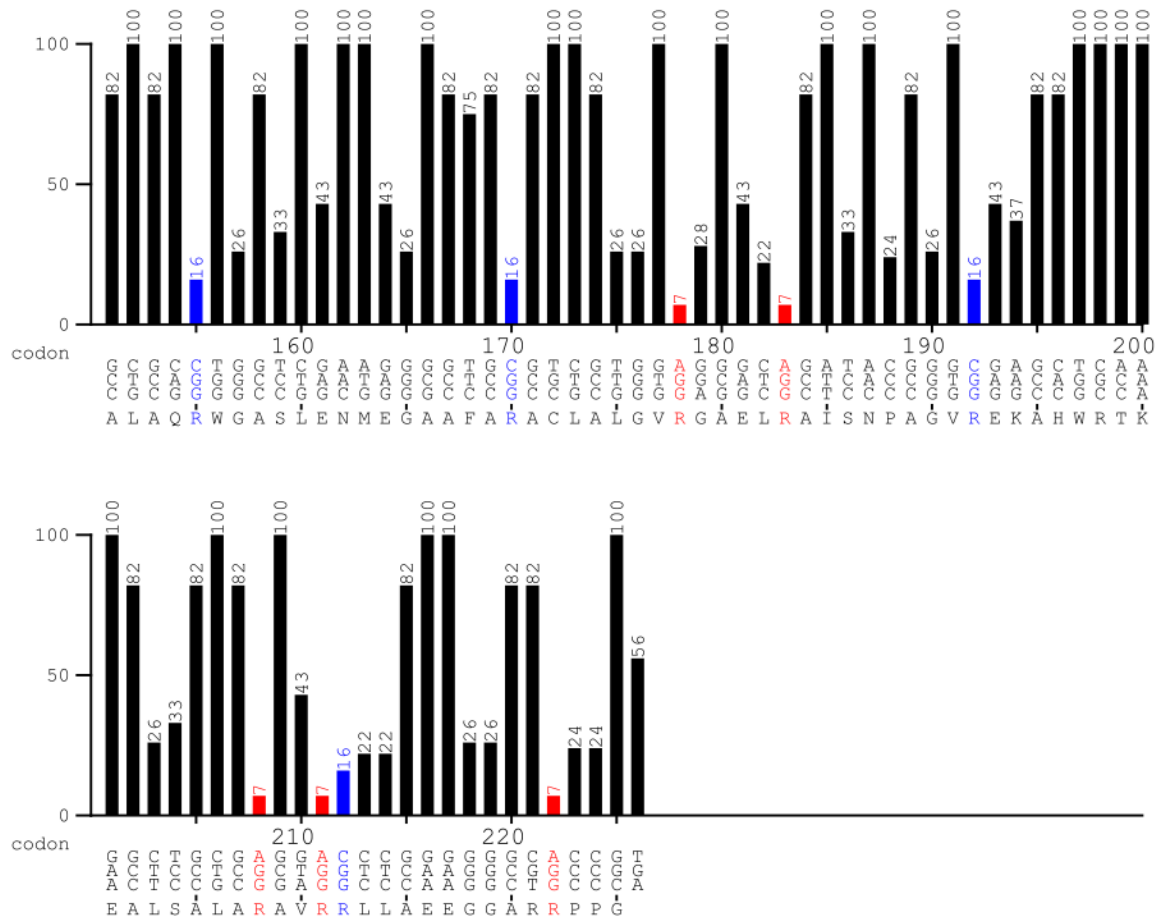


Figure 8.11. Graphical codon-usage analysis. Comparison of the necessary codons of TtMqnB with the use of them in *E. coli* K-12 strains. The y-axis shows the relative adaptability of each codon. The most frequently used triplet is set to 100%. Blue and red bars show the codons which the relative adaptability is lower than 20% and 10%, respectively (Fuhrmann *et al.*, 2004).

Figure 8.12. PISA analysis of TtMqnB-apo structure.

PISA Interface List.

Interfaces in MqnB_apo_refine_21-coot-0.pdb crystal.
Space symmetry group: P 31 2 1

Session Map (id=246-11-5FJ)
Start Interfaces Interface Search
Monomers
Assemblies

Interfaces XML View Details Download Search

##	Structure 1	x	Structure 2	interface	ΔG	ΔG	N_{HB}	N_{SB}	N_{DS}	CSS	
Id	NN	Range	N _{at.} N _{res.} Surface Å ²	Range	Symmetry op-n	Sym.ID	N _{at.} N _{res.} Surface Å ²	area, Å ²	kcal/mol	P-value	
1	1	C	161 45 11128	B	x,y,z	1_555	161 45 10397	1607.4	-27.3	0.051	10 2 0 1.000
	2	D	115 32 10291	A	x,y,z	1_555	115 32 10802	1102.3	-16.8	0.166	7 2 0 1.000
							Average:	1354.9	-22.1	0.109	9 2 0 1.000
2	3	A	84 21 10802	C	x-y,-y+1,-z+2/3	6_565	93 23 11128	769.1	-5.2	0.513	10 1 0 0.000
3	4	C	61 18 11128	A	-y+1,x-y+1,z+1/3	2_665	64 18 10802	591.9	-7.1	0.359	6 0 0 0.000
	5	D	59 17 10291	B	x,y,z	1_555	56 17 10397	578.0	-5.8	0.456	4 1 0 0.000
							Average:	584.9	-6.5	0.407	5 1 0 0.000
4	6	B	62 19 10397	A	x-y,-y+1,-z+2/3	6_565	58 18 10802	536.0	-5.2	0.517	8 0 0 0.000
5	7	C	54 14 11128	A	x,y,z	1_555	50 13 10802	507.6	-7.0	0.290	3 0 0 0.000
6	8	B	47 14 10397	D	-y+1,x-y+1,z+1/3	2_665	47 14 10291	463.4	-7.5	0.245	4 0 0 0.000
7	9	D	26 7 10291	D	x-y+1,-y+2,-z+2/3	6_675	26 7 10291	243.7	2.3	0.889	2 0 0 0.000
8	10	D	27 9 10291	C	x,y,z	1_555	19 7 11128	234.2	-1.9	0.287	2 0 0 0.000
	11	B	18 6 10397	A	-y+1,x-y+1,z+1/3	2_665	25 9 10802	221.8	-2.0	0.362	2 1 0 0.000
	12	C	19 8 11128	D	-y+1,x-y+1,z+1/3	2_665	11 4 10291	142.7	-2.2	0.274	1 0 0 0.000
	13	B	19 8 10397	A	x,y,z	1_555	10 3 10802	141.7	-2.3	0.229	1 0 0 0.000

Figure 8.12. PISA interface analysis of TtMqnB-apo structure. PISA interface list indicates potential interface between monomers C and B (NN1) and between monomers D and A (NN2) with interface area of 1607.4 Å² and 1102.3 Å², respectively. Both interfaces were scored with 1.0 in complexation significance score (CSS) indicating that they play a role in complexation (Krissinel und Henrick 2007).

Figure 8.13. Superposition of monomer C of apo-TtMnqB with hypo-TtMnqB

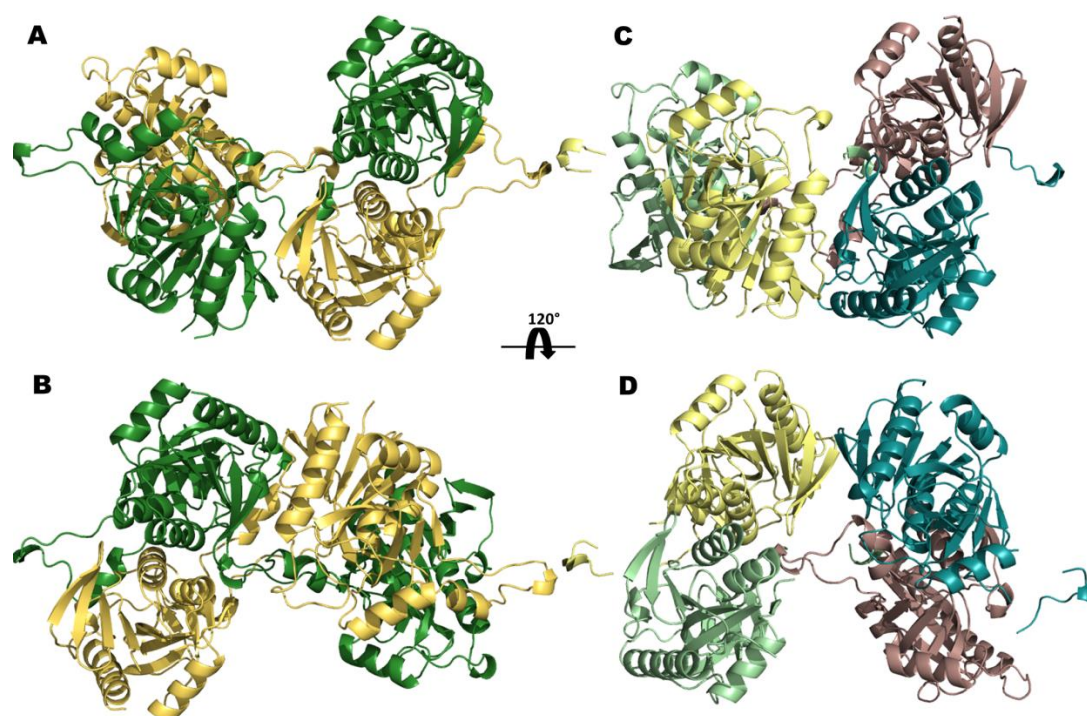


Figure 8.13. Crystal packing of TtMnqB. (A) (B) Crystal packing of hypo-TtMnqB. The TtMnqB crystal structure presented two molecules in the asymmetric unit and the space group $P3_221$. The tetramer structure was generated using the symmetry mates in PyMOL. **(C) (D) Crystal packing of apo-TtMnqB.** TtMnqB-apo crystals showed four molecules in the asymmetric unit and the space group $P3_112$. Although both crystals presented a trigonal space group, it is possible to observe different packing between the structures.

Figure 8.14. Superposition of monomer C of apo-TtMnqB with hypo-TtMnqB

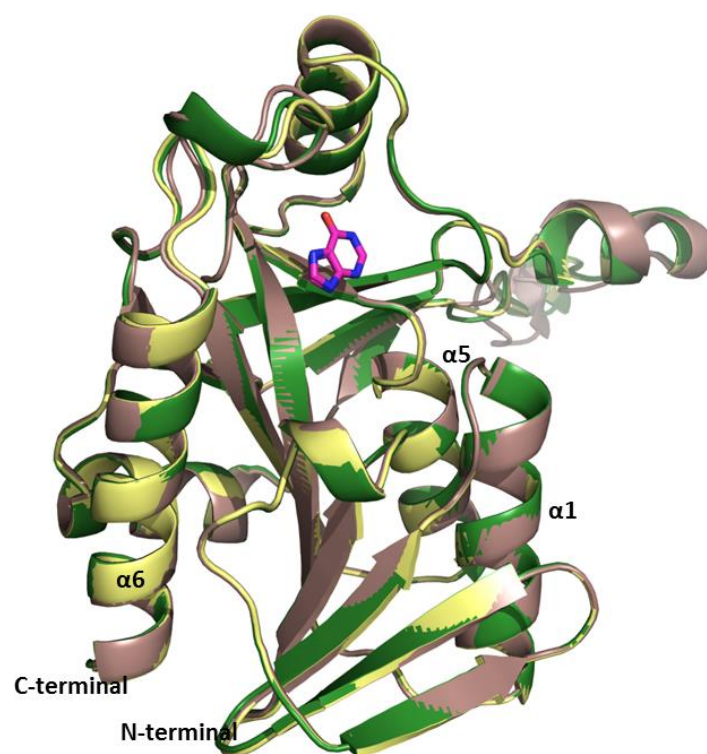


Figure 8.14. Superposition of both monomers of hypo-TtMnqB-hypo (shown in green) with monomer C of apo-TtMnqB (shown in brown). Comparison between both monomers shows no significant conformational modifications after hypoxanthine (magenta sticks) binding

Figure 8.15. Docking conformation from Autodock Vina program

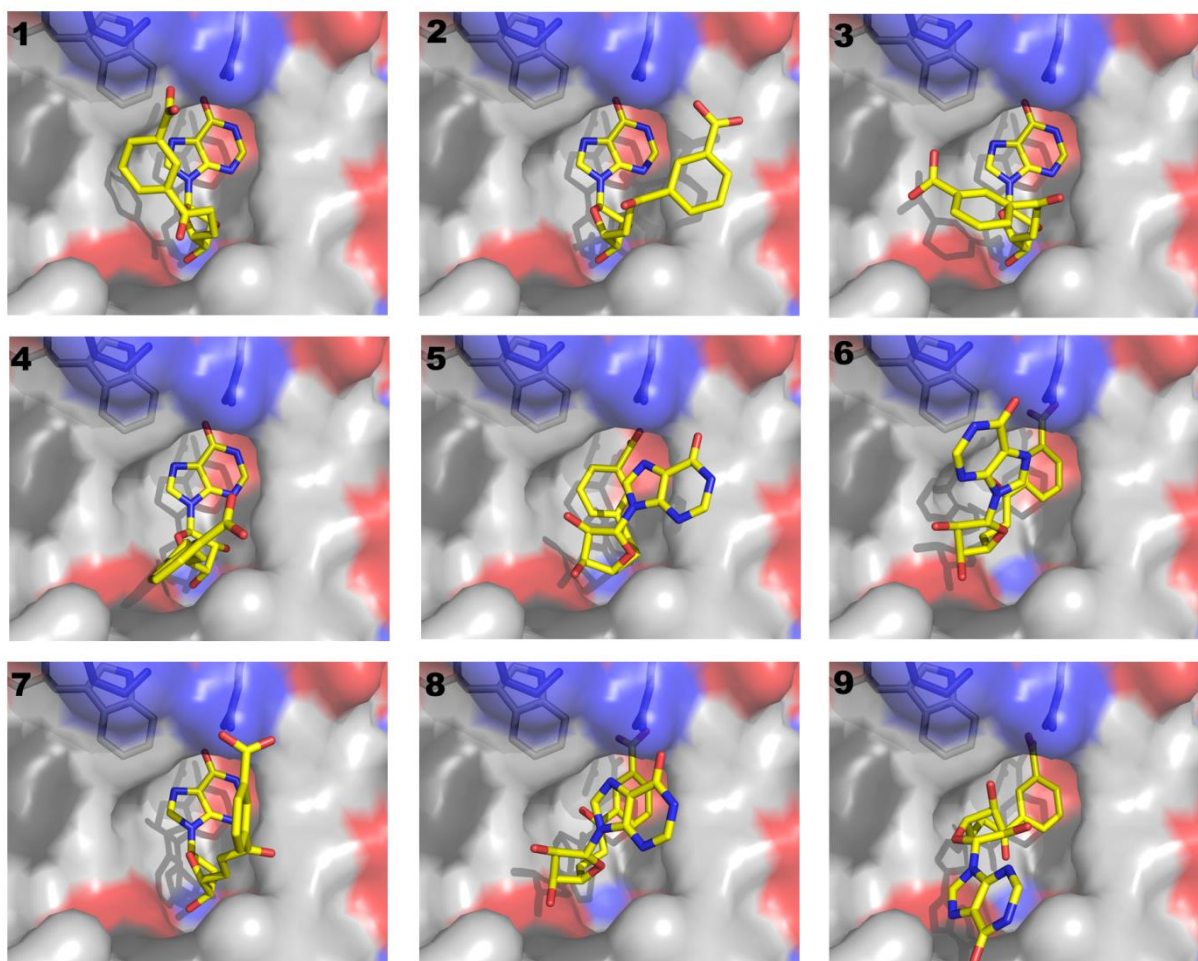


Figure 8.15. Docking solutions using the program AutoDock Vina. Numbers from 1 to 9 indicate different binding of futalosine in the active site of TtMqnB. The output containing the binding affinity and RMSD values is shown below. Two variants of RMSD are provided, rmsd/lb (lower bound) and rmsd/ub (upper bound), differing in how the atoms are matched in the distance calculation: rmsd/ub matches each atom in one conformation with itself in the other conformation, ignoring any symmetry and rmsd/lb is defined as follows: $\text{rmsd/lb}(c_1, c_2) = \max(\text{rmsd}'(\text{rmsd}(c_1, c_2)), \text{rmsd}'(c_1, c_2))$ (Trott and Olson, 2010).

Output of AutoDock Vina

mode	affinity (kcal/mol)	dist from best mode	
		rmsd l.b.	rmsd u.b.
1	-9.3	0.000	0.000
2	-9.2	2.860	3.744
3	-8.9	1.576	2.173
4	-8.4	2.228	2.842
5	-8.4	3.022	5.745
6	-7.7	3.174	6.985
7	-7.7	2.263	2.781
8	-7.4	3.284	6.751
9	-7.3	3.889	8.202

9. Abbreviations

4PP	4-phenylphenol
ACN	Acetonitrile
ADA	N-(2-Acetamido)iminodiacetic acid, N-(Carbamoylmethyl)iminodiacetic acid
CD	Circular dichroism
CMC	Critical micelle concentration
Cymal-6	6-Cyclohexyl-1-hexyl- β -D-maltopyranoside
DDM	n-Dodecyl- β -D-maltopyranoside
DHNA-2	1,4-dihydroxy-2-naphthoic acid
DHNA-6	1,4-dihydroxy-6-naphthoic acid
DM	n-Decyl- β -D-maltopyranoside
DMAPP	Dimethylallyl pyrophosphate
DMK	Demethylmenaquinone
EDO	Ethylene glycol
EDTA	Ethylenediamine tetraacetic acid
FPP	Farnesyl pyrophosphate
GFPP	Geranylgeranyl pyrophosphate
GGPP	Geranylgeranyl pyrophosphate
GHB	3-geranyl-4-hydroxybenzoate
GPP	Geranyl pyrophosphate
HPLC	High performance liquid chromatography
IMAC	Immobilized metal ion affinity chromatography
IPTG	Isopropyl- β -D-thiogalacto-pyranosid
LB	Luria Bertoni
LePTG1	Lithospermum erythrorhizon p-hydroxybenzoate geranyltransferase
LCP	Lipid cubic phase
MF	Membrane fraction
MK	Menaquinone
MR	Molecular replacement

Abbreviations

MTA	5'-methylthioadenosine
MTAN	5'-methylthioadenosine nucleosidase
β -OG	n-octyl- β -D-glucoside
PAGE	Polyacrylamid gelectrophoresis
PDB	Protein data bank
PHB	4-hydroxybenzoic acid
PCR	Polymerase chain reaction
PVDF	Polyvinylidene fluoride
RMSD	Root-mean-square deviation
RP-HPLC	Reverse phase
SEC	Size Exclusion chromatography
SDS	Sodium dodecyl sulphate
TEV	Tobacco etch virus
Tris	Tris(hydroxymethyl)-aminomethane
UQ	Ubiquinone

Resume

Personal data

Name: Camila A. Cotrim
Date of birth: 3th April, 1985
Place of birth: Campinas, São Paulo - Brazil
Marital status: Married

Education

- Since 02/2016: Research officer (Postdoc) at Institute of Molecular Bioscience (IMB) at The University of Queensland – Brisbane, Australia.
 Supervisor: Prof. Dr. Jennifer Martin
 Thema: “Structure and function of human zinc transporter membrane proteins”.
- 08/2015 – 01/2016: Visiting academic at School of Chemistry and Molecular Biosciences at The University of Queensland – Brisbane, Australia.
 Supervisor: Prof. Dr. Bostjan Kobe
 Thema: “Structural characterization of UDP-glucose pyrophosphorylase from *Saccharum hybrid cultivar* (ScUGPase)”.
- 04/2011 – 05/2015: PhD at Department of Biochemistry/Biotechnology at Martin-Luther-Universität Halle-Wittenberg – Germany.
 Supervisor: Prof. Dr. Milton T. Stubbs.
 Thema: “Biochemical and structural studies on enzymes of menaquinone biosynthesis”.
- 02/2009 – 01/2011: MSc in Molecular Biology and Functional Biology – Specialization in Biochemistry at State University of Campinas (UNICAMP) – Brazil.
 Supervisor: Prof. Dr. Marcos Hikari Toyama.
 Thema: “Evaluation of quercetin and hecogenin effects of the pharmacological enzymatic activities of sPLA2 isolated from *Crotalus terrificus* and *Bothrops pirajai*”.
- 03/2004 – 12/2008: BSc in Chemistry at São Paulo State University (UNESP) - Brazil.
 Supervisor: Prof. Dr. Reinaldo Marchetto.
 Thema: “Characterization of DNA Gyrase inhibition using analogue peptides based on CcdB protein”.
- 03/2000 – 12/2002: Secondary school, Colégio Oswaldo Cruz - COC Campinas, São Paulo – Brazil.
- 03/1992 – 12/1999: Primary school, E.M.P.G Correa de Mello, Campinas, São Paulo – Brazil.

Publications

1. Camargo, E.A.; Santana, D.G.; Silva, C.I.; Teixeira, M.H.; **Cotrim, C.A.**; Landucci, E.C.T.; Antunes, E.; Muscara, M.N.; Costa, S.K.P (2013). Inhibition of inducible nitric oxide synthase-derived nitric oxide as a therapeutical target for acute pancreatitis induced by secretory phospholipase A2. *European Journal of Pain* 18 (5), 691-700.
2. **Cotrim, Camila A.**; de Oliveira, Simone Cristina Buzzo; Diz Filho, Eduardo B.S.; Fonseca, Fabiana Vieira; Baldissera Jr., Lineu; Antunes, Edson; Ximenes, Rafael Matos; Monteiro, Helena Serra Azul; Rabello, Marcelo Montenegro; Hernandez, Marcelo Zaldini (2011). Quercetin as an inhibitor of snake venom secretory phospholipase A2. *Chemical Biological Interactions* 189, 9-16.
3. Santos, Marcelo L.; Toyama, Daniela O.; Oliveira, Simone C. B.; **Cotrim, Camila A.**; Diz-Filho, Eduardo B. S.; Fagundes, Fábio H. R.; Soares, Veronica C. G.; Aparicio, Ricardo; Toyama, Marcos H. (2011). Modulation of the pharmacological activities of secretory phospholipase A2 from *Crotalus durissus cascavella* induced by Naringin. *Molecules* 16, 738-761.
4. Toyama, Daniela de Oliveira; Diz Filho, Eduardo Britto dos Santos; Cavada, Benildo Sousa; da Rocha, Bruno Anderson Matias; de Oliveira, Simone Cristina Buzzo; **Cotrim, Camila A.**; Soares, Veronica Cristina Gomes; Delatorre, Plinio; Marangoni, Sergio; Toyama, Marcos Hikari (2011). Umbelliferone induces changes in the structure and pharmacological activities of Bn IV, a phospholipase A2 isoform isolated from *Bothrops neuwiedi*. *Toxicon* 57, 851-860.
5. Soares, Veronica Cristina Gomes; Bonacorsi Cibele; Andrela, Alana L B; Bortoloti, Lígia V; de Campos, Stepheny C; Fagundes, Fábio H. R.; Piovani, Márcio; **Cotrim, Camila A.**; Vilegas, Wagner; Toyama, Marcos H. (2011). Cytotoxicity of active ingredients extracted from plants of the Brazilian "Cerrado". *Natural Product Communications* 6, 983-984.
6. Fonseca, F.V.; Baldissera Jr., L.; Camargo, E.A.; Antunes, E.; Diz-Filho, E.B.S.; Corrêa, A.G.; Beriam, L.O.S.; Toyama, D.O.; **Cotrim, C. A.**; Toyama, M.H. (2010). Effect of the synthetic coumarin, ethyl 2-oxo-2H-chromene-3-carboxylate, on activity of *Crotalus durissus ruruima* sPLA2 as well as on edema and platelet aggregation induced by this factor. *Toxicon* 55, 1527-1530.
7. **Cotrim, Camila A.**; Garrido, Saulo S; Trovatti, Eliane; Marchetto, Reinaldo (2010). Síntese, Caracterização e Estudos de Interação de um análogo da Antitoxina CcdA Empregando Fluorescência no Estado Estacionário. *Química Nova* 33, 841-845.
8. Trovatti, Eliane; **Cotrim, Camila A.**; Garrido, Saulo S.; Barros, Ronaldo S.; Marchetto, Reinaldo (2008). Peptides based on CcdB protein as novel inhibitors of bacterial topoisomerases. *Bioorganic & Medicinal Chemistry Letters* 18, 6161-6164.

9. Marchetto, Reinaldo; Garrido, Saulo S.; Barros, R. S.; Trovatti E.; **Cotrim, Camila A.** (2008). Peptides from CcdB protein as novel inhibitors of DNA gyrase. *Journal of Peptide Science* 14, 102-103.

Book chapter

1. Marcos Toyama, Selma D. Rodrigues, Daniela O. Toyama, Veronica C.G. Soares, **Camila Ap Cotrim**, Rafael Ximenes, Marcelo L. Santos (2012). Phospholipases A2 Protein Structure and Natural Products Interactions in Development of New Pharmaceuticals. *Protein Structure*, Chapter 16 Eshel Faraggi (Ed.), ISBN: 978-953-51-0555-8.

Danksagung

Hiermit möchte ich mich bei all denjenigen bedanken, die zum Gelingen dieser Arbeit beigetragen haben.

Zuallererst danke ich **Prof. Dr. Milton T. Stubbs** für die Möglichkeit diese interessanten Themen zu arbeiten und für die Freiheit in der Planung und Durchführung der Experimente. Insbesondere danke ich ihm für seinen Optimismus sogar als die Experimente mit der Membranproteine nicht gut geklappt hatten und natürlich bin ich ihm sehr dankbar für die Möglichkeit ein neues Land und eine neue Kultur entdecken zu können.

Ein großes Dankeschön gilt **Dr. Annett Weidner** für die Unterstützung von Anfang dieser Arbeit, die konstruktiven Diskussionen und für die zahlreichen Hinweise. Außerdem danke ich ihr für die schöne Zeit im Labor.

Bei **Dr. Christoph Parthier** und **Dr. Michael Schöpfel** möchte ich mich für die große Hilfe mit der Prozesse der Datensammlung, Prozessierung und Strukturaufklärung bedanken.

Bei **Dr. Mikio Tanabe** und seiner Arbeitsgruppe (**Dr. Frank Jaenecke**, **Dr. Caroline Haupt** und **Kumar Nagarathinam**) möchte ich mich für die zahlreichen Diskussionen und Tipps über Membranproteine bedanken.

Der Arbeitsgruppe von **Prof. Dr. Ludger Wessjohann**, insbesondere **Dr. Tula Beck Bisol** und **Dr. Ricardo W. Neves Filho** danke ich für die organisch Synthese von verschiedenen Moleküle. Ein besonderer Dank auch an **Dr. Danilo Meyer** und **Hans Felix Schreckenbach** für die Hilfe mit der Aktivitätstests und für die konstruktiven Diskussionen.

Der Arbeitsgruppe von **Prof. Dr. Gary Sawers**, insbesondere **Dr. Lydia Beyer**, **Claudia Bielak** und **Monique Jaroschinsky** danke ich für die Hilfe mit der Mikrobiologie-Experimente sowie für ihre geduldige Beantwortung all meiner Fragen zum Thema.

Bei **PD Dr. Hauke Lilie** möchte ich mich für die Durchführung der analytischen Ultrazentrifugation bedanken.

Bei **Dr. Nadine Strehmel**, **Dr. Christoph Böttcher** und **Dr. Angelika Schierhorn** möchte ich mich für die Durchführung der Massenspektrometrie-Experimente bedanken.

Bei der gesamten Arbeitsgruppe (**AG Stubbs**) danke ich mich für den vielen Diskussionen und Tipps sowie die schöne Zeit. Es war toll mit euch zu arbeiten. Ein besonderer Dank gilt **Anja Greschuchna**, **Pia Rosenburg**, **Anke Piechotta**, **Sabrina Pfennig**, **Luise Quil** und **Nadja Reiter** für das schöne Arbeitsklima im Labor und Büro sowie für die Hilfe mit der deutschen Sprache.

Ich danke allen Mitgliedern des **Pronet T³** und **HALOmem** für die Diskussionsbereitschaft und für die interessanten Meetings. Ein großer Dank an **Dr. Mathias Strutz**, **Katja Möritz**, **Rositta Mothes** und **Ulla Niesbach-Klösgen** für die Unterstützung.

Ich danke allen **meinen Freunden**, besonders **Robert und Helgard**, die immer ein offenes Ohr für mich und meine Probleme hatten. Vielen Dank für die tolle Zeit und die großartigen Erfahrungen, die wir zusammen verbracht haben.

Der größte Dank gilt **meiner lieben Familie** und vor allem meinem Mann **Rafael** für die liebevolle Unterstützung, ohne die diese Doktorarbeit nicht möglich gewesen wäre.

Vielen Dank!

Declaration

Erklärung

Hiermit erkläre ich, dass ich die vorliegende Arbeit selbständig und ohne fremde Hilfe verfasst habe. Ich habe keine anderen als die hier angegebenen Quellen und Hilfsmittel benutzt und wörtlich oder inhaltlich entnommenen Stellen als solche kenntlich gemacht habe. Ferner erkläre ich, dass ich mich mit dieser Arbeit an keiner anderen Hochschule oder Universität um die Erlangung eines akademischen Grades beworben habe.

Declaration

I hereby declare that I have written this thesis independently and without external assistance other than the mentioned sources and aids being cited in this dissertation. Therefore any extracts of external works used literally or figuratively in the present thesis are outlined and cited accordingly. I also declare that I have not applied this thesis at any other college or university in order to obtain an academic degree.

Halle (Saale), den

Camila A. Cotrim